Electrostatic Interactions during Multicomponent Ionic Transport in Porous Media

Dissertation

der Mathematisch-Naturwissenschaftlichen Fakultät

der Eberhard Karls Universität Tübingen

zur Erlangung des Grades eines

Doktors der Naturwissenschaften

(Dr. rer. nat.)

vorgelegt von

M.Sc. Muhammad Muniruzzaman

aus Dhaka/Bangladesch

Tübingen

2016

Gedruckt mit Genehmigung der Mathematisch-Naturwissenschaftlichen Fakultät der Eberhard Karls Universität Tübingen.

Tag der mündlichen Qualifikation:	19.09.2016
Dekan:	Prof. Dr. Wolfgang Rosenstiel
1. Berichterstatter:	Prof. Dr. Massimo Rolle
2. Berichterstatter:	Prof. Dr. Peter Grathwohl
3. Berichterstatter:	Dr. George Redden

To my family

“ভাব ন হোই অভাব ণ জাই ।
অইস সংবোহেঁ কো পতিআই ॥ধ্রু॥
লুই ভণই বঢ় দুলক্খ বিণাণা ।
তিঅ ধাএ বিলসই উহ লাগে ণা ॥ধ্রু॥
জাহের বানচিহ্ন রূব ণ জাণী ।”

লুই’পা, চর্যা- ২৯, চর্যাপদ

“It is neither being nor non being.
Who will believe this explanation?
Luyi says: O foot!
Real wisdom is very difficult to understand.
It is manifested in three elements.
But its location cannot be ascertained.”

- Luyipada, Charyapada 29

Abstract

Solute transport of charged species in porous media is significantly affected by the electrochemical migration term resulting from the charge-induced interactions among the dissolved ions as well as with solid surfaces. Therefore, the characterization of such electrochemical processes is of utmost importance for assessing the fate and transport of charged solutes in porous media. This work presents a detailed investigation of the electrochemical effects during conservative and reactive multicomponent ionic transport in homogeneous and heterogeneous domains by means of laboratory bench-scale experiments and numerical simulations. The investigation aims at quantifying the key role of small-scale electrostatic interactions in flow-through systems, especially when advection is the dominant mass-transfer process. By performing a series of quasi two-dimensional flow-through experiments with different electrolyte solutions, we study the specific influence of charge effects on steady-state and transient transport of multicomponent ionic species in saturated porous media. The outcomes of steady-state experiments reveal that Coulombic cross-coupling of diffusive/dispersive fluxes significantly affects the lateral displacement of charged species not only in diffusion-dominated systems but also in advection-dominated flow regimes. We also show that these charge effects do not vanish during transport in spatially variable flow-fields in physically heterogeneous porous media. Furthermore, the electrostatic interactions were found to significantly impact the pH fronts propagation depending on the solution composition as well as on the concentration gradients of the other charged species in a multicomponent environment. Experiments were also performed under transient transport conditions. The results demonstrate that ionic interactions significantly influence the transient multicomponent ionic transport and lead to remarkable differences in solute breakthroughs and dilution behaviors of different ionic species. Each experiment has been quantitatively evaluated with numerical simulations. The experiments have been accompanied by stepwise model development in which a multicomponent ionic formulation, explicitly accounting for charge interactions, was adopted. A new two-dimensional multicomponent ionic transport model has been proposed. The modeling approach is based on the local charge balance, multicomponent formulation of diffusive/dispersive fluxes, and improved description of compound-specific hydrodynamic dispersion coefficients. The multicomponent ionic transport code was coupled with the widely used geochemical code PHREEQC (using IPhreeqc module) and, thus, provides a comprehensive framework to perform Darcy- to field-scale reactive transport simulations, explicitly considering electrochemical migration as well as geochemical calculations included in PHREEQC's reaction package. Numerical simulations, performed with the newly proposed model, showed that electrostatic interactions among charged species affect conservative and reactive transport also in field-scale domains containing both physical and geochemical heterogeneities.

Kurzfassung

Der Transport geladener Teilchen in Porösen Medien wir signifikant durch den ‘electrochemical migration’-Term beeinflusst, der aus der ladungsinduzierten Interaktion zwischen den gelösten Ionen sowie geladener Oberflächen resultiert. Die Charakterisierung solcher elektrochemischen Prozesse ist daher von höchster Relevanz um den Transport und das Verhalten geladenen Teilchen in Porösen Medien zu Beschreiben. Die vorliegende Arbeit umfasst eine detaillierte Untersuchung elektrochemischer Effekte während des konservativen sowie des reaktiven Mehrkomponententransports geladener Teilchen in homogenen und heterogenen Medien durch Laborexperimente und numerische Simulationen. Die Arbeit hat zum Ziel die Schlüsselrolle kleinskaliger elektrostatischer Wechselwirkungen in Durchflusssystemen zu untersuchen, speziell wenn die Advektion der dominante Transportmechanismus ist. Hierfür wurde eine Reihe von Quasi-2-D-Tankexperimenten mit unterschiedlichen Elektrolytlösungen durchgeführt um den Einfluss von Ladungseffekten auf den stationären sowie den instationären Mehrkomponententransport geladener Teilchen in wassergesättigten Porösen Medien zu analysieren. Die Ergebnisse der stationären Transportexperimente zeigen auf, dass der „Coulombic cross coupling“-Effekt der diffusiven/dispersiven Massenflüsse nicht nur einen signifikanten Einfluss in diffusionsdominierten Systemen hat sondern auch in advektionsdominierten Systemen einen großen Einfluss haben kann. Mit weiteren Experimenten konnten wir zeigen, dass dieser Effekt auch in heterogenen Systemen bestehen bleibt. Weiter konnten durch die vorliegende Arbeit gezeigt werden, dass die elektrostatische Wechselwirkung die Propagation einer ph-Front beeinflusst, in Abhängigkeit der Zusammensetzung der Lösung sowie der Konzentrationsgradienten der anderen Ionen im Wasser. Zusätzlich zu den stationären Experimenten wurden auch Transportexperimente unter instationären Bedingungen durchgeführt. Die Ergebnisse legen nah, dass die ionische Wechselwirkung auch den transienten Multikomponententransport beeinflusst und zu Unterschieden im Durchbruch sowie der Verdünnung der gelösten Ionen führt. Jedes der durchgeführten Experimente wurde mittels numerischer Simulationen quantitativ ausgewertet. Hierbei wurden die Experimente begleitet von der schrittweisen Weiterentwicklung des numerischen Modells, welches eine Mehrkomponenten-Formulierung für den Ionen-Transport berücksichtigt, die explizit die elektrostatische Wechselwirkung berücksichtigt. Ein neues 2-D-Mehrkomponenten-Transportmodel für Ionen wurde entwickelt. Die Modellierung beruht hierbei auf der lokalen Ladungsbilanz, der Mehrkomponenten-Formulierung der diffusiven/dispersiven Massenflüsse sowie der verbesserten Beschreibung der hydrodynamischen Dispersion. Das Mehrkomponententransportmodell wurde mit der geochemischen Simulationssoftware PHREEQC (IPhreeqc Modul) gekoppelt und bietet somit einen umfassenden Rahmen für die Simulation des reaktiven Transports, unter expliziter Berücksichtigung der elektrochemischen Wechselwirkung geladener gelöster Teilchen, von der Darcy- bis hin zur Feldskale. Die durchgeführten Simulationen mit dem neu entwickelten Modell zeigen, dass die elektrostatische Wechselwirkungen zwischen geladenen Spezies auch auf der Feldskala in pysikalisch und chemische heterogenen Systemen den konservativen sowie den reaktiven Transport beeinflussen.

Acknowledgements

This work would not have been possible without the support and encouragement from many people. I would like to express my explicit gratitude to a number of individuals, who, in some ways, contributed to the completion of this work:

First of all, I would like to thank Prof. Dr. Massimo Rolle for providing me the opportunity to work on this dissertation. His detailed guidance, patience, inspiration, and continuous input of ideas during the last five years (starting from my master) help me to grow scientifically. Without his constant support it would have been much more difficult to achieve this goal.

I also want to express my deepest gratitude to my other supervisor, Prof. Dr. Peter Grathwohl. He provided an excellent lab and working place and constantly encouraged me throughout all the past years.

I am indebted to Prof. Dr. Olaf A. Cirpka, who provided generous support when I was lost working with his streamline-oriented code, especially in the beginning of my PhD. I also deeply appreciate his readiness for spontaneous discussions from time to time. In fact, the courses offered by him during the first three semesters of my MSc provided me the basis for the modeling skills needed for this work.

I owe very special thanks to Dr. Christina Haberer for helping me to learn the techniques of the flow-through transport and diffusion experiments. It was a great opportunity to work with her closely and learn from her experiences. At the end, we shared three joint publications.

Thanks to the *administration* and *technical* teams (Dr. Wolfgang Bott, Elisabetha Kraft, Marion Schäffling, Willi Kappler…) of Center for Applied Geoscience for helping me to survive with all the bureaucracies (auf Deutsch, of course) and IT issues. I owe a great deal to Dr. Peter Merkel and Monika Jekelius for finding me a scholarship during my MSc and their cooperativeness in the last six years.

I also want to thank our *laboratory* team, especially Dr. Thomas Wendel, Bernice Nisch, Annegret Walz, Sara Cafisso, Wolfgang Kürner….. Additionally, I also greatly appreciate the support from the people working in *DTU Environment laboratory* (Jens Schaarup Sørensen, Sinh Hy Nguyen, Mikael Emil Olsson, Hector Diaz…) during my exchange period at the last year of my PhD.

Special thanks to all former and recent members of *Mensa* team: Jin Biao, Dominik Eckert, Alexander Lübben, Farhana Huq, Olaf Cirpka, Carsten Leven, Chuanhe Lu, Kennedy Doro, Daniel Erdal, Stéphane Ngueleu, Emilio Sanchez….. Also thanks to the *Canteen* team of DTU: Klaus, Claus, Sheng, Bentje, Filippo, Monica, Ursula, Anne, Lucien, Maria, Grith…… They helped me surviving after so many lunches in the Mensa/Canteen and made this period enjoyable as well. Furthermore, I would like to especially thank Dominik Eckert for helping me getting used to the details of streamline code and having patience for answering all of my questions.

Thanks to all of my officemates in Tübingen as well as in DTU: Haiyan Li, Alexander Lübben, Raphael Schneider, Louise Rosenberg, Chunyu Wen, and Liguang Jiang….

I would like to thank my friends and colleagues in ZAG, and former/current group members of Hydrogeochemistry group: Yu Ye, Zhongwen, Gaëlle, Bijendra, Jenia, Dominik …

I want to thank all my friends, spread all around the world, for helping me to cope with occasional (ups and) downs and for sharing with me many happy moments. In particular, special thanks go to Syed Hadiuzzaman, Farhana Huq, Shabab Hannan, Sobuj Mia, Didarul Alam Tusher, Syeda Tasneem Towhid, Salima Sultana Daisy, Tanvir Hassan, Aron Habteghebriel… who made my life in Tübingen very enjoyable.

Last but not the least, I want to thank my entire family, especially my father and mother, grandparents, siblings, and others who never stopped encouraging me in all these years. Without their support and motivation, it would have been impossible for me to finish this dissertation. In particular, I would like to especially dedicate this work to my grandfather (who was the first university graduate in our whole family, and is not with us is anymore), who had initiated the very first step of my educational life starting from how to read and write.

This work was funded by Baden-Württemberg Stiftung under Eliteprogram for Postdocs, which is gratefully acknowledged here. I also acknowledge the support (Baden-Württemberg Stipendium) from the same organization during my MSc studies.

Contents

Abstract ..... **v**

Kurzfassung ..... **vii**

Contents ..... **xi**

List of Figures ..... **xiii**

List of Tables ..... **xvii**

Introduction **1**

Coulombic effects in advection-dominated transport of electrolytes in porous media: Multicomponent ionic dispersion **9**
2.1 Introduction 10
2.2 Theoretical Background 11
2.3 Experimental Setup 12
2.4 Modeling Approach 15
2.5 Results and Discussion 18
2.5.1 Experiments at flow velocity v=1.5 m/day 18
2.5.2 Experiments at flow velocity v=6 m/day 22
2.5.3 Flux-related dilution index 24
2.6 Summary and Conclusions 26
References 28

Multicomponent ionic dispersion during transport of electrolytes in heterogeneous porous media: Experiments and model-based interpretation **31**
3.1 Introduction 32
3.2 Theoretical Background 33
3.3 Two-dimensional Multicomponent Transport Model 34
3.4 Experimental Setup 39
3.5 Results and Discussion 41
3.5.1 Flow-through experiments with a low-permeability inclusion (HET A) 42
3.5.2 Flow-through experiments with high-permeability inclusions (HET B) 47
3.6 Summary and Conclusions 51
References 53

Impact of multicomponent ionic transport on pH fronts propagation in saturated porous media **57**
4.1 Introduction 58
4.2 Equations of Multicomponent Ionic Transport 59
4.3 Experimental Setup 61
4.4 Modeling Approach 64
4.5 Results and Discussion 66
4.5.1 Scenario 1: Transport of HCl with similar molar concentration of $MgCl_2$ 66

4.5.2 Scenario 2: Transport of HCl with excess molar concentration of $MgCl_2$ 69
4.5.3 Analysis of the electrical potential gradient 71
4.5.4 Dilution of the ionic plumes 74
4.5.5 Propagation of pH fronts 77
4.6 Summary and Conclusions 79
References 82
S4. Supporting Information 86

Modeling multicomponent ionic transport in groundwater with IPhreeqc coupling: electrostatic interactions and geochemical reactions in homogeneous and heterogeneous domains 89
5.1 Introduction 90
5.2 Multicomponent Ionic Transport 92
5.3 Modeling Approach 93
5.3.1 Solution of Flow and Transport Equations 94
5.3.2 Reaction Calculations and IPhreeqc Coupling 98
5.4 Benchmark Problems 98
5.4.1 Benchmark of Transient Multicomponent Ionic Transport 98
5.4.2 Benchmark of IPhreeqc Coupling: Ion-Exchange with Multicomponent Ionic Transport and Charge Interactions 102
5.5 Examples of Multicomponent Ionic Transport Simulations 103
5.5.1 Conservative Transport 103
5.5.2 Multicomponent Reactive Transport 111
5.6 Summary and Conclusions 115
References 117
S5. Supplementary Material 123

Experimental investigation of the impact of compound-specific dispersion and electrostatic interactions on transient transport and solute breakthrough 127
6.1 Introduction 128
6.2 Experimental Setup 129
6.3 Modeling Approach and Data Evaluation 132
6.3.1 Analysis of Breakthrough Curves (BTC) 133
6.3.2 Quantification of Transverse Dispersion 137
6.3.3 Evaluation of Plume Dilution 138
6.3.4 Modeling Multicomponent Ionic Dispersion 138
6.4 Results and Discussion 140
6.4.1 Multi-tracer Experiments 140
6.4.2 Multicomponent Ionic Experiments 151
6.5 Summary and Conclusions 155
References 157

Conclusions 163

List of Figures

Figure 2.1. Schematic of the experimental setup. The insert highlights the high-resolution sampling at the outlet of the flow-through chamber.....13
Figure 2.2. Comparison between the 2-D steady-state analytical solution (Eq. 2.14) and the 1-D transient multicomponent numerical model for transport of NaCl (1:1 electrolyte, a and b) and $MgCl_2$ (1:2 electrolyte, c and d) in pure water at v=1.5 m/day (Eq. 2.10). The 1-D PHREEQC multicomponent results obtained for the upper half of the 2-D domain are extended by symmetry in the lower half (gray area). 18
Figure 2.3. Transverse profiles at the end of the flow-through system for NaCl (a) and $MgCl_2$ (b) in Milli-Q water (Experiment 1 and 2): measured cation and anion concentrations (symbols) and multicomponent modeling results (lines).....19
Figure 2.4. Transverse profiles at the end of the flow-through system for transport of mixed electrolytes, KCl and $MgCl_2$ (Experiment 3): measured cation and anion concentrations (symbols) and multicomponent modeling results (lines).....20
Figure 2.5. Observed and simulated profiles for ionic transport in buffer electrolyte solutions under the conditions and initial concentrations of Experiment 4 (a and b) and Experiment 5 (c and d). The concentrations are normalized by the values at the inlet central ports.....21
Figure 2.6. Multicomponent ionic transport at high flow velocity (v=6 m/day): (a) Experiment 1: NaCl injection with water as ambient solution; (b) Experiment 3: KCl and $MgCl_2$ injection with water as ambient solution; (c) and (d) Experiment 4: $MgCl_2$ injection with NaBr as ambient solution. 23
Figure 2.7. Computed (lines) and observed (symbols) flux-related dilution index for the experiments at v=1.5 m/day: (a) Experiment 1: NaCl injection with water as ambient solution; (b) Experiment 3: KCl and $MgCl_2$ injection with water as ambient solution; (c) Experiment 4: $MgCl_2$ injection with NaBr as ambient solution.....25
Figure 3.1. Multicomponent ionic fluxes in the transverse direction at the end of the flow-through domain: Total fluxes (a, b); Dispersive fluxes (c, d); Electrochemical migration fluxes (e, f), for transport of NaCl in pure water (a, c, and e), and transport of $MgCl_2$ in NaBr solution (b, d, and f). The lines represent the values calculated with the 2-D transport code developed in this study and the symbols are the results of 1-D multicomponent simulations using PHREEQC. 38
Figure 3.2. Experimental setups with steady-state color tracer (New Coccine) plumes (a, b); computed streamlines and hydraulic conductivities (c, d); velocity distribution (e, f); and calculated flux-related dilution index of the color tracer (with D_{aq}=3.43×10^{-10} m^2/s estimated after Worch, 1993). The flow direction is from left to right.....40
Figure 3.3. 2-D concentration distributions (a and b), and cross-sectional profiles at 20 cm (c), 50 cm (d), and 80 cm (e) from the inlet of the flow-through domain (*HET A*), computed for the case of NaCl transport in Milli-Q water.....42
Figure 3.4. Transverse concentration profiles at the outlet of the flow-through system (*HET A*) for transport of NaCl in Milli-Q water: measured cation and anion concentrations (symbols) and modeling results (lines).....43
Figure 3.5. Maps of multicomponent ionic transverse fluxes: Total fluxes (a, b); Dispersive fluxes (c, d); Electrochemical migration fluxes (e, f), for transport of NaCl in Milli-Q water (*HET A*). Note that the direction from the core to the fringe of the plume is considered positive for the calculated fluxes. .44
Figure 3.6. 2-D concentration distributions of Mg^{2+} (a), Cl^- (b), Na^+ (c), and Br^- (d); and cross-sectional profiles at 20 cm (e), 50 cm (f), and 80 cm (g) from the inlet of the flow-through domain (*HET A*), computed for the case of $MgCl_2$ transport in NaBr solution.....45
Figure 3.7. Transverse concentration profiles at the end of the flow-through system (*HET A*) for transport of $MgCl_2$ in NaBr solution: measured cation and anion concentrations (symbols) and modeling results (lines).....46
Figure 3.8. Transverse electrochemical migration fluxes of Mg^{2+} (a), Cl^- (b), Na^+ (c), and Br^- (d) during transport of $MgCl_2$ in NaBr solution in *HET A* setup. The direction from the core to the fringe of the plume is considered positive for the calculated fluxes.....46

Figure 3.9. 2-D concentration distributions (a and b), and cross-sectional profiles at 20 cm (c), 50 cm (d), and 80 cm (e) from the inlet of the flow-through domain (*HET B*), computed for the case of NaCl transport in Milli-Q water. 47
Figure 3.10. Transverse concentration profiles at the end of the flow-through system (*HET B*) for transport of NaCl in Milli-Q water: measured cation and anion concentrations (symbols) and modeling results (lines). 48
Figure 3.11. Maps of multicomponent ionic transverse fluxes: Total fluxes (a, b); Dispersive fluxes (c, d); Electrochemical migration fluxes (e, f), for transport of NaCl in Milli-Q water (*HET B*). Note that the direction from the core to the fringe of the plume is considered positive for the calculated fluxes. .49
Figure 3.12. 2-D concentration distributions of Mg^{2+} (a), Cl^- (b), Na^+ (c), and Br^- (d); and cross-sectional profiles at 20 cm (e), 50 cm (f), and 80 cm (g) from the inlet of the flow-through domain (*HET B*), computed for the case of $MgCl_2$ transport in NaBr solution. 50
Figure 3.13. Transverse concentration profiles at the outlet of the flow-through system (*HET B*) for transport of $MgCl_2$ in NaBr solution: measured cation and anion concentrations (symbols) and modeling results (lines). 50
Figure 3.14. Transverse electrochemical migration fluxes of Mg^{2+} (a), Cl^- (b), Na^+ (c), and Br^- (d) in the transverse direction for transport of $MgCl_2$ in NaBr solution in the *HET B* setup. Note that the direction from the core to the fringe of the plume is considered positive for the calculated fluxes. 51
Figure 4.1. Laboratory flow-through setup. The red shaded area represents the steady-state plume of ionic species (H^+, Mg^{2+} and Cl^-) injected from the 8 bottom inlet ports. The inset shows the high-resolution sampling at the outlet of the flow-through chamber. 62
Figure 4.2. Transverse ion concentrations (a) and pH (b) profiles at the outlet of the flow-through system (x = 1 m) for multicomponent transport in Scenario 1 ($C_{H+}/C_{Mg2+}\approx1$): measured ion concentrations and pH (symbols) and modeling results (lines). 66
Figure 4.3. Maps of multicomponent ionic transverse fluxes for Scenario 1: Total fluxes (a, b, c), Dispersive fluxes (d, e, f) and Electrochemical migration fluxes (g, h, i). The lower panels (j, k, l) show the vertical profiles of multicomponent ionic fluxes at the outlet of the flow-through domain. The vertical red line represents the width of the tracer solution at the inlet. The direction from the core to the fringe (upward) of the plume is considered positive for the calculated fluxes. 68
Figure 4.4. Transverse ion concentrations (a) and pH (b) profiles at the outlet of the flow-through system (x = 1 m) for multicomponent transport in Scenario 2 ($C_{H+}/C_{Mg2+} \approx 0.01$): measured ion concentrations and pH (symbols) and modeling results (lines). 69
Figure 4.5. Maps of multicomponent ionic transverse fluxes for Scenario 2: Total fluxes (a, b, c), Dispersive fluxes (d, e, f) and Electrochemical migration fluxes (g, h, i). The lower panels (j, k, l) show the vertical profiles of multicomponent ionic fluxes at the outlet of the flow-through domain. The vertical red line represents the width of the tracer solution at the inlet. The direction from the core to the fringe (upward) of the plume is considered positive for the calculated fluxes. Additionally, notice that the scale used in the H^+ maps and profiles is 100-fold smaller because the absolute concentrations of Mg^{2+} and Cl^- are two orders of magnitude higher compared to the H^+ concentration. 70
Figure 4.6. Maps of the transverse component of the electrostatic potential gradient produced during multicomponent ionic transport: The net electrical gradient (a, f), proton component (b, g), magnesium component (c, h), chloride component (d, i), and the outlet cross-sectional profiles (e, j) for Scenario 1 (a-e) and Scenario 2 (f-j). 73
Figure 4.7. Observed (symbols) and simulated (lines) flux-related dilution index for the two experimental scenarios: (a) Scenario 1: Injection of HCl and $MgCl_2$ with similar concentration (i.e., $C_{H+}/C_{Mg2+} \approx1$) in Milli-Q water; (b) Scenario 2: Injection of HCl and $MgCl_2$ with excess $MgCl_2$ concentration (i.e., $C_{H+}/C_{Mg2+} \approx0.01$) in Milli-Q water. The term liberated refers to the case without electrostatic coupling (i.e., the species are transported as uncharged species with their own diffusive/dispersive properties). 76
Figure 4.8. The symbols represents the observed (blue and pink colors for Scenario 1 and 2, respectively) penetration depths (a) and penetration velocities (b) of pH fronts in the two experimental scenarios. The lines are the simulated values including the case of penetration depth (black dotted line) computed for liberated state (i.e., without electrostatic coupling). Penetration depth refers to the distance of pH front migration. The pH front is tracked considering a difference of 1.5 pH units from the initial solution pH. 78

Figure S4.1. Schematic diagram of 1D setup for the benchmark problem. 86
Figure S4.2. Comparison of the multicomponent transport code used in this study with the geochemical code PHREEQC for a 1D multicomponent diffusion problem. The profiles are taken after 12 hours of simulation: Scenario 1 (a, b, c), Scenario 2 (d, e, f).....87
Figure 5.1. Schematic diagram of the structure of the multicomponent reactive transport model. 94
Figure 5.2. Comparison of the multicomponent ionic transport model and 2-D analytical solution for the transport of NaCl in pure water at v = 1 m/day: 2-D concentration distributions after t = 18 hours (a-c); longitudinal cross sectional profiles at z = 6 cm (d); transverse cross sectional profiles at x = 80 cm (e). 101
Figure 5.3. Benchmark of IPhreeqc coupling with the 2-D transport code for an example of ion-exchange coupled to multicomponent ionic transport with electrochemical migration.....103
Figure 5.4. Breakthrough curves (a-c and g-i) and flux-related dilution indices (d-f and j-l) for simulations at v = 0.1 m/day (a-f) and v = 1 m/day 1 (g-l) in a homogeneous domain. $E_{Q,i}$ values are calculated for a concentration threshold equal to 10^{-6} of the peak concentration for each species.....106
Figure 5.5. Seepage velocity distribution and streamlines (a); 2-D concentration maps (b-d) for mixed electrolyte case at v = 1 m/day after t = 7 days. The red rectangle represents the initial location of the solute slug (b-d). 108
Figure 5.6. Breakthrough curves (a-c and g-i) and flux-related dilution indices (d-f and j-l) for simulations at v = 0.1 m/day (a-f) and 1 m/day (g-l) in a heterogeneous domain. $E_{Q,i}$ values are calculated for a concentration threshold equal to 10^{-6} of the peak concentration for each species.....109
Figure 5.7. Maps of multicomponent ionic transverse fluxes for the transport of mixed electrolytes after 70 days (v = 0.1 m/day): Total fluxes (a, b, c), Dispersive fluxes (d, e, f) and Electrochemical migration fluxes (g, h, i). The direction from the core to the fringe of the plume is considered positive for the calculated fluxes.....111
Figure 5.8. (a) Spatial distribution of hydraulic conductivity K (m/s) used in the simulated reactive transport scenarios A and B. (b) Spatial distribution of cation exchange capacity, CEC (eq/L) used in Scenario B. 112
Figure 5.9. 2-D concentration distribution of cations in Scenario A (a-c) and B (d-f) after 75 days of simulation.....113
Figure 5.10. Depth-integrated breakthrough curves of Ca^{2+} at the end of the heterogeneous domain in Scenario A and B, considering multicomponent ionic transport (solid lines) as well as transport in "liberated" state (dotted lines). (a) Simulations with same average *CEC* between Scenario A and B; (b) Simulations with same total *CEC* between Scenario A and B. 115
Figure S5.1. 2-D steady-state plumes for different ionic species obtained from the simulation of the transport of KCl and $MgCl_2$ in pure water using the proposed 2-D multicomponent ionic transport code. 124
Figure S5.2. Comparison between the experimental data (markers) obtained from the 2-D flow-through system (Rolle et al., 2013) and the simulation outcomes (solid lines) of the proposed multicomponent ionic dispersion model. 125
Figure S5.3. Comparison between the outcomes of the proposed 2-D multicomponent ionic dispersion code (solid lines) and 1-D PHREEQC simulations (dashed lines). 125
Figure S5.4. Schematic diagram of the transport and ion-exchange problem of Example 11 in PHREEQC manual.....126
Figure S5.5: Benchmark of IPhreeqc coupling with the 2-D transport code for a classical transport and ion-exchange problem presented in the PHREEQC manual (Example 11).....126
Figure 6.1. Laboratory flow-through setup. The yellowish-shaded areas represent the schematic illustration of the temporal evolution of the tracer plumes injected from the four central inlet ports. The inset shows a photograph of fluorescein samples collected at different vertical locations at the outlet as a function of time. 130
Figure 6.2. Breakthrough curves of the flux-weighted integrated-concentrations normalized by the flux-weighted inflow boundary conditions (a-c), and flux-related dilution indices (d-f) at the outlet cross-section for the seepage velocity of $v \approx 0.5$ m/day (a,d), 5 m/day (b,e) and 25 m/day (c,f).....141
Figure 6.3. Breakthrough curves of the flux-weighted integrated-concentrations normalized by the flux-weighted inflow boundary conditions in logarithmic scale (a,b), and the model fitted weighted residuals (c,d) at the seepage velocity of $v \approx 25$ m/day.....143

Figure 6.4. 2-D maps of concentration measurements performed at each individual outlet port as a function of time for different flow velocities: measured data points (a-f), and cubic interpolation of the measured values (g-l). The contour lines are shown for normalized concentration values of 0.02 and 0.1 with dots representing the interpolated measured values and the solid lines being the ADE predicted values. 145
Figure 6.5. Breakthrough curves measured at each individual port for the seepage velocity of $v \approx 5$ m/day. 148
Figure 6.6. Time-integrated transverse profiles normalized by the temporal integral of inflow boundary condition for the seepage velocity of 0.5 (a), 5 (b), and 25 (c) m/day. 149
Figure 6.7. Comparison between the D_T values computed from the measurements performed in this study (markers) and the predictions from the non-linear compound-specific parameterization (lines).150
Figure 6.8. Integrated breakthrough curves (a,c) and vertical concentration profiles (b,d) during the transport of $MgCl_2$ in pure water (a-b) and in NaBr background solution (c-d). The markers indicate the measured quantities whereas the lines represent the fitted profiles with 1-D ADE model (solid lines) and the simulated profiles with the 2-D multicomponent ionic transport model (dotted lines).....152
Figure 6.9. Maps of multicomponent ionic flux components in the longitudinal (a-f) and transverse (g-i) direction for the transport of $MgCl_2$ in pure water after $t = 50$, 150, and 250 minutes. The direction from the core to the fringe of the plume is considered positive in the flux calculations. 154

List of Tables

Table 2.1: Geometry and flow and transport parameters of the experimental setup.....14
Table 2.2: Flow-through experiments performed at two different flow velocities: v=1.5 m/day and v=6 m/day. 14
Table 3.1: Algorithm for the solution of the steady-state multicomponent transport problem by Picard iteration. 36
Table 3.2: Summary of flow and transport parameters in the two heterogeneous experimental setups (*HET A* and *HET B*). 41
Table 4.1: Summary of geometry and flow and transport parameters of the laboratory experimental system 63
Table 4.2: Chemical composition of the inlet solutions in the flow-through experiments. 64
Table 4.3: Flux-related dilution index computed from ion concentrations and volumetric discharge measured at the outlet of the flow-through setup. 77
Table S4.1: Experimental measurements performed at the outlet of the flow-through setup for multicomponent transport in Scenario 1. Concentration and pH values used in Figure 4.2. 87
Table S4.2: Experimental measurements performed at the outlet of the flow-through setup for multicomponent transport in Scenario 2. Concentration and pH values used in Figure 4.4. 88
Table 5.1: Algorithm for transient multicomponent ionic transport and reaction computation. 97
Table 5.2: Aqueous diffusion coefficients of different ions.....100
Table 5.3: Summary of geometry, flow and transport parameters of the homogeneous and heterogeneous domains. 108
Table 5.4: Description of the multicomponent reactive transport scenarios. 111
Table 6.1: Summary of geometry and transport parameters of the experimental system. 131
Table 6.2: Tracers' inlet concentrations, pulse duration, sampling intervals and number of samples..132
Table 6.3: Summary of the fitted parameters for the breakthrough curves integrated over the outlet cross-section. 147
Table 6.4: Summary of local breakthrough curves fitting at $v \approx 5$ m/day.....147

Chapter 1

Introduction

The transport of dissolved solutes in porous media is collectively affected by different physical (e.g., advection, diffusion, dispersion), electrochemical (e.g., Coulombic interactions, ion-pairing), and/or reactive (e.g., equilibrium/kinetic chemical reactions) processes. In groundwater systems, these mechanisms occur at different scales. For instance, aqueous diffusion, electrostatic effects, and most of the chemical transformations are mainly related to the fundamental property of solute species and usually occur at small microscopic or even at molecular scales. On the other hand, processes like hydrodynamic dispersion, caused by diffusive properties coupled with the variation of fluid velocity in the complex geometry of porous networks, need to be described at the so called Darcy scale (also known as local scale) (e.g., Bear and Bachmat, 1967). In addition, heterogeneity and anisotropy in natural sediment formations or in geochemical properties occur at larger field scales. In natural aquifer systems, mixing, spreading or dilution behaviors of conservative and reactive plumes are ultimately determined by the complex interplay between these mechanisms in act (e.g., Kitanidis, 1994). Therefore, fundamental understanding of different processes is extremely important for characterizing fate and transport in natural subsurface environments or in designing engineered remediation schemes (e.g., Bear, 1972; Dentz et al., 2011).

In subsurface solute transport, the key role of small-scale processes has been found to be critical in determining the ultimate fate of contaminants plumes. In fact, considerable research effort has been devoted to identify the impact of microscopic processes during large scale solute transport (e.g., Kitanidis, 1994; Thullner et al., 2005; Steefel and Maher, 2009; Zhang et al., 2010; Molins et al., 2012). Furthermore, small-scale mixing processes occurring at thin fringes of contaminant plumes have been recognized to control the fate of continuously released contaminants in aquifer systems (e.g., Cirpka et al., 1999; Liedl et al., 2005; Maier and Grathwohl, 2006). Providing the accurate description of these microscopic processes during the large-scale solute transport is a very challenging task. Models with pore-scale resolution open great possibilities in allowing the description of real physical, electrochemical or reactive processes. However, for most applications such description is too detailed and in fact impractical. A common alternative is using an up-scaled description of the relevant processes by conserving the main features of the microscopic processes (e.g., Bear, 1972).

Such approach, also known as continuum description, portrays macro-scale transport having constant local properties (i.e., averaged pore-scale properties) in a particular grid block.

In the range of typical groundwater flow conditions, diffusion is the only physical processes responsible for the mass-exchange between neighboring streamlines and it brings initially segregated reactants into physical contact by mixing (e.g., Kitanidis, 1994; Cao and Kitanidis, 1998). The crucial role of aqueous diffusion as a controlling mass-transfer process is increasingly recognized in subsurface solute transport and considerable advances has been made by means of experimental studies as well as theoretical concepts (e.g., Kitanidis, 1994; Haggerty and Gorelick, 1995; Rolle et al., 2008; Bauer et al., 2009). Numerous studies focusing on controlled laboratory and field-scale experiments and/or numerical modeling established that diffusion is also important in large-scale solute transport in porous media and it can significantly affect the mixing, spreading or dilution of a particular transported solute species (e.g., Carrera et al., 1998; LaBolle and Fogg, 2001; Chiogna et al., 2011; Hadley and Newell, 2014; Rolle et al., 2013a). The impact of this physical process is found to be relevant not only at low velocities (i.e., diffusion-dominated) but also at high flow velocities (i.e., advection-dominated), where steep concentration gradients exist leading to incomplete mixing in pore-channels (e.g., Rolle et al., 2012; Hochstelter et al., 2013). These outcomes have led to the improved description of Darcy-scale local dispersion coefficients, which are essential prerequisites for correctly capturing diffusive/dispersive fluxes, involving a direct dependence of the mechanical dispersion term on both compound-specific diffusion as well as fluid velocity (e.g., Delgado, 2006; Chiogna et al., 2010; Scheven et al., 2014).

The transport of charged species in a multicomponent environment is conceptually different compared to transport of uncharged solutes because of the electrochemical migration term. This additional contribution, induced from the charge of dissolved species and/or solid surfaces, electrostatically affects the diffusive movement of a particular ionic species due to the interactions between different diffusing molecules. Therefore, diffusion of such solutes is not independent, but rather connected to the presence and concentration gradients of other charged solutes in the system (e.g., Lasaga, 1979). Multicomponent diffusion models, based on Nernst-Planck formulation, are usually used to describe diffusion of such multi-ionic species by accounting for electrochemical potential gradients (e.g., Cussler, 2009). These electrostatic effects during the multicomponent ionic transport have been found to significantly affect the movement of charged species by modifying their diffusive fluxes both in laboratory (e.g., Vinograd and McBain, 1941; Ben-Yaakov, 1972; Felmy and Weare, 1991; Liu et al., 2011) and field (e.g., Giambalvo et al., 2002; Appelo and Wersin, 2007; Appelo et al., 2008) scale investigations.

The characterization of the electrochemical effects is of utmost importance because the dissolved species of interest are often charged in natural and/or engineered systems including subsurface conservative/reactive solute transport, natural attenuation of contaminants, electrokinetic remediation, minerals dissolution and precipitation, nuclear waste repositories, or geologic carbon sequestration. Therefore, the quality of the prediction of multicomponent ionic transport in such systems is highly dependent on the detailed knowledge of Coulombic interactions between transported species. Besides subsurface hydrogeochemistry, the understandings of electrostatic interactions are also highly relevant in other scientific and engineering disciplines where the mass-transfer of ionic species is involved. For instance, fields like chemical engineering (e.g., fluidized bed reactors), physiology (e.g., transport of ions between extra-and-intra cellular fluids), or marine hydrology (e.g., mixing between fresh and seawater) are examples of areas in which electrostatic interactions are relevant.

Although considerable efforts have been undertaken to identify the relevance of electrostatic effects during multicomponent ionic transport in porous media, most of the study in the literature focuses mainly on diffusion-dominated conservative transport (e.g., Vinograd and McBain, 1941; Felmy and Weare, 1991; Liu, 2007). Only a few contributions addressed multicomponent diffusion coupled with other physical or chemical processes (e.g., Giambalvo et al., 2002; Maher et al., 2006; Appelo and Wersin, 2007; Li et al., 2008; Liu et al., 2011). However, no data are available for transport in flow-through systems and/or under advection-dominated flow regimes. In such flow conditions, besides aqueous diffusion, fluid flow and local hydrodynamic dispersion will also affect mass-exchange between the plume ions and ambient groundwater species. In addition, studies involving multidimensional ionic transport explicitly considering electrostatic effects are also not common (Rasouli et al., 2015). There is also a lack of attention towards including these charge interactions into large scale multicomponent reactive transport codes. Among the available models that accounts for Coulombic interactions coupled with other geochemical reactions, applicability is often limited to one-dimensional transport or domains with spatially uniform properties. Therefore, the development of modeling tool capable of rigorously accounting for different physical, geochemical, and electrostatic effects during the multicomponent ionic transport is essential. Furthermore, knowledge gaps also exist, especially in identifying the relevance of these fundamental electrochemical mechanisms in the field-scale multi-ionic transport scenarios where heterogeneity of hydraulic conductivities and geochemical properties can lead to significant levels of complexity.

The aim of the current work is to initiate the investigation of the role of electrostatic effects during multicomponent ionic transport in flow-through systems, especially when advection is

the dominant mass-transfer process. The motivation has been provided by the increased recognition of the significant role of aqueous diffusion for solute transport across a range of different scales (e.g., Carrera et al., 1998; LaBolle and Fogg, 2001; Hadley and Newell, 2014). Recent multitracer laboratory experiments (e.g., Chiogna et al., 2010; Rolle et al., 2010) and pore-scale simulations (e.g., Rolle et al., 2012; Hochstelter et al., 2013; Rolle and Kitanidis, 2014) demonstrated that macro-scale local dispersion is compound specific even at high groundwater flow velocities due to pore-scale mass-transfer limitations. Furthermore, for charged species, the charge induced electrostatic potential is ultimately related to the diffusion term (e.g., Lasaga, 1979). Therefore, the influence of this charge effect is also finally reflected in the diffusive/dispersive movements of the ionic species involved. In particular, the main objectives of the present work address these specific research points: (i) relevance of Coulombic effects in flow-through systems; (ii) influence of such effects in advection-dominated transport and in spatially variable flow-regimes; (iii) development of multicomponent reactive transport models including electrochemical migration; (iv) impact of charge effects on field-scale scenarios including physical and geochemical heterogeneity. This dissertation is structured into five main chapters, which are concisely described below.

In Chapter 2, a detailed investigation of multicomponent ionic transport under advection-dominated flow-through conditions is presented. Laboratory bench-scale experiments were performed in quasi two-dimensional porous media using dilute electrolyte solutions to study the relevance of charge interactions on transverse displacement of different ionic species (Rolle et al., 2013b). The experiments were conducted, under steady-state transport conditions, with different combinations of ionic species as well as at different flow velocities. Chapter 3 further extends the investigation by considering heterogeneous flow-fields including flow-focusing in high-permeability inclusions and flow-diverging in low-permeability inclusions (Muniruzzaman et al., 2014). Experiments were conducted with different grain-sized material inclusions in the porous matrix to identify the key role of electrochemical migration during transport in spatially variable domains. A two-dimensional multicomponent ionic dispersion model was proposed to rigorously account for the charge interactions during steady-state transport of ionic admixtures. The modeling approach is based on the multicomponent formulation of diffusive/dispersive fluxes and the proper recognition of aqueous diffusion in the dispersion terms. The experimental results were successfully reproduced with the proposed numerical model and thus verify the validity of the proposed approach.

Chapter 4 presents the impact of electrostatic effects on pH fronts propagation during multicomponent ionic transport in saturated porous media. Laboratory experiments were performed in quasi two-dimensional flow-through setup under steady-state flow and transport

conditions (Muniruzzaman and Rolle, 2015). This study also specifically focused on the influence of solution composition on multicomponent ionic transport. Different compositions of acidic solutions were injected into the saturated porous media applying identical flow and transport conditions. The experimental outcomes were matched with the multicomponent ionic dispersion model, which was also used to explain ion-specific interactions.

Chapter 5 demonstrates the extension of the proposed multicomponent ionic dispersion modeling framework to transient transport conditions as well as to the coupling of physical and reactive transport processes (Muniruzzaman and Rolle, under review). The modeling approach is based on an improved description of cross-coupled longitudinal and transverse diffusive/dispersive fluxes. The latter relies on the accurate description of hydrodynamic dispersion coefficients with the direct dependence on species diffusivity and advective velocity. In heterogeneous domains, these local dispersion coefficients as well as diffusive/dispersive fluxes should also be spatially variable and connected to the local velocities. The multicomponent ionic transport code was coupled with the widely used geochemical code PHREEQC-3 (Parkhurst and Appelo, 2013) using the recently released IPhreeqc module (Charlton and Parkhurst, 2011). This provides a generalized platform to perform reactive transport simulations explicitly considering electrochemical migration as well as a wide range of geochemical reactions available in PHREEQC's reaction package. In addition, numerical simulations of different scenarios explore the relevance of charge interactions during the large-scale reactive transport involving physical and geochemical heterogeneity.

In the sixth and final chapter of this thesis, first experimental evidence showing the importance of compound-specific and electrostatic effects on transient multicomponent ionic transport has been provided (Muniruzzaman and Rolle, in preparation). By performing laboratory experiments, the influence of charge effects as well as compound-specific dispersion on solute breakthrough curves was shown. In addition to the charged solutes, uncharged tracers were also used in this study to identify the compound-specific effects on solute breakthroughs and plume dilution. The concept of flux-related dilution index (Rolle et al., 2009; Rolle and Kitanidis, 2014) was applied to characterize the dilution of different solute plumes. Dilution breakthrough curves were used in combination with traditional concentration breakthrough curves to distinguish between mixing and longitudinal spreading of different tracer plumes and to quantify the impact of electrostatic interactions on solutes' breakthrough.

References

Appelo, C. A. J., Vinsot, A., Mettler, S., and Wechner, S. (2008). Obtaining the porewater composition of a clay rock by modeling the in- and out-diffusion of anions and cations from an in-situ experiment. *Journal of Contaminant Hydrology, 101*(1-4), 67-76. doi:DOI 10.1016/j.jconhyd.2008.07.009

Appelo, C. A. J., and Wersin, P. (2007). Multicomponent diffusion modeling in clay systems with application to the diffusion of tritium, iodide, and sodium in opalinus clay. *Environmental Science & Technology, 41*(14), 5002-5007. doi:Doi 10.1021/Es0629256

Bauer, R. D., Rolle, M., Bauer, S., Eberhardt, C., Grathwohl, P., Kolditz, O., and Griebler, C. (2009). Enhanced biodegradation by hydraulic heterogeneities in petroleum hydrocarbon plumes. *Journal of Contaminant Hydrology, 105*(1–2), 56-68. doi:10.1016/j.jconhyd.2008.11.004

Bear, J. (1972). *Dynamics of fluids in porous media*. New York, American Elsevier Pub. Co.

Bear J., and Bachmat Y. (1967) A generalized theory on hydrodynamic dispersion in porous media. In *IASH Symposium on Artificial Recharge and Management of Aquifers*, Haifa, Israel,vol. 72, pp. 7–16.

Ben-Yaakov, S. (1972). Diffusion of sea water ions—I. Diffusion of sea water into a dilute solution. *Geochimica et Cosmochimica Acta, 36*(12), 1395-1406. doi:10.1016/0016-7037(72)90069-5

Cao, J., and Kitanidis, P. K. (1998). Pore-scale dilution of conservative solutes: An example. *Water Resources Research, 34*(8), 1941-1949. doi:10.1029/98WR01468

Carrera, J., Sanchez-Vila, X., Benet, I., Medina, A., Galarza, G., and Guimera, J. (1998). On matrix diffusion: formulations, solution methods and qualitative effects. *Hydrogeology Journal, 6*(1), 178-190. doi:DOI 10.1007/s100400050143

Charlton, S. R., and Parkhurst, D. L. (2011). Modules based on the geochemical model PHREEQC for use in scripting and programming languages. *Computers & Geosciences, 37*(10), 1653-1663. doi:http://dx.doi.org/10.1016/j.cageo.2011.02.005

Chiogna, G., Cirpka, O. A., Grathwohl, P., and Rolle, M. (2011). Relevance of local compound-specific transverse dispersion for conservative and reactive mixing in heterogeneous porous media. *Water Resour. Res., 47*(7), W07540. doi:10.1029/2010wr010270

Chiogna, G., Eberhardt, C., Grathwohl, P., Cirpka, O. A., and Rolle, M. (2010). Evidence of Compound-Dependent Hydrodynamic and Mechanical Transverse Dispersion by Multitracer Laboratory Experiments. *Environmental Science & Technology, 44*(2), 688-693. doi:10.1021/es9023964

Cirpka, O. A., Frind, E. O., and Helmig, R. (1999). Numerical simulation of biodegradation controlled by transverse mixing. *Journal of Contaminant Hydrology, 40*(2), 159-182. doi:http://dx.doi.org/10.1016/S0169-7722(99)00044-3

Cussler, E. L. (2009). *Diffusion : Mass transfer in fluid systems* (3rd ed.). Cambridge ; New York: Cambridge University Press.

Delgado, J. M. P. Q. (2006). A critical review of dispersion in packed beds. *Heat and Mass Transfer, 42*(4), 279-310. doi:10.1007/s00231-005-0019-0

Dentz, M., Le Borgne, T., Englert, A., and Bijeljic, B. (2011). Mixing, spreading and reaction in heterogeneous media: A brief review. *Journal of Contaminant Hydrology, 120–121*(0), 1-17. doi:10.1016/j.jconhyd.2010.05.002

Felmy, A. R., and Weare, J. H. (1991). Calculation of Multicomponent Ionic-Diffusion from Zero to High-Concentration .1. The System Na-K-Ca-Mg-Cl-So4-H2o at 25-Degrees-C. *Geochimica et Cosmochimica Acta, 55*(1), 113-131. doi:Doi 10.1016/0016-7037(91)90405-T

Giambalvo, E. R., Steefel, C. I., Fisher, A. T., Rosenberg, N. D., and Wheat, C. G. (2002). Effect of fluid-sediment reaction on hydrothermal fluxes of major elements, eastern flank of the Juan de Fuca Ridge. *Geochimica et Cosmochimica Acta, 66*(10), 1739-1757. doi:10.1016/S0016-7037(01)00878-X

Hadley, P. W., and Newell, C. (2014). The New Potential for Understanding Groundwater Contaminant Transport. *Groundwater, 52*(2), 174-186. doi:10.1111/gwat.12135

Haggerty, R., and Gorelick, S. M. (1995). Multiple-Rate Mass-Transfer for Modeling Diffusion and Surface-Reactions in Media with Pore-Scale Heterogeneity. *Water Resources Research, 31*(10), 2383-2400. doi:Doi 10.1029/95wr10583

Hochstetler, D. L., Rolle, M., Chiogna, G., Haberer, C. M., Grathwohl, P., and Kitanidis, P. K. (2013). Effects of compound-specific transverse mixing on steady-state reactive plumes: Insights from pore-scale simulations and Darcy-scale experiments. *Advances in Water Resources, 54*, 1-10. doi:DOI 10.1016/j.advwatres.2012.12.007

Kitanidis, P. K. (1994). The concept of the Dilution Index. *Water Resources Research, 30*(7), 2011-2026. doi:10.1029/94WR00762

LaBolle, E. M., and Fogg, G. E. (2001). Role of molecular diffusion in contaminant migration and recovery in an alluvial aquifer system. *Transport in Porous Media, 42*(1-2), 155-179. doi:Doi 10.1023/A:1006772716244

Lasaga, A. C. (1979). The treatment of multi-component diffusion and ion pairs in diagenetic fluxes. *American Journal of Science, 279*(3), 324-346. doi:10.2475/ajs.279.3.324

Li, L., Steefel, C. I., and Yang, L. (2008). Scale dependence of mineral dissolution rates within single pores and fractures. *Geochimica et Cosmochimica Acta, 72*(2), 360-377. doi:DOI 10.1016/j.gca.2007.10.027

Liedl, R., Valocchi, A. J., Dietrich, P., and Grathwohl, P. (2005). Finiteness of steady state plumes. *Water Resour. Res., 41*(12), W12501. doi:10.1029/2005wr004000

Liu, C. X. (2007). An ion diffusion model in semi-permeable clay materials. *Environmental Science & Technology, 41*(15), 5403-5409. doi:Doi 10.1021/Es0624117

Liu, C. X., Shang, J. Y., and Zachara, J. M. (2011). Multispecies diffusion models: A study of uranyl species diffusion. *Water Resources Research, 47*. doi 10.1029/2011wr010575

Maher, K., Steefel, C. I., DePaolo, D. J., and Viani, B. E. (2006). The mineral dissolution rate conundrum: Insights from reactive transport modeling of U isotopes and pore fluid chemistry in marine sediments. *Geochimica et Cosmochimica Acta, 70*(2), 337-363. doi:http://dx.doi.org/10.1016/j.gca.2005.09.001

Maier, U., and Grathwohl, P. (2006). Numerical experiments and field results on the size of steady state plumes. *Journal of Contaminant Hydrology, 85*(1–2), 33-52. doi:http://dx.doi.org/10.1016/j.jconhyd.2005.12.012

Molins, S., Trebotich, D., Steefel, C. I., and Shen, C. P. (2012). An investigation of the effect of pore scale flow on average geochemical reaction rates using direct numerical simulation. *Water Resources Research, 48*. doi: 10.1029/2011wr011404

Muniruzzaman, M., Haberer, C. M., Grathwohl, P., and Rolle, M. (2014). Multicomponent ionic dispersion during transport of electrolytes in heterogeneous porous media: Experiments and model-based interpretation. *Geochimica et Cosmochimica Acta, 141*(0), 656-669. doi:http://dx.doi.org/10.1016/j.gca.2014.06.020

Muniruzzaman, M., and Rolle, M. (2015). Impact of multicomponent ionic transport on pH fronts propagation in saturated porous media. *Water Resources Research, 51*(8), 6739-6755. doi:10.1002/2015WR017134

Muniruzzaman, M., and Rolle, M., (2016). Modeling multicomponent ionic transport in groundwater with IPhreeqc coupling: electrostatic interactions and geochemical reactions in homogeneous and heterogeneous domains. *Advances in Water Resources,* (under review).

Muniruzzaman, M., and Rolle, M., (2016). Experimental investigation of the impact of compound-specific dispersion and electrostatic interactions on transient transport and solute breakthrough. (in preparation).

Parkhurst, D. L., and Appelo, C. A. J. (2013). *Description of input and examples for PHREEQC version 3- A computer program for speciation, batch-reaction, one dimensional transport, and inverse geochemical calculations* Vol. book 6, chapter. A43. (pp. 497 p.). doi:http://pubs.usgs.gov/tm/06/a43

Rasouli, P., Steefel, C. I., Mayer, K. U., and Rolle, M. (2015) Benchmarks for multicomponent diffusion and electrochemical migration. *Computatutational Geosciences*, *19*, 523-33. doi: 10.1007/s10596-015-9481-z.

Rolle, M., Bauer, R. D., Griebler, C., Meckenstock, R. U., Bauer, S., Kolditz, O., and Grathwohl, P. (2008). Aerobic degradation of a toluene plume in homogeneous and heterogeneous porous media. IAHS, from AHS-AISH Publication http://iahs.info/redbooks/a324/iahs_324_0356.pdf

Rolle, M., Chiogna, G., Bauer, R., Griebler, C., and Grathwohl, P. (2010). Isotopic fractionation by transverse dispersion: flow-through microcosms and reactive transport modeling study. *Environmental Science & Technology, 44*(16), 6167-6173. doi:10.1021/es101179f

Rolle, M., Chiogna, G., Hochstetler, D. L., and Kitanidis, P. K. (2013a). On the importance of diffusion and compound-specific mixing for groundwater transport: An investigation from pore to field scale. *Journal of Contaminant Hydrology, 153*(0), 51-68. doi:http://dx.doi.org/10.1016/j.jconhyd.2013.07.006

Rolle, M., Eberhardt, C., Chiogna, G., Cirpka, O. A., and Grathwohl, P. (2009). Enhancement of dilution and transverse reactive mixing in porous media: Experiments and model-based interpretation. *Journal of Contaminant Hydrology, 110*(3–4), 130-142. doi:10.1016/j.jconhyd.2009.10.003

Rolle, M., Hochstetler, D. L., Chiogna, G., Kitanidis, P. K., and Grathwohl, P. (2012). Experimental Investigation and Pore-Scale Modeling Interpretation of Compound-Specific Transverse Dispersion in Porous Media. *Transport in Porous Media, 93*(3), 347-362. doi:10.1007/s11242-012-9953-8

Rolle, M., and Kitanidis, P. K. (2014). Effects of compound-specific dilution on transient transport and solute breakthrough: A pore-scale analysis. *Advances in Water Resources, 71*, 186-199. doi:http://dx.doi.org/10.1016/j.advwatres.2014.06.012

Rolle, M., Muniruzzaman, M., Haberer, C. M., and Grathwohl, P. (2013b). Coulombic effects in advection-dominated transport of electrolytes in porous media: Multicomponent ionic dispersion. *Geochimica et Cosmochimica Acta, 120*(0), 195-205. doi:http://dx.doi.org/10.1016/j.gca.2013.06.031

Scheven, U. M., Khirevich, S., Daneyko, A., and Tallarek, U. (2014). Longitudinal and transverse dispersion in flow through random packings of spheres: A quantitative comparison of experiments, simulations, and models. *Physical Review E, 89*(5), 053023.

Steefel, C. I., and Maher, K. (2009). Fluid-Rock Interaction: A Reactive Transport Approach. *Thermodynamics and Kinetics of Water-Rock Interaction, 70*, 485-532. doi:DOI 10.2138/rmg.2009.70.11

Thullner, M., Van Cappellen, P., and Regnier, P. (2005). Modeling the impact of microbial activity on redox dynamics in porous media. *Geochimica et Cosmochimica Acta, 69*(21), 5005-5019. doi:DOI 10.1016/j.gca.2005.04.026

Vinograd, J. R., and McBain, J. W. (1941). Diffusion of Electrolytes and of the Ions in their Mixtures. *Journal of the American Chemical Society, 63*(7), 2008-2015. doi:10.1021/ja01852a063

Zhang, C. Y., Dehoff, K., Hess, N., Oostrom, M., Wietsma, T. W., Valocchi, A. J., and Werth, C. J. (2010). Pore-Scale Study of Transverse Mixing Induced CaCO3 Precipitation and Permeability Reduction in a Model Subsurface Sedimentary System. *Environmental Science & Technology, 44*(20), 7833-7838. doi:Doi 10.1021/Es1019788

Chapter 2

Coulombic effects in advection-dominated transport of electrolytes in porous media: Multicomponent ionic dispersion*

Abstract

We study the influence of Coulombic effects on transport of charged species in saturated porous media in advection-dominated flow regimes. We focus on transverse hydrodynamic dispersion and we performed quasi two-dimensional flow-through experiments to investigate transport of dilute electrolyte solutions. The experiments were repeated for two average flow velocities (1.5 and 6 m/day) representing advection-dominated and strongly advection-dominated flow conditions, respectively. Numerical transport simulations have been conducted to quantitatively interpret the experimental results. The adopted modeling approach is based on a multicomponent formulation and on the accurate description of transverse dispersion. The latter entails a non-linear dependence of the transverse dispersion coefficient on the flow velocity as well as a compound-specific dependence on the molecular diffusion of the transported solute. These dependencies hold true at low and also at high flow velocities. Our experimental and modeling results show that Coulombic cross-coupling of dispersive fluxes of charged species in porous media significantly affects the lateral displacement of charged species in flow-through systems. Such effects are remarkable not only in diffusion-dominated but also in advection-dominated flow regimes. Their accurate description requires a multicomponent modeling approach and the recognition of the key role of molecular diffusion for both the pore diffusion and the mechanical dispersion terms of hydrodynamic dispersion.

* Reproduced from: Rolle, M., Muniruzzaman, M., Haberer, C. M., and Grathwohl, P. (2013). Coulombic effects in advection-dominated transport of electrolytes in porous media: Multicomponent ionic dispersion. *Geochimica et Cosmochimica Acta, 120*(0), 195-205. doi:http://dx.doi.org/10.1016/j.gca.2013.06.031

2.1 Introduction

Diffusive and dispersive mass transfer in natural porous media are important for many processes including diagenesis (Boudreau, 1997; Wang and Van Cappellen, 1996), exchange of gases and volatile compounds between the atmosphere and the subsurface (e.g., McCarthy and Johnson, 1993; Holocher et al., 2002; Haberer et al., 2011 and 2012), geological carbon sequestration (e.g., Zhang et al., 2010; Molins et al., 2012), solute transport in sediments and groundwater (e.g., Kitanidis, 1994; Haggerty and Gorelick, 1995), and subsurface biogeochemical transformations (e.g., Thullner et al., 2005; Rolle et al., 2008; Bauer et al., 2009; Steefel and Maher, 2009). In particular, molecular diffusion controls transport in aquatic sediments, in low permeability materials such as silt and clay, and determines the sorption/desorption kinetics and the overall rate of many geochemical and biological reactions (e.g., Grathwohl, 1998). The diffusive fluxes of neutral species in dilute solutions can be described by Fick's law in which the flux is proportional to the concentration gradient, and the molecular diffusion coefficient (corrected by the tortuosity in porous media) is the constant of proportionality. When dissolved species are charged, the interactions between diffusing molecules and electrochemical migration terms need to be considered. This has led to the formulation of multicomponent diffusion models (e.g., Ben Yaakov, 1972; Lasaga, 1979; Felmy and Weare, 1991; Van Cappellen and Gaillard, 1996; Boudreau, 2004; Liu, 2007; Appelo and Wersin, 2007; Steefel and Maher, 2009). These models have been used to describe the multicomponent diffusion effects in laboratory (e.g., Vinograd and McBain, 1941; Ben Yaakov, 1972; Felmy and Weare, 1991) and field observations (e.g., Giambalvo et al., 2002; Appelo and Wersin, 2007; Appelo et al., 2008). Only a few contributions have addressed the coupling between multicomponent ionic diffusion and other physical and chemical processes in porous media. Notable examples include the works of Giambalvo et al. (2002), Maher et al. (2006), Li et al. (2008), Appelo et al. (2010) and Liu et al. (2011).

The goal of the present study is to investigate the role of multicomponent ionic interactions during transport in saturated porous media at different flow velocities. In particular, we consider flow regimes where advection is the dominant mass-transfer process. The motivation has been provided by recent multitracer laboratory experiments and pore-scale simulations (e.g., Chiogna et al., 2010; Rolle et al., 2010 and 2012; Hochstetler et al., 2013) which have shown that transverse dispersion is compound-specific even at high groundwater flow velocities because of pore-scale diffusion limitations. Furthermore, high-resolution field observations and numerical simulations also indicated that the effects of diffusion in groundwater systems are still important at the larger field scale (e.g., LaBolle and Fogg, 2001; Liu and Ball, 2002; Chiogna et al., 2011; Rasa et al., 2011; Van Breukelen and Rolle, 2012).

We performed flow-through laboratory experiments in saturated porous media to investigate transport of different electrolytes and to identify and quantify the effects of charge interactions on transverse dispersion. We show that Coulombic cross-coupling of dispersive fluxes is significant not only at low but also at high groundwater flow velocities. The experimental results are quantitatively interpreted with a model based on a multicomponent ionic formulation of diffusive/dispersive fluxes.

2.2 Theoretical Background

The theory of multicomponent diffusion has been derived following two different approaches based on the pragmatic extension of Fick's law and on first principles from the theory of non-equilibrium thermodynamics (Boudreau, 2004). In this study we follow the first approach which has been adopted by a number of authors in the geochemical and water research literature (e.g., Ben Yakov, 1972; Lasaga, 1979; Van Cappellen and Gaillard, 1996; Giambalvo et al., 2002; Boudreau, 2004; Liu et al., 2004; Appelo, 2007; Liu et al., 2011). Detailed derivations can be found in the above-mentioned studies; in the present section we only summarize the fundamental steps leading to the governing equations of multicomponent diffusion. The starting point is the recognition that interactions among charged species can be captured by including an electrochemical migration term to the description of diffusive fluxes. Therefore, the diffusive flux of an ionic species i in solution depends on a chemical and an electrical potential gradient. In dilute solutions, the chemical potential gradient can be approximated by the concentration gradient and the diffusive flux can be written as (Cussler, 2009):

$$J_i = -D_i \nabla C_i - D_i \frac{z_i F}{RT} C_i \nabla \psi \qquad i = 1, 2, ..., n \tag{2.1}$$

where D_i is the self-diffusion coefficient, z_i is the charge and C_i is the concentration of the ionic species i, F is the Faraday constant, R is the gas constant, T is the temperature, ψ is the electrical potential and n the number of species. In the absence of electrical current (i.e., zero net flow of electrical charge: $\sum_{i=1}^{N} z_i J_i = 0$), the electrical potential gradient can be written as (e.g., Lasaga, 1979):

$$\nabla \psi = \frac{-\sum_{i=1}^{n} \left(z_i D_i \nabla C_i \right)}{\sum_{i=1}^{n} \left(z_i^2 F D_i C_i \right) / RT} \tag{2.2}$$

Substituting Eq. 2.2 into the expression of the diffusive flux (Eq. 2.1) yields:

$$J_i = -D_i \nabla C_i + \frac{z_i D_i C_i}{\sum_{j=1}^{n} (z_j^2 D_j C_j)} \sum_{k=1}^{n} z_k D_k \nabla C_k \tag{2.3}$$

which explicitly represents the dependence of the diffusive flux of the charged species *i* not only on its concentration gradient but also on the concentration gradients of the other species in solution. Eq. 2.3 can be further rearranged to:

$$J_i = -\sum_{j=1}^{n} D_{ij} \nabla C_j \tag{2.4}$$

where D_{ij} is the matrix of inter-diffusion coefficients coupling the flux of ion *i* and the gradient of ion *j*:

$$D_{ij} = \delta_{ij} D_i - \frac{z_i z_j D_i D_j C_i}{\sum_{k=1}^{n} (z_k^2 D_k C_k)} \tag{2.5}$$

in which δ_{ij} is the Kronecker delta that is equal to 1 if $i=j$ and equal to 0 if $i \neq j$. Replacing the diffusive flux (Eq. 2.3) in the mass balance equation yields the governing equation of multicomponent diffusion, which for non-reactive species reads as:

$$\frac{\partial C_i}{\partial t} = \nabla \cdot \left(\sum_{j=1}^{n} D_{ij} \nabla C_j \right) \tag{2.6}$$

2.3 Experimental Setup

Laboratory bench-scale experiments were performed to investigate ionic interactions under flow-through conditions. The experiments were carried out in a quasi two-dimensional setup (Fig. 2.1) with inner dimensions 100 cm × 19 cm × 1 cm (L × H × W). We established a uniform horizontal flow field by connecting two high-precision peristaltic pumps (IPC-N24 Ismatec, Glattbrugg, Switzerland) at the inlet and outlet of the flow-through chamber. Twenty-three and 24 ports, spaced 5 mm apart, were used at the inlet and outlet of the system, respectively. The small spacing between the ports allowed us sampling the tracers and the ambient solutions at high spatial resolution. All injection and extraction ports were made of Alltech rubber septa pierced by hollow needles. The needles were directly connected to Fluran HCA pump tubing (Ismatec, Glattbrugg, Switzerland) with inner diameter of 0.64 mm. The flow-through chamber was homogeneously filled with glass beads, with grain diameters ranging between 1.00 mm and 1.50 mm (Sartorius, Göttingen, Germany). We applied a wet-

packing procedure in which the water level was always maintained above the upper limit of the porous medium to avoid entrapment of air within the glass beads. The experiments were performed in a temperature-controlled room at a temperature of 20 °C.

The 24-channel pumps at the inlet and at the outlet of the flow-through system were calibrated before each experimental run and a steady-state flow field was established in the homogeneous porous medium.

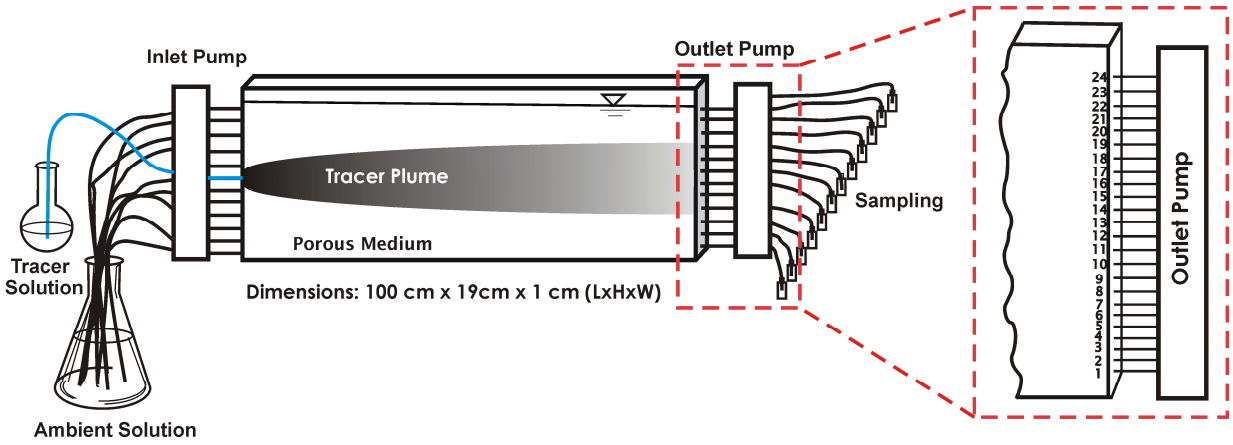

Figure 2.1. Schematic of the experimental setup. The insert highlights the high-resolution sampling at the outlet of the flow-through chamber.

Transport experiments were carried out by injecting a tracer solution through the central inlet ports (port 11 and 12, at 5.5 cm and 6 cm from the bottom of the tank, respectively). An ambient solution was injected through the remaining ports. The experiments were performed using strong 1:1 and 1:2 electrolytes (KCl, NaCl and $MgCl_2$) as tracer solutions and ultra-pure Milli-Q water (Millipore, MA, USA) or a 1:1 electrolyte (NaBr) as ambient solutions. Low electrolyte concentrations (0.29-1.6 mM) were used in the different experiments to avoid density effects. The tracer and the ambient solutions were continuously injected for at least two pore volumes to obtain steady-state plumes. For each experimental run, duplicate samples were taken at the 24 outlet ports and analyzed by ion-chromatography (Dionex Dx-120, Fisher Scientific, Schwerte, Germany). The solution sampled at the outlet ports consisted of a mixture of cations and anions which underwent conservative multispecies transport under identical hydraulic conditions. To prevent cross-contamination the 7 mL sampling vials and the glass beads were washed with hydrochloric acid (pH ≈ 4) and with Milli-Q water before each experiment. After sampling, we additionally determined the flow rate of each outlet port by collecting the effluent for a given period of time and weighing the collected volume. The

parameters summarizing the characteristics of the experimental setup and the self-diffusion coefficients of the considered ionic species are reported in Table 2.1.

Table 2.1: Geometry and flow and transport parameters of the experimental setup.

Experimental Settings		
Tank dimensions ($L \times H \times W$) [cm]		100 × 19 × 1
Number of inlet/outlet ports used [-]		23/24
Ports spacing [mm]		5
Grain size [mm]		1.00 – 1.50
Porosity [-]		0.41
Diffusion Coefficients		
Ion	D_{aq} [m^2/s] at 18° C[a]	D_{aq} [m^2/s] at 20° C[b]
K^+	1.67×10^{-9}	1.77×10^{-9}
Na^+	1.13×10^{-9}	1.20×10^{-9}
Mg^{2+}	5.94×10^{-10}	6.26×10^{-10}
Cl^-	1.71×10^{-9}	1.81×10^{-9}
Br^-	1.76×10^{-9}	1.86×10^{-9}

[a] Values from Lasaga (1998)

[b] Values corrected for temperature and viscosity changes

The flow-through experiments were performed at two different flow velocities: 1.5 m/day and 6 m/day. These values of seepage velocity are representative of fast groundwater flow encountered in rather permeable sand and gravel formations. Under these conditions the transport regime is advection-dominated. In fact, considering the average grain size (d=1.25 mm) and a reference diffusion coefficient of 1×10^{-9} m^2/s, the grain Péclet number ($Pe=vd/D$), expressing the relative balance between advection and diffusion, is 21.7 and 86.8 for the experiments at 1.5 m/day and 6 m/day, respectively. Table 2.2 summarizes the experiments carried out in this study including the inlet concentrations of the electrolytes in the tracer and ambient solutions.

Table 2.2: Flow-through experiments performed at two different flow velocities: v=1.5 m/day and v=6 m/day.

Experiment	**Tracer solution [mM]**	**Ambient solution [mM]**
1	NaCl (0.73; 1.05)[a]	Milli-Q water
2	$MgCl_2$ (0.40; 0.48)	Milli-Q water
3	KCl and $MgCl_2$ (0.29; 0.30)	Milli-Q water
4	$MgCl_2$ (0.40; 0.46) and NaBr (1.60; 1.58)	NaBr (1.60; 1.58)
5	$MgCl_2$ (0.35; 0.43)	NaBr (1.57; 0.44)

[a] The first values are the inlet concentrations in the experiments at v=1.5 m/day, the second ones refer to the experiments performed at v=6 m/day

2.4 Modeling Approach

The governing transport equation for a conservative species in a two-dimensional domain representing our experimental setup, with a uniform horizontal velocity field and a constant porosity can be written as:

$$\frac{\partial C_i}{\partial t} + v\frac{\partial C_i}{\partial x} - \frac{\partial}{\partial x}\left(D^L \frac{\partial C_i}{\partial x} \right) - \frac{\partial}{\partial z}\left(D^T \frac{\partial C_i}{\partial z} \right) = 0 \tag{2.7}$$

where v is the horizontal average linear velocity, and D^L and D^T are the longitudinal and transverse hydrodynamic dispersion coefficients, respectively.

Considering steady-state transport and the release of the compound from a continuously emitting source, the contribution of longitudinal dispersion becomes negligible compared to the one in the transverse direction (e.g., Cirpka et al., 2011) and Eq. 2.7 simplifies to:

$$v\frac{\partial C_i}{\partial x} - \frac{\partial}{\partial z}\left(D^T \frac{\partial C_i}{\partial z} \right) = 0 \tag{2.8}$$

Under the same conditions, the governing equation for multicomponent transport of charged species in a flow-through system is:

$$v\frac{\partial C_i}{\partial x} - \frac{\partial}{\partial z}\left(\sum_{j=1}^{n} D_{ij}^T \frac{\partial C_i}{\partial z} \right) = 0 \tag{2.9}$$

where D^T_{ij} is the matrix of multicomponent ionic transverse dispersion coefficients. This matrix is formally identical to the purely diffusive counterpart (Eq. 2.5) and its elements couple the dispersive fluxes of an ion i with the concentration gradients of the other species in solution.

The steady-state transport equation in a two-dimensional homogeneous domain is equivalent to a 1-D transient diffusive/dispersive problem. In fact, the longitudinal spatial coordinate in Eq. 2.9 can be written as $x=vt$ and the uniform velocity can be simplified, yielding the one-dimensional transient diffusive/dispersive equation of the multicomponent problem:

$$\frac{\partial C_i}{\partial t} = \frac{\partial}{\partial z}\left(\sum_{j=1}^{n} D_{ij}^T \frac{\partial C_i}{\partial z} \right) \tag{2.10}$$

This equation was solved with PHREEQC (Parkhurst and Appelo, 1999) taking advantage of the multicomponent diffusion capability of the code (Appelo and Wersin, 2007). Setting the simulation time to the residence time in the flow-through system, the calculated transient profiles at the last time step can be directly compared to the concentration profiles measured at the outlet ports of the experimental setup. To be able to solve this multicomponent transport problem, the transverse dispersion coefficients for each ion in solution need to be provided as

input parameter. This was done using the non-linear compound-specific parameterization of transverse dispersion, which was inspired by an earlier statistical model (Bear and Bachmat, 1967) and was developed in the works of Chiogna et al. (2010) and Rolle et al. (2012). The parameterization takes the form:

$$D^T = D^P + D\left(\frac{Pe^2}{Pe + 2 + 4\delta^2}\right)^{\beta} \tag{2.11}$$

where D^P is the pore diffusion approximated as the product of the aqueous diffusion coefficient, D, and the porosity (Boving and Grathwohl, 2001), Pe is the grain Péclet number, δ is the ratio between the length of a pore channel and its hydraulic radius, and β is an empirical exponent accounting for the incomplete mixing in the pore channels. In a similar flow-through system and with the same porous medium used in this study, Rolle et al. (2012) determined values of δ=6.2 and β=0.47 in a number of multitracer experiments performed in a flow velocity range 0.5-35 m/day. These parameters were used to calculate the transverse dispersion coefficients of the different ionic species in liberated state (i.e., "self-dispersion", the transverse dispersion coefficient of a solute without interactions with other species). The cross-coupling between the different species is then given by:

$$D_{ij}^T = \delta_{ij} D_i^T - \frac{z_i z_j D_i^T D_j^T C_i}{\sum_{k=1}^{n} (z_k^2 D_k^T C_k)} \tag{2.12}$$

To test the validity of our modeling approach we consider the case of electrolyte transport in pure water. Under such conditions, the solute-solute interactions result in a coupled displacement of the charged species. Therefore, in this case, despite the fact that the strong electrolytes fully ionize in solution, their diffusion can be described by a single diffusion coefficient which characterizes the displacement of the salt (e.g., Lasaga, 1979; Cussler, 2009):

$$D_{salt} = \frac{|z_1| + |z_2|}{|z_1|/D_2 + |z_2|/D_1} \tag{2.13}$$

where z_1, z_2 and D_1, D_2 are the charge and the aqueous diffusion coefficients of the cation and anion which constitute the salt.

We consider a two-dimensional domain (100 cm × 12 cm), representing the saturated zone of our laboratory flow-through system, and two distinct cases of continuous injection of a 1:1 electrolyte (NaCl) and a 1:2 electrolyte ($MgCl_2$), respectively. The NaCl and $MgCl_2$ solutions are injected from a line source (with width w=1 cm and corresponding to the central inlet ports in our setup) and pure water from the remaining portion of the inlet boundary. Under such conditions, a unique diffusion coefficient for the injected salts can be calculated (Eq. 2.13): we obtained D_{NaCl}=1.44×10^{-9} m^2/s and D_{MgCl2}=1.18×10^{-9} m^2/s using the self-diffusion coefficients

for the different ions at T=20 °C (Table 2.1). The analytical solution for this two-dimensional steady-state transport problem, considering the salt as a single uncharged species, is given by (Domenico and Palciauskas, 1982):

$$\frac{C(x,z)}{C_0} = \frac{1}{2}\left[erf\left(\frac{z + w/2}{2\sqrt{D^T_{salt} x / v}} \right) - erf\left(\frac{z - w/2}{2\sqrt{D^T_{salt} x / v}} \right) \right] \tag{2.14}$$

where C_0 is the concentration at the source (0.25 mM) and D^T_{salt} is the transverse dispersion coefficient for the considered salts calculated according to Eq. 2.11, with D_{NaCl} and D_{MgCl2} as diffusion coefficients. The results of the 2-D steady-state analytical solution can be compared with the outcome of the 1-D multicomponent transport problem solved numerically with PHREEQC. The latter is based on the solution of Eq. 2.10 with the cross-coupling dispersion coefficients calculated according to Eqs. 2.11-2.12. The simulation domain was a 1-D column, 6 cm long (half the height of the saturated porous medium in the experimental setup and in the 2-D modeling domain) and discretized into 120 cells (Δz=0.5 mm). An initial concentration of 0.25 mM was assigned at the first 10 cells (5 mm corresponding to half the width of the 2-D source) and the simulations were run for 16 hours and 4 hours for the flow-through experiments with v=1.5 m/day and v=6 m/day, respectively. Such simulation times correspond to the outlet cross sections in the two-dimensional domains according to the applied transformation of coordinate (x=vt). Therefore, the vertical profiles computed with the analytical solution at the outlet cross section (x=100 cm) can be directly compared with the results of the transient numerical model at the last simulation time step. The outcomes of such comparison are shown in Fig. 2.2 for the seepage velocity of 1.5 m/day. An excellent agreement was obtained between the 2-D steady-state analytical solution and the 1-D transient multicomponent numerical simulations. The computed profiles have a Gaussian shape. In the case of the 1-D PHREEQC model, the results are obtained for the upper half of the 2-D domain and extended by symmetry to the lower half (gray area). For both the 1:1 (NaCl) and the 1:2 electrolytes ($MgCl_2$), the PHREEQC solution of the multicomponent transport problems, considering the interactions between the ionic species (Eqs. 2.10-2.12), perfectly matches the outcomes of the single-tracer analytical solution. This shows that, under the conditions of transverse displacement in pure water, the transport of the dissociated ionic pairs (Na^+ and Cl^- for the sodium chloride solution, and Mg^{2+} and Cl^- for the magnesium chloride solution) is fully coupled and occurs as a single species. In the following section we adopt the 1-D transient multicomponent PHREEQC model to interpret the outcome of the performed quasi 2-D steady-state flow-through experiments to account for the different coupling between the transverse dispersive fluxes of the ionic species.

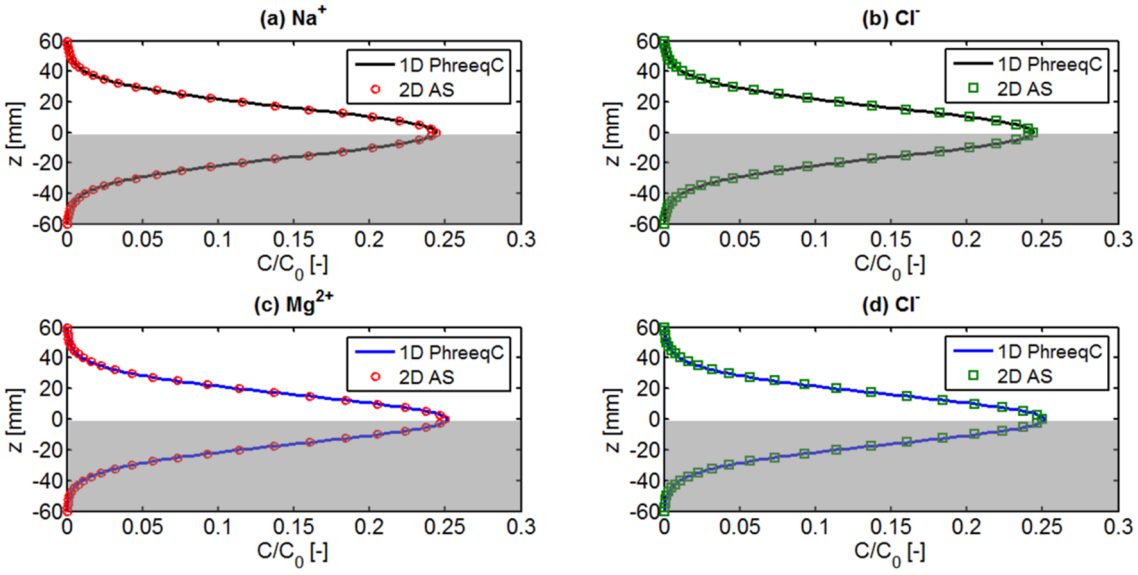

Figure 2.2. Comparison between the 2-D steady-state analytical solution (Eq. 2.14) and the 1-D transient multicomponent numerical model for transport of NaCl (1:1 electrolyte, a and b) and $MgCl_2$ (1:2 electrolyte, c and d) in pure water at v=1.5 m/day (Eq. 2.10). The 1-D PHREEQC multicomponent results obtained for the upper half of the 2-D domain are extended by symmetry in the lower half (gray area).

2.5 Results and Discussion

The results of the flow-through experiments, performed under two distinct advection-dominated flow regimes (i.e., flow velocity of 1.5 m/day and 6 m/day), are interpreted with pure forward simulations of multicomponent transport according to the modeling approach outlined in the previous section.

2.5.1 Experiments at flow velocity v=1.5 m/day

2.5.1.1 Transport of single electrolytes in pure water

In the first flow-through experiments (1 and 2 in Table 2.2) we investigated the transport of electrolytes in Milli-Q water. In Experiment 1, we continuously injected a 1:1 electrolyte solution (0.73 mM NaCl) through the two central inlet ports of the flow-through chamber and measured the concentrations of the cation and the anion at the outlet. The results are shown in Fig. 2.3a. Notice that even though the cation and anion have significantly different diffusion coefficients in their liberated state (1.20×10^{-9} m^2/s for Na^+ and 1.81×10^{-9} m^2/s for Cl^-), they appear to travel together as indicated by their practically identical transverse displacement at

the outlet of the flow-through system. This behavior is due to the cross-coupling between the transverse dispersion fluxes of the charged species. In fact, Coulombic interactions between the ions with opposite charge couple the two ions and result in the enhancement of the displacement of the slower ion, Na^+, and in the decrease of the displacement of the faster ion, Cl^-. Therefore, the ionic species are electrostatically tied together and their displacement in the flow-through system can be accurately described by a single dispersion coefficient (Eq. 2.11 and Eq. 2.13). The multicomponent numerical simulations substantiate the experimental observations. In fact, the transverse profiles of the ions at the outlet, calculated solving Eq. 2.10 and taking into account the cross-coupling between the transverse dispersion coefficients of the different species (Eq. 2.12), results in overlapping curves for the positively and negatively charged species. Furthermore, the purely forward multicomponent numerical simulations show an excellent agreement with the measurements at the outlet of the flow-through system.

Similar results were obtained in Experiment 2, in which a dilute solution of a 1:2 electrolyte (0.40 mM $MgCl_2$) was injected through the central inlet ports. Mg^{2+} has an aqueous diffusion coefficient (6.26×10^{-10} m^2/s) that is significantly smaller than the one of Na^+ and the one of Cl^-. Even though chloride has a diffusivity almost three times larger than the one of Mg^{2+}, the electrostatic interactions between the two charged species results in a coupled transverse displacement of the ions in pure water. This is shown by the measurement at the outlet ports of the flow-through system and by the outcome of the multicomponent simulations (Fig. 2.3b).

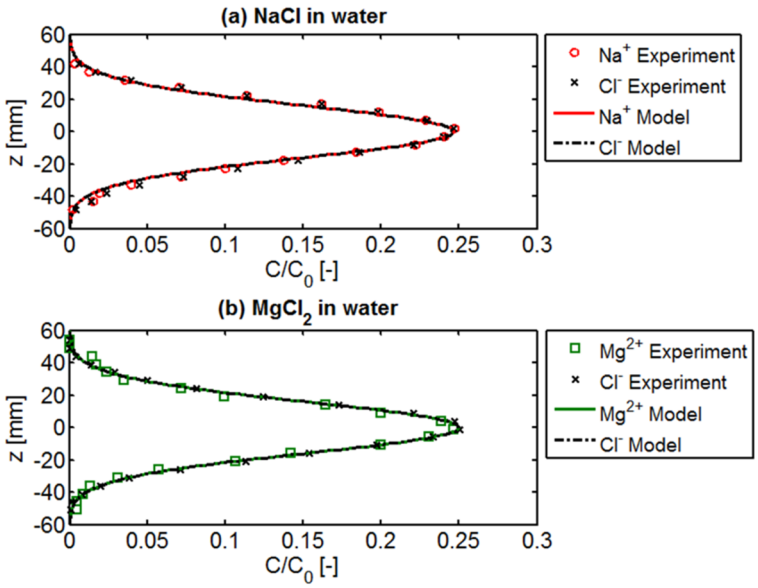

Figure 2.3. Transverse profiles at the end of the flow-through system for NaCl (a) and $MgCl_2$ (b) in Milli-Q water (Experiment 1 and 2): measured cation and anion concentrations (symbols) and multicomponent modeling results (lines).

2.5.1.2 Transport of mixed electrolytes in pure water

In Experiment 3 we investigated the transport of mixed electrolytes, a dilute solution of KCl and $MgCl_2$, in Milli-Q water. The solution, containing two cations (K^+ and Mg^{2+}) and a common anion (Cl^-), was continuously injected through the two central inlet ports and ambient Milli-Q water was injected through the remaining 21 ports. Measurements at the outlet were performed to determine the concentration of the two cations and the anion. Unlike the previous experiments, the outlet profiles show a clearly distinct pattern in the transverse displacement of the charged species (Fig. 2.4). The two cations have significantly different profiles: Mg^{2+} has a more peaked distribution than K^+. Both cations show an enhancement of their transverse displacement, relative to their liberated state, due to the coupling with the anion (Cl^-). This results in a positive contribution of the electrochemical migration terms to the overall dispersive fluxes of the two cations. The chloride ion, despite having the highest self-diffusion coefficient (Table 2.1), has a profile in between the ones of the cations since its transverse displacement is affected by a negative contribution of the electrochemical migration term. These results demonstrate the coupling between the dispersive fluxes of the charged species in our flow-through system and are in agreement with the observations made by Vinograd and McBain (1941) in their pioneering work on diffusion of electrolytes. The numerical multicomponent simulations (lines in Fig. 2.4), based on the cross-coupling between the transverse displacement of the different species, reproduce quite closely the experimental results. The simulated profiles also clearly indicate a distinct pattern of the different ionic species, injected as a mixture of two different electrolytes (KCl and MgCl2), due to the electrostatic coupling of their transverse dispersive fluxes.

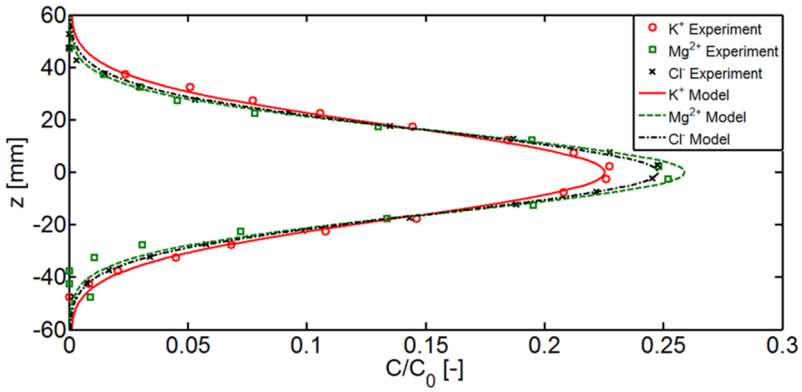

Figure 2.4. Transverse profiles at the end of the flow-through system for transport of mixed electrolytes, KCl and $MgCl_2$ (Experiment 3): measured cation and anion concentrations (symbols) and multicomponent modeling results (lines).

2.5.1.3 Transport of ionic species in an ambient buffer electrolyte solution

In Experiments 4 and 5 we focused on transport of a 1:2 electrolyte ($MgCl_2$) in an ambient buffer electrolyte solution (NaBr). In Experiment 4, a solution with a concentration of 0.4 mM $MgCl_2$ and an approximately fourfold (1.6 mM) concentration of the background electrolyte (NaBr) was continuously injected through the two central inlet ports. An ambient solution with the same concentration of NaBr was injected in parallel through the surrounding inlet ports. The measurements of Mg^{2+} and Cl^- at the outlet show a distinct pattern of the two ions. This behavior can be explained by the presence of the buffer electrolyte (NaBr) at higher concentration which tends to suppress the electrical gradient and allows the ionic species injected at lower concentration through the central inlet ports (Mg^{2+} and Cl^-) to move with a diffusivity very close to their own self-diffusivity. The observed and simulated profiles show a clear difference between the displacement of magnesium and chloride, with the cation presenting higher peak concentration and lower transverse spreading than the anion (Fig. 2.5a). The lines are the outcomes of the multicomponent simulations and are very similar to the results of simulations performed considering the ions as independent species, each characterized by its self-diffusion coefficient (results not shown). We measured also the concentration of the buffer ions at the outlet (Fig. 2.5b). The experimental results and the simulations show the formation of vertical gradients of these species even though they were injected with the same concentration throughout the entire thickness of the porous medium.

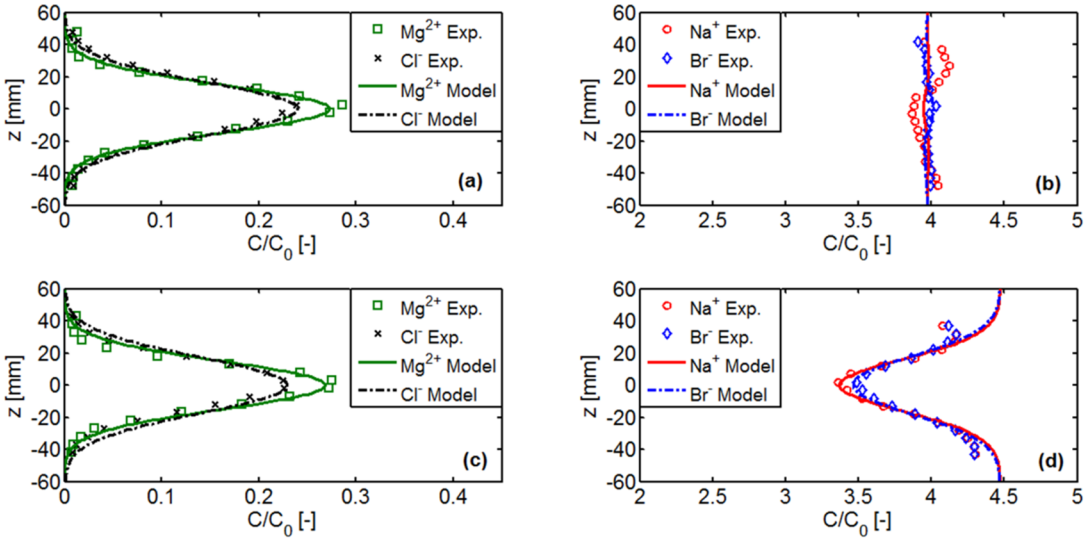

Figure 2.5. Observed and simulated profiles for ionic transport in buffer electrolyte solutions under the conditions and initial concentrations of Experiment 4 (a and b) and Experiment 5 (c and d). The concentrations are normalized by the values at the inlet central ports.

The concentration of Br^- increases at the center of the plume to maintain the charge neutrality and to counterbalance the excess of positive charge in this region due to the relative increase of the concentration of Mg^{2+}, which shows a lower transverse displacement than Cl^-. The situation is the opposite at the plume fringes: here chloride is in excess and the background cation (Na^+) displaces outwards, against its concentration gradient, to maintain electroneutrality. A similar outcome for the injected $MgCl_2$ solution (0.35 mM), with a slightly enhanced difference between the two ions, was observed in Experiment 5. In this experiment the background electrolyte (NaBr) was not injected from the two central inlet ports and therefore moved, by transverse dispersion, towards the center. A difference between the displacement of the background electrolyte ions, Na^+ and Br^-, can be appreciated in particular in the central region where bromide is present at higher concentration than sodium, thus balancing the difference between Mg^{2+} and Cl^- in the injected plume (Fig. 2.5c and d).

2.5.2 Experiments at flow velocity *v*=6 m/day

The experiments summarized in Table 2.2 were also performed at a higher flow velocity, in a strongly advection-dominated flow regime. Under such conditions, transverse dispersion is dominated by the mechanical dispersion term, which has a much greater contribution than that of pore diffusion. The results were similar to the ones obtained at a lower flow velocity (v=1.5 m/day) and confirm the Coulombic cross-coupling of the transverse dispersion fluxes. Fig. 2.6 reports the experimental observations and modeling results for transport of an electrolyte solution in pure water (Experiment 1), transport of a mixture of electrolytes in pure water (Experiment 3), and ionic transport in a buffer electrolyte solution (Experiment 4).

It is worth pointing out that most of our experimental observations could not be accurately reproduced with a model based on a multicomponent formulation but implementing a classical parameterization (Scheidegger, 1961) of transverse dispersion:

$$D_{ij}^{T} = D_{ij}^{P} + \alpha_T v \tag{2.15}$$

where α_T is the transverse dispersivity, which is typically assumed to be a property of the porous medium, but in reality it is a function of both the flow-velocity and the diffusivity of the transported solutes (Rolle et al., 2012; Hochstetler et al., 2013).

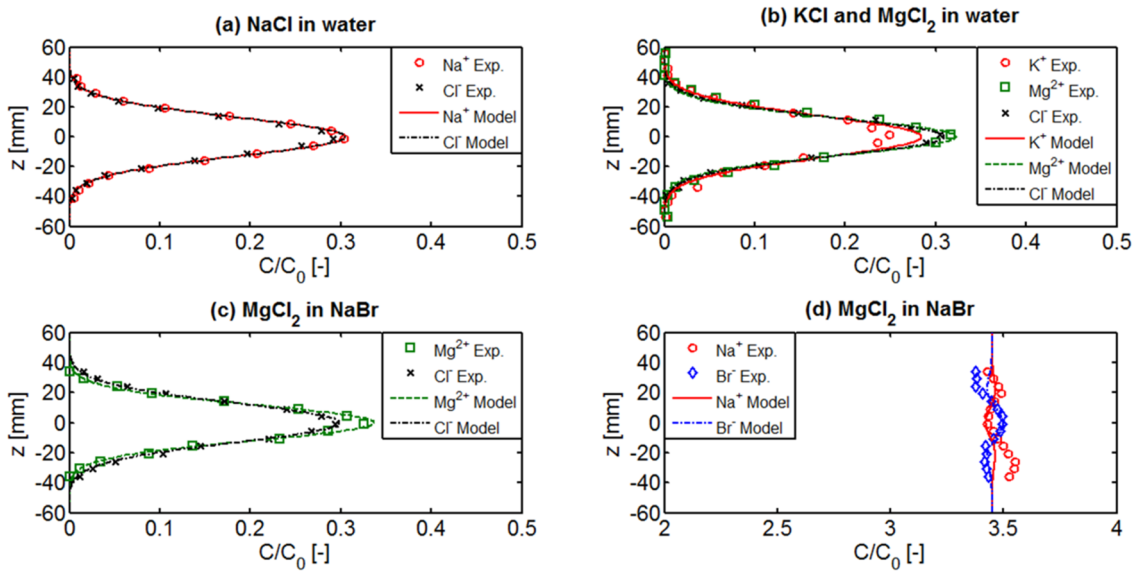

Figure 2.6. Multicomponent ionic transport at high flow velocity (v=6 m/day): (a) Experiment 1: NaCl injection with water as ambient solution; (b) Experiment 3: KCl and $MgCl_2$ injection with water as ambient solution; (c) and (d) Experiment 4: $MgCl_2$ injection with NaBr as ambient solution.

Taking the data of transport of NaCl in pure water (Fig. 2.6a) as reference case and considering the salt as a single species with diffusivity D_{NaCl}=1.44×10^{-9} m^2/s (Eq. 2.13) one can calculate the transverse dispersivity, α_T, from Eq. 2.15, with a best fit procedure. In fact, Eq. 2.14 can be fitted to the experimental data, using D^T_{salt} as fitting parameter. With such approach, the best-fit value of the transverse dispersion coefficient was found to be D^T_{salt} = 5.49×10^{-9} m^2/s, thus resulting in a transverse dispersivity α_T=7.6×10^{-5} m. A modeling approach using the same multicomponent formulation described above but with the classical dispersion parameterization (Eq. 2.15) would only reproduce the data reported in Fig. 2.6a, which were used to determine the value of transverse dispersivity. For the other experiments, the model will predict only very small differences between the ions, since every species undergoes practically the same transverse displacement. Such displacement is dominated by the mechanical dispersion term ($\alpha_T v$), which, in the strongly advection-dominated regime, overwhelms the multicomponent ionic diffusion effects of the pore diffusion term. The latter represents only ~1/10 of the hydrodynamic dispersion coefficient under the considered fast flow conditions. Thus, the classical parameterization (Eq. 2.15) is not suitable to accurately describe the behavior observed in the flow-through experiments. In fact, such a formulation does not allow capturing the specific displacement of the different ionic species and the gradients developing in the background electrolyte to maintain charge neutrality (Fig. 2.6b-d).

2.5.3 Flux-related dilution index

Metrics of mixing based on the concept of information (Shannon) entropy have been applied to appropriately quantify solute dilution during transport in porous media (e.g., Kitanidis, 1994; Rolle et al., 2009; Chiogna et al., 2012). The dilution index quantifies dilution as the "act of distributing solute mass over a larger volume" (Kitanidis, 1994). To quantify dilution in our setup, with continuous injection of tracer solutions at the inlet, we used the flux-related dilution index (Rolle et al., 2009). This metric expresses dilution as the "act of distributing a given solute mass flux over a larger water flux". The flux-related dilution index quantifies the effective volumetric discharge transporting the solute flux at a given longitudinal position x and its mathematical expression reads as:

$$E_Q(x) = \exp\left(-\int_{\Omega} p_Q(\boldsymbol{x}) \ln(p_Q(\boldsymbol{x})) q_x(\boldsymbol{x}) d\Omega \right) \tag{2.16}$$

where $q_x = v\theta$ is the component of the specific discharge normal to the cross-sectional area Ω, θ is the porosity, and p_Q is the flux-related probability density function:

$$p_Q(\boldsymbol{x}) = \frac{C_i(\boldsymbol{x})}{\int_{\Omega} C_i(\boldsymbol{x}) q_x(\boldsymbol{x}) d\Omega} \tag{2.17}$$

We use the flux-related dilution index to quantify the transverse displacement of the charged species in our multicomponent dispersion experiments. In the flow-through experiments E_Q can be computed from the measured concentrations and flow rates at the inlet and outlet of the flow-through system. The model simulations allowed us to calculate the flux-related dilution index at different cross sections (i.e., at different times with the modeling formulation adopted, Eq. 2.10) inside the porous medium. According to Eq. 2.16 and Eq. 2.17, these calculations are based on the concentration distribution of the different species and the flow rate at a given longitudinal cross-section. The results are reported in Fig. 2.7 for Experiment 1, 3 and 4 at the flow velocity of 1.5 m/day. Notice that the flux-related dilution index, being a measure of entropy, monotonically increases with increasing distance from the inlet source. At the inlet, the flux-related dilution index is the same for every ion, since the tracer electrolyte is injected through the two central inlet ports and, therefore, the charged species are distributed over an identical water flux. In Experiment 1, NaCl was the tracer electrolyte surrounded by pure water as ambient solution. In this case, the Coulombic coupling between the multicomponent transverse dispersive fluxes of Na^+ and Cl^- results in an identical flux-related dilution index for the two charged species (Fig. 2.7a). These species move together and, therefore, at every cross section, they are distributed over the same volumetric discharge. The measurements at the outlet ports also results in a practically identical flux-related dilution index for the cation and the anion and substantiate the outcome of the multicomponent transport simulation. The

situation is different when a mixture of electrolytes is simultaneously injected and transported in pure water (Experiment 3). The electrostatic interactions between the two cations (K^+ and Mg^{2+}) and the common anion (Cl^-) result in distinct dilution (Fig. 2.7b). The flux-related dilution index starts at the same point at the inlet but evolves differently throughout the porous medium. In fact, as also indicated by the transverse profiles measured at the outlet (Fig. 2.4), the different ions show distinct transverse displacements which result in progressively different values of the flux-related dilution index. The measurements at the outlet agree with the outcomes of the simulation and show that the value of E_Q for K^+ is 15% larger than the one for Mg^{2+}. This indicates that the mass flux of potassium is distributed over a volumetric discharge 15% larger than the one carrying the magnesium ion. In Experiment 4, $MgCl_2$ was injected with NaBr as background electrolyte. Under these conditions the cation and the anion tend to displace with aqueous diffusion coefficients very close to their own self-diffusivities. As a result, the flux-related dilution index calculated for Mg^{2+} and Cl^- progressively diverges from the initial common inlet value. Due to its larger transverse dispersion, the chloride ion is more effectively distributed over a larger water flux and, at the end of the flow-through system, the relative difference in the dilution between the two ionic species is 12.3%.

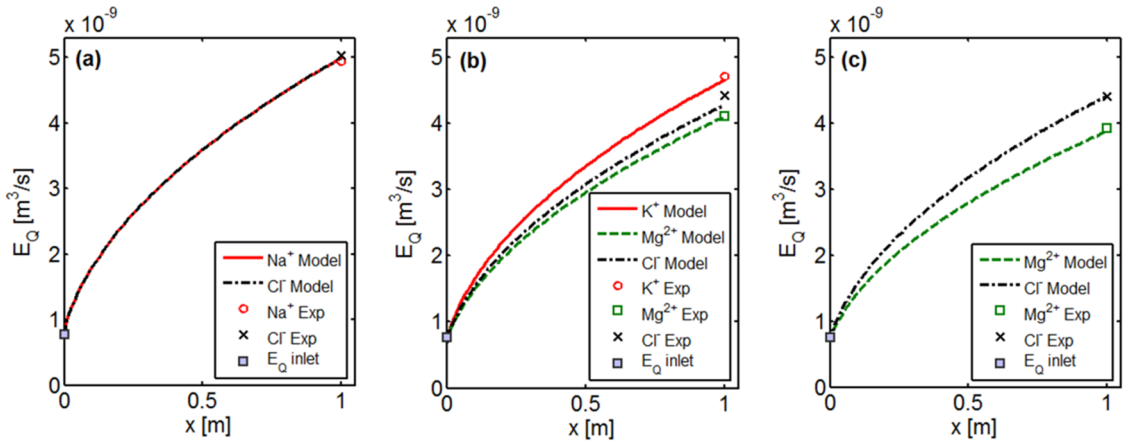

Figure 2.7. Computed (lines) and observed (symbols) flux-related dilution index for the experiments at v=1.5 m/day: (a) Experiment 1: NaCl injection with water as ambient solution; (b) Experiment 3: KCl and $MgCl_2$ injection with water as ambient solution; (c) Experiment 4: $MgCl_2$ injection with NaBr as ambient solution.

2.6 Summary and Conclusions

In this study we have shown the presence of significant Coulombic interactions during transport of charged species in porous media in advection-dominated flow regimes. We focused on transverse dispersion and have demonstrated the need for a multicomponent ionic dispersion formulation to account for the cross-coupling between the dispersive fluxes of ionic species undergoing transport in porous media. We used flow-through experiments, performed at 1.5 and 6 m/day, to investigate transport of dilute electrolyte solutions under advection-dominated and strongly advection-dominated flow conditions. Numerical transport simulations have been performed to quantitatively interpret the experimental results. The adopted modeling approach was based on a multicomponent formulation and on the accurate description of transverse dispersion. The latter entails a non-linear and compound-specific parameterization of the transverse dispersion coefficient, as demonstrated by recent multitracer experiments and pore-scale simulations (Chiogna et al., 2010; Rolle et al., 2012; Hochstetler et al., 2013). Such parameterization allows capturing the dependence of D^T on molecular diffusion not only at low but also at high flow velocities, where compound-specific concentration gradients develop at the subcontinuum scale due to incomplete mixing in the pore channels (Rolle et al., 2012). The results of the multicomponent simulations for electrolyte transport performed in this study show a good agreement with the experimental observations and demonstrate the relevance of Coulombic interactions between charged species in flow-through systems.

To clearly identify the effects of multicomponent ionic dispersion, we decided to work in simplified flow through systems. Underlying simplifying assumptions to our work are: (i) the choice of a macroscopically homogeneous porous medium, (ii) steady-state flow and transport conditions, (iii) the use of dilute solutions, and (iv) the limited complexity of the selected chemical systems that comprised only strong electrolytes, thus avoiding the effects of ion pairs in the multicomponent coupling of the fluxes (Lasaga, 1979). Relaxing these assumptions can further lead to interesting findings in the fundamental understanding of coupled transport of charged species in porous media and for practical applications in both natural and engineered systems, such as the use of electrokinetic techniques to displace contaminants and inject amendments in the subsurface (e.g., Saicheck and Reddy, 2005; Wu et al., 2012). For instance, considering transient conditions will require extending the proposed framework to include important effects like the exchange of charged species among different domains in a porous medium, such as the bulk solution and the diffuse double layer surrounding charged solid surfaces (e.g., Gvirtzman and Gorelick, 1991; Appelo and Wersin, 2007), and mass-transfer effects between low and high permeability zones in natural geologic formations (Haggerty and Gorelick, 1995). Furthermore, for transient solute transport, the interactions of the dissolved

charged species with the solid grains, such as sorption and ion exchange, will play an important role (e.g., Bjerg et al., 1993; Appelo, 1994). Concerning the physical properties of the porous medium, the study of multicomponent effects in heterogeneous media represents an interesting and broadly unexplored field of investigation. Spatially-variable flow fields in heterogeneous formations significantly influence solute transport. In heterogeneous systems, the mathematical description can no longer be based on the simplifying assumptions adopted in this study but requires the development of a multidimensional flow and multicomponent transport modeling approach. Finally, of great interest is also the study of multicomponent effects in reactive systems which, to date, has received limited consideration, with only a few studies addressing these effects with experimental and/or modeling approaches (e.g., Boudreau et al., 2004; Li et al., 2008; Liu et al., 2011; Molins et al., 2012).

Acknowledgments

The authors thank Bernice Nisch and Annegret Walz for their assistance with the ion-chromatography measurements.

M.R. acknowledges the support of the Marie Curie International Outgoing Fellowship (DILREACT project) within the 7th European Community Framework Programme. M.R. and M.M. acknowledge the Baden-Württemberg Stiftung for the financial support of this research project by the Eliteprogram for Postdocs.

References

Appelo C. A. J. (1994) Some calculations on multicomponent transport with cation exchange in aquifers. *Ground Water* **32**, 968-975.

Appelo C. A. J. and Wersin P. (2007) Multicomponent diffusion modeling in clay systems with application to the diffusion of tritium, iodide, and sodium in Opalinus Clay. *Environ. Sci. Technol.* **41**, 5002-5007.

Appelo C. A. J., Vinsot A., Mettler S. and Wechner S. (2008) Obtaining the porewater composition of a clay rock by modeling the in- and out-diffusion of anions and cations from an in-situ experiment. *J. Contam. Hydrol.* **101**, 67-76.

Appelo C. A. J., Van Loon L. R. and Wersin P. (2010) Multicomponent diffusion of a suite of tracers (HTO, Cl, Br, I, Na, Sr, Cs) in a single sample of Opalinus Clay. *Geochim. Cosmochim. Acta* **74**, 1201-1219.

Bauer R.D., Rolle M., Kürzinger P., Grathwohl P., Meckenstock R.U. and Griebler C. (2009). Two-dimensional flow-through microcosms – versatile test systems to study biodegradation processes in porous aquifers. *J. Hydrol.*, 369, 284–295.

Bear J. and Bachmat Y. (1967) A generalized theory on hydrodynamic dispersion in porous media. In IASH Symposium on Artificial Recharge and Management of Aquifers, Haifa, Israel, vol. 72, 7-16.

Ben-Yaakov S. (1972) Diffusion of sea water ions: I. Diffusion of sea water into a dilute solution. *Geochim. Cosmochim. Acta* **36**, 1395-1406.

Boudreau B. P. (1997) Diagenetic models and their implementation: Modelling transport and reactions in aquatic sediments. Springer-Verlag, Heidelberg.

Boudreau B. P., Meysman F. J. R. and Middelburg J.J. (2004) Multicomponent ionic diffusion in porewaters: Coulombic effects revisited. *Earth Planet. Sci. Lett.* **222**, 653-666.

Boving T. and Grathwohl P. (2001) Matrix diffusion coefficients in sandstones and limestones: Relationship to permeability and porosity. *J. Contam. Hydrol.* **53**, 85-100.

Bierg P. L., Ammentorp H. C. and Christensen T. H. (1993) Model simulations of a field experiment on cation exchange-affected multicomponent solute transport in a sandy aquifer. *J. Contam. Hydrol.* **12**, 291-311.

Chiogna G., Eberhardt C., Grathwohl P., Cirpka O. A. and Rolle M. (2010) Evidence of compound dependent hydrodynamic and mechanical transverse dispersion by multi-tracer laboratory experiments. *Environ. Sci. Technol.* **44**, 688-693.

Chiogna G., Cirpka O. A., Grathwohl, P. and Rolle M. (2011) Relevance of local compound-specific transverse dispersion for conservative and reactive mixing in heterogeneous porous media. *Water Resour. Res.* **47**, W06515, doi:10.1029 /2010WR010270.

Chiogna G., Hochstetler D. L., Bellin A., Kitanidis P. K. and Rolle M. (2012) Mixing, entropy and reactive solute transport. *Geophys. Res. Lett.* **39**, L20405, doi:10.1029/2012GL053295.

Cirpka O. A., de Barros F. P. J., Chiogna G., Rolle M. and Nowak W. (2011) Stochastic flux-related analysis of transverse mixing in two-dimensional heterogeneous porous media. *Water Resour. Res.* **47**, W07540, doi:10.1029 /2010WR010279.

Cussler E. L. (2009) Diffusion: Mass transfer in fluid systems. Third Edition, Cambridge University Press, New York, USA.

Domenico P. A. and Palciauskas V. (1982) Alternative boundaries in solid waste management. *Ground Water* **20**, 303-311.

Felmy A. R. and Weare J. H. (1991) Calculation of multicomponent ionic diffusion from zero to high concentration: I. The system Na-K-Ca-Mg-Cl-SO_4-H_2O at 25C. *Geochim. Cosmochim. Acta* **55**, 113-131.

Giambalvo E. R., Steefel C. I., Fisher A. T., Rosenberg N. D. and Wheat C. G. (2002) Effect of fluid-sediment reaction on hydrothermal fluxes of major elements, eastern flank of the Juan de Fuca Ridge. *Geochim. Cosmochim. Acta* **66**, 1739-1757.

Grathwohl P. (1998) Diffusion in natural porous media: Contaminant transport, sorption/desorption, and dissolution kinetics. Kluwer Academic Publishers, Boston, USA.

Gvirtzman H. and Gorelick S. M. (1991) Dispersion and advection in unsaturated porous media enhanced by anion exclusion. *Nature* **352**, 793-795.

Haberer C. M., Rolle M., Liu S., Cirpka O. A. and Grathwohl P. (2011) A high-resolution non-invasive approach to quantify oxygen transport across the capillary fringe and within the underlying groundwater. *J. Contam. Hydrol.* **122**, 26-39.

Haberer C.M., Rolle M., Cirpka O.A. and Grathwohl P. (2012). Oxygen transfer in a fluctuating capillary fringe. *Vadose Zone J.*, **11**, doi: 10.2136/vzj2011.0056.

Haggerty R. and Gorelick S.M. (1995) Multiple-rate mass transfer for modeling diffusion and surface reactions in media with pore-scale heterogeneity. *Water Resour. Res.* **31**, 2383-2400.

Hochstetler D. L., Rolle M., Chiogna G., Haberer C. M., Grathwohl P. and Kitanidis P. K. (2013) Effects of compound-specific transverse mixing on steady-state reactive plumes: insights from pore-scale simulations and Darcy-scale experiments. *Adv. Water Resour.* **54**, 1-13.

Holocher J., Peeters F., Aeschbach-Hertig W., Hofer M., Brennwald M., Kinzelbach W. and Kipfer R. (2002) Experimental investigations on the formation of excess air in quasi-saturated porous media. *Geochim. Cosmochim. Acta* **66**, 4103-4117.

Kitanidis P. K. (1994) The concept of the dilution index. *Water Resour. Res.* **30**, 2011-2026.

Lasaga A. C. (1979) The treatment of multi-component diffusion and ion pairs in diagenetic fluxes. *Am. J. Sci.* **279**, 324-346.

Lasaga A. C. (1998) Kinetic theory in the earth sciences. Princeton University Press, Princeton, New Jersey.

LaBolle E. M and Fogg, G. E. (2001) Role of molecular diffusion in contaminant migration and recovery in alluvial aquifer system. *Transport Porous Med.*, 42, 155-179.

Li L., Steefel C. I. and Yang L. (2008) Scale dependence of mineral dissolution rates within single pores and fractures. *Geochim. Cosmochim. Acta* **72**, 360-377.

Liu C. X. (2007) An ion diffusion model in semi-permeble clay materials. *Environ. Sci. Technol.* **41**, 5403-5409.

Liu C. X. and Ball W. P. (2002) Back diffusion of chlorinated solvents from a natural aquitard to a remediated aquifer under controlled field conditions: Predictions and measurements. *Ground Water* **40**, 175-184.

Liu C. X., Zachara J. M., Felmy A. R. and Gorby Y. A. (2004) An electrodynamics-based model for ion diffusion in microbial polysaccharides. *Colloids Surf. A and B* **38**, 55-65.

Liu C. X., Shang J. and Zachara J. M. (2011) Multispecies diffusion models: A study of uranyl species diffusion. *Water Resour. Res.* **47**, W12514, doi:10.1029/2011WR010575.

Maher K., Steefel C.I., DePaolo D. and Viani B. (2006) The mineral dissolution rate conundrum: Insights from reactive transport modeling of U isotopes and pore fluid chemistry in marine sediments. *Geochim. Cosmochim. Acta* **70**, 337-363.

McCarthy K. A. and Johnson R. L. (1993) Transport of volatile organic compounds across the capillary fringe. *Water Resour. Res.* **29**, 1675-1683.

Molins S., Trebotich D., Steefel C. I. and Shen C. (2012) An investigation of pore scale flow on average geochemical reaction rates using different numerical simulation. *Water Resour. Res.* **48**, W03527, doi:10.1029/2011WR011404.

Parkhurst D. L. and Appelo C. A. J. (1999) User's guide to PHREEQC – a computer program for speciation, reaction path, 1-D transport, and inverse geochemical calculations. Technical Report 99-4259, US Geol. Survey Water Resources Investigation Report, 1999.

Rasa E., Chapman S. W., Bekins B. A., Fogg G. E., Scow K. M. and Mackay D. M. (2011) Role of back diffusion and biodegradation reactions in sustaining an MTBE/TBA plume in alluvial media. *J. Contam. Hydrol.* **126**, 235-247.

Rolle M., Clement T.P., Sethi R. and Di Molfetta A. (2008) A kinetic approach for simulating redox-controlled fringe and core biodegradation processes in groundwater: model development and application to a landfill site in Piedmont, Italy. *Hydrol. Process.*, **22**, 4905-4921.

Rolle M., Eberhardt C., Chiogna G., Cirpka O. A. and Grathwohl P. (2009) Enhancement of dilution and transverse reactive mixing in porous media: experiments and model-based interpretation. *J. Contam. Hydrol.* **110**, 130-142.

Rolle M., Chiogna G., Bauer R., Griebler C. and Grathwohl P. (2010) Isotopic fractionation by transverse dispersion: Flow-through microcosms and reactive transport modeling study. *Environ. Sci. Technol.* **44**, 6167-6173.

Rolle M., Hochstetler D. L., Chiogna G., Kitanidis P. K. and Grathwohl P. (2012) Experimental investigation and pore-scale modeling interpretation of compound-specific transverse dispersion in porous media. *Transport Porous Med.* **93**, 347-362.

Saichek R. E. and Reddy K. R. (2005) Electrokinetically enhanced remediation of hydrophobic compounds in soils: a review. *Crit. Rev. Environ. Sci. Technol.* **35**, 115-192.

Scheidegger A. (1961) General theory of dispersion in porous media. *J. Geophys. Res.* **66**, 3273-3278.

Steefel C. I. and Maher K. (2009) Fluid-rock interactions: A reactive transport approach. *Rev. Mineral. Geochem.* **70**, 485-532.

Thullner M., Van Cappellen P. and Regnier P. (2005) Modeling the impact of microbial activity on redox dynamics in porous media. *Geochim. Cosmochim. Acta* **69**, 5005-5019.

Van Breukelen B. M. and Rolle M. (2012) Transverse hydrodynamic dispersion effects on isotope signals in groundwater chlorinated solvents‘ plumes. *Environ. Sci. Technol.* **46**, 7700-7708.

Van Cappellen P. and Gaillard J.-F. (1996) Biogeochemical Dynamics in aquatic sediments. In: Reactive Transport in Porous Media: General Principles and Application to Geochemical Processes (eds. P. C. Lichtner, C. I. Steefel and E. H.Oelkers). Mineral. Soc. Amer. pp. 335–376.

Vinograd J. R. and McBain J. W. (1941) Diffusion of electrolytes and of the ions in their mixtures. *J. Am. Chem. Soc.* **63**, 2008-2015.

Wang Y. and Van Cappellen P. (1996) A multicomponent reactive transport model of early diagenesis: application to redox cycling in coastal marine sediments. *Geochim. Cosmochim. Acta* **60**, 2993-3014.

Wu M. Z., Reynolds D. A., Fourie A., Prommer H. and Thomas D. G. (2012) Electrokinetic in situ oxidation remediation: assessment of parameter sensitivities and the influence of aquifer heterogeneity on remediation efficiency. *J. Contam. Hydrol.* **136-137**, 72-85.

Zhang C., Dehoff K., Hess N., Oostrom M., Wietsma T. W., Valocchi A. J., Fouke B. W. and Werth C. (2010) Pore-scale study of transverse mixing induced CaCO3 precipitation and permeability reduction in a model subsurface sedimentary system. *Environ. Sci. Technol.* **44**, 7833-7838.

Chapter 3

Multicomponent ionic dispersion during transport of electrolytes in heterogeneous porous media: Experiments and model-based interpretation[†]

Abstract

This study investigates the effects of Coulombic interactions during transport of electrolytes in heterogeneous porous media under steady-state flow and transport conditions. We performed flow-through experiments in a quasi two-dimensional setup using dilute solutions of strong 1:1 and 1:2 electrolytes to study the influence of electrochemical cross-coupling on mass transfer of charged species in saturated porous media. The experiments were carried out under advection-dominated conditions (seepage velocity: 1 and 1.5 m/day) in two well-defined heterogeneous domains where flow diverging around a low-permeability inclusion and flow focusing in high-permeability zones occurred. To quantitatively interpret the outcomes of our laboratory experiments in the spatially variable flow fields we developed a two-dimensional numerical model based on a multicomponent formulation and on charge conservation. The results of the multicomponent transport simulations were compared with the high-resolution concentration measurements of the ionic species at the outlet of the flow-through domain. The excellent agreement between the measured concentrations and the results of purely forward numerical simulations demonstrates the capability of the proposed two-dimensional multicomponent approach to describe transport of charged species and to accurately capture the Coulombic interactions between the ions, which are clearly observed in the flow-through experiments. Furthermore, the model allowed us to directly quantify and visualize the ionic interactions by mapping the Coulombic cross-coupling between the dispersive fluxes of the charged species in the heterogeneous domains.

[†] Reproduced from: Muniruzzaman, M., Haberer, C. M., Grathwohl, P., and Rolle, M. (2014). Multicomponent ionic dispersion during transport of electrolytes in heterogeneous porous media: Experiments and model-based interpretation. *Geochimica et Cosmochimica Acta, 141*(0), 656-669.
doi:http://dx.doi.org/10.1016/j.gca.2014.06.020

3.1 Introduction

Aqueous diffusion of charged species is significantly affected by the electrochemical migration term resulting from the interactions among the dissolved species and/or with charged surfaces (e.g., Vinograd and McBain, 1941; Ben-Yaakov, 1972; Lasaga, 1979; Felmy and Weare, 1991; van Chappellen and Gaillard, 1996; Liu, 2007; Appelo and Wersin, 2007; Steefel and Maher, 2009). In such systems, the diffusive flux of a species is not just function of its properties and concentration gradient but it is linked to the presence and to the concentration gradients of other charged species in the system (Lasaga, 1979). Thus, a simple expression of Fick's law does not allow providing a rigorous and accurate description. Hence, a multicomponent formulation is required to model diffusion (e.g., Ben-Yaakov, 1972; Lasaga, 1979; Felmy and Weare, 1991; Boudreau et al., 2004; Liu et al., 2004; Liu 2007; Appelo and Wersin, 2007; Li et al., 2008; Steefel and Maher, 2009). In several earlier studies, multicomponent diffusion models, based on local charge balance approaches, have been developed to interpret conservative and reactive transport of charged species in both laboratory (e.g., Vinograd and McBain, 1941; Ben-Yakov, 1972; Felmy and Weare, 1991; Liu et al., 2011) and field conditions (e.g., Giambalvo et al., 2002; Appelo and Wersin, 2007; Appelo et al., 2008 and 2010).

In flow-through systems, the exchange of mass between different streamlines occurs through diffusion and local dispersion. The quantification of such processes is of critical importance to accurately describe conservative and reactive solute transport in the subsurface (e.g., Kitanidis, 1994; Wang and van Chappellen, 1996; Boudreau, 1997; Thullner et al., 2005; Zhang et al., 2010; Haberer et al., 2011; Molins et al., 2012). In particular, the importance of diffusion in saturated porous media and its role as controlling transport mechanism not only at the small pore and Darcy scales but also at larger field scales is increasingly recognized in studies of subsurface solute transport (e.g., Carrera et al., 1998; LaBolle and Fogg, 2001; Chiogna et al., 2011; Rolle et al., 2013b; Hadley and Newell, 2013). Focusing on multicomponent transport of charged species, in a recent contribution (Rolle et al., 2013a) we proved the existence and relevance of Coulombic effects in homogeneous saturated porous media under advection-dominated flow regimes. In that work we performed quasi 2-D steady-state flow-through experiments, at high groundwater flow velocities (1.5 and 6 m/day) in homogeneously packed flow-through systems, along with 1-D transient numerical modeling. We showed that electrostatic cross-coupling of dispersive-fluxes of ionic species in porous media substantially affects the lateral displacement of charged species not only under purely diffusive but also under flow-through conditions.

In this study, we extend the investigation of multicomponent ionic transport of electrolytes to heterogeneous porous formations. We perform flow-through bench-scale laboratory experiments in advection-dominated flow regimes and under steady-state flow and transport conditions. We work in two different heterogeneous saturated porous media containing well-defined coarse and fine material inclusions, respectively. The aim of the study is to investigate transport of charged species and to identify Coulombic cross-coupling effects among the different ions in solution and their impact on lateral spreading and mixing in spatially variable flow fields. To quantitatively interpret the experimental results we present a two-dimensional numerical model based on a multicomponent formulation of ionic transport and on the cross-coupling of dispersive fluxes.

3.2 Theoretical Background

Multicomponent diffusive fluxes of ionic species in dilute solutions can be described by the Nernst-Plank equation (Bard and Faulkner, 2001; Cussler, 2009), which in absence of strong gradients of ionic strength (Lasaga, 1979) reads as:

$$J_i = -D_i \nabla C_i - D_i \frac{z_i F}{RT} C_i \nabla \Phi \quad i = 1, 2, 3, ..., N \tag{3.1}$$

where D_i is the self-diffusion coefficient, C_i is the concentration of ionic species i, z_i is the charge, F is the Faraday's constant, R is the ideal gas constant, T is the temperature, Φ is the electrostatic potential, and N is the number of the species. The multicomponent formulation is derived using electroneutrality, which is associated with two distinct physical constraints (Boudreau et al., 2004): (i) vanishing charge in every point of the solution (i.e., $\sum_{i=1}^{N} z_i C_i = 0$) and no electrical current (i.e., $\sum_{i=1}^{N} z_i J_i = 0$). Substituting the expression for the diffusive flux into the solute mass balance equation yields the governing equation for multicomponent diffusion problems (e.g., Ben-Yakov, 1972; Lasaga, 1979; van Cappellen and Gaillard, 1996; Boudreau et al., 2004; Liu et al., 2004 and 2011; Appelo and Wersin, 2007). Under flow-through conditions, the advective component should also be considered and mass transfer between different streamlines occurs through local dispersion. Therefore, in multicomponent flow-through problems, the diffusion coefficient of a charged species (D_i) needs to be replaced by its hydrodynamic dispersion coefficient. The latter depends on the interaction between the basic transport mechanisms of advection and diffusion and it is commonly parameterized as the additive contribution of a velocity-independent pore diffusion term and a mechanical dispersion term, accounting for the variability of the velocity in the pore space.

Following an analogous procedure as in the case of purely diffusive problems (e.g., Boudreau et al., 2004), we use the zero charge constraint and we substitute the dispersive flux into the classical advection-dispersion equation. This yields the governing transport equation of charged species for multicomponent flow-through problems:

$$\frac{\partial C_i}{\partial t} + \boldsymbol{v} \cdot \nabla C_i - \nabla \cdot \left(\sum_{j=1}^{N} \boldsymbol{D}_{ij} \nabla C_j \right) = 0 \tag{3.2}$$

in which t is time, $\boldsymbol{v}$ is the velocity vector, and $\boldsymbol{D}_{ij}$ is the dispersion tensor. The entries of $\boldsymbol{D}_{ij}$ in a two-dimensional domain, considering a reference system oriented along the principal directions, can be expressed as:

$$\boldsymbol{D}_{ij} = \begin{bmatrix} \boldsymbol{D}_{ij}^{L} & 0 \\ 0 & \boldsymbol{D}_{ij}^{T} \end{bmatrix}$$

$$\boldsymbol{D}_{ij}^{L} = \delta_{ij} D_i^{L} - \frac{z_i z_j D_i^{L} D_j^{L} C_i}{\sum_{k=1}^{N} \left(z_k^2 D_k^{L} C_k \right)} \tag{3.3}$$

$$\boldsymbol{D}_{ij}^{T} = \delta_{ij} D_i^{T} - \frac{z_i z_j D_i^{T} D_j^{T} C_i}{\sum_{k=1}^{N} \left(z_k^2 D_k^{T} C_k \right)}$$

where $\boldsymbol{D}_{ij}^{L}$ and $\boldsymbol{D}_{ij}^{T}$ are the matrices of longitudinal and transverse cross-coupled dispersion coefficients, respectively, with D_i^{L} being the longitudinal component and D_i^{T} being the transverse component of the dispersion coefficient for species i in its liberated state (i.e., "self-dispersion"). δ_{ij} is the Kronecker delta which has a value of 1 (if $i=j$) or 0 (if $i \neq j$).

3.3 Two-dimensional Multicomponent Transport Model

The governing flow equations in a two-dimensional domain under steady-steady conditions can be described as (Cirpka et al., 1999a):

$$\nabla \cdot \left(\boldsymbol{K} \nabla h \right) = 0$$

$$\nabla \cdot \left(\frac{1}{\boldsymbol{K}} \nabla \psi \right) = 0 \tag{3.4}$$

in which, h and ψ are the hydraulic head and the stream-function, and $\boldsymbol{K}$ is the tensor of hydraulic conductivity. We solve Eq. 3.4 numerically by bilinear finite elements on a rectangular coordinate system. For the hydraulic head problem, constant head boundaries (Dirichlet) are applied both at the inlet and at the outlet, and no-flow boundary (Neumann) conditions are considered at the top and bottom of the 2-D domain. The steady-state stream-

function equation is solved applying fixed values at the top and bottom boundaries. The difference between these values equals the volumetric flux through the domain.

In order to solve the multicomponent transport problem for different ionic species, we construct streamline-oriented grids based on the results of the flow simulations and solve the advective and dispersive terms with the finite volume scheme described by Cirpka et al. (1999b), which minimizes artificial mixing. We restrict our analysis to steady-state transport problems for which the governing multicomponent equations read as:

$$\boldsymbol{v} \cdot \nabla C_i - \nabla \cdot \left(\sum_{j=1}^{N} \boldsymbol{D}_{ij} \nabla C_j \right) = 0 \tag{3.5}$$

This system of equations is solved on the generated streamline-oriented grid using the direct solver UMFPACK implemented in MATLAB (Davis and Duff, 1997). We consider a constant concentration boundary at the inflow and zero dispersive-flux conditions at the remaining boundaries. The simulation domain is 100 cm × 12 cm. It represents the saturated zone of our 2-D experimental setup and was discretized into 100 × 240 cells (Δx=1 cm, Δz=0.5 mm).

The electrostatic coupling between the dispersive fluxes of different ionic species, introduces non-linearities in the multicomponent transport equations. Thus, we implement an iterative scheme to linearize the set of non-linear transport equations within a Picard loop, applying the direct matrix solver in each iteration. The computational steps are summarized in Table 3.1. The iteration starts with an initial guess neglecting the cross-coupling term (Eq. 3.3) between different species and considering the transport identical to uncharged compounds (i.e., off-diagonal elements of $\boldsymbol{D}_{ij}$ as zero). In *step 1*, the matrix of the cross-coupling dispersion coefficients is determined for every cell of the heterogeneous domain, discretized on the generated streamline-oriented grid. Successively (*step 2*), we calculate the mobility matrix ($\boldsymbol{Mmob}_i$) describing the divergence of advective-dispersive fluxes for each compound, using the finite volume method (Cirpka et al., 1999b). The parameters determined in *step 1* and *step 2* are used to calculate the concentration vector for a charged species *i* in *step 3*, where $\boldsymbol{b}_i$ denotes the right-hand side vector resulting from the inlet boundary conditions. The iterative process continues until the *norm* of the differences between the concentration vectors in two consecutive iterations converges to a user-defined threshold value, ε ($=1\times10^{-15}$ in our simulations).

Table 3.1: Algorithm for the solution of the steady-state multicomponent transport problem by Picard iteration.

while	$norm\left(\boldsymbol{C}_i^{\kappa+1} - \boldsymbol{C}_i^{\kappa}\right) > \varepsilon$; i = 1, 2, 3,..., N	
	Step 1:	$\boldsymbol{D}_{ij}^{L,\kappa} = \delta_{ij} D_i^L - \frac{z_i z_j D_i^L D_j^L C_i^{\kappa}}{\sum_{k=1}^{N}\left(z_k^2 D_k^L C_k^{\kappa}\right)}$
	Step 1:	$\boldsymbol{D}_{ij}^{T,\kappa} = \delta_{ij} D_i^T - \frac{z_i z_j D_i^T D_j^T C_i^{\kappa}}{\sum_{k=1}^{N}\left(z_k^2 D_k^T C_k^{\kappa}\right)}$
	Step 2:	*Calculate* $\boldsymbol{Mmob}_i^{\kappa}$
	Step 3:	*Solve for the concentration:* $\boldsymbol{C}_i^{\kappa} = \left(\boldsymbol{Mmob}_i^{\kappa}\right)^{-1} \boldsymbol{b}_i$
	Step 4:	*Next iteration:* $\kappa = \kappa + 1$
end		

The hydrodynamic dispersion coefficients for each ion were parameterized following the non-linear compound-specific relationship developed to interpret the multitracer experiments of Chiogna et al. (2010) and Rolle et al. (2012) and inspired by the earlier statistical model of Bear and Bachmat (1967):

$$D_i = D_i^P + D_i^{aq}\left(\frac{Pe^2}{Pe + 2 + 4\delta^2}\right)^{\beta} \tag{3.6}$$

in which D_i^P is the pore diffusion coefficient, defined by the ratio of aqueous diffusion coefficient (D_i^{aq}) and the tortuosity of the porous medium and approximated as $D_i^P \approx \theta D_i^{aq}$, where θ is the porosity. *Pe* is the grain Péclet number: $Pe = vd / D_i^{aq}$, where v is the seepage velocity and d is the grain size diameter of the porous material. δ expresses the ratio between the length of a pore channel and its hydraulic radius, and β is an empirical exponent taking into account the incomplete mixing at the pore scale. Values of δ=6.2 and β=0.5 were determined for the transverse dispersion coefficient with an excellent agreement between laboratory experiments and numerical pore-scale simulations (Rolle et al., 2012; Hochstetler et al., 2013). As done in a recent study (Rolle et al., 2013b), we use the same parameterization for the local longitudinal dispersion coefficient (with same δ and β=0.89, derived from transient pore-scale simulations) even though for steady-state transport problems, as considered in this study, D_i^L is not a sensitive parameter.

In heterogeneous porous media the average grain size diameter, d, used to calculate the mechanical dispersion term is spatially variable and directly linked to the hydraulic conductivity at a given location. As proposed in previous studies on transport in heterogeneous

formations (e.g., Chiogna et al., 2011; Eckert et al., 2012), we express the relationship between the average grain size and the hydraulic conductivity using the approximation of Hazen (1892):

$$d \approx 0.01\sqrt{K} \tag{3.7}$$

This approach results in an accurate representation of spatially variable local dispersion coefficients that is required to describe solute transport in heterogeneous flow fields. As outlined above (Eq. 3.3 and Table 3.1), for multicomponent transport problems the local dispersion coefficients are used to calculate the cross-coupled dispersive fluxes.

In order to test the validity of our 2-D multicomponent transport code, we compared with 1-D transient multicomponent simulations using PHREEQC (Parkhurst and Appelo, 1999; Appelo and Wersin, 2007). Such comparison is possible in a homogeneous medium since the transport equation in such a 2-D domain under steady-state conditions and in absence of significant longitudinal dispersive fluxes is mathematically equivalent to a 1-D transient diffusive/dispersive problem (e.g., Maier and Grathwohl, 2006; Van Breukelen and Rolle, 2012). The simulations were performed for two different scenarios at a flow velocity of 1.5 m/day (Rolle et al., 2013a): transport of (*i*) NaCl (1:1 electrolyte, continuously injected through the two central inlet ports of the setup) in pure ambient water, and (*ii*) $MgCl_2$ (1:2 electrolyte, continuously injected through the two central inlet ports of the setup) in an ambient solution of NaBr (1:1 electrolyte). In both scenarios we found an excellent agreement between the concentration profiles obtained with the 2-D steady-state solution and with the 1-D transient multicomponent PHREEQC solution. We also compared the different components of the transverse fluxes for the ionic species at the outlet of the flow-through domain as illustrated in Fig. 3.1. According to Eq. 3.1, the total flux component in the transverse direction can be decomposed into the additive contribution of a purely dispersive flux (J_i^{dis}) and of an electrochemical migration flux (J_i^{mig}):

$$J_i = J_i^{dis} + J_i^{mig} \tag{3.8}$$

Fig. 3.1a and Fig. 3.1b represent the total fluxes, J_i for the transport of NaCl in pure water, and for the transport of $MgCl_2$ in an ambient/background solution of buffer electrolyte (NaBr), respectively. The purely dispersive components (J_i^{dis}) are shown in Fig. 3.1c and 3.1d, whereas the contribution due to the electrical gradients (J_i^{mig}) are presented in Fig. 3.1e and 3.1f.

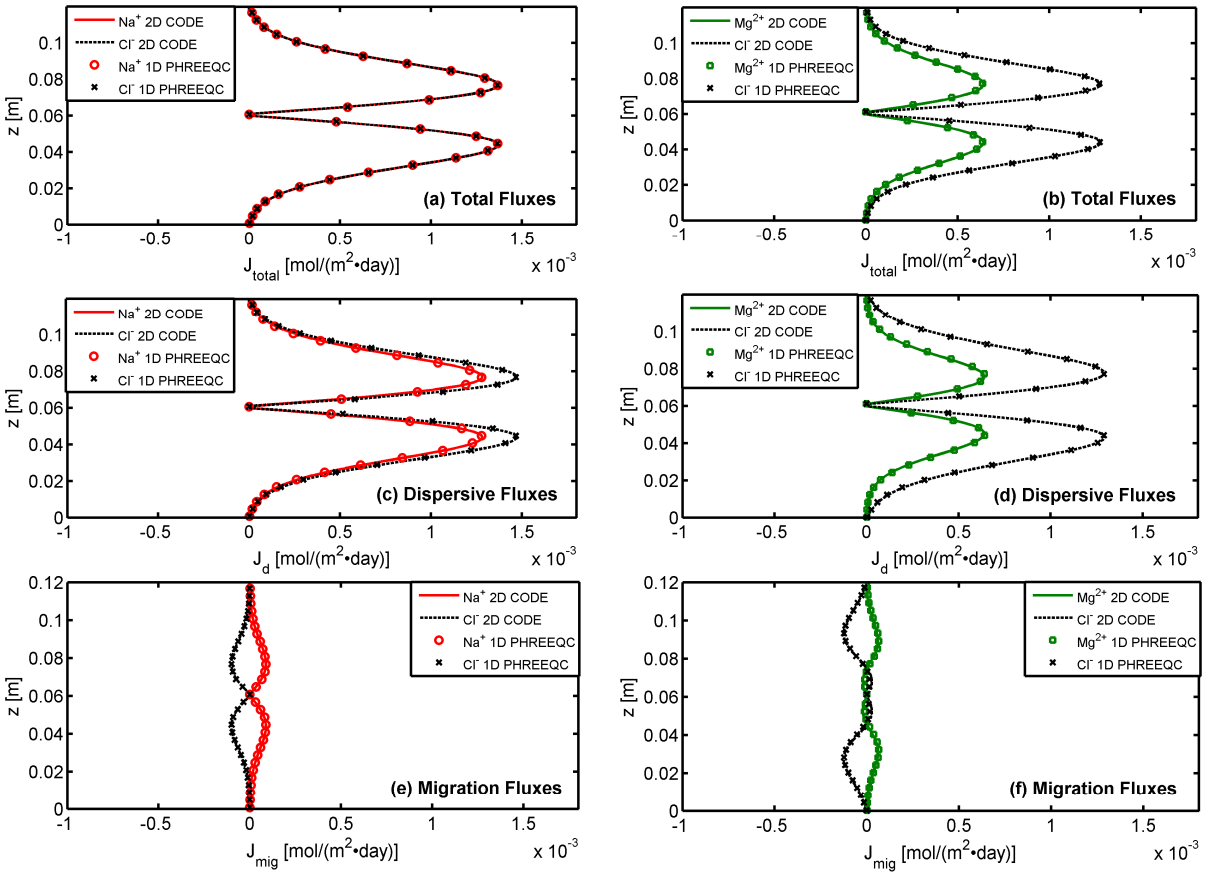

Figure 3.1. Multicomponent ionic fluxes in the transverse direction at the end of the flow-through domain: Total fluxes (a, b); Dispersive fluxes (c, d); Electrochemical migration fluxes (e, f), for transport of NaCl in pure water (a, c, and e), and transport of $MgCl_2$ in NaBr solution (b, d, and f). The lines represent the values calculated with the 2-D transport code developed in this study and the symbols are the results of 1-D multicomponent simulations using PHREEQC.

The code was also validated with experimental data in homogeneous porous media (Rolle et al., 2013). The simulation results showed a good agreement with the measured data. The data could also be reproduced with the multidimensional transport codes MIN3P (Mayer et al., 2002) and CrunchFlow (Steefel, 2009) which also have the capability of solving multicomponent ionic transport (results not shown). The validated 2-D code described above was used to interpret the results of the experiments in heterogeneous porous media performed in this study and illustrated in the following section, for which a 1-D model representation would not be adequate to capture the main features of multicomponent ionic transport in the spatially variable flow fields.

3.4 Experimental Setup

The experiments were performed in the same flow-through setup used in our previous study (Rolle et al., 2013a). Therefore, here we only briefly summarize the main features of the experimental system. The setup consists of a quasi 2-D flow-through chamber with inner dimensions of 100 cm length, 19 cm height and 1 cm width (Fig. 3.2a and 3.2b). The chamber was equipped with 24 equally spaced (5 mm distance) ports both at the inlet and at the outlet, allowing high-resolution sampling of the injected tracers. All ports were made of Alltech pierced rubber septa and the injection needles were directly connected to Fluran HCA pump tubings (Ismatec, Glattbrugg, Switzerland) with inner diameter of 0.64 mm. In order to establish steady-state flow conditions, two high-precision peristaltic pumps (Ismatec IPC-N24, Ismatec, Glattbrugg, Switzerland) were used at the inlet and outlet of the flow-through chamber. The experiments were carried out in a temperature-controlled room at 20 °C.

The tank was filled with glass beads by following a wet-packing procedure, in which the water level was always kept above the upper limit of the porous medium to avoid air entrapment within the water-saturated domain (Haberer et al., 2012). The experiments were carried out in two distinct heterogeneous porous media. In the first setup (Fig. 3.2a), denoted as *HET A*, a low-permeability inclusion made of fine glass beads (0.25-0.30 mm, Sartorius AG, Göttingen, Germany) was embedded into a more permeable matrix with glass beads of 1.00-1.50 mm (Sartorius AG, Göttingen, Germany). The length and thickness of the inclusion were 30 cm and 4 cm respectively, and it was placed directly in line with the center of plume's injection. The distance of the fine material zone from the inlet was 35 cm (Fig. 3.2a). In the second experimental setup (*HET B*, Fig. 3.2b), two high-conductivity inclusions, made of coarse glass beads (2.00-2.50 mm, Sartorius AG, Göttingen, Germany), were embedded into the same matrix (glass beads of 1.00-1.50 mm). The coarse-grained zones were placed 1.5 cm away from the center-line of plume's injection and their thickness was 1 cm. The length of the inclusions was 20 cm and the distance from the inlet was 70 cm (Fig. 3.2b).

Fig. 3.2c and Fig. 3.2d depict the hydraulic conductivity distribution and the flow-lines computed with the model. The variation of local velocities is shown in Fig. 3.2e and Fig. 3.2f for *HET A* and *HET B*, respectively. Fig. 3.2g and Fig. 3.2h show the mixing behavior of the steady-state plumes in the two heterogeneous flow-through systems using the flux-related dilution index, $E_Q(x)$ (Rolle et al., 2009; Chiogna et al., 2012) as metric of mixing:

$$E_Q(x) = \exp\left(-\int_{\Omega} p_Q(\boldsymbol{x}) \ln(p_Q(\boldsymbol{x})) q_x(\boldsymbol{x}) d\Omega \right) \qquad (3.9)$$

where $q_x=v\theta$ is the specific discharge, Ω is the cross-sectional area, θ is the porosity, and p_Q is the flux-related probability density function:

$$p_Q(\boldsymbol{x}) = \frac{C_i(\boldsymbol{x})}{\int_{\Omega} C_i(\boldsymbol{x}) q_x(\boldsymbol{x}) d\Omega} \tag{3.10}$$

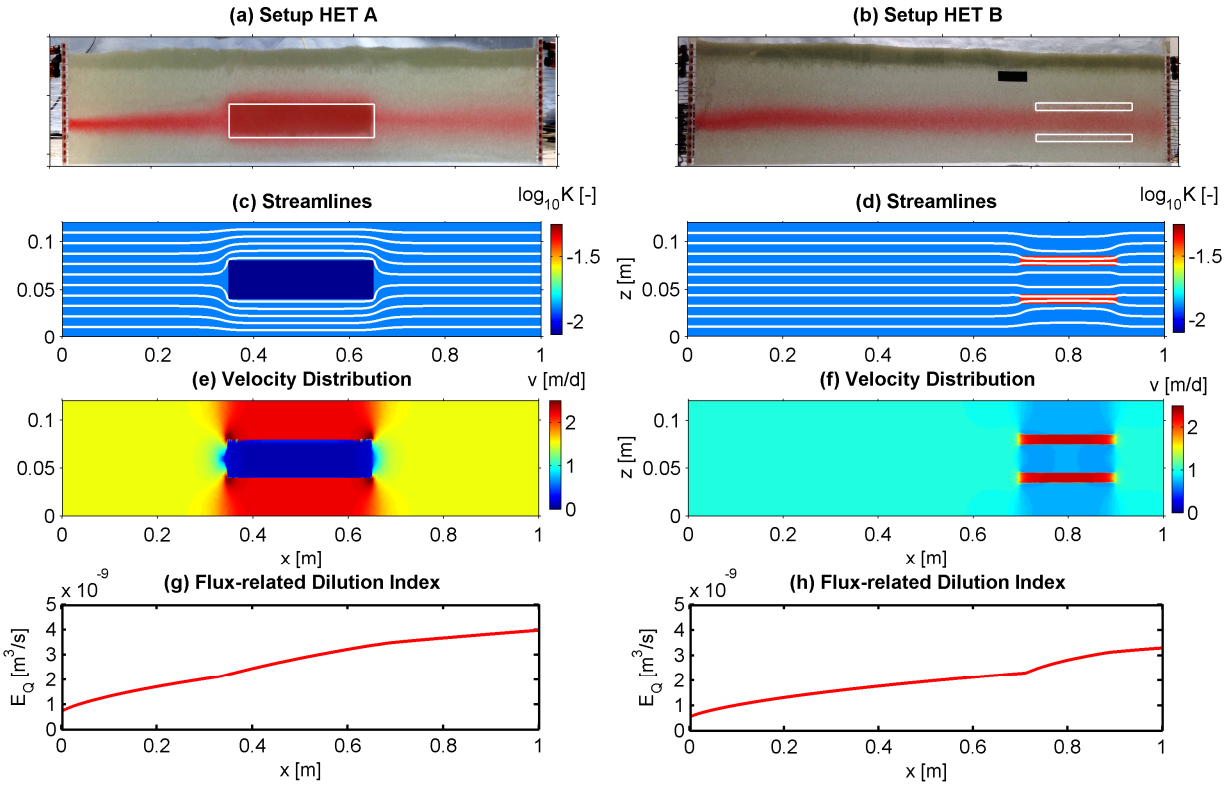

Figure 3.2. Experimental setups with steady-state color tracer (New Coccine) plumes (a, b); computed streamlines and hydraulic conductivities (c, d); velocity distribution (e, f); and calculated flux-related dilution index of the color tracer (with D_{aq}=3.43×10^{-10} m^2/s estimated after Worch, 1993). The flow direction is from left to right.

$E_Q(x)$ quantifies the distribution of the mass flux of a dissolved species over the volumetric water flux at a given longitudinal location x and refers to the color tracer experiments performed to visualize the flow and transport patterns in the flow-through systems. After the ionic experiments, a color tracer (New Coccine solution, 90 mg/L; CAS: 2611-82-7) was injected through the two central inlet ports and a steady-state plume was established in order to observe the shape of the plume in the heterogeneous setups (Fig. 3.2a and Fig. 3.2b). The trend of $E_Q(x)$ in Fig. 3.2g and Fig. 3.2h shows a change of the slope at the locations of the inclusions, indicating the variation of mixing properties due to flow focusing and de-focusing in these zones with different grain sizes and permeability.

The transport experiments were performed, by injecting tracer electrolyte solutions through the central injection ports (port 11 and 12, at 5.5 cm and 6 cm from the bottom, respectively) and

ambient solutions through the remaining ports, after a steady-state flow condition was achieved in the flow-through systems. Strong 1:1 (NaCl) and 1:2 ($MgCl_2$) electrolytes were used as tracer solutions, and Milli-Q water (Millipore, MA, USA) or a 1:1 electrolyte (NaBr) were used as ambient solutions. When the plumes reached steady-state conditions samples were collected at all 24 outlet ports and the ion concentrations were measured by ion-chromatography (Dionex Dx-120, Fisher Scientific, Schwerte, Germany). The electrolyte concentrations used in the different experiments were in the range of 0.4 mM to 1.70 mM. The flow-through experiments were performed at an average linear horizontal flow velocity of 1.5 m/day for *HET A* and 1.0 m/day for *HET B*. The parameters summarizing the flow and transport properties of the experimental setups are reported in Table 3.2.

Table 3.2: Summary of flow and transport parameters in the two heterogeneous experimental setups (*HET A* and *HET B*).

Experimental settings and hydraulic properties	**Value**
Tank inner dimensions ($L \times H \times W$) [cm]	100×19×1
Number of inlet/outlet ports used	23/24
Port spacing [mm]	5
Fine grain diameter, low-*K* inclusion in *HET A* [mm]	0.25-0.30
Intermediate grain diameter, porous matrix [mm]	1.00-1.50
Coarse grain diameter, high-*K* inclusions in *HET B* [mm]	2.00-2.50
Hydraulic conductivity, low-*K* inclusion in *HET A* [m/s]	6.14×10^{-4}
Hydraulic conductivity, porous matrix [m/s]	1.27×10^{-2}
Hydraulic conductivity, high-*K* inclusions in *HET B* [m/s]	4.12×10^{-2}
Average horizontal flow velocity [a] [m/day]	1.5; 1.0
Average porosity [-]	0.41
Diffusion coefficients	D^{aq} [m^2/s][b]
Na^+	1.20×10^{-9}
Mg^{2+}	0.63×10^{-9}
Cl^-	1.81×10^{-9}
Br^-	1.86×10^{-9}

[a] the first value is for *HET A* and the second one is for *HET B*

[b] values from Lasaga (1998) at 18°C, and corrected for temperature and viscosity changes of the experimental conditions at 20°C

3.5 Results and Discussion

For each heterogeneous setup, *HET A* and *HET B*, two different flow-through experiments were performed: (*i*) transport of NaCl (1:1 electrolyte) in Milli-Q water, and (*ii*) transport of $MgCl_2$ (1:2 electrolyte) in NaBr (1:1 electrolyte) buffer electrolyte solution. The results obtained from these experiments are interpreted with the 2-D multicomponent numerical model presented in section 3.3.

3.5.1 Flow-through experiments with a low-permeability inclusion (HET A)

In this flow-through setup (*HET A*, Fig. 3.2a) we used a well-defined low-permeability zone (K=6.14×10^{-4} m/s) embedded into a higher permeability matrix (K=1.27×10^{-2} m/s); this leads to the divergence of the streamlines around the low-permeability inclusion (Fig. 3.2c). In the first experiment, a 1:1 electrolyte solution (0.80 mM NaCl) and Milli-Q water were continuously injected through the two central and the remaining inlet ports, respectively. The steady-state concentration profiles of the cation and of the anion were measured at the outlet of the flow-through domain. Fig. 3.3 depicts the concentration distribution and the vertical profiles of Na^+ and Cl^- at three different cross sections (20, 50, and 80 cm from the inlet) simulated with the 2-D multicomponent model.

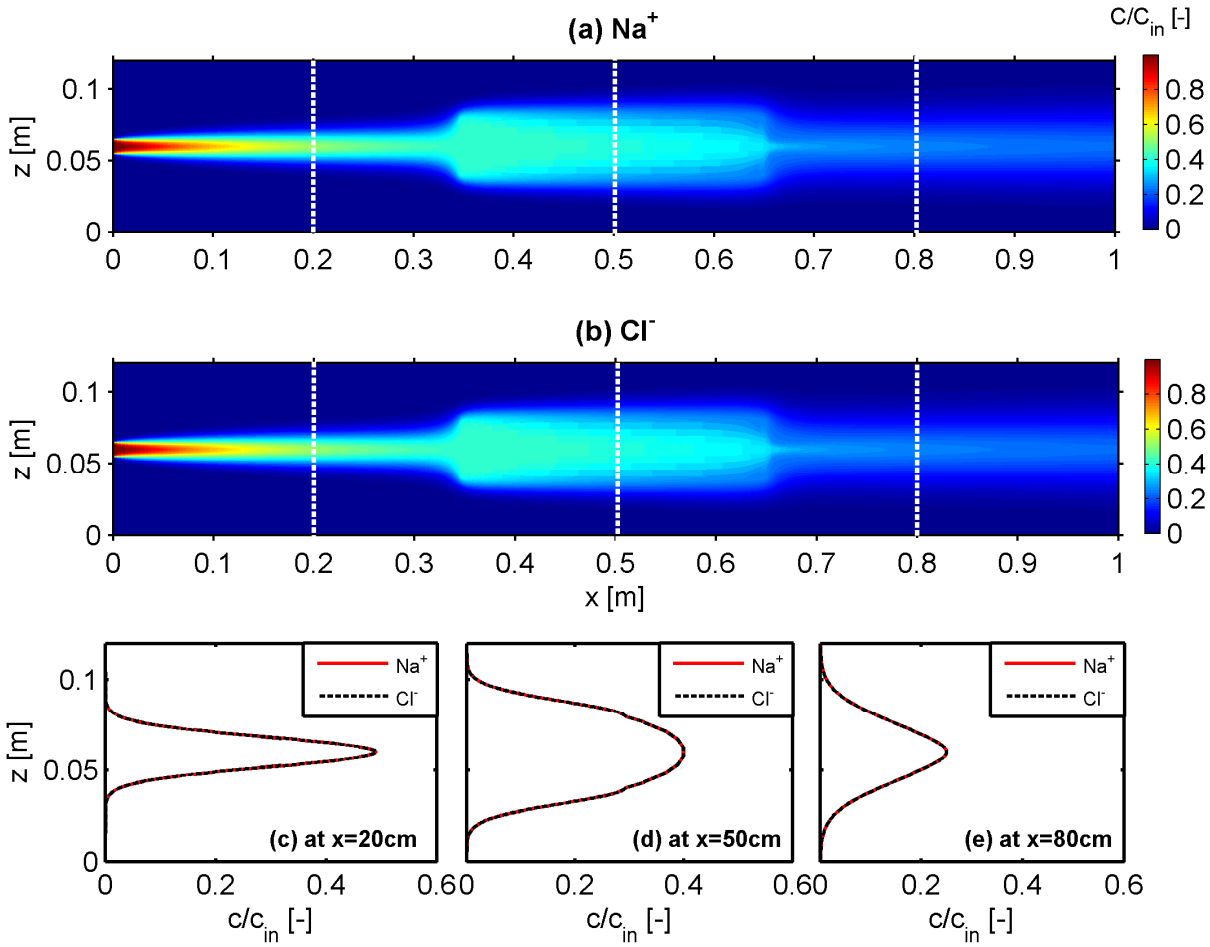

Figure 3.3. 2-D concentration distributions (a and b), and cross-sectional profiles at 20 cm (c), 50 cm (d), and 80 cm (e) from the inlet of the flow-through domain (*HET A*), computed for the case of NaCl transport in Milli-Q water.

The plumes of both cation and anion show more spreading near the low-permeability inclusion (Fig. 3.3a and 3.3b). This behavior is, in fact, induced from the bypassing of flow lines around the low-conductivity zone (Fig. 3.2c), due to the permeability contrast (K ratio =0.05) between

the two different grain sizes. Downgradient, the streamlines become closer and the computed plumes exhibit smaller spreading compared to the central region. These characteristics are also illustrated by the concentration profiles at different cross sections. At 20 cm from the inlet, the profiles have a Gaussian shape (Fig. 3.3c) since the plume is travelling in a homogeneous medium whereas the ionic profiles are distorted and show more spreading in the center of the setup due to the presence of the low-*K* inclusion (Fig. 3.3d). The profiles of sodium and chloride have a more regular shape at the cross-section after the inclusion (*x*=80 cm, Fig. 3.3e). The comparison between the measured and the computed profiles of the ions at the outlet of the flow-through system are shown in Fig. 3.4.

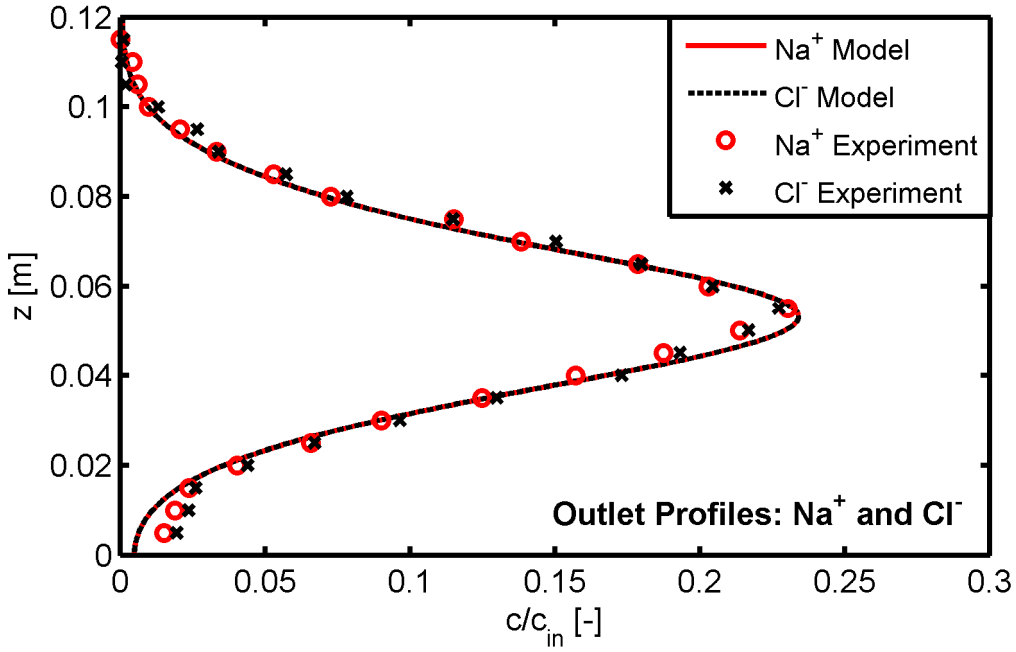

Figure 3.4. Transverse concentration profiles at the outlet of the flow-through system (*HET A*) for transport of NaCl in Milli-Q water: measured cation and anion concentrations (symbols) and modeling results (lines).

The cation and anion appear to travel together in spite of having significantly different self-diffusion (and thus self-dispersion) coefficients ($D^{aq}_{Na^+} = 1.20 \times 10^{-9}$ m^2/s and $D^{aq}_{Cl^-} = 1.81 \times 10^{-9}$ m^2/s). Their concentration profiles at the outlet overlap and a very good agreement exists between the measured concentrations and the outcomes of the purely forward multicomponent simulations (i.e., without any fitting parameters). The observed behavior is due to the existence of Coulombic interactions, which lead to the cross-coupling of the transverse dispersive fluxes, between the positively and the negatively charged species. These Coulombic effects for Na^+ and Cl^- can be effectively visualized by mapping the different contributions of transverse dispersive fluxes (Fig. 3.5).

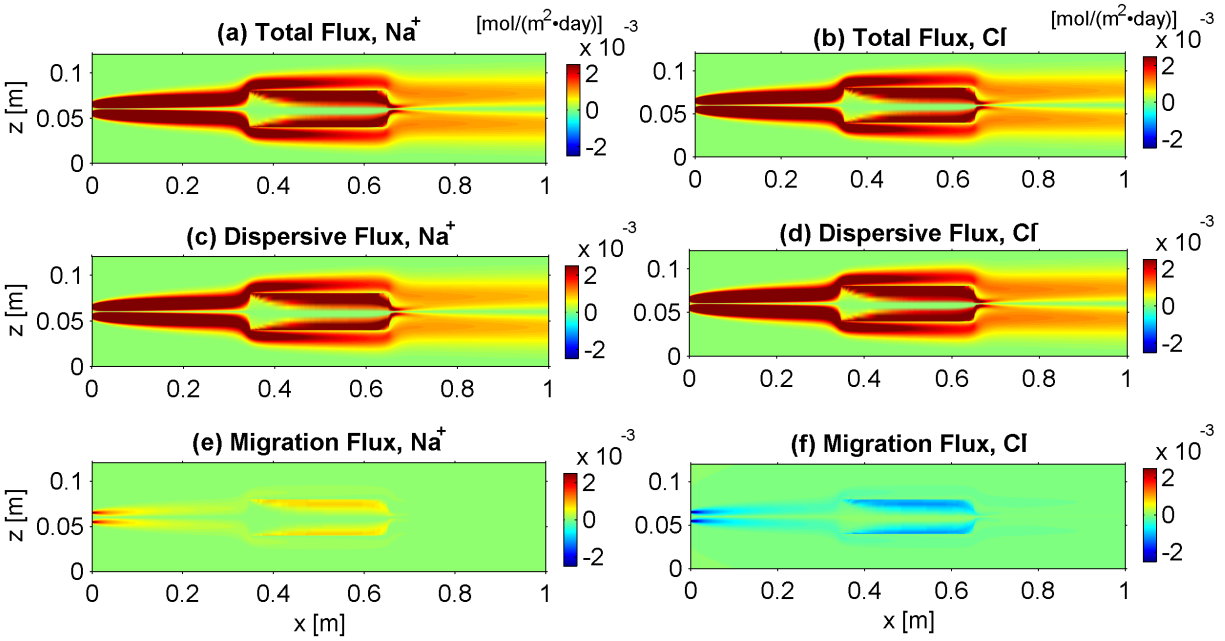

Figure 3.5. Maps of multicomponent ionic transverse fluxes: Total fluxes (a, b); Dispersive fluxes (c, d); Electrochemical migration fluxes (e, f), for transport of NaCl in Milli-Q water (*HET A*). Note that the direction from the core to the fringe of the plume is considered positive for the calculated fluxes.

Fig. 3.5a and Fig. 3.5b show that the total transverse flux (J_i) has exactly the same distribution for both Na^+ and Cl^-. However, these identical total fluxes have different contributions of the dispersive and the electrochemical migration terms (Eq. 3.8). In fact, chloride has larger values of the dispersive flux component (J_i^{dis}) compared to Na^+ (Fig. 3.5c and Fig. 3.5d) since it has higher diffusion and transverse dispersion coefficients. Fig. 3.5e and Fig. 3.5f map the electrochemical migration fluxes (J_i^{mig}) for both the cation and the anion. These electrochemical coupling components have the same distribution but opposite signs: positive for Na^+ and negative for Cl^-. Thus, a positive contribution for Na^+ (Fig. 3.5e) and a negative contribution for Cl^- (Fig. 3.5f) facilitate, respectively, the enhancement of the transverse flux for the slower species, Na^+, and the reduction of the transverse flux for the faster ion, Cl^-. Hence, the electrostatic interactions couple the two oppositely charged species and lead to an equal transverse displacement, which allows attaining identical vertical concentration profiles for both ions at the outlet (Fig. 3.4).

In the second experiment, we investigated the transport of a 1:2 electrolyte (0.44 mM $MgCl_2$) through an ambient buffer electrolyte solution (1.70 mM NaBr) in the same setup, *HET A*. Fig. 3.6 illustrates the results obtained from the multicomponent simulations. Unlike the previous experiment (i.e., transport of NaCl in Milli-Q water), the 2-D concentration distribution of the

cation and the anion injected through the central inlet ports show a dissimilar pattern (Fig. 3.6a and Fig. 3.6b). The concentration maps show that in the low-permeability inclusion, magnesium has relatively higher concentration than chloride, as can be observed from the slight color differences in Fig 3.6a and Fig 3.6b.

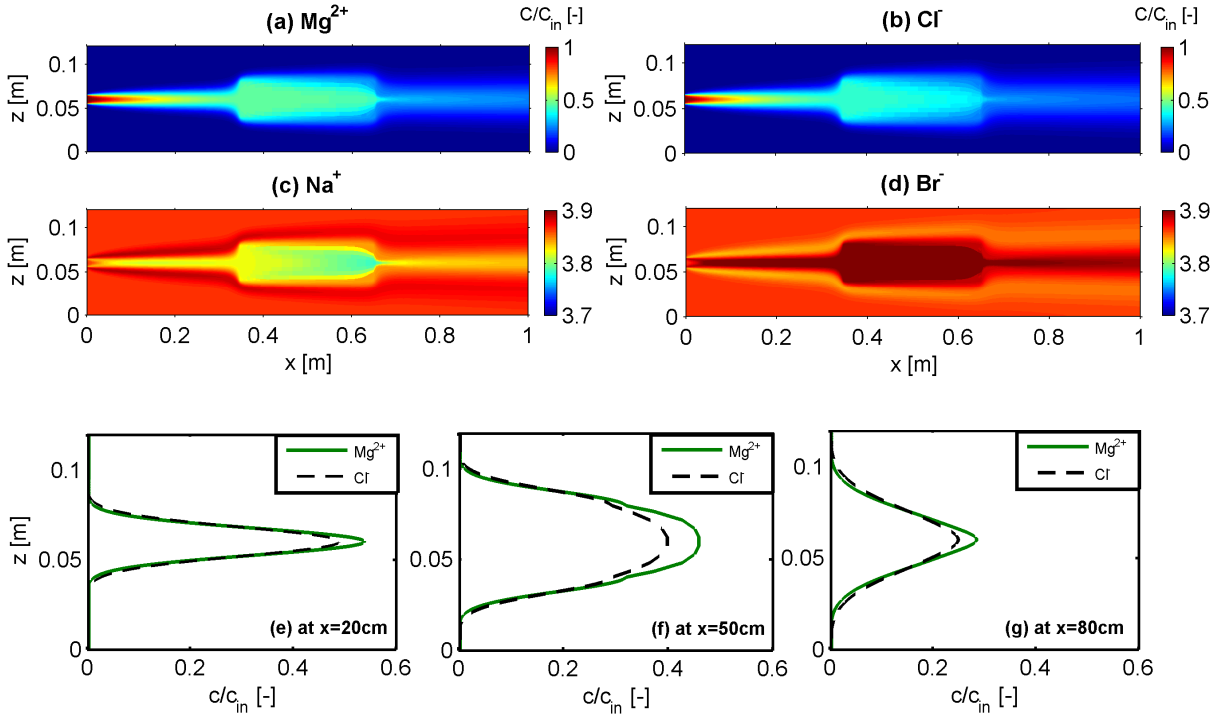

Figure 3.6. 2-D concentration distributions of Mg^{2+} (a), Cl^- (b), Na^+ (c), and Br^- (d); and cross-sectional profiles at 20 cm (e), 50 cm (f), and 80 cm (g) from the inlet of the flow-through domain (*HET A*), computed for the case of $MgCl_2$ transport in NaBr solution.

This pattern is consistent with the calculated concentration profiles at different cross sections of the flow-through chamber, for which the peak concentration of the cation, Mg^{2+}, is higher than the one of the anion, Cl^- (Fig. 3.6e-g). Interesting is also the behavior of the background electrolyte (NaBr) solution. In fact, Na^+ shows comparatively smaller concentrations than Br^- in the core of the plume (Fig. 3.6c and Fig. 3.6d), although they were injected at a uniform concentration throughout the inlet boundary.

The measured concentration profiles of the ionic species at the outlet of the flow-through chamber and the results of the multicomponent simulations are reported in Fig. 3.7. From Fig. 3.7a, it is evident that Mg^{2+} and Cl^- have clearly distinct profiles, with Mg^{2+} having a higher peak and smaller spreading than Cl^-.

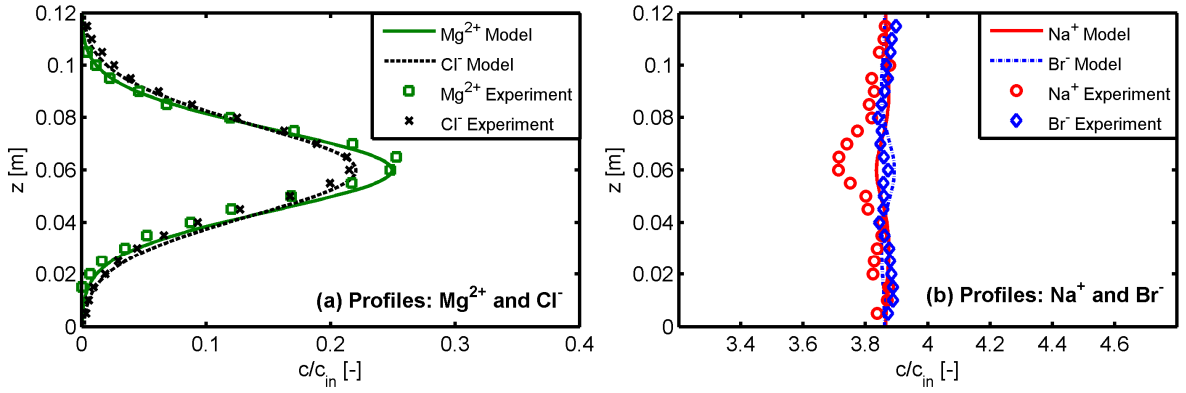

Figure 3.7. Transverse concentration profiles at the end of the flow-through system (*HET A*) for transport of $MgCl_2$ in NaBr solution: measured cation and anion concentrations (symbols) and modeling results (lines).

The behavior observed at the outlet depends on the Coulombic interactions between the charged species. Such effects can be rationalized and effectively visualized by mapping the fluxes of the different ions. For the sake of brevity, in Fig. 3.8 we present only the electrochemical migration component (J_i^{mig}) of the total fluxes of the cations and anions in the tracer and buffer electrolyte solutions.

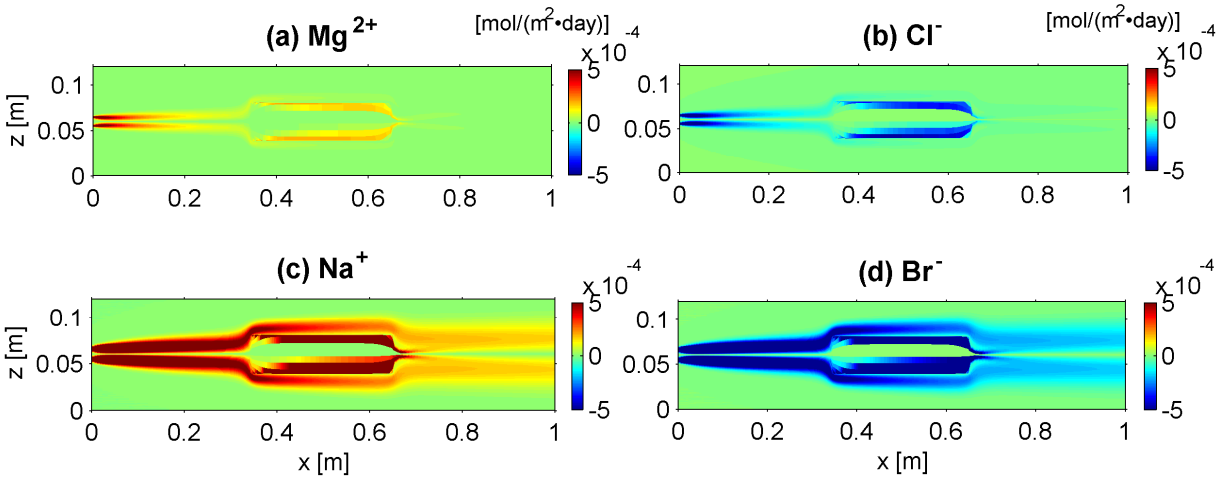

Figure 3.8. Transverse electrochemical migration fluxes of Mg^{2+} (a), Cl^- (b), Na^+ (c), and Br^- (d) during transport of $MgCl_2$ in NaBr solution in *HET A* setup. The direction from the core to the fringe of the plume is considered positive for the calculated fluxes.

The outward, positive migration flux component of Na^+ (Fig. 3.8c) and inward, negative component of Br^- displace these ions, respectively, towards the fringe (Na^+) and towards the centerline (Br^-) of the plume. This induces a relative increase of Br^- concentration in the plume's core and a decrease in the plume's fringe and an opposite effect for Na^+. Due to the higher concentration of the ambient buffer electrolyte solution (approximately fourfold), the

electrochemical gradients of Mg^{2+} and Cl^- injected in the central ports are almost suppressed by counter balancing the charge differences with the vertical displacement of background ions (Na^+ and Br^-). The electrochemical migration flux components of Mg^{2+} and Cl^- (Fig. 3.8a and Fig. 3.8b) are significantly smaller than those of the background ionic species (Na^+ and Br^-; Fig. 3.8c and Fig. 3.8d). Therefore, the displacement of Mg^{2+} and Cl^- is dominated by the dispersive flux components. This explains the differences in the measured concentration profiles of these ions whose displacement approaches the one determined by their self-diffusion and self-dispersion coefficients.

3.5.2 Flow-through experiments with high-permeability inclusions (HET B)

The experiments mentioned in the previous section were also carried out in the second heterogeneous setup, *HET B* (Fig. 3.2b), where two high-permeability inclusions (K=4.12×10^{-2} m/s) were embedded into a matrix of lower hydraulic conductivity (K=1.27×10^{-2} m/s). Fig. 3.9 reports the modeling results for the transport of 1:1 electrolyte (NaCl) in Milli-Q water.

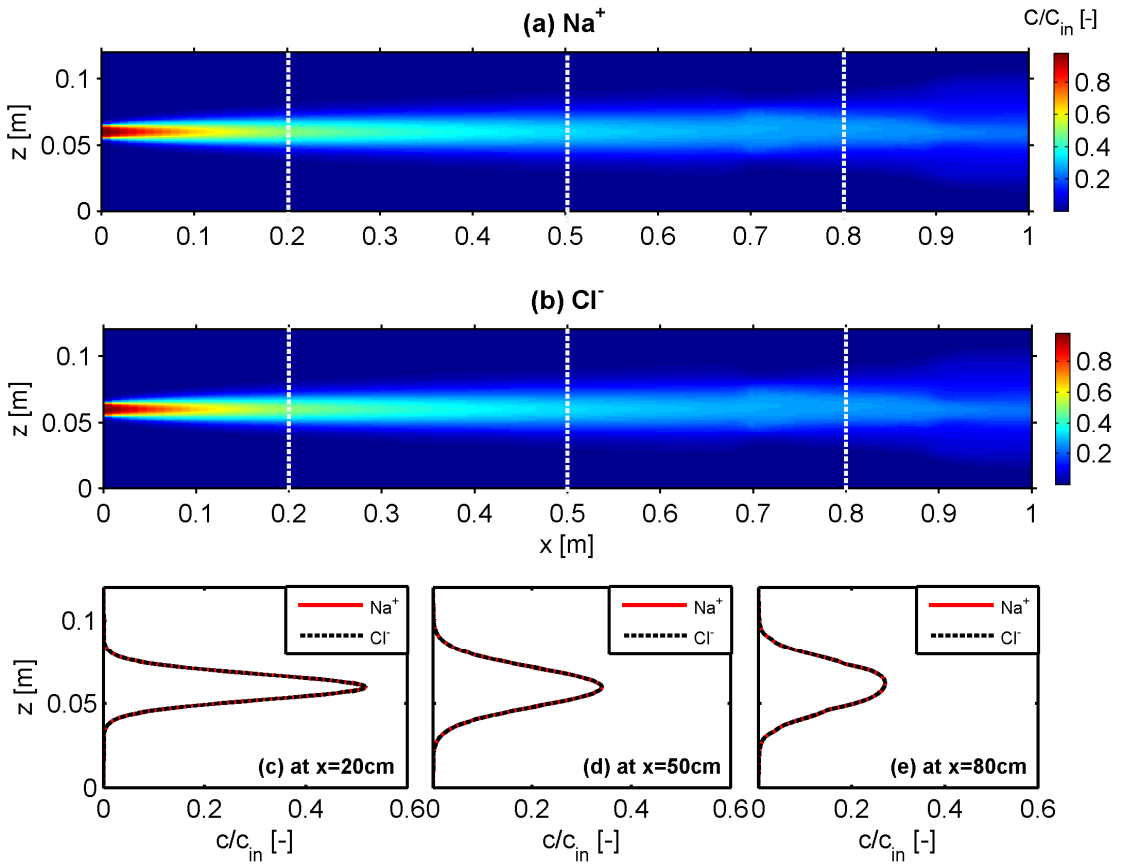

Figure 3.9. 2-D concentration distributions (a and b), and cross-sectional profiles at 20 cm (c), 50 cm (d), and 80 cm (e) from the inlet of the flow-through domain (*HET B*), computed for the case of NaCl transport in Milli-Q water.

Upstream of the high-conductivity zones, the plume has the regular shape characteristic of transport in homogeneous porous media. As the ionic plumes approach the inclusions, they appear to spread over a larger area (Fig. 3.9a and Fig. 3.9b). Due to the permeability contrast (*K* ratio=3.24) the flow lines are focused within the high-permeability inclusions (Fig. 3.2d). Consequently, the small distance among the streamlines in the high-conductivity zones facilitates dispersive mass transfer of solute mass and enhances the transverse mixing in the fringe area of the plume. The situation is opposite along the centerline of the plume: in this zone the distance among the streamlines is larger (Fig. 3.2d) and this leads to a decrease of transverse mass exchange. These effects are also reflected in the calculated transverse profiles at different cross sections (Fig. 3.9c, 3.9d, and 3.9e). The profiles at both 20 cm and 50 cm from the inlet show a Gaussian shape whereas the computed ionic profiles directly at the high-*K* inclusion (Fig. 3.9e) show higher spreading when compared to the upstream cross sections. Fig. 3.10 illustrates the measured outlet profiles of the cation and the anion. Both Na^+ and Cl^- have a distorted and clearly non-Gaussian shape with the higher peak concentrations presenting lower transverse spreading and the lateral lower concentrations significantly more spread due to enhanced mixing in the fringe areas. Also in this setup the measurements of the outlet ports clearly show the electrochemical coupling between the two ions, which travel together. Similarly to the findings for *HET A*, also for this setup the forward multicomponent simulations show a satisfactory agreement with the experimental data.

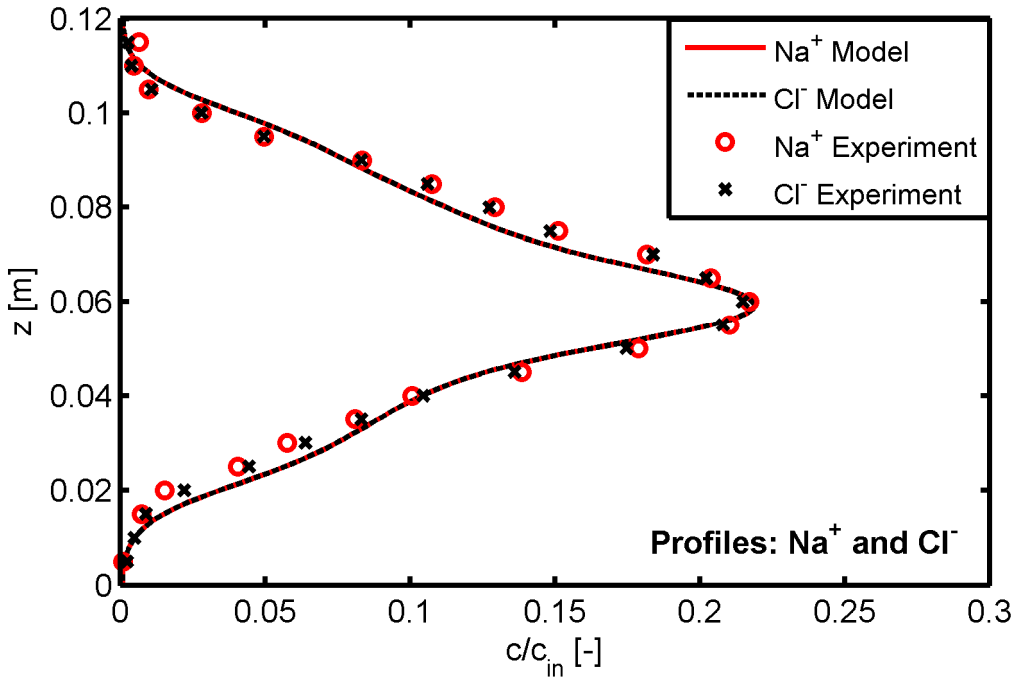

Figure 3.10. Transverse concentration profiles at the end of the flow-through system (*HET B*) for transport of NaCl in Milli-Q water: measured cation and anion concentrations (symbols) and modeling results (lines).

The different components of the transverse dispersive fluxes calculated with the 2-D code are shown in Fig. 3.11. The total and dispersive fluxes of both Na^+ and Cl^- are enhanced (higher color intensity) within the coarse-material inclusions due to flow focusing in these zones.

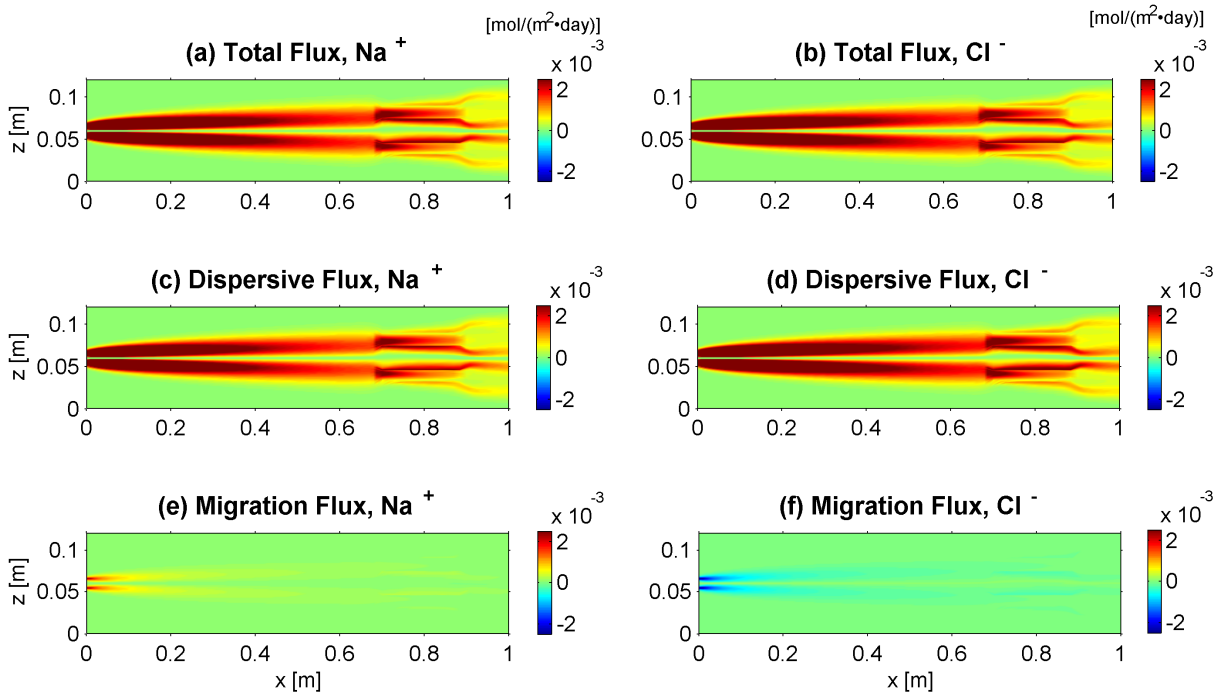

Figure 3.11. Maps of multicomponent ionic transverse fluxes: Total fluxes (a, b); Dispersive fluxes (c, d); Electrochemical migration fluxes (e, f), for transport of NaCl in Milli-Q water (*HET B*). Note that the direction from the core to the fringe of the plume is considered positive for the calculated fluxes.

Similarly to what observed in *HET A*, the positive component for Na^+ (Fig. 3.11e) and the negative component for Cl^- (Fig. 3.11f) of the electrochemical migration flux show the magnitude of Coulombic interactions between the two ions. Such effects cause the overlapping of measured outlet concentration profiles (Fig. 3.10) as well as identical distributions of the total transverse dispersive fluxes (Fig. 3.11a and Fig. 3.11b).

Fig. 3.12 and Fig. 3.13 show the modeling and experimental outcomes for the transport of $MgCl_2$ in an ambient buffer electrolyte solution (NaBr) in the heterogeneous setup *HET B*. The boundary conditions and the initial concentrations of the electrolyte solutions (0.44 mM $MgCl_2$ and 1.70 mM NaBr) where the same used in the analogous experiment performed in *HET A*. Also in this heterogeneous scenario we observed a clear separation between the profiles of Mg^{2+} and Cl^- in the peak area of the plume inside the porous medium (Fig. 3.12e-g) and at the outlet of the flow-through system (Fig. 3.13a), as well as the appearance of concentration gradients for the ions in the buffer electrolyte solution (Fig. 3.13b).

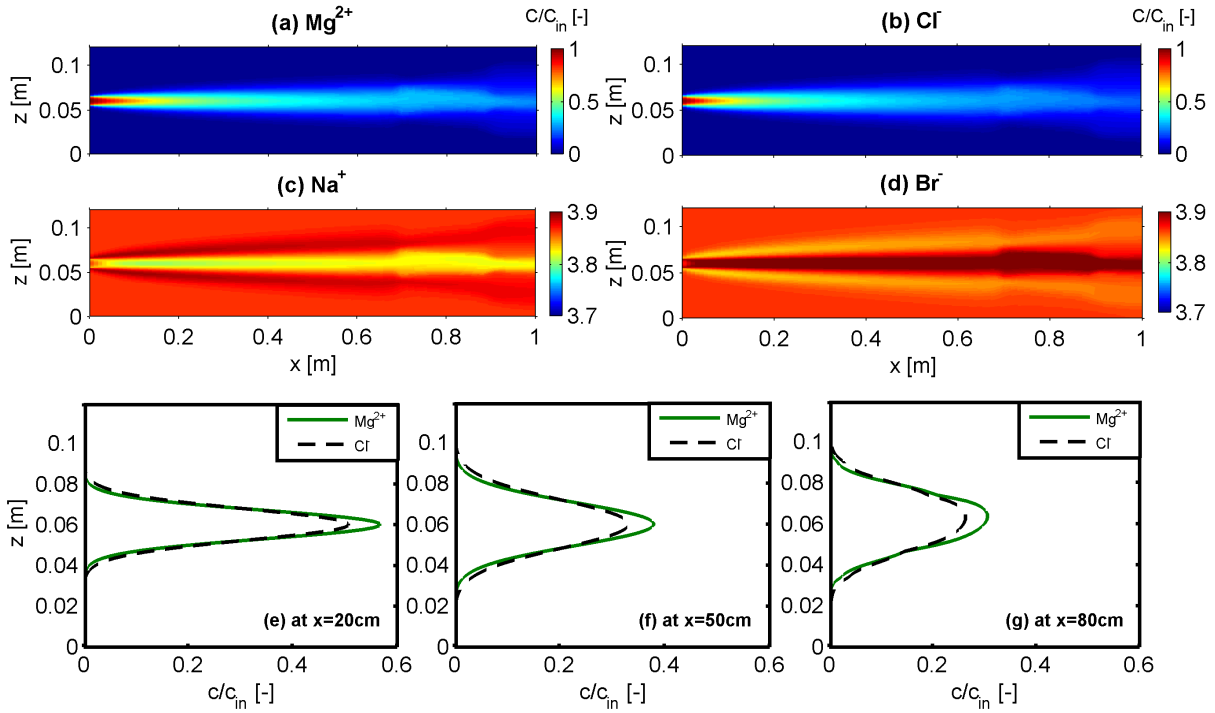

Figure 3.12. 2-D concentration distributions of Mg^{2+} (a), Cl^- (b), Na^+ (c), and Br^- (d); and cross-sectional profiles at 20 cm (e), 50 cm (f), and 80 cm (g) from the inlet of the flow-through domain (*HET B*), computed for the case of $MgCl_2$ transport in NaBr solution.

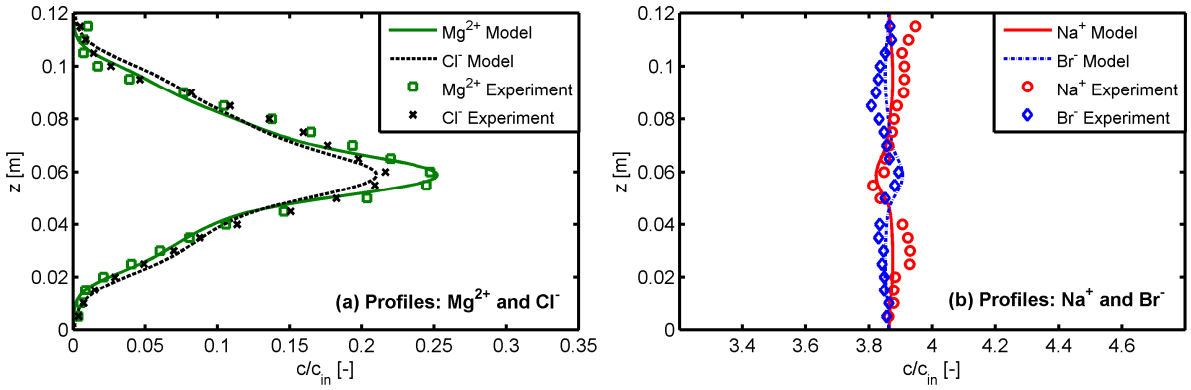

Figure 3.13. Transverse concentration profiles at the outlet of the flow-through system (*HET B*) for transport of $MgCl_2$ in NaBr solution: measured cation and anion concentrations (symbols) and modeling results (lines).

The 2-D distribution of transverse electrochemical migration fluxes (Fig. 3.14) of the different ions show similar patterns as the ones obtained in the *HET A* setup. The higher values of the electrochemical flux components for the background buffer ions show that Na^+ and Br^- provide a substantial contribution in maintaining the electroneutrality condition. Consequently, the ions in the tracer solutions (Mg^{2+} and Cl^-) are loosely coupled and can travel with diffusive/dispersive properties close to their self-diffusion and self-dispersion coefficients.

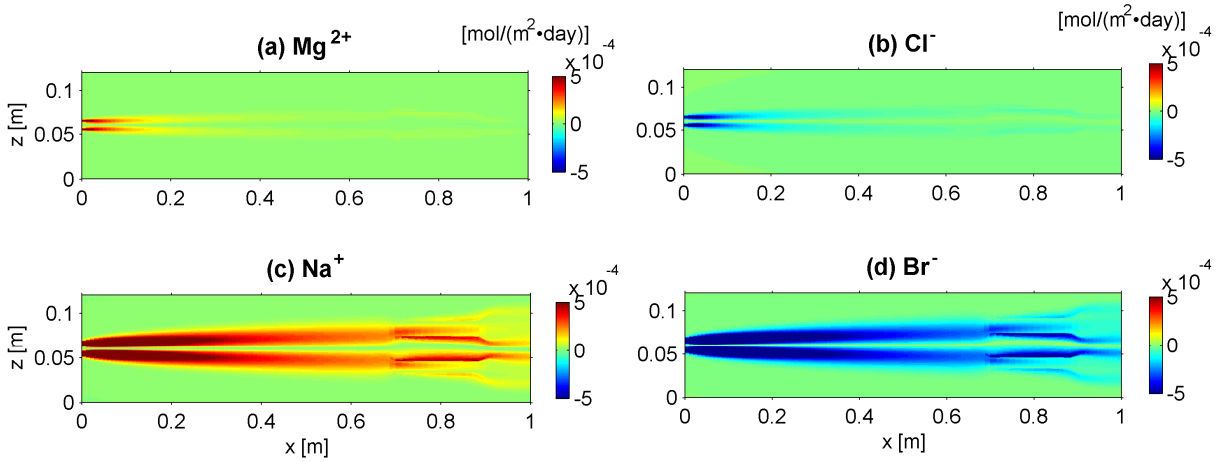

Figure 3.14. Transverse electrochemical migration fluxes of Mg^{2+} (a), Cl^- (b), Na^+ (c), and Br^- (d) in the transverse direction for transport of $MgCl_2$ in NaBr solution in the *HET B* setup. Note that the direction from the core to the fringe of the plume is considered positive for the calculated fluxes.

3.6 Summary and Conclusions

In this paper, we presented a detailed investigation of Coulombic effects during multicomponent ionic transport in spatially variable flow fields. The experiments were performed in two different heterogeneous porous media: one containing a low-conductivity inclusion in a more permeable matrix (*HET A*), and the other containing two high-conductivity inclusions in a less permeable porous matrix (*HET B*). We worked in advection-dominated flow regimes with an average flow velocity of 1.5 m/day for *HET A* and of 1.0 m/day for *HET B*.

A two-dimensional multicomponent numerical model was developed to capture the Coulombic interactions among charged species in the two-dimensional heterogeneous systems under steady-state flow and transport conditions. The model was validated in homogeneous porous media against 1-D PHREEQC simulations and previous experimental results (Rolle et al., 2013a). Successively, the 2-D model was applied to quantitatively interpret the results of the flow-through experiments in the heterogeneous porous media performed in this study. For the different experiments in both setups (*HET A* and *HET B*), a very good agreement was observed between the experimental results and the outcomes of purely forward numerical simulations. This substantiates the capability of the proposed modeling approach, based on a multicomponent ionic formulation and on the accurate and spatially variable description of

local dispersion, to precisely capture the physical processes governing the transport and the interactions of the charged species in the heterogeneous flow-through systems.

We have restricted our investigation to multicomponent steady-state conservative transport of charged species in dilute solutions. Under such conditions, our experimental and modeling findings show that microscopic Coulombic interactions occurring at the molecular scale affect the macro-scale transport and the observations at the laboratory Darcy scale. Such effects most commonly related to diffusion of charged species do not vanish under the advection-dominated flow regimes and in the heterogeneous porous media tested in this work. To improve the understanding of electrochemical migration of charged species in geologic formations under flow-through conditions future experimental and modeling studies should address the next level of upscaling from the laboratory to the field scale under natural and engineered conditions (e.g., Saichek and Reddy, 2005; Wu et al., 2012). In such larger scale setups, transport occurs in complex flow fields in which heterogeneity, anisotropy and flow topology influence mixing and, thus, affect the magnitude and the impact of Coulombic effects on the migration of charged species. Furthermore, additional work is necessary to investigate the effects of multicomponent ionic dispersion coupled to accurate description of geochemical reaction rates (e.g., Maher et al., 2006; Li et al., 2007 and 2014; Molins et al., 2012) and to processes such as sorption and ion exchange (e.g., Gvirtzman and Gorelick, 1991; Bjerg et al., 1993; Bjerg and Christensen, 1993; Appelo, 1994; Liu et al., 2011; Holden et al., 2012 and 2013).

Acknowledgments

This work was supported by the Baden-Württemberg Stiftung under the Eliteprogram for Postdocs. We thank Bernice Nisch and Annegret Walz for their assistance with the ion-chromatography measurements, and Olaf A. Cirpka and Dominik Eckert for their help in developing the multicomponent streamline-oriented code. M.R. acknowledges the support of the Marie Curie International Outgoing Fellowship (DILREACT project) within the 7th European Community Framework Programme. Finally, we would like to thank the Associate Editor (C. Steefel) and two anonymous reviewers for their constructive comments and suggestions.

References

Appelo C. A. J. (1994) Some calculations on multicomponent transport with cation exchange in aquifers. *Ground Water* **32**, 968-975.

Appelo C. A. J. and Wersin P. (2007) Multicomponent diffusion modeling in clay systems with application to the diffusion of tritium, iodide, and sodium in Opalinus Clay. *Environ. Sci. Technol.* **41**, 5002-5007.

Appelo C. A. J., Vinsot A., Mettler S. and Wechner S. (2008) Obtaining the porewater composition of a clay rock by modeling the in- and out-diffusion of anions and cations from an in-situ experiment. *J. Contam. Hydrol.* **101**, 67-76.

Appelo C. A. J., Van Loon L. R. and Wersin P. (2010) Multicomponent diffusion of a suite of tracers (HTO, Cl, Br, I, Na, Sr, Cs) in a single sample of Opalinus Clay. *Geochim. Cosmochim. Acta* **74**, 1201-1219.

Bard A. J. and Faulkner L. R. (2001) *Electrochemical Methods Fundamentals and Applications,* second ed. Wiley Weinheim, New York.

Bear J. and Bachmat Y. (1967) A generalized theory on hydrodynamic dispersion in porous media. In *IASH Symposium on Artificial Recharge and Management of Aquifers, Haifa, Israel*, vol. 72, 7-16.

Ben-Yaakov S. (1972) Diffusion of sea water ions—I. Diffusion of sea water into a dilute solution. *Geochim. Cosmochim. Acta* **36**, 1395-1406.

Bjerg P. L., Ammentorp H. C. and Christensen T. H. (1993) Model simulations of a field experiment on cation exchange-affected multicomponent solute transport in a sandy aquifer. *J. Contam. Hydrol.* **12**, 291-311.

Bjerg P. L. and Christensen T. H. (1993) A field experiment on cation exchange-affected multicomponent solute transport in a sandy aquifer. *J. Contam. Hydrol.* **12**, 269-290.

Boudreau B. P. (1997) *Diagenetic Models and their Implementation: Modelling Transport and Reactions in Aquatic Sediments*. Springer-Verlag, Heidelberg.

Boudreau B. P., Meysman F. J. R. and Middelburg J. J. (2004) Multicomponent ionic diffusion in porewaters: Coulombic effects revisited. *Earth Planet. Sci. Lett*. **222**, 653-666.

Carrera J., Sanchez-Vila X., Benet I., Medina A., Galarza G. and Guimera J. (1998) On matrix diffusion: formulations, solution methods and qualitative effects. *Hydrogeol. J*. **6**, 178-190.

Chiogna G., Eberhardt C., Grathwohl P., Cirpka O. A. and Rolle M. (2010) Evidence of compound-dependent hydrodynamic and mechanical transverse dispersion by multitracer laboratory experiments. *Environ. Sci. Technol.* **44**, 688-693.

Chiogna G., Cirpka O. A., Grathwohl P. and Rolle M. (2011) Relevance of local compound-specific transverse dispersion for conservative and reactive mixing in heterogeneous porous media. *Water Resour. Res*. **47**, W06515, doi:10.1029 /2010WR010270.

Chiogna G., Hochstetler D. L., Bellin A., Kitanidis P. K. and Rolle M. (2012) Mixing, entropy and reactive solute transport. *Geophys. Res. Lett*. **39**, L20405, doi:10.1029/2012GL053295.

Cirpka O. A., Frind E. O. and Helmig R. (1999a) Streamline-oriented grid generation for transport modelling in two-dimensional domains including wells. *Adv. Water Resour.* **22**, 697-710. doi: 10.1016/s0309-1708(98)00050-5

Cirpka O. A., Frind E. O. and Helmig R. (1999b) Numerical methods for reactive transport on rectangular and streamline-oriented grids. *Adv. Water Resour.* **22**, 711-728. doi: http://dx.doi.org/10.1016/S0309-1708(98)00051-7

Cussler E. L. (2009) *Diffusion: Mass Transfer in Fluid Systems,* third ed. Cambridge University Press, New York, USA.

Davis T. and Duff I. (1997) An unsymmetric-pattern multifrontal method for sparse LU factorization. *SIAM J. Matrix Anal. A.* **18**, 140-158. doi: doi:10.1137/S0895479894246905

Eckert D., Rolle M. and Cirpka O. A. (2012). Numerical simulation of isotope fractionation in steady-state bioreactive transport controlled by transverse mixing. *J. Contam. Hydrol*. **140–141**, 95-106.

Felmy A. R. and Weare J. H. (1991) Calculation of multicomponent ionic-diffusion from zero to high-concentration: I. The system Na-K-Ca-Mg-Cl-So4-H2o at 25-degrees-C. *Geochim. Cosmochim. Acta* **55**, 113-131.

Giambalvo E. R., Steefel C. I., Fisher A. T., Rosenberg N. D. and Wheat C. G. (2002) Effect of fluid-sediment reaction on hydrothermal fluxes of major elements, eastern flank of the Juan de Fuca Ridge. *Geochim. Cosmochim. Acta* **66**, 1739-1757.

Gvirtzman H. and Gorelick S. M. (1991) Dispersion and advection in unsaturated porous media enhanced by anion exclusion. Nature **352**, 793-795.

Hadley P. W. and Newell C. (2013) The new potential for understanding groundwater contaminant transport. *Ground Water* (in press).

Haberer C. M., Rolle M., Liu S., Cirpka O. A. and Grathwohl P. (2011) A high-resolution non-invasive approach to quantify oxygen transport across the capillary fringe and within the underlying groundwater. *J. Contam. Hydrol.* **122**, 26-39.

Haberer C.M., Rolle M., Cirpka O.A. and Grathwohl P. (2012). Oxygen transfer in a fluctuating capillary fringe. *Vadose Zone J*. **11**, doi: 10.2136/vzj2011.0056.

Hazen A. (1892) Some physical properties of sands and gravels special reference to their use in filtration. *Ann. Rep. State Board of Health Mass*. **24**, 541-556.

Hochstetler D. L., Rolle M., Chiogna G., Haberer C. M., Grathwohl P. and Kitanidis P. K. (2013) Effects of compound-specific transverse mixing on steady-state reactive plumes: Insights from pore-scale simulations and Darcy-scale experiments. *Adv. Water Resour.* **54**, 1-13. doi: 10.1016/j.advwatres.2012.12.007

Holden A. A., Mayer K. U. and Ulrich A. C. (2012) Evaluating methods for quantifying cation exchange in mildly calcareous sediments in Northern Alberta. *Appl. Geochem.* **27**, 2511-2523.

Holden A. A., Haque S. E., Mayer K. U. and Ulrich A. C. (2013) Biogeochemical processes controlling the mobility of major ions and trace metals in aquitard sediments beneath an oil sand tailing pond: Laboratory studies and reactive transport modeling. *J. Contam. Hydrol.* **151**, 55-67.

Kitanidis P. K. (1994) The concept of the dilution index. *Water Resour. Res.* **30**, 2011-2026.

LaBolle E.M and Fogg G.E. (2001) Role of molecular diffusion in contaminant migration and recovery in alluvial aquifer system. *Transp. Porous Med*. **42**, 155-179.

Lasaga A. C. (1979) The treatment of multi-component diffusion and ion pairs in diagenetic fluxes. *Am. J. Sci.* **279**, 324-346.

Lasaga A. C. (1998) *Kinetic Theory in the Earth Sciences*. Princeton University Press, Princeton, New Jersey.

Li L., Peters C. A. and Celia M. A. (2007) Effects of mineral spatial distribution on reaction rates in porous media. *Water Resour. Res*. **43**, W01419. doi: 10.1029/2005WR004848

Li L., Steefel C. I. and Yang L. (2008) Scale dependence of mineral dissolution kinetics within single pores and fractures. *Geochim. Cosmochim. Acta* **72**, 360-377.

Li L., Salehikhoo F., Brantley S. and Heidari P. (2014) Spatial zonation limits magnesite dissolution in porous media. *Geochim. Cosmochim. Acta* **126**, 555-573.

Liu C., Zachara J. M., Felmy A. and Gorby Y. (2004) An electrodynamics-based model for ion diffusion in microbial polysaccharides. *Colloids Surf. A and B* **38**, 55-65.

Liu C. X. (2007) An ion diffusion model in semi-permeable clay materials. *Environ. Sci. Technol.* **41**, 5403-5409.

Liu C. X., Shang J. and Zachara J. M. (2011) Multispecies diffusion models: A study of uranyl species diffusion. *Water Resour. Res*. **47**, W12514, doi:10.1029/2011WR010575.

Maher K., Steefel C. I., DePaolo D. and Viani B. (2006) The mineral dissolution rate conundrum: Insights from reactive transport modeling of U isotopes and pore fluid chemistry in marine sediments. *Geochim. Cosmochim. Acta* **70**, 337-363.

Maier U. and Grathwohl P. (2006) Numerical experiments and field results on the size of steady state plumes. *J. Contam. Hydrol.* **85**, 33-52.

Mayer K. U., Frind E. O., Blowes D. W. (2002) Multicomponent reactive transport modeling in variably saturated porous media using a generalized formulation for kinetically controlled reactions. *Water Resour. Res*. **38**, 1174-1194.Molins S., Trebotich D., Steefel C. I. and Shen C. (2012) An investigation of pore scale flow on average geochemical reaction rates using different numerical simulation. *Water Resour. Res*. **48**, W03527, doi:10.1029/2011WR011404.

Parkhurst D. L. and Appelo C. A. J. (1999) *User's guide to PHREEQC – a computer program for speciation, reaction path, 1-D transport, and inverse geochemical calculations*. Technical Report 99-4259, US Geol. Survey Water Resources Investigation Report, 1999.

Rolle M., Hochstetler D. L., Chiogna G., Kitanidis P. and Grathwohl P. (2012) Experimental investigation and pore-scale modeling interpretation of compound-specific transverse dispersion in porous media. *Transp. Porous Media* **93**, 347-362.

Rolle M., Muniruzzaman M., Haberer C. M. and Grathwohl P. (2013a) Coulombic effects in advection-dominated transport of electrolytes in porous media: Multicomponent ionic dispersion. *Geochim. Cosmochim. Acta* **120**, 195-205.

Rolle M., Chiogna G., Hochstetler D. L. and Kitanidis P. K. (2013b) On the importance of diffusion and compound-specific mixing for groundwater transport: An investigation from pore to field scale. *J. Contam. Hydrol*. **153**, 51-68.

Rolle M., Eberhardt C., Chiogna G., Cirpka O. A. and Grathwohl P. (2009) Enhancement of dilution and transverse reactive mixing in porous media: experiments and model-based interpretation. *J. Contam. Hydrol.* **110**, 130-142.

Saichek R. E. and Reddy K. R. (2005) Electrokinetically enhanced remediation of hydrophobic compounds in soils: a review. *Crit. Rev. Environ. Sci. Technol*. **35**, 115-192.

Steefel C. I. (2009) CrunchFlow. Software for Modeling Multicomponent Reactive Flow and Transport. User's Manual. Lawrence Berkeley National Laboratory, Berkeley, USA.

Steefel C. I. and Maher K. (2009) Fluid-rock interactions: A reactive transport approach. *Rev. Mineral. Geochem.* **70**, 485-532.

Thullner M., Van Cappellen P. and Regnier P. (2005) Modeling the impact of microbial activity on redox dynamics in porous media. *Geochim. Cosmochim. Acta* **69**, 5005-5019.

Van Breukelen B. M. and Rolle M. (2012) Transverse hydrodynamic dispersion effects on isotope signals in groundwater chlorinated solvents' plumes. *Environ. Sci. Technol.* **46**, 7700-7708.

Van Cappellen P. and Gaillard J.-F. (1996) Biogeochemical dynamics in aquatic sediments. In *Reactive Transport in Porous Media: General Principles and Application to Geochemical Processes* (eds. P. C. Lichtner, C. I. Steefel and E. H.Oelkers). Mineral. Soc. Amer. pp. 335–376.

Vinograd J. R. and McBain J. W. (1941) Diffusion of electrolytes and of the ions in their mixtures. *J. Am. Chem. Soc.* **63**, 2008-2015.

Wang Y. F. and Van Cappellen P. (1996) A multicomponent reactive transport model of early diagenesis: Application to redox cycling in coastal marine sediments. *Geochim. Cosmochim. Acta* **60**, 2993-3014.

Worch E. (1993) Eine neue Gleichung zur Berechnung von Diffusionskoeffizienten gelöster Stoffe (A new equation for the calculation of diffusion coefficients for dissolved substances), Vom Wasser 81, 289-297.

Wu M. Z., Reynolds D. A., Fourie A., Prommer H. and Thomas D. G. (2012) Electrokinetic in situ oxidation remediation: assessment of parameter sensitivities and the influence of aquifer heterogeneity on remediation efficiency. *J. Contam. Hydrol.* **136-137**, 72-85.

Zhang C. Y., Dehoff K., Hess N., Oostrom M., Wietsma T. W., Valocchi A. J. and Werth C. J. (2010) Pore-scale study of transverse mixing induced $CaCO_3$ precipitation and permeability reduction in a model subsurface sedimentary system. *Environ. Sci. Technol.* **44**, 7833-7838.

Chapter 4

Impact of multicomponent ionic transport on pH fronts propagation in saturated porous media[‡]

Abstract

We investigate the propagation of pH fronts during multicomponent ionic transport in saturated porous media under flow-through conditions. By performing laboratory bench-scale experiments combined with numerical modeling we show the important influence of Coulombic effects on proton transport in the presence of ionic admixtures. The experiments were performed in a quasi two-dimensional flow-through setup under steady-state flow and transport conditions. Dilute solutions of hydrochloric acid with $MgCl_2$ (1:2 strong electrolyte) were used as tracer solutions to experimentally test the effect of electrochemical cross-coupling on the migration of diffusive/dispersive pH fronts. We focus on two experimental scenarios, with different composition of tracer solutions, causing remarkably different effects on the propagation of the acidic fronts with relative differences in the penetration depth of pH fronts of 36% between the two scenarios and of 25% and 15% for each scenario with respect to the transport of ions at liberated state (i.e., without considering the charge effects). Also differences in the dilution of the distinct ions plumes up to 28% and 45% in experiment 1 and 2, respectively, were measured at the outflow of the flow-through system. The dilution of the pH plumes also changed considerably (26% relative difference) in the two flow-through experiments only due to the different composition of the pore water solution and to the electrostatic coupling of the ions in the flow-through setups. Numerical transport simulations were performed to interpret the laboratory experiments. The simulations were based on a multicomponent ionic formulation accurately capturing the Coulombic interactions between the transported ions in the flow-through system. The results of purely forward simulations show a very good agreement with the high-resolution measurements performed at the outlet of the flow-through setup and confirms the importance of charge effects on pH transport in porous media.

[‡] Reproduced from: Muniruzzaman, M., and Rolle, M. (2015). Impact of multicomponent ionic transport on pH fronts propagation in saturated porous media. *Water Resources Research, 51(8),* 6739-6755. http://dx.doi.org/10.1002/2015WR017134

4.1 Introduction

The correct quantification of pH distribution is of utmost importance in various areas of subsurface research including the study of groundwater acidification [e.g., *Moss and Edmunds*., 1992; *de Caritat*, 1995; *Hansen and Postma*, 1995; *Donovan et al*., 1997; *Kjøller et al*., 2004; *Fest et al*., 2005, 2007; *Franken et al*., 2009], sorption-desorption and surface complexation of trace metals onto mineral surfaces [e.g., *Davis and Kent*, 1990; *Zachara et al*., 1991; *Kent et al*., 2000; *Davis et al*., 2004; *Prigiobbe and Bryant*, 2014], ion exchange [e.g., *Griffioen*, 1993; *Appelo*, 1994], redox-controlled reaction fronts [e.g., *Engesgaard and Kipp*, 1992], as well as mineral equilibria and reactive transport [e.g., *Maher et al*., 2006; *Li et al*., 2007, 2014; *Molins et al*., 2012; *Redden et al.*, 2014; *Haberer et al*., 2015]. In particular, groundwater acidification, mainly caused by acid rain precipitation, has been identified as a serious problem especially in aquifers with sediments containing low pH buffering capacity [*Edmunds and Kinniburgh*, 1986; *Hansen and Postma*, 1995; *Kjøller et al*., 2004; *Franken et al*., 2009]. In such systems, the acidic recharge reaches the saturated zone where the pH front penetrates downwards and mixes with the underlying ambient groundwater. Key processes leading to vertical mixing are molecular diffusion and transverse hydrodynamic dispersion. Diffusion of charged species is significantly affected by electrochemical migration effects induced by the charge of dissolved species and/or mineral surfaces [e.g., *Vinograd and McBain*, 1941; *Lasaga*, 1979; *Van Cappellen and Gaillard*, 1996; *Liu*, 2007; *Appelo and Wersin*, 2007; *Steefel and Maher*, 2009]. Multispecies diffusion models, which are traditionally represented by Nernst-Planck formulations, are used to predict diffusive fluxes under such conditions [e.g., *Boudreau et al*., 2004; *Liu et al*., 2004; *Appelo and Wersin*, 2007; *Li et al*., 2008]. These models allow capturing inter-species interactions by preserving local charge balance, and thus represent valuable tools to accurately describe multicomponent conservative and reactive solute transport occurring in both laboratory and field scale domains [e.g., *Vinograd and McBain*, 1941; *Giambalvo et al*., 2002; *Appelo et al*., 2008, 2010; *Liu et al*., 2011]. In two recent contributions we studied multicomponent ionic transport in saturated porous media and we showed that, in addition to purely diffusive processes, the charge-induced Coulombic interactions significantly affect transverse hydrodynamic dispersion and the transport of ionic species in advection-dominated homogeneous and heterogeneous flow-through systems [*Rolle at al*., 2013a; *Muniruzzaman et al*., 2014]. These studies were restricted to transport of soluble salts and, to the best of our knowledge, no investigation has yet focused on the effects of charge interactions on pH-front propagation in saturated porous media under flow-through conditions.

The main objective of this work is to study the evolution of diffusive/dispersive pH fronts in the presence of an ionic admixture during conservative solute transport in porous media. To investigate the macroscopic impact of electrostatic effects on acidic front migration under flow-through conditions, we performed quasi two-dimensional bench-scale experiments in a saturated homogeneous porous domain and studied the transport of acidic plumes, undergoing transverse mixing with pure water, under different compositions of the injected electrolyte solution. The experimental results were quantitatively interpreted with a two-dimensional multicomponent transport model taking into account the effects of ionic interactions on pH distribution. The multicomponent simulations allowed us to explain the experimental observations and to quantify the specific components of the transverse dispersive fluxes, including the electromigration term due to the electrostatic coupling between the different ionic species. Our flow-through experiments and modeling results show that the impact of electrostatic microscopic effects is remarkable and causes macroscopic variations in pH-front development and dilution of acidic plumes that are significantly controlled by the presence and concentration of other electrolytes in the pore water solution.

4.2 Equations of Multicomponent Ionic Transport

Multicomponent diffusion models for species with nonzero charge are commonly derived based on the Nernst-Planck equation [*Bard and Faulkner*, 2001]. The formulations of such models involve the pragmatic extension of Fick's first law by considering an additional charged-induced electrostatic term. In dilute solutions and in the condition of negligible ionic strength gradients, the diffusive flux of an ionic species i in a multicomponent environment, is expressed as [*Lasaga*, 1979; *Cussler*, 2009]:

$$J_i = -D_i \nabla C_i - D_i \frac{z_i F}{RT} C_i \nabla \Phi \quad i = 1, 2, 3, ..., N \tag{4.1}$$

where C_i is the concentration, z_i is the charge, D_i is the self-diffusion coefficient, F is the Faraday's constant, R is the ideal gas constant, T is the absolute temperature, Φ is the electrostatic potential, and N is the number of species in solution. Equation (4.1) indicates that the flux of a charged species, i, is not only driven by its own concentration gradient but also by the electrical field created by the movement of different ions present in the system.

A detailed derivation of the governing equations for the multicomponent diffusion problem can be found in previous studies [e.g., *Ben Yaakov*, 1972; *Lasaga*, 1979, *Van Cappellen and Gaillard*, 1996; *Boudreau et al*, 2004; *Appelo and Wersin*, 2007; *Liu et al*., 2011]. Key steps in the derivation are the physical constraints associated with the electroneutrality of the aqueous

solution: (i) local preservation of charge balance in all spatial locations ($\sum_{i=1}^{N} z_i C_i = 0$), and (ii) the absence of electrical current ($\sum_{i=1}^{N} z_i J_i = 0$). Using these constraints, the gradient of electrical potential, $\nabla\Phi$ in equation (4.1) can be expressed in terms of easily quantifiable parameters such as concentration and charge of the ions in solution as well as their self-diffusion coefficients:

$$\nabla\Phi = \frac{-\sum_{i=1}^{N}\left(z_i D_i \nabla C_i\right)}{\sum_{i=1}^{N}\left(z_i^2 F D_i C_i\right)/RT} \tag{4.2}$$

After substitution of equation (4.2) into equation (4.1), the diffusive flux readily reduces solely to a function of diffusion coefficients, charge and concentration of the ions in solution, and concentration gradients:

$$J_i = -D_i \nabla C_i + \frac{z_i D_i C_i}{\sum_{j=1}^{N}\left(z_j^2 D_j C_j\right)} \sum_{k=1}^{N}\left(z_k D_k \nabla C_k\right) \tag{4.3}$$

Equation (4.3) can be further rearranged in a more compact notation by introducing a matrix of inter-diffusion coefficients, cross-coupling fluxes and concentration gradients of the dissolved species. The multicomponent formulation of diffusive processes has been adopted and shown to be relevant in numerous studies in the geochemical and water research literature [e.g., *Lasaga*, 1979; *Van Cappellen and Gaillard*, 1996; *Giambalvo et al*., 2002; *Boudreau et al*., 2004; *Liu et al*., 2004, 2011; *Appelo and Wersin*, 2007].

In flow-through systems, solute mass exchange also depends on the advective movement of the fluid. Therefore, under such conditions, hydrodynamic dispersion coefficients should be considered in the derivation of the multicomponent transport problem in porous media [*Rolle at al*., 2013a; *Muniruzzaman et al*., 2014]. By substituting the multicomponent dispersive fluxes (formally similar to equation (4.3)) into the classical advection-dispersion equation, the governing transport equation of ionic species in saturated porous domain takes the form:

$$\frac{\partial C_i}{\partial t} = -\boldsymbol{v}\cdot\nabla C_i + \nabla\cdot\left(\sum_{j=1}^{N}\mathbf{D}_{ij}\nabla C_j\right) \tag{4.4}$$

where t is time, $\boldsymbol{v}$ is the velocity vector, and $\mathbf{D}_{ij}$ is the dispersion tensor. In a two-dimensional system oriented along the principal flow direction the entries of $\mathbf{D}_{ij}$ are $\mathbf{D}_{ij}^{L}$ and $\mathbf{D}_{ij}^{T}$, which represent the longitudinal and transverse cross-coupled dispersion coefficients [*Muniruzzaman et al*., 2014]:

$$\mathbf{D}_{ij}^{L} = \delta_{ij} D_i^{L} - \frac{z_i z_j D_i^{L} D_j^{L} C_i}{\sum_{k=1}^{N} \left(z_k^2 D_k^{L} C_k \right)}$$

$$\mathbf{D}_{ij}^{T} = \delta_{ij} D_i^{T} - \frac{z_i z_j D_i^{T} D_j^{T} C_i}{\sum_{k=1}^{N} \left(z_k^2 D_k^{T} C_k \right)} \qquad (4.5)$$

where D_i^L is the longitudinal and D_i^T is the transverse component of the hydrodynamic self-dispersion coefficient of species *i* (i.e., when the ion is "liberated" from the other charged species in solution), δ_{ij} is the Kronecker symbol which has a value of 1 when $i=j$ or 0 when $i \neq j$. The combination of equation (4.4) and equation (4.5) ensures that the movement of a specific ion depends on its own dispersion coefficient and concentration gradient (first terms in equation (4.5)) as well as on the properties and concentration gradients of other charged species in solution (second terms in equation (4.5)).

The general formulation of the multicomponent transport problem (equations (4.1-4.5)) reduces to the classical advection-dispersion equation for non-charged species, since all the electrostatic cross-coupling terms in equation (4.5) drop out.

4.3 Experimental Setup

The experiments were performed in a quasi two-dimensional flow-through setup in a homogeneous porous medium. The flow-through chamber has inner dimensions of 100 cm × 19 cm × 1cm (L × H × W) and is equipped with 24 ports both at the inlet and at the outlet (Figure 4.1). These ports, constructed with Alltech rubber septa pierced with hollow injection needles, are directly connected to two 24-channel high-precision peristaltic pumps (ISMATEC IPC-N24, Ismatec, Glattburg, Switzerland) through Fluran HCA pump tubings (inner diameter 0.64 mm; Ismatec, Glattburg, Switzerland). The porous medium was prepared by filling the flow-through chamber with glass beads with grain diameter in the range 1.00–1.50 mm (Sartorius AG, Göttingen, Germany). A wet-packing procedure was followed by maintaining the water level always above the upper limit of the porous medium to avoid possible air entrapment [*Haberer et al.*, 2012]. The pumps, calibrated before each experiment, allowed establishing a uniform horizontal flow field and the small spacing between the ports (5 mm) allowed high-resolution sampling of the injected tracer solutions. The experiments were performed in a temperature controlled room at a temperature of 20 °C.

The flow-through experiments were initiated by injecting tracer solutions through 8 injection ports at the bottom of the chamber (port 1–8; 0–4 cm from the bottom) and an ambient solution of ultra-pure Milli-Q water (Millipore, MA, USA) through the remaining inlet ports. Such solutions were continuously injected until steady-state transport conditions were achieved and samples were taken afterwards at all 24 outlet extraction ports (Figure 4.1).

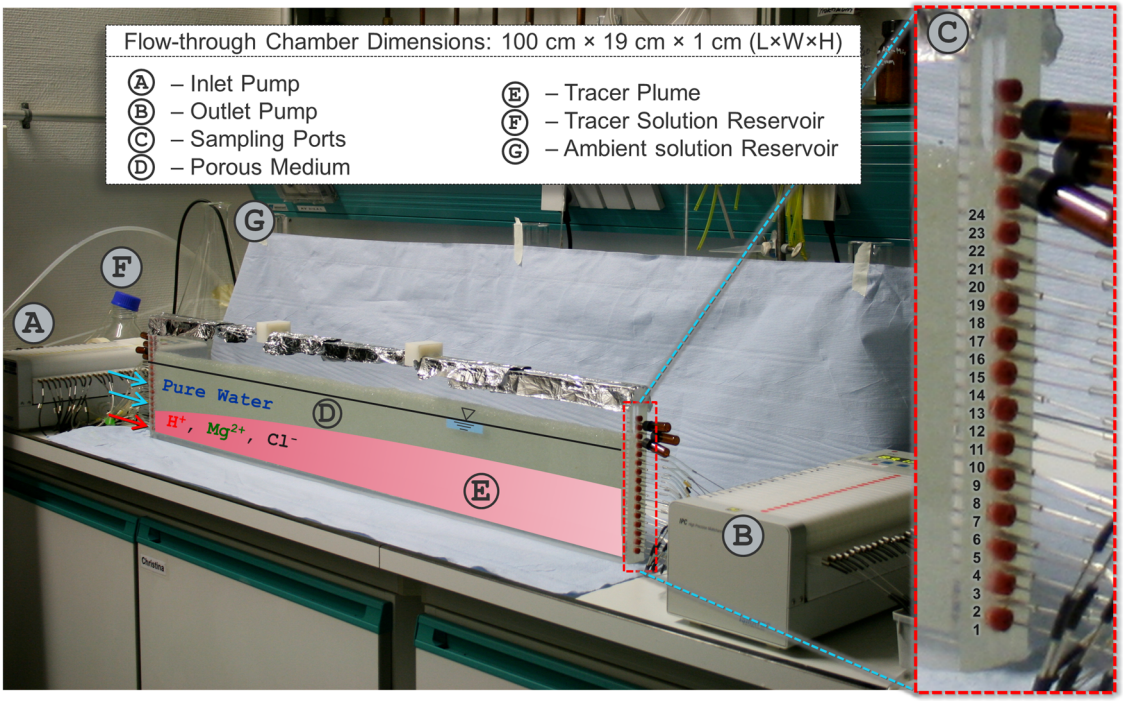

Figure 4.1. Laboratory flow-through setup. The red shaded area represents the steady-state plume of ionic species (H^+, Mg^{2+} and Cl^-) injected from the 8 bottom inlet ports. The inset shows the high-resolution sampling at the outlet of the flow-through chamber.

The acidic solutions injected from the bottom inlet ports contained HCl and $MgCl_2$, a strong 1:2 electrolyte injected at similar and hundredfold concentrations relative to HCl in different experimental runs. Mg^{2+} and Cl^- concentrations were measured by ion-chromatography (Dionex Dx-120, Fisher Scientific, Schwerte, Germany) and pH measurements were performed by pH electrode (ORION 8103BN, Thermo Fisher Scientific Inc., USA). For each experimental run, duplicate measurements at each outlet port were taken. Additionally, the flow rate at each port was determined gravimetrically, by collecting and weighing the effluent volume for a given period of time. The flow rate measurement was always carried out after sampling for the ion concentration measurements. The transport experiments were performed in an advection-dominated regime, at a seepage velocity of 0.8 m/day. The parameters summarizing the main features of the flow-through setup as well as the flow and transport properties are reported in Table 4.1.

Table 4.1: Summary of geometry and flow and transport parameters of the laboratory experimental system

Experimental settings	
Flow-through chamber inner dimensions (L×H×W) [cm]	100×19×1
Number of inlet/outlet ports used	23/24
Port spacing [mm]	5
Grain diameter of the porous matrix, d [mm]	1.00-1.50
Hydraulic conductivity, K [m/s]	1.27×10^{-2}
Average horizontal flow velocity, v [m/day]	0.8
Average porosity, θ [-]	0.41
Diffusion coefficients	D^{aq} [m^2/s][a]
H^+	8.65×10^{-9}
Mg^{2+}	0.63×10^{-9}
Cl^-	1.81×10^{-9}

[a] values from *Lasaga* [1998] at 18°C, and corrected for temperature and viscosity changes of the experimental conditions at 20°C

The values of the ion diffusion coefficients reported in Table 4.1 are important for this study. Such values represent the aqueous self-diffusion coefficients of the ionic species under the experimental conditions of the flow-through experiments. It is interesting to notice the variability of the diffusivity constants which depend not only on the size of the different ions but also on the electrostatic interactions of the ions with the polar solvent. These effects cause a cohort of solvation molecules, denoted as first solvation shell, to follow the movement of the ions [*Møller et al.*, 2005]. Particularly striking is the value of D^{aq} for the hydrogen ion, which is more than one order of magnitude larger than the diffusivity of the other cations in solution. The large diffusivity of H^+ cannot be explained by hydrodynamic considerations and arise from specific "Grotthuss-type" mechanisms resulting in proton hopping through a chain reaction between water molecules [*Cussler*, 2009]. These properties are of primary importance for the propagation of pH fronts that can advance at a considerably higher speed than the other ions in the pore water solution. As illustrated in this study, the ions in solution have the capability to strongly influence the displacement of the hydrogen ions.

The laboratory experiments were performed considering a ternary electrolyte system containing two cations (H^+, Mg^{2+}) and a common anion Cl^-. In particular, two experimental scenarios with different composition of the inlet solutions were tested: (i) Scenario 1: transport of a HCl and $MgCl_2$ solution with similar concentration of the two cations (i.e., $C_{H+}/C_{Mg2+} \approx 1$) in ambient Milli-Q water, and (ii) Scenario 2: transport of a HCl and $MgCl_2$ solution with

excess of $MgCl_2$ (i.e., $C_{H+}/C_{Mg2+} \approx 0.01$) in ambient Milli-Q water. The chemical composition of the inlet solutions in the flow-through experiments are summarized in Table 4.2.

Table 4.2: Chemical composition of the inlet solutions in the flow-through experiments.

Parameter	Scenario 1	Scenario 2
pH	3.8	4.1
Mg^{2+} concentration, C_{Mg2+} [mM]	0.15	12.0
Cl^- concentration, C_{Cl-} [mM]	0.46	24.1
C_{H+}/C_{Mg2+} [-]	1.14	0.007
Ionic Strength [M]	6×10^{-4}	3.61×10^{-2}

4.4 Modeling Approach

A two-dimensional steady-state model for flow and multicomponent transport in saturated porous media has been adopted in the present study. The flow problem for hydraulic head, h, and stream–function, ψ, under steady-state conditions reads as [*Cirpka et al*., 1999a]:

$$\begin{aligned} \nabla \cdot \left(\mathbf{K} \nabla h \right) &= 0 \\ \nabla \cdot \left(\mathbf{K}^{-1} \nabla \psi \right) &= 0 \end{aligned} \tag{4.6}$$

where **K** is the hydraulic conductivity tensor. Equation (4.6) is solved numerically by bilinear finite elements on Cartesian grids. Dirichlet boundary conditions are applied at the inlet and outlet boundaries for the head problem, and at the top and bottom boundaries for the stream-function problem.

Under steady-state conditions the governing equation describing multicomponent solute transport, written in local coordinates x_L and x_T oriented along and perpendicular to the direction of the flow, writes as:

$$v \frac{\partial C_i}{\partial x_L} - \frac{\partial}{\partial x_L} \left(\sum_{j=1}^{N} \mathbf{D}_{ij}^{L} \frac{\partial C_j}{\partial x_L} \right) - \frac{\partial}{\partial x_T} \left(\sum_{j=1}^{N} \mathbf{D}_{ij}^{T} \frac{\partial C_j}{\partial x_T} \right) = 0 \tag{4.7}$$

The transport problem is computed with finite volume method (FVM) on streamline-oriented grids constructed by the approach of *Cirpka et al*. [1999a, 1999b]. The use of such grids oriented along the flow direction reduces numerical errors by avoiding artificial mixing. The system of equations is solved using the direct matrix solver UMFPACK [*Davis and Duff*,

1997] and all associated calculations are performed in MATLAB. A Picard iterative scheme is used to linearize the non-linear set of transport equations (equation (4.7)), in which the non-linearity arises from the electrostatic cross-coupling between the dispersive fluxes of the different ions. A detailed description including the development and validation of the two-dimensional multicomponent dispersion model can be found in *Muniruzzaman et al*. [2014].

To simulate the flow-through laboratory experiments the two-dimensional model domain (100 cm × 12 cm) is discretized into 100 cells (Δx = 1 cm) and 120 cells (Δz = 1 mm) along the longitudinal and transverse dimension, respectively. A constant concentration boundary at the inflow and zero dispersive flux conditions at the remaining boundaries are applied. A key parameter for the accurate representation of the displacement of the different ionic species is the hydrodynamic dispersion coefficient which was parameterized according to a non-linear compound-specific formulation [*Chiogna et al*., 2010; *Rolle et al*., 2012]:

$$D_i = D_i^P + D_i^{aq}\left(\frac{Pe^2}{Pe+2+4\delta^2}\right)^{\beta} \tag{4.8}$$

where D_i^P is the pore diffusion coefficient approximated as $D_i^P \approx \theta D_i^{aq}$. Pe is the grain Péclet number defined as, $Pe = vd / D_i^{aq}$, with v and d being the seepage velocity and the grain diameter, respectively. δ is the ratio between the length of a pore channel and its hydraulic radius, and β is an empirical exponent accounting for incomplete mixing in the pore channels. For the transverse dispersion coefficient, which is the key parameter for steady-state transport, the values of δ = 6.2 and β = 0.5 were determined in previous multitracer experiments and pore-scale simulations performed in the same porous medium used in this study [*Rolle et al*., 2012; *Hochstetler et al*., 2013]. The same empirical parameterization was used for the longitudinal dispersion coefficient [*Rolle et al*., 2013b; *Muniruzzaman et al*., 2014], with the same value for δ and δ = 0.89, determined in transient pore-scale simulations, even though the longitudinal dispersion term in equation (4.7) becomes negligible for steady-state transport and continuous injection of the tracer solutions [*Cirpka et al*., 2011].

The electrostatic coupling between the different charged species in the flow-through setup is performed by implementing the equations of multicomponent ionic interactions described in Section 4.2. A simplified approach was followed, considering exclusively the coupling between the major ions measured in the flow-through experiments (H^+, Mg^{2+} and Cl^-). Such approach is adequate for the experimental conditions considered in this study, as shown by the excellent agreement of the simulation results with the outcome of PHREEQC (Parkhurst and Appelo, 1999) for a 1D multicomponent diffusion problem described in the Supporting Information. Instead, more complex aqueous chemistry as well as higher concentrations would

require a full coupling of a multidimensional transport simulator with a geochemical code allowing considering the full aqueous speciation reactions as well as the influence of ionic strength and the gradients in the activity coefficients.

4.5 Results and Discussion

Laboratory experiments were performed considering two different systems of ternary electrolytes, containing two cations (H^+, Mg^{2+}) and a common anion Cl^- (Table 4.2). The results obtained from these two experimental scenarios are quantitatively analyzed with purely forward 2-D multicomponent simulations based on the approach outlined in section 4.4.

4.5.1 Scenario 1: Transport of HCl with similar molar concentration of $MgCl_2$

In this experiment, a dilute solution containing similar molar concentrations of hydrochloric acid (0.17 mM) and $MgCl_2$ (0.15 mM) was continuously injected through 8 inlet ports at the bottom of the flow-through setup; Milli-Q water was injected as ambient solution through the remaining ports. The injected ions underwent conservative multispecies transport through the saturated porous medium until the establishment of steady-state plumes. Figure 4.2 reports the steady-state concentration profiles for Mg^{2+} and Cl^- as well as the pH profiles measured at high vertical resolution at the outlet of the flow-through domain.

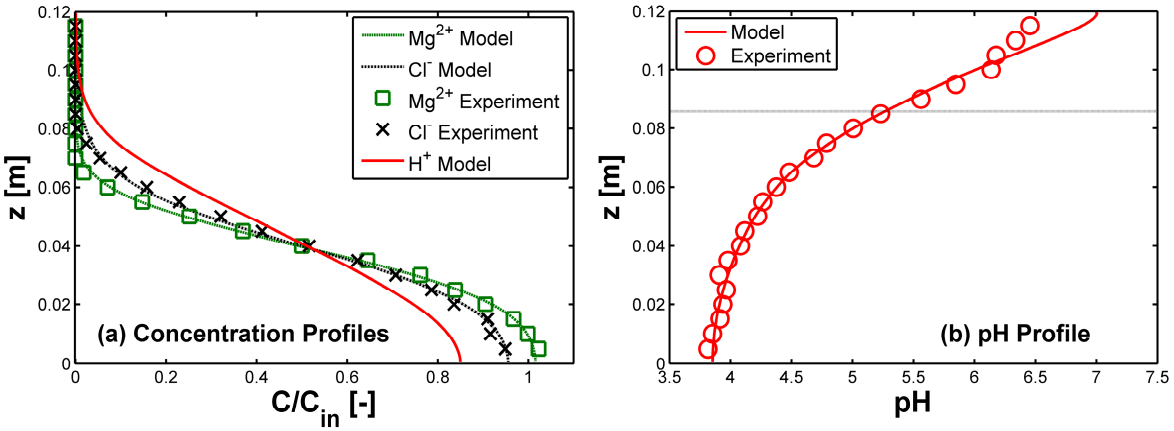

Figure 4.2. Transverse ion concentrations (a) and pH (b) profiles at the outlet of the flow-through system (x = 1 m) for multicomponent transport in Scenario 1 ($C_{H+}/C_{Mg2+}\approx1$): measured ion concentrations and pH (symbols) and modeling results (lines).

The measured vertical concentration profiles show distinct patterns in transverse displacement of injected species (Figure 4.2a). Such patterns are substantiated by the multicomponent

simulations that show a very good agreement with the measurements of the ion concentrations. The distinct patterns confirm the importance of diffusion and compound-specific dispersion under the advection-dominated regime (i.e., seepage velocity of 0.8 m/day) of the flow-through experiments. As expected from their diffusion coefficients (Table 4.1), the two cations, fast H^+ and slow Mg^{2+}, show different spreading and the common anion Cl^- has a profile that lies in-between the ones of the cations. The pH was the parameter measured to track the displacement of hydrogen ions. In dilute solution the pH can be approximated as the negative logarithm of H^+ concentrations. Considering a change of 1.5 pH units from the inlet solution, the results show that at the end of the flow-through system the dispersive pH front has migrated up to a distance of ~8.6 cm (gray dotted line in Figure 4.2b, 4.6 cm above the 4 cm injection zone) from the bottom of the flow-through system. An excellent agreement also exists between the measured pH profiles and the results of the multicomponent transport simulations.

The multicomponent model allows us to map the distinct contributions of steady-state transverse flux components for the different ionic species in solution. In fact, the total dispersive flux, formally identical to equation (4.1) but considering hydrodynamic dispersion instead of diffusion, consists of an additive contribution of a purely dispersive flux (J_i^{dis}) and an electrochemical migration flux (J_i^{mig}). The latter represents the contribution due to the electrostatic coupling between the charged species:

$$J_i = J_i^{dis} + J_i^{mig} \tag{4.9}$$

Mapping the different flux contributions is useful to illustrate the coupled transport of the charged species in the multicomponent setup. Maps of the different dispersive flux components are shown in Figure 4.3 (a-i). The figures illustrates that the total and dispersive fluxes of H^+ are significantly more spread than those of the other ions, in particular of Mg^{2+} (Figure 4.3a-f). The electrochemical migration term (J_i^{mig}) shows an interesting distribution with both cations having negative contributions and the anion (Cl^-) having a positive contribution (Figure 4.3g-i). Therefore, due to negative electrochemical migration flux components, protons and magnesium ions experience a decrease of their transverse displacement. The situation is opposite for Cl^-, for which a positive electrochemical flux component leads to an enhancement of its transverse flux. As a consequence, in this scenario, both cations slowed down and the anion accelerated compared to their liberated state. This is also evident from the profiles of the transverse fluxes computed at the outlet of the domain (Figure 4.3j-l). Notice that for both cations the total flux components have smaller magnitude compared to the purely dispersive flux terms. For Cl^-, instead, both the dispersive and the electrochemical migration fluxes have a positive contribution and add up to a larger total flux. In this scenario the Coulombic

interactions between the different ionic species is particularly effective in limiting the transverse dispersion of the protons whose displacement is considerably reduced compared to the case of transport in the absence of electrostatic effects (i.e., liberated state).

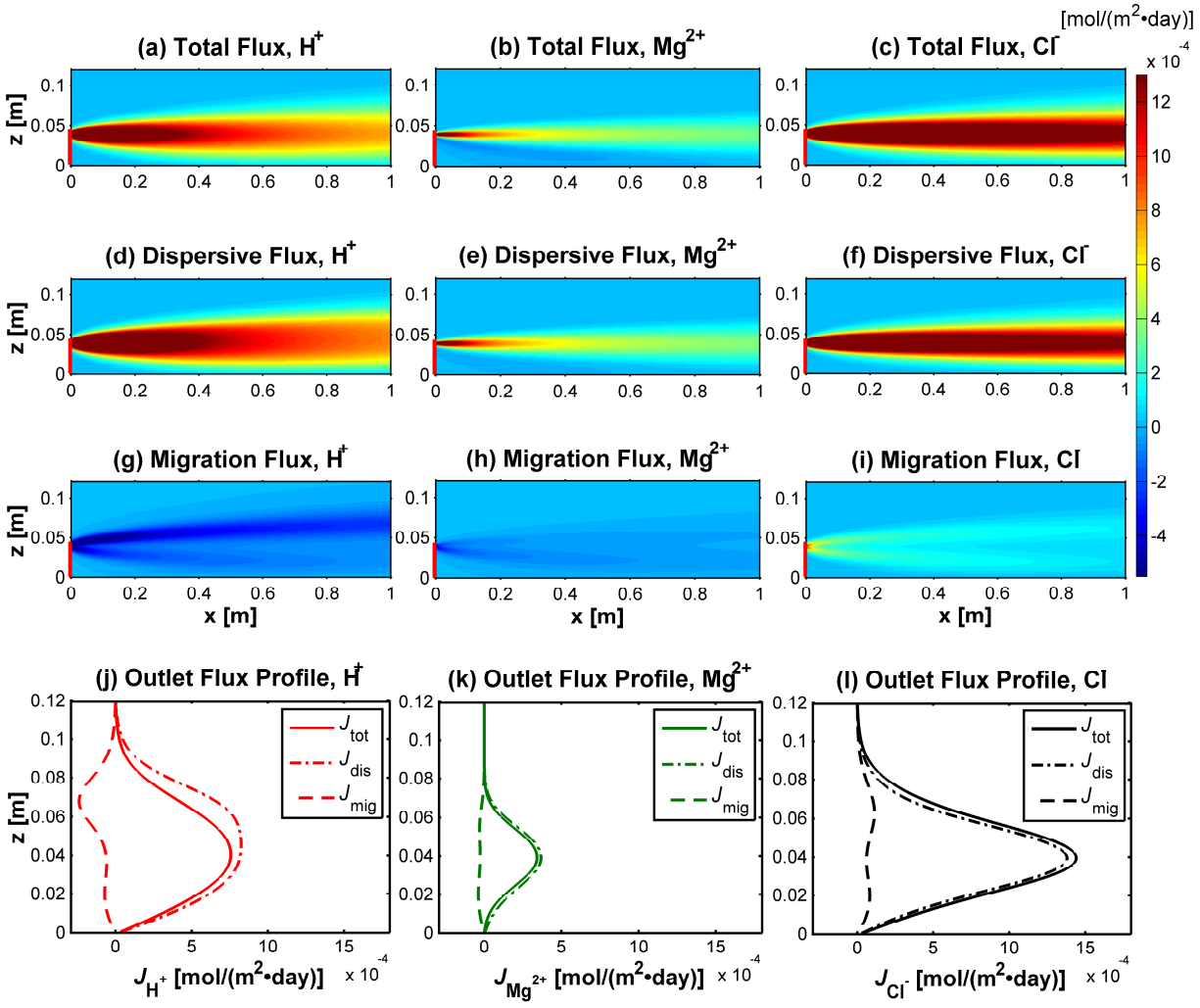

Figure 4.3. Maps of multicomponent ionic transverse fluxes for Scenario 1: Total fluxes (a, b, c), Dispersive fluxes (d, e, f) and Electrochemical migration fluxes (g, h, i). The lower panels (j, k, l) show the vertical profiles of multicomponent ionic fluxes at the outlet of the flow-through domain. The vertical red line represents the width of the tracer solution at the inlet. The direction from the core to the fringe (upward) of the plume is considered positive for the calculated fluxes.

4.5.2 Scenario 2: Transport of HCl with excess molar concentration of $MgCl_2$

In this scenario, we investigated the transport of HCl in the presence of excess $MgCl_2$. The tracer solution contained 0.08 mM hydrochloric acid and 12 mM $MgCl_2$. As in the previous experiment, this electrolyte solution was continuously injected through the 8 bottom inlet ports and Milli-Q water was injected from the remaining inlet ports. When the plume reached steady-state, samples were taken at the 24 outlet ports of the flow-through chamber. The measured and simulated outlet profiles are shown in Figure 4.4.

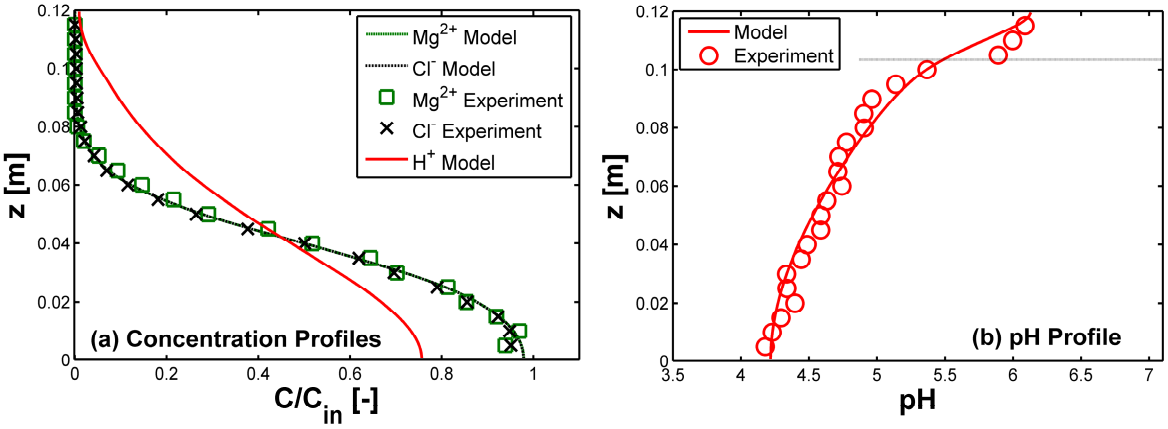

Figure 4.4. Transverse ion concentrations (a) and pH (b) profiles at the outlet of the flow-through system (x = 1 m) for multicomponent transport in Scenario 2 ($C_{H+}/C_{Mg2+} \approx 0.01$): measured ion concentrations and pH (symbols) and modeling results (lines).

Unlike Scenario 1, Mg^{2+} and Cl^-, present in excess concentration, appear to travel together resulting in overlapping concentration profiles (Figure 4.4a). The hydrogen ion, present in relatively smaller concentration, travels much further compared to the other two ions. This is reflected in a more spread vertical profile with a smaller peak concentration. The pH measurements and simulations shows that the dispersive pH front (1.5 pH units change from the inlet solution) has advanced up to a vertical distance of ~10.2 cm from the bottom (i.e., 6.2 cm above the 4 cm injection zone), at the outlet of the flow-through chamber (Figure 4.4b). Also in this case, the agreement between the measured profiles and the profiles calculated with the purely forward multicomponent simulations is very good. Also for this scenario it is illustrative to visualize the different flux components of the ionic plumes in the two-dimensional setup. Figure 4.5 shows the maps of the steady-state transverse dispersive fluxes and the corresponding profiles at the outlet boundary of the domain.

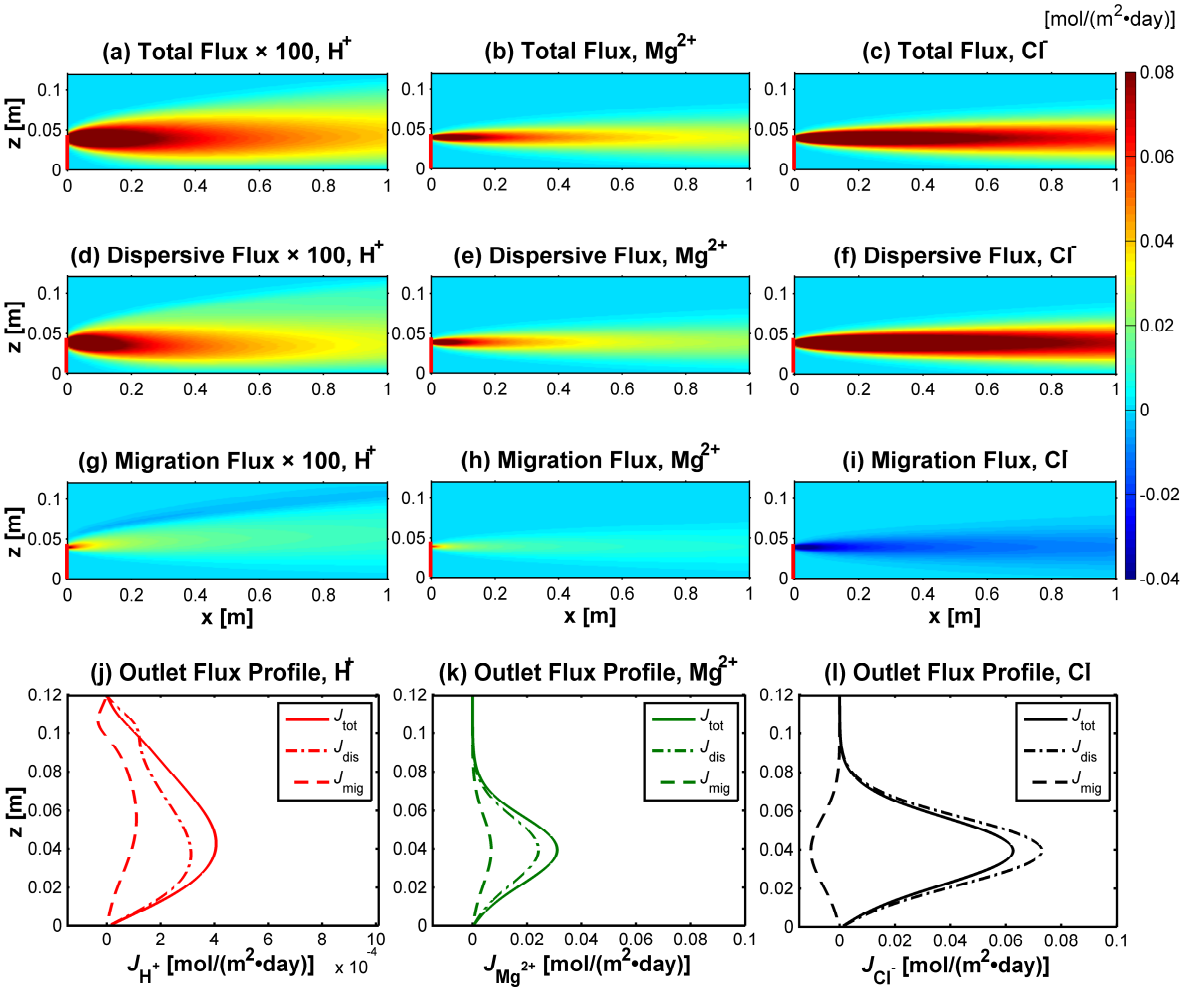

Figure 4.5. Maps of multicomponent ionic transverse fluxes for Scenario 2: Total fluxes (a, b, c), Dispersive fluxes (d, e, f) and Electrochemical migration fluxes (g, h, i). The lower panels (j, k, l) show the vertical profiles of multicomponent ionic fluxes at the outlet of the flow-through domain. The vertical red line represents the width of the tracer solution at the inlet. The direction from the core to the fringe (upward) of the plume is considered positive for the calculated fluxes. Additionally, notice that the scale used in the H^+ maps and profiles is 100-fold smaller because the absolute concentrations of Mg^{2+} and Cl^- are two orders of magnitude higher compared to the H^+ concentration.

It is clear from Figure 4.5a-c that the total transverse flux for H^+ has a wider distribution compared to the other two ions. This pattern is also consistent with the outlet concentration profiles of the ions shown in Figure 4.4a. In fact, the transverse flux for H^+ interest a wider portion of the domain and this is reflected also by the higher spreading of the H^+ plume compared to Mg^{2+} and Cl^-. Notable differences between the different ions in solution can be observed also for the dispersive flux components J_i^{dis} (Figure 4.5d-f). The electrochemical migration flux distributions (Figure 4.5g-i) show an interesting behavior, completely opposite

to the one observed in Scenario 1. In this case, both cations (Mg^{2+} and H^+) have a positive contribution and the anion (Cl^-) has a negative contribution. This causes an enhancement of Mg^{2+} and a reduction of Cl^- transverse displacements, which leads to the practically identical movement of these two species due to the electrochemical coupling. These effects are also well reflected in the flux profiles computed at the outlet of the domain (Figure 4.5j-l). Particularly interesting is to examine the additive contribution of the transverse flux components for the hydrogen ions. Specifically, the electromigration term, $J_{H^+}^{mig}$, shows a positive contribution that accelerates H^+ for most of the transverse thickness of the H^+ plume. However, at the very edge of the plume (z > 8 cm at the outlet cross-section), $J_{H^+}^{mig}$ decreases and becomes negative again (Figures 4.5g and 4.5j). This happens because in this outer fringe area, the other two ions (Mg^{2+} and Cl^-) are present only in trace amount and the concentration ratio between protons and magnesium ions becomes similar ($C_{H+}/C_{Mg2+}\approx1$) or even larger ($C_{H+}/C_{Mg2+}>1$) than in Scenario 1. Consequently, as observed in Scenario 1, a negative contribution of $J_{H^+}^{mig}$ reduces the dispersive flux, $J_{H^+}^{dis}$, and leads to a reduction of transverse movement of H^+ in this particular small region of the domain.

The results found in Scenario 1 and 2 clearly show the existence and significance of ionic interactions during acidic plume migration in advection-dominated flow-through systems and how their extent can vary depending on the composition of the same ternary electrolyte system.

4.5.3 Analysis of the electrical potential gradient

A deeper understanding of the interactions between individual species and insights into the mechanisms of electromigration can be obtained by evaluating the electrical potential gradient produced by different ions on the course of multicomponent transport. The electrical potential gradient is a key term for the electrochemical migration flux (equation (4.1)) and describes the effect of the additional force, acting on a given ion *i,* arising from electric fields induced by the different diffusion rates of the charged species in solution [*Lasaga*, 1998]. According to equation (4.2), the gradient of electrical potential (also known as diffusion potential) in the transverse direction can be calculated as:

$$\frac{\partial \Phi}{\partial x_T} = \frac{-\sum_{i=1}^{N}\left(z_i D_i \frac{\partial C_i}{\partial x_T}\right)}{\sum_{i=1}^{N}\left(z_i^2 F D_i C_i\right)/RT} \tag{4.10}$$

in which the diffusion coefficients of equation (4.2) are replaced by transverse hydrodynamic dispersion coefficients for flow-through systems. By considering an electrolyte system with the three major ions considered in our experimental scenarios, the electrical gradient component in the above equation is the additive contribution of the gradients caused by each ion and can be expressed as:

$$\frac{\partial \Phi}{\partial x_T} = \frac{\partial \Phi_{H^+}}{\partial x_T} + \frac{\partial \Phi_{Mg^{2+}}}{\partial x_T} + \frac{\partial \Phi_{Cl^-}}{\partial x_T} \tag{4.11}$$

Figure 4.6 represents the calculated electrical gradient and its different components (equation (4.11)) for both experimental scenarios. Figure 4.6a also shows that the net electrical potential gradient produced by the movement of different ionic species is negative in Scenario 1. Such net electrical potential gradient consists of a negative contribution for both cations (H^+ and Mg^{2+}) and a positive contribution for the common anion (Cl^-) (Figure 4.6b-d). The outlet vertical profiles of ion-specific electrical potential gradients for this experimental scenario are shown in Figure 4.6e.

In the source zone (z=0-4 cm), the components from the cations ($\frac{\partial \Phi_{H^+}}{\partial x_T}$ and $\frac{\partial \Phi_{Mg^{2+}}}{\partial x_T}$) tend to counterbalance the anionic component, $\frac{\partial \Phi_{Cl^-}}{\partial x_T}$. However, due to the differences in their diffusivities, the electrostatic gradient develops in the fringe area. The gradient in the electrostatic potential generates an electrical field, under which electrical forces are exerted on the dissolved charged species in the solution. The magnitude of the force imposed on individual species is dependent on the charge of the dissolved species and the overall electrical gradient. The flux due to the electrical gradient for an individual species is directly proportional to the force active on that species and the species' concentration (Probstein, 1989). As a result, the active electric field enforces the dissolved ionic species' diffusive movement (electromigration) in the solution to maintain electroneutrality. In particular, for this specific experimental scenario, the negative electrostatic gradient limits the overall diffusive/dispersive movement of positively charged ions and enhances the movement of the negatively charged ion. This behavior is also evident from equation (4.1) and (4.9); in fact, for a cation, a negative electrical potential gradient leads to a migration flux component in the direction opposite to the diffusive/dispersive component and thus reduces its total flux. The situation is opposite for an anion where the same electrical potential gradient produces J_i^{mig} in the same direction as J_i^{dis} and consequently enhances the total transverse flux. Such behavior is also observed during the experiment as illustrated in the maps of fluxes in Figure 4.3.

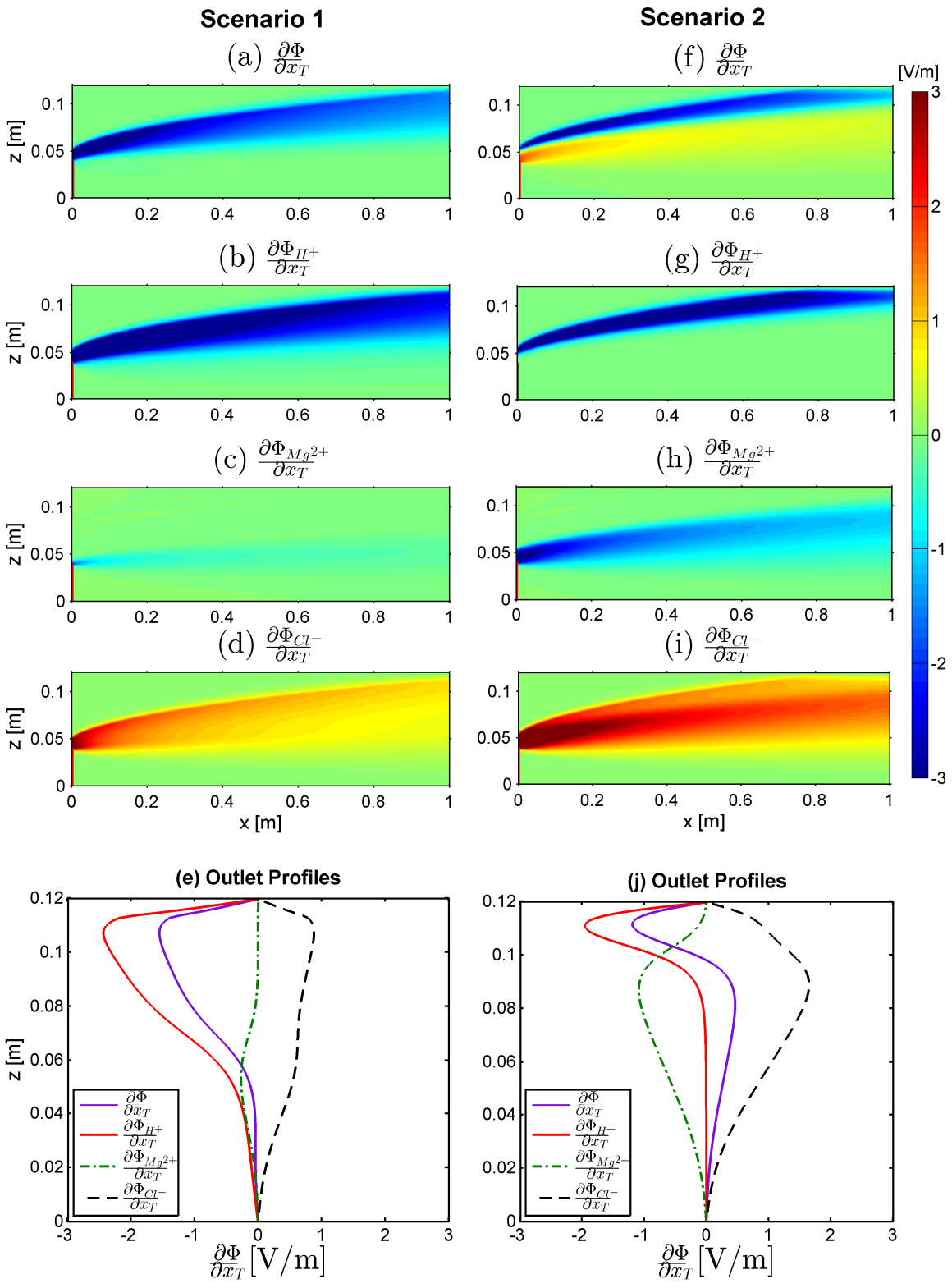

Figure 4.6. Maps of the transverse component of the electrostatic potential gradient produced during multicomponent ionic transport: The net electrical gradient (a, f), proton component (b, g), magnesium component (c, h), chloride component (d, i), and the outlet cross-sectional profiles (e, j) for Scenario 1 (a-e) and Scenario 2 (f-j).

In Scenario 2, the distribution of the net electrical potential gradient is significantly different compared to that of Scenario 1. In this experiment, $\frac{\partial \Phi}{\partial x_T}$ is negative in the outer fringe area whereas it is positive in the inner fringe of the ionic plume. The opposite behavior of $\frac{\partial \Phi}{\partial x_T}$ in these two fringe zones is clearly illustrated in Figure 4.6f. This outcome further explains the behavior observed in the flux maps in Figure 4.5, where the positive electromigration flux of the cations and the negative migration flux of the anion are induced by the positive electrical potential gradient in the inner fringe. However, in the outer fringe, $\frac{\partial \Phi}{\partial x_T}$ is negative and the situation is similar as in Scenario 1. Consequently, in this region, the negative electrostatic gradient retards the cations and accelerates the anion. The ions present in great excess (Mg^{2+} and Cl^-) have larger electrical gradient components compared to those of Scenario 1 (Figure 4.6c-j). On the other hand, the proton component, $\frac{\partial \Phi_{H^+}}{\partial x_T}$ is around zero until the outer fringe (z = ~8.5 cm at the outlet), where it becomes negative (Figure 4.6j). Such behavior in the outlet cross-sectional profiles also implies that H^+ is the least involved species in the electrostatic coupling for most of the vertical cross section with the exception of the outer fringe area. However, in Scenario 1 the opposite is observed where H^+ is the most involved ion in the electrostatic coupling and major contributor to the net electrical potential gradient (Figure 4.6e).

4.5.4 Dilution of the ionic plumes

It is interesting to analyze the multicomponent transport problems and the flow-through experiments of this study using metrics of plume dilution. We use the flux-related dilution index [*Rolle et al*., 2009] to quantify the dilution of the different ionic plumes due to their lateral displacement and mixing with deionized water. This metric, based on the concept of Shannon entropy, describes the distribution of a solute mass flux over the volumetric water flux at a given location along the main flow direction. The flux-related dilution index is particularly suited to study the dilution of solute plumes continuously emitted from a contamination source [*Chiogna et al*., 2012; *Rolle et al*., 2012]. For a multicomponent ionic transport problem, the flux-related dilution index of a charged species, i, reads as:

$$E_{Q,i}(x) = \exp\left(-\int_{\Omega} p_{Q,i}(\boldsymbol{x}) \ln(p_{Q,i}(\boldsymbol{x})) q_x(\boldsymbol{x}) d\Omega \right) \tag{4.12}$$

where $q_x = v\theta$ is the specific discharge in the main flow direction normal to the cross-sectional area Ω, θ is the porosity and $p_{Q,i}$ is the flux-related probability density function:

$$p_{Q,i}(\boldsymbol{x}) = \frac{C_i(\boldsymbol{x})}{\int_{\Omega} C_i(\boldsymbol{x}) q_x(\boldsymbol{x}) d\Omega} \tag{4.13}$$

The flux-related dilution index has been used as metric of plume dilution in both Stokes' and Darcy's flows [*Rolle et al.*, 2013b; *Rolle and Kitanidis*, 2014]. Physically $E_{Q,i}(x)$ represents an effective volumetric flux transporting the solute flux of a given ion i at the longitudinal position x. The values of $E_{Q,i}(x)$ monotonically increase with the travel distance in the flow-through system. For multicomponent transport, a higher value of the flux-related dilution index for a species i compared to the other ions in solution quantifies the higher dilution of the plume of that species. Figure 4.7 reports the computed flux-related dilution index, $E_{Q,i}$ at different longitudinal cross sections for the investigated experimental scenarios. At the inflow boundary, the flux-related dilution index is identical for each ion because they are injected from the same inlet ports and thus show the same extent of dilution. However, E_Q profiles evolve differently for different ionic species in the porous media because the transported ions have different diffusive and dispersive properties leading to a distinct distribution of the ions' mass fluxes over the volumetric flux in the flow-through setup (Figure 4.7a-b).

The experimental flux-related dilution index, calculated from the concentrations and volumetric discharges measured at the inlet and outlet of the flow-through domain, shows a reasonable agreement with the model simulations. In Scenario 1, where two electrolytes (HCl and $MgCl_2$) were simultaneously injected at the same concentration level, all ions show distinct profiles that monotonically increase along the travel distance (Figure 4.7a). The dotted lines denote the simulated dilution of each species at their liberated state (i.e., as if they were transported as uncharged species). Both cations (H^+ and Mg^{2+}) show a reduction and the common anion (Cl^-) shows an enhancement of dilution compared to the case of displacement at liberated state conditions. In particular, the H^+ plume, although being clearly the most diluted one, shows a considerable decrease in the E_Q value compared to the outcomes of the multicomponent simulations describing H^+ undergoing transverse displacement according to its liberated state diffusive/dispersive properties. As discussed above this limitation in dilution is due to the electrostatic interactions with the other charged species. This results in coupled dispersive fluxes that are caused by the development of an electrical potential gradient induced by the different diffusive rates of the ionic species in the solution (section 4.5.3) and by the dependence of local dispersion coefficients on the solutes' diffusivities, not only at slow but also at high flow velocities. The latter effect arises from incomplete mixing and compound-specific gradients of different solutes in the pore channels [*Rolle et al.*, 2012].

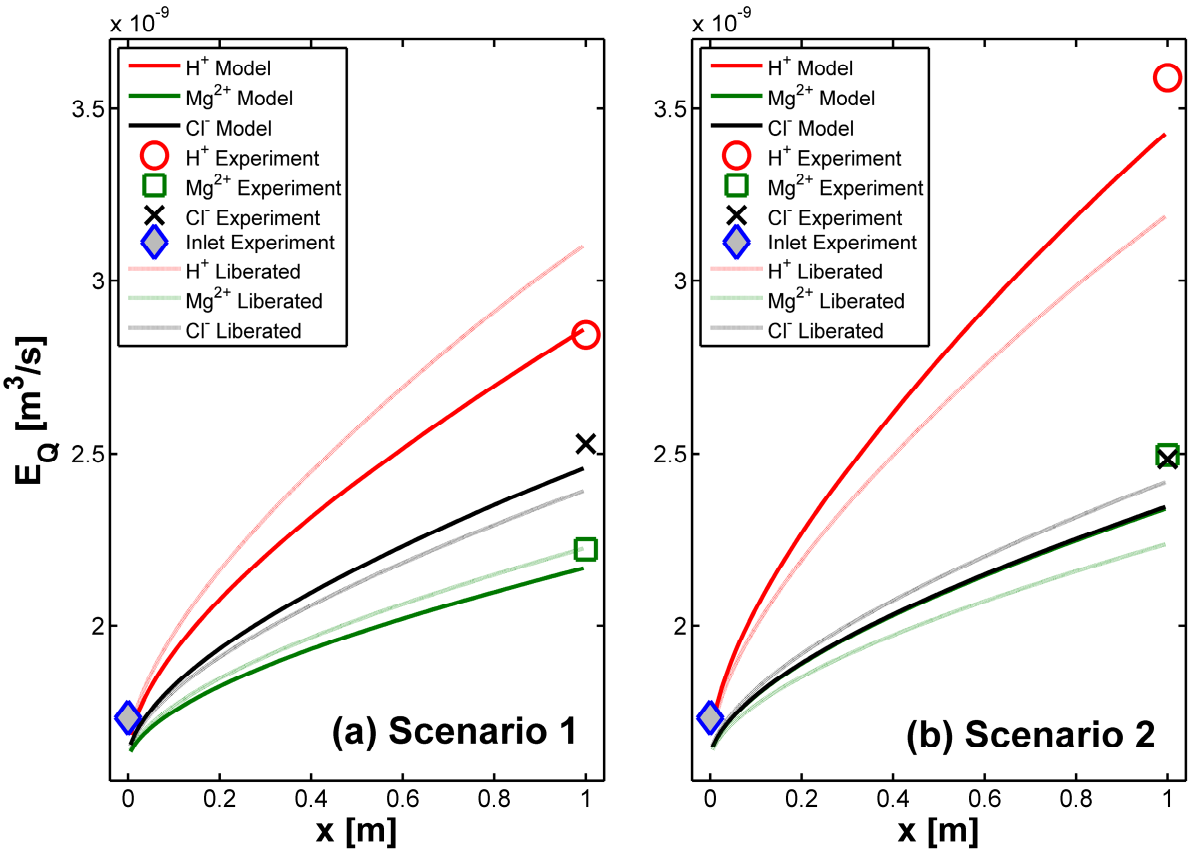

Figure 4.7. Observed (symbols) and simulated (lines) flux-related dilution index for the two experimental scenarios: (a) Scenario 1: Injection of HCl and $MgCl_2$ with similar concentration (i.e., $C_{H+}/C_{Mg2+} \approx 1$) in Milli-Q water; (b) Scenario 2: Injection of HCl and $MgCl_2$ with excess $MgCl_2$ concentration (i.e., $C_{H+}/C_{Mg2+} \approx 0.01$) in Milli-Q water. The term liberated refers to the case without electrostatic coupling (i.e., the species are transported as uncharged species with their own diffusive/dispersive properties).

In Scenario 2, Mg^{2+} and Cl^- have identical profiles of flux-related dilution index and they also show practically the same measured values of E_Q (Figure 4.7b). This behavior is, in fact, induced from the composition of the injected electrolyte solution and the associated Coulombic cross-coupling of dispersive fluxes. Although $MgCl_2$ fully ionizes in solution, the cation and anion appear to travel together, nearly as a single salt. However, a close inspection of the concentrations of these ions reveals a tendency of Cl^- to displace slightly further in the transverse direction resulting in a small excess of Mg^{2+} in the core of the plume. This also affects the behavior of H^+ which tends to displace faster out of this region, thus receiving a positive electrostatic contribution to its lateral movement. As a result, the hydrogen ions displace at a rate that is even larger than the one expected under liberated state conditions. The

enhanced displacement of H^+ results in a very dilute plume showing values of flux-related dilution index 45% higher than the other ionic species in the setup. Comparing the dilution of the H^+ plumes in the two experimental scenarios it is interesting to notice that, based on the measured values at the outlet, the acidic plume in Scenario 2 is effectively distributed over a water flux which is 26% larger compared to the one carrying the acidic plume in Scenario 1. This outcome is quite striking since it shows that the extent of mixing for H^+ varies remarkably depending on the composition of the aqueous solution. This variation is solely due to the electrostatic Coulombic effects since both multicomponent ionic flow-through experiments were performed using the same electrolytes and under identical flow and transport conditions. The values of the flux-related dilution index measured at the outlet of the flow-through setup are summarized in Table 4.3.

Table 4.3: Flux-related dilution index computed from ion concentrations and volumetric discharge measured at the outlet of the flow-through setup.

Ions	**Flux-related dilution index, $E_{Q,i}$ [m^3/s]**	
	Scenario 1	**Scenario 2**
H^+	2.84×10^{-9}	3.59×10^{-9}
Mg^{2+}	2.22×10^{-9}	2.50×10^{-9}
Cl^-	2.53×10^{-9}	2.48×10^{-9}

4.5.5 Propagation of pH fronts

As seen in the previous sections, the laboratory experiments with a ternary mixture of strong electrolytes have shown specific features of the concentration profiles of the different ions, the interaction of purely dispersive and electromigration fluxes as well a distinct dilution of the ionic plumes. Focusing on the proton displacement, the transport of H^+ in the saturated porous medium can be regarded and analyzed as a problem of propagation of dispersive pH fronts in the transverse direction. Figure 4.8 illustrates the results of the propagation of pH fronts for the two experimental scenarios. Figure 4.8a represents the vertical distances, beyond the injection zone, reached by the acidic fronts at different longitudinal cross sections in the flow-through setup. The calculation of such vertical distances, that can be regarded as a penetration depth travelled by the pH fronts, refers to changes of 1.5 units in pH compared to the inlet solution. These pH values were chosen as threshold for the edge of the acidic plumes.

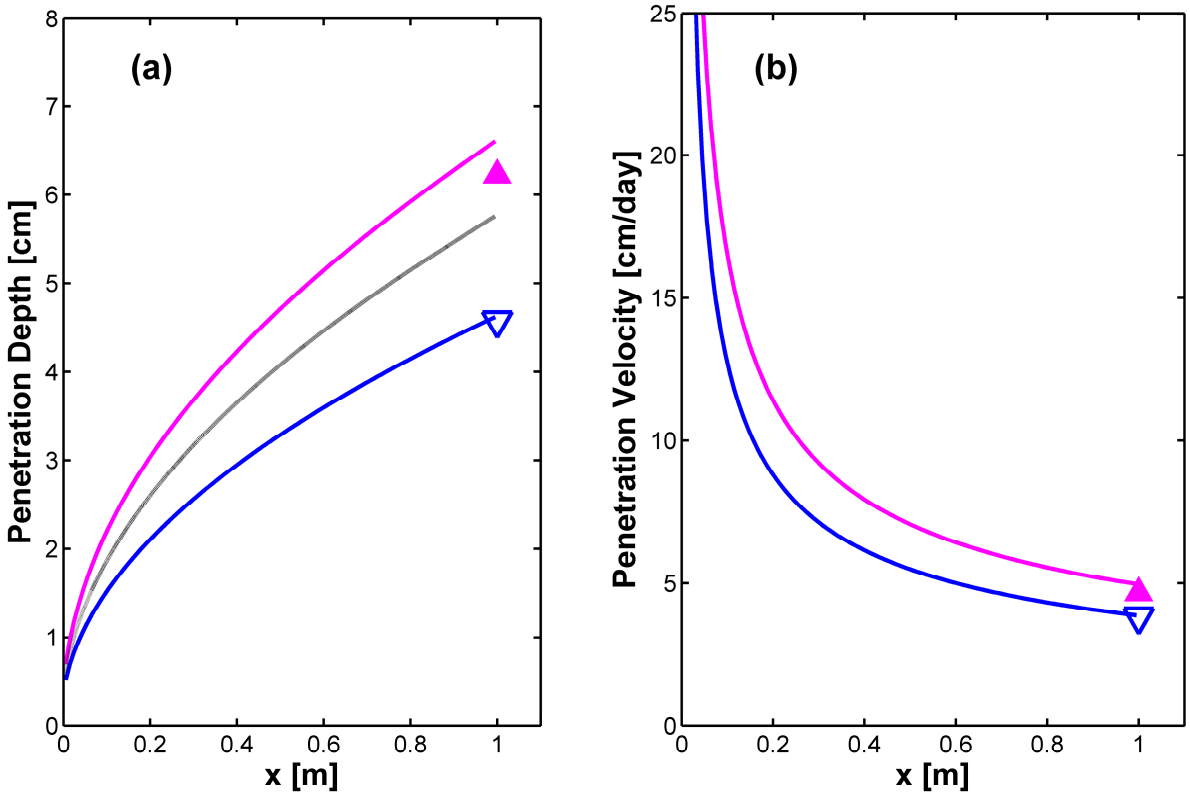

Figure 4.8. The symbols represent the observed (blue and pink colors for Scenario 1 and 2, respectively) penetration depths (a) and penetration velocities (b) of pH fronts in the two experimental scenarios. The lines are the simulated values including the case of penetration depth (black dotted line) computed for liberated state (i.e., without electrostatic coupling). Penetration depth refers to the distance of pH front migration. The pH front is tracked considering a difference of 1.5 pH units from the initial solution pH.

Figure 4.8a clearly shows that the pH front at any longitudinal cross section migrates to a larger distance in Scenario 2 compared to Scenario 1. At the end of the flow-through domain (x = 1 m), the difference among the measured penetration depths in the two experimental scenarios reaches 1.6 cm. This behavior is consistent with the observations of the outlet pH profiles (Figures 4.2b and 4.4b) and of the flux-related dilution indices (Figure 4.7). The use of a different solution composition in Scenario 2 and the resultant Coulombic interactions between transported ionic species significantly accelerate the protons compared to the conditions tested in Scenario 1, thus causing a more effective penetration of the acidic front in Scenario 2. The different and increasing penetration depth of the acidic fronts at different cross-sections along the water flow direction allow us to calculate a speed of propagation of the dispersive pH fronts in the vertical direction. The results are reported in Figure 4.8b and

show distinct behaviors for the two experimental scenarios with faster propagation velocity of the pH front observed in Scenario 2. In both cases the trend of such propagation velocities show that they reach their maximum close to the inlet of the flow-through setup, where due to the injection boundary conditions very high H^+ gradients occur. Due to hydrodynamic dispersion, those gradients tend to smooth along the water flow direction causing a reduced penetration velocity of the pH fronts at increasing longitudinal distances.

4.6 Summary and Conclusions

This study shows the significance of ionic interactions for the propagation of pH fronts in porous media. We have presented detailed flow-through experiments on multicomponent ionic transport in saturated porous media under steady-state conditions. In particular, we have studied the propagation of acidic fronts considering two distinct transport scenarios for mixed electrolyte solutions. Such experimental scenarios were chosen to demonstrate significantly different electromigration effects of the ions in solution on the transverse displacement of hydrogen ions, and thus on the propagation of dispersive pH fronts. The experiments have been quantitatively interpreted with a two-dimensional multicomponent ionic transport model based on an accurate description of local dispersion and accounting for charge conservation and for electrochemical cross-coupling of charged species in the solution. Purely forward numerical simulations showed an excellent agreement with the high resolution ion concentrations and pH profiles measured at the outlet of the laboratory setup.

The experimental and modeling results clearly show the importance of charge interactions and the cross-coupling of ion displacement also for advective-dispersive transport in porous media. Specifically, the effects of Coulombic interactions on acidic front migration were explored in this study and were shown to be particularly important for the propagation of pH fronts, since the displacement of hydrogen ions can be significantly accelerated or retarded depending on the concentration of other ions in solution. Considerable differences have been observed between the two experimental scenarios, both in terms of penetration depth of the pH fronts (relative difference of 36% between the two flow-through experiments) as well as for plume dilution (26% relative difference). Furthermore, the differences were also significant (up to 25% and 19% in penetration depth and plume dilution, respectively) compared to transport at liberated state (i.e., without considering the electrostatic cross-coupling). Coulombic interactions at the basis of multicomponent ionic transport occur at the small molecular scale; however, their effect propagates through the scales and impacts macroscopic solute transport. This was observed both in the flow-through experiments and from the outcomes of the

numerical simulations. Furthermore, the conditions investigated highlight the importance of electromigration interactions not only at slow horizontal flow velocity but also for fast groundwater flow, under advection-dominated conditions. Two main factors contribute to these effects: the electrochemical coupling between different charged species and the incomplete mixing in the pore channels which is captured by macroscopic parameterizations of local transverse dispersion depending on solutes diffusivities not only at slow but also at high flow velocities [*Rolle et al.*, 2012; *Scheven*, 2013]. The latter effect has been proven to be relevant and to propagate also at larger field scales, in heterogeneous flow fields, provided that the spatial variability and dependence from the grain size of local dispersion coefficients is acknowledged [e.g., *Chiogna et al.*, 2011; *Eckert et al.*, 2012]. The experimental findings of this study also contribute to support the conclusions of recent investigations that pointed out the key role of aqueous diffusion for groundwater transport also at large scales [*La Bolle and Fogg*, 2008; *Rolle et al*., 2013b; *Hadley and Newell*, 2014].

The effects of electromigration on pH front propagation, studied in this work under simplified conditions, can also impact more complex situations of subsurface flow and transport including transient transport conditions as well as additional physical and (bio)geochemical processes like sorption, ion-exchange, surface complexation [e.g., *Gvirtzman and Gorelick*, 1991; *Zachara et al*., 1991; *Bjerg and Christensen*, 1993; *Appelo*, 1994; *Liu et al*., 2011; *Holden et al*., 2012, 2013], geochemical weathering of sediments, pH buffering, release/mobilization of trace metals, mineral dissolution-precipitation and degradation reactions [e.g., *Hansen and Postma*, 1995; *Kjøller et al*., 2004; *Maher et al*., 2006; *Tartakovsky et al.*, 2008; *Liu et al*, 2011; *Molins et al*., 2012; *Li et al*., 2014].

Finally, recent investigation of solute transport in homogeneous and heterogeneous three-dimensional experimental setups [*Ye et al*., 2015a and 2015b] suggests that the charge interactions and the cross-coupling effects, studied in this work in (quasi) two-dimensional domains, would be even more pronounced for fully three-dimensional ionic transport in porous media.

Acknowledgments

The experimental data of this study are provided in the Supporting Information. Specifically, Table S4.1 and Table S4.2 summarize the concentration and pH values used in Figure 4.2 and Figure 4.4, respectively. Furthermore, a 1D multicomponent diffusion problem is presented to benchmark the modeling approach of this study with the geochemical code PHREEQC.

We thank Bernice Nisch and the hydrogeochemistry laboratory at the University of Tuebingen (Prof. P. Grathwohl) for assistance with the ion-chromatography measurements. Constructive comments of three anonymous reviewers and associate editor helped in improving the quality of the manuscript. This work was supported by the Baden-Württemberg Stiftung under the Eliteprogram for Postdocs.

References

Appelo, C. A. J. (1994), Cation and proton exchange, pH variations, and carbonate reactions in a freshening aquifer, *Water Resour. Res*., *30*(10), 2793-2805.

Appelo, C. A. J., and P. Wersin (2007), Multicomponent diffusion modeling in clay systems with application to the diffusion of tritium, iodide, and sodium in opalinus clay, *Environ. Sci. Technol.*, *41*(14), 5002-5007.

Appelo, C. A. J., L. R. Van Loon, and P. Wersin (2010), Multicomponent diffusion of a suite of tracers (HTO, Cl, Br, I, Na, Sr, Cs) in a single sample of Opalinus Clay, *Geochim. Cosmochim. Acta*, *74*(4), 1201-1219.

Appelo, C. A. J., A. Vinsot, S. Mettler, and S. Wechner (2008), Obtaining the porewater composition of a clay rock by modeling the in- and out-diffusion of anions and cations from an in-situ experiment, *J. Contam. Hydrol.*, *101*(1-4), 67-76.

Bard, A. J., and L. R. Faulkner (2001), *Electrochemical Methods: Fundamentals and Applications*, 718 pp., John Wiley, New York.

Ben-Yaakov, S. (1972), Diffusion of sea water ions—I. Diffusion of sea water into a dilute solution, *Geochim. Cosmochim. Acta*, *36*(12), 1395-1406.

Bjerg, P. L., and T. H. Christensen (1993), A field experiment on cation exchange-affected multicomponent solute transport in a sandy aquifer, *J. Contam. Hydrol.. 12*, 269-290.

Boudreau, B. P., F. J. R. Meysman, and J. J. Middelburg (2004), Multicomponent ionic diffusion in porewaters: Coulombic effects revisited, *Earth Planet. Sci. Lett.*, *222*(2), 653-666.

Chiogna, G., O. A. Cirpka, P. Grathwohl, and M. Rolle (2011), Relevance of local compound-specific transverse dispersion for conservative and reactive mixing in heterogeneous porous media, *Water Resour. Res.*, *47*(7), W07540.

Chiogna, G., C. Eberhardt, P. Grathwohl, O. A. Cirpka, and M. Rolle (2010), Evidence of compound-dependent hydrodynamic and mechanical transverse dispersion by multitracer laboratory experiments, *Environ. Sci. Technol.*, *44*(2), 688-693.

Chiogna, G., D. L. Hochstetler, A. Bellin, P. K. Kitanidis, and M. Rolle (2012), Mixing, entropy and reactive solute transport, *Geophys. Res. Lett.*, *39*(20), L20405.

Cirpka, O. A., E. O. Frind, and R. Helmig (1999a), Streamline-oriented grid generation for transport modelling in two-dimensional domains including wells, *Adv. Water Resour*., *22*(7), 697-710.

Cirpka, O. A., E. O. Frind, and R. Helmig (1999b), Numerical methods for reactive transport on rectangular and streamline-oriented grids, *Adv. Water Resour*., *22*(7), 711-728.

Cirpka, O. A., F. P. J. de Barros, G. Chiogna, M. Rolle, and W. Nowak (2011), Stochastic flux-related analysis of transverse mixing in two-dimensional heterogeneous porous media, *Water Resour. Res.*, *47*(6), W06515.

Cussler, E. L. (2009), *Diffusion : Mass Transfer in Fluid Systems*, third ed., 631 pp., Cambridge University Press, Cambridge, New York.

Davis, J. A., and D. B. Kent (1990), Surface complexation modeling in aqueous geochemistry, Eds. M.F. Hochella and A. F. White, Mineral-Water Interface Geochemistry, Min. Soc. Am., *Rev. Mineral.*, *23*, 177-260.

Davis, J. A., D. E. Meece, M. Kohler, and G. P. Curtis (2004), Approaches to surface complexation modeling of Uranium(VI) adsorption on aquifer sediments, *Geochim. Cosmochim. Acta*, *68*(18), 3621-3641.

Davis, T., and I. Duff (1997), An unsymmetric-pattern multifrontal method for sparse LU factorization, *SIAM J. Matrix Anal. A.*, *18*(1), 140-158.

de Caritat, P. (1995), Intensifying groundwater acidification at Birkenes, southern Norway, *J. Hydrol*., *170*(1–4), 47-62.

Donovan, J. J., K. W. Frysinger, and T. P. Maher Jr. (1997), Geochemical response of acid groundwater to neutralization by alkaline recharge, *Aq. Geochem.*, *2*(3), 227-253.

Eckert, D., M. Rolle, and O. A. Cirpka (2012), Numerical simulation of isotope fractionation in steady-state bioreactive transport controlled by transverse mixing, *J. Contam. Hydrol.*, *140–141*(0), 95-106.

Edmunds, W.M., and D. G. Kinniburgh, (1986), The susceptibility of UK groundwaters to acidic deposition, *J. Geol. Soc.*, *143*, 707–720.

Engesgaard, P., and K. L. Kipp (1992), A geochemical transport model for redox-controlled movement of mineral fronts in groundwater flow systems: A case of nitrate removal by oxidation of pyrite, *Water Resour. Res.*, *28*(10), 2829-2843.

Fest, E. P. M. J., E. J. M. Temminghoff, J. Griffioen, and W. H. Van Riemsdijk (2005), Proton buffering and metal leaching in sandy soils, *Environ. Sci. Technol.*, *39*(20), 7901-7908.

Fest, E. P. M. J., E. J. M. Temminghoff, J. Griffioen, B. Grift, and W. H. Van Riemsdijk (2007), Groundwater chemistry of Al under Dutch acid sandy soils: effects of land use and depth, *Appl. Geochem.*, *22*(7), 1427-1438.

Franken, G., D. Postma, W. H. M. Duijnisveld, J. Böttcher, and J. Molson (2009), Acid groundwater in an anoxic aquifer: Reactive transport modelling of buffering processes, *Appl. Geochem.*, *24*(5), 890-899.

Giambalvo, E. R., C. I. Steefel, A. T. Fisher, N. D. Rosenberg, and C. G. Wheat (2002), Effect of fluid-sediment reaction on hydrothermal fluxes of major elements, eastern flank of the Juan de Fuca Ridge, *Geochim. Cosmochim. Acta*, *66*(10), 1739-1757.

Griffioen, J. (1993), Multicomponent cation exchange including alkalinization/ acidification following flow through sandy sediment, *Water Resour. Res.*, *29*(9), 3005-3019.

Gvirtzman, H., and S. M. Gorelick (1991), Dispersion and advection in unsaturated porous media enhanced by anion exclusion, *Nature 352*, 793-795.

Haberer, C. M., M. Muniruzzaman, P. Grathwohl, and M. Rolle (2015), Diffusive/Dispersive and reactive fronts in porous media: Fe (II)-oxidation at the unsaturated/saturated interface, *Vadose Zone J.*, doi:10.2136/vzj2014.07.0091.

Haberer, C. M., M. Rolle, O. A. Cirpka, and P. Grathwohl (2012), Oxygen transfer in a fluctuating capillary fringe, *Vadose Zone J.*, *11*(3).

Hadley, P. W., and C. Newell (2014), The new potential for understanding groundwater contaminant transport, *Groundwater*, *52*(2), 174-186.

Hansen, B. K., and D. Postma (1995), Acidification, buffering, and salt effects in the unsaturated zone of a sandy aquifer, Klosterhede, Denmark, *Water Resour. Res.*, *31*(11), 2795-2809.

Hochstetler, D. L., M. Rolle, G. Chiogna, C. M. Haberer, P. Grathwohl, and P. K. Kitanidis (2013), Effects of compound-specific transverse mixing on steady-state reactive plumes: Insights from pore-scale simulations and Darcy-scale experiments, *Adv. Water Resour.*, *54*, 1-10.

Holden, A. A., K. U. Mayer and A. C. Ulrich (2012), Evaluating methods for quantifying cation exchange in mildly calcareous sediments in Northern Alberta. *Appl. Geochem.*, *27*, 2511-2523.

Holden A. A., S. E. Haque, K. U. Mayer and A. C. Ulrich (2013) Biogeochemical processes controlling the mobility of major ions and trace metals in aquitard sediments beneath an oil sand tailing pond: Laboratory studies and reactive transport modeling, *J. Contam. Hydrol.*, *151*, 55-67.

Kent, D. B., R. H. Abrams, J. A. Davis, J. A. Coston, and D. R. LeBlanc (2000), Modeling the influence of variable pH on the transport of zinc in a contaminated aquifer using semiempirical surface complexation models, *Water Resour. Res.*, *36*(12), 3411-3425.

Kjøller, C., D. Postma, and F. Larsen (2004), Groundwater acidification and the mobilization of trace metals in a sandy aquifer, *Environ. Sci. Technol.*, *38*(10), 2829-2835.

LaBolle, E. M., and G. E. Fogg (2001), Role of molecular diffusion in contaminant migration and recovery in an alluvial aquifer system, *Transp. Porous Med.*, *42*(1-2), 155-179.

Lasaga, A. C. (1979), The treatment of multi-component diffusion and ion pairs in diagenetic fluxes, *Am. J. Sci.*, *279*(3), 324-346.

Lasaga, A. C. (1998), *Kinetic Theory in the Earth Sciences*, 811 pp., Princeton University Press, Princeton, N. J.

Li, L., C. A. Peters, and M. A. Celia (2007), Effects of mineral spatial distribution on reaction rates in porous media, *Water Resour. Res*., *43*(1), W01419.

Li, L., C. I. Steefel, and L. Yang (2008), Scale dependence of mineral dissolution rates within single pores and fractures, *Geochim. Cosmochim. Acta*, *72*(2), 360-377.

Li, L., F. Salehikhoo, S. L. Brantley, and P. Heidari (2014), Spatial zonation limits magnesite dissolution in porous media, *Geochim. Cosmochim. Acta*, *126*(0), 555-573.

Liu, C. X. (2007), An ion diffusion model in semi-permeable clay materials, *Environ. Sci. Technol.*, *41*(15), 5403-5409.

Liu, C. X., J. Shang, and J. M. Zachara (2011), Multispecies diffusion models: A study of uranyl species diffusion, *Water Resour. Res*., *47*(12), W12514.

Liu, C. X., J. M. Zachara, A. Felmy, and Y. Gorby (2004), An electrodynamics-based model for ion diffusion in microbial polysaccharides, *Colloids Surf. A and B*, *38*(1-2), 55-65.

Maher, K., C. I. Steefel, D. J. DePaolo, and B. E. Viani (2006), The mineral dissolution rate conundrum: Insights from reactive transport modeling of U isotopes and pore fluid chemistry in marine sediments, *Geochim. Cosmochim. Acta*, *70*(2), 337-363.

Molins, S., D. Trebotich, C. I. Steefel, and C. P. Shen (2012), An investigation of the effect of pore scale flow on average geochemical reaction rates using direct numerical simulation, *Water Resour. Res*., *48*.

Moss, P. D., and W. M. Edmunds (1992), Processes controlling acid attenuation in the unsaturated zone of a Triassic sandstone aquifer (U.K.), in the absence of carbonate minerals, *Appl. Geochem.*, *7*(6), 573-583.

Møller, K. B., R. Rey, , M. Masia, , and J. T. Hynes (2005), On the coupling between molecular diffusion and solvation shell exchange, *J. Chem. Phys.*, 122, 114508,1-12.

Muniruzzaman, M., C. M. Haberer, P. Grathwohl, and M. Rolle (2014), Multicomponent ionic dispersion during transport of electrolytes in heterogeneous porous media: Experiments and model-based interpretation, *Geochim. Cosmochim. Acta*, *141*(0), 656-669.

Prigiobbe, V., and S. L. Bryant (2014), pH-dependent transport of metal cations in porous media, *Environ. Sci. Technol.* 48(7): 3752-3759.

Probstein, R. F. (1989), Physicochemical hydrodynamics: An introduction, 337 pp., Butterworth Publishers, Stoneham.

Redden, G., D. Fox, , C. Zhang, , Y. Fujita, , L. J. Guo, , and P. Huang (2014) CaCO3 precipitation, transport and sensing in porous media with in situ generation of reactants, *Environ. Sci. Technol.* 48(1): 542-549.

Rolle, M., M. Muniruzzaman, C. M. Haberer, and P. Grathwohl (2013a), Coulombic effects in advection-dominated transport of electrolytes in porous media: Multicomponent ionic dispersion, *Geochim. Cosmochim. Acta*, *120*(0), 195-205.

Rolle, M., G. Chiogna, D. L. Hochstetler, and P. K. Kitanidis (2013b), On the importance of diffusion and compound-specific mixing for groundwater transport: An investigation from pore to field scale, *J. Contam. Hydrol.*, *153*(0), 51-68.

Rolle, M., C. Eberhardt, G. Chiogna, O. A. Cirpka, and P. Grathwohl (2009), Enhancement of dilution and transverse reactive mixing in porous media: Experiments and model-based interpretation, *J. Contam. Hydrol.*, *110*(3–4), 130-142.

Rolle, M., D. L. Hochstetler, G. Chiogna, P. K. Kitanidis, and P. Grathwohl (2012), Experimental investigation and pore-scale modeling interpretation of compound-specific transverse dispersion in porous media, *Transp. Porous Med.*, *93*(3), 347-362.

Rolle, M., and P. K. Kitanidis (2014), Effects of compound-specific dilution on transient transport and solute breakthrough: A pore-scale analysis, *Adv. Water Resour.*, 71, 186-19.

Scheven, U. M. (2013), Pore-scale mixing and transverse dispersivity of randomly packed monodisperse spheres, *Phys. Rev. Let.,* 110, 214504.Steefel, C. I., and K. Maher (2009), Fluid-rock interaction: A reactive transport approach, *Rev. Mineral. Geochem.*, *70*, 485-532.

Tartakovsky, A.M., G. D. Redden, P. C. Lichtner, T. C. Scheibe, and P. Meakin (2008), Mixing-induced precipitation: Experimental study and multi-scale numerical analysis. *Water Resour. Res*., *44*, W06S04. doi:10.1029/2006WR005725.

Van Cappellen, P., and J. F. Gaillard (1996), Biogeochemical dynamics in aquatic sediments, *Rev. Mineral. Geochem*., *34*(1), 335-376.

Vinograd, J. R., and J. W. McBain (1941), Diffusion of electrolytes and of the ions in their mixtures, *J. Am. Chem. Soc.*, *63*(7), 2008-2015.

Ye, Y., G. Chiogna, O. A. Cirpka, P. Grathwohl, and M. Rolle (2015a), Experimental investigation of compound-specific dilution of solute plumes in saturated porous media: 2-D vs. 3-D flow-through systems, *J. Contam. Hydrol.*, *172*(0), 33-47.

Ye, Y., G. Chiogna, O. A. Cirpka, P. Grathwohl, and M. Rolle (2015b), Enhancement of plume dilution in two- and three-dimensional porous media by flow focusing in high-permeability inclusions, *Water Resour. Res.*, *51,* doi:10.1002/2015WR016962.

Zachara, J. M., C. E. Cowan, and C. T. Resch (1991), Sorption of divalent metals on calcite, *Geochim. Cosmochim. Acta*, *55*(6), 1549-1562.

S4. Supporting Information

S4.1 Introduction

This document includes the benchmarking of the transport model, used in this study to interpret the laboratory results, with the code PHREEQC (Parkhurst and Appelo, 1999) for a 1D multicomponent diffusion problem. The document also provides a summary of the concentrations and pH data measured in the flow-through experiments. The values reported are average of duplicate measurements performed at the outlet of the flow-through setup.

S4.2 Benchmarking of the transport code with PHREEQC

The transport code used in this study is validated by comparing the simulation results with PHREEQC in a one dimensional multicomponent diffusive transport problem. We consider a 1D column of 12 cm in which half the length contains the tracer solution (source zone) and the other half only pure water (Figure S4.1). The simulations are performed considering purely diffusive multicomponent transport using the tracer solution compositions of both experimental scenarios and the diffusion coefficients reported in Table 4.1. The spatial profiles from the two codes are compared after 12 hours of simulation time (Figure S4.2).

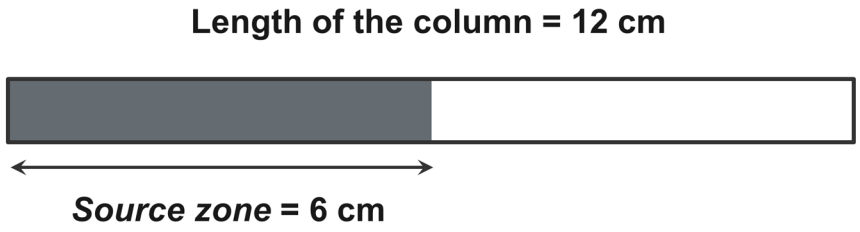

Figure S4.1. Schematic diagram of 1D setup for the benchmark problem.

Figure S4.2 shows an excellent agreement between the results obtained with our model formulation and the outcomes of PHREEQC. It should be noted that, the effect of ionic strength, activity gradients, aqueous reactions and the presence of other ions and aqueous complexes (e.g., OH^-, $MgOH^+$) are included in the PHREEQC formulation. However, the PHREEQC outcomes do not deviate from our model results obtained considering only the coupling between the major cations and anions measured in the flow-through experiments (H^+, Mg^{2+} and Cl^-). This implies that these processes do not have a significant impact on the ionic

transport in these particular scenarios and neglecting them does not introduce any noticeable errors in interpreting the results of the flow-through experiments performed in this study.

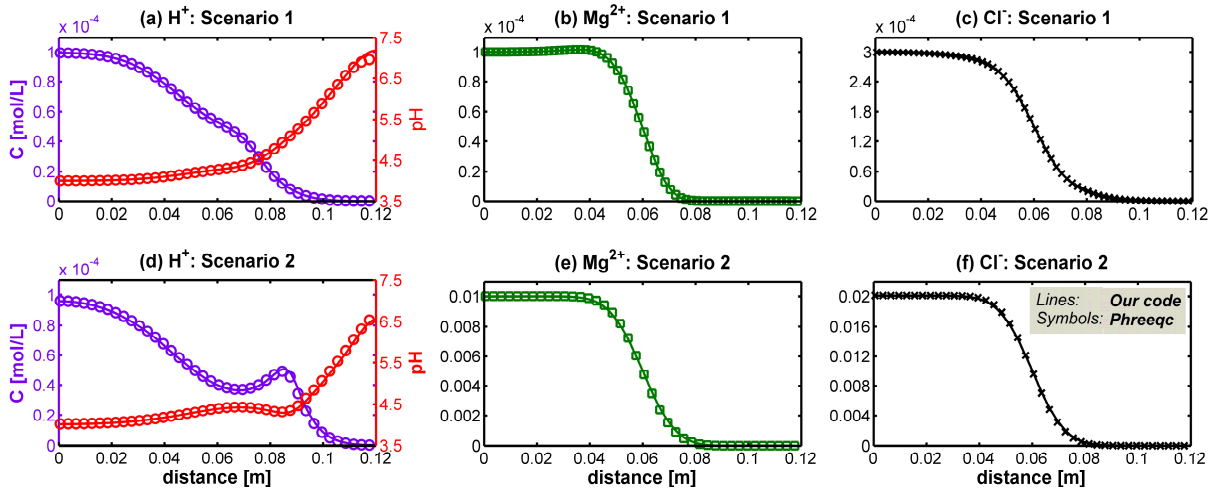

Figure S4.2. Comparison of the multicomponent transport code used in this study with the geochemical code PHREEQC for a 1D multicomponent diffusion problem. The profiles are taken after 12 hours of simulation: Scenario 1 (a, b, c), Scenario 2 (d, e, f).

Table S4.1: Experimental measurements performed at the outlet of the flow-through setup for multicomponent transport in Scenario 1. Concentration and pH values used in Figure 4.2.

Sampling Location z [cm]	Mg^{2+} Concentration [mol/L]	Cl^- Concentration [mol/L]	pH
0.5	1.48E-04	4.32E-04	3.81
1.0	1.45E-04	4.17E-04	3.85
1.5	1.40E-04	4.14E-04	3.91
2.0	1.31E-04	3.80E-04	3.94
2.5	1.22E-04	3.58E-04	3.97
3.0	1.10E-04	3.22E-04	3.91
3.5	9.34E-05	2.83E-04	3.98
4.0	7.25E-05	2.35E-04	4.08
4.5	5.36E-05	1.88E-04	4.12
5.0	3.65E-05	1.46E-04	4.22
5.5	2.14E-05	1.04E-04	4.26
6.0	1.03E-05	7.16E-05	4.38
6.5	2.63E-06	4.54E-05	4.48
7.0	0	2.44E-05	4.68
7.5	0	1.09E-05	4.79
8.0	0	1.69E-06	5.01
8.5	0	0	5.23
9.0	0	0	5.56
9.5	0	0	5.85
10.0	0	0	6.14
10.5	0	0	6.18
11.0	0	0	6.34
11.5	0	0	6.45
Injected solution (8 bottom inlet ports)	1.45E-4	4.55E-4	3.78

Table S4.2: Experimental measurements performed at the outlet of the flow-through setup for multicomponent transport in Scenario 2. Concentration and pH values used in Figure 4.4.

Sampling Location z **[cm]**	**Mg^{2+} Concentration [mol/L]**	**Cl^- Concentration [mol/L]**	**pH**
0.5	1.13E-02	2.29E-02	4.18
1.0	1.16E-02	2.28E-02	4.23
1.5	1.10E-02	2.22E-02	4.30
2.0	1.02E-02	2.06E-02	4.40
2.5	9.76E-03	1.90E-02	4.34
3.0	8.43E-03	1.68E-02	4.34
3.5	7.73E-03	1.49E-02	4.44
4.0	6.21E-03	1.21E-02	4.49
4.5	5.06E-03	9.08E-03	4.59
5.0	3.49E-03	6.37E-03	4.59
5.5	2.58E-03	4.37E-03	4.63
6.0	1.76E-03	2.78E-03	4.74
6.5	1.12E-03	1.67E-03	4.71
7.0	6.23E-04	1.01E-03	4.72
7.5	2.35E-04	5.15E-04	4.78
8.0	6.63E-05	3.10E-04	4.91
8.5	0	1.54E-04	4.90
9.0	0	1.17E-04	4.96
9.5	0	7.99E-05	5.14
10.0	0	7.06E-05	5.37
10.5	0	6.77E-05	5.89
11.0	0	4.37E-05	6.00
11.5	0	0	6.09
Injected solution (8 bottom inlet ports)	1.20E-2	2.41E-2	4.10

Chapter 5

Modeling multicomponent ionic transport in groundwater with IPhreeqc coupling: Electrostatic interactions and geochemical reactions in homogeneous and heterogeneous domains[§]

Abstract

The key role of small-scale processes like molecular diffusion and electrochemical migration has been increasingly recognized in multicomponent reactive transport in saturated porous media. In this study, we propose a two-dimensional multicomponent reactive transport model taking into account the electrostatic interactions during transport of charged ions in physically and chemically heterogeneous porous media. The modeling approach is based on the local charge balance and on the description of compound-specific and spatially variable diffusive/dispersive fluxes. The multicomponent ionic transport code is coupled with the geochemical code PHREEQC-3 by utilizing the IPhreeqc module, thus enabling to perform the geochemical calculations included in the PHREEQC's reaction package. The multicomponent reactive transport code is benchmarked with different 1-D and 2-D transport problems. Successively, conservative and reactive transport examples are presented to demonstrate the capability of the proposed model to simulate transport of charged species in heterogeneous porous media with spatially variable physical and chemical properties. The results reveal that the Coulombic cross-coupling between dispersive fluxes can significantly influence conservative as well as reactive transport of charged species both at the laboratory and at the field scale.

[§] Reproduced from: Muniruzzaman, M., and Rolle, M., (2016). Modeling multicomponent ionic transport in groundwater with IPhreeqc coupling: Electrostatic interactions and geochemical reactions in homogeneous and heterogeneous domains. *Advances in Water Resources, 98,* 1-15.
doi:http://dx.doi.org/10.1016/j.advwatres.2016.10.013.

5.1 Introduction

The importance of coupling subsurface solute transport models with geochemical codes, capable of simulating a wide variety of equilibrium and kinetic reactions, has been increasingly recognized and has led to major developments of reactive transport codes for subsurface environmental simulation (e.g., [1,2]). The coupling of fluid flow, mass transport and geochemical reactions is instrumental for understanding and predicting the complex interplay between physical and bio-geochemical processes in sediments and groundwater systems, as well as for the quantitative interpretation of experimental observations both at the laboratory and field scales. Combining flow and transport codes with geochemical reaction packages has led to a first generation of now well-established reactive transport simulators for both groundwater (e.g., CrunchFlow [3]; Geochemist's Workbench [4]; PHT3D [5]; PHAST [6]) and unsaturated/multiphase flow (e.g., HYDROGEOCHEM [7]; TOUGHREACT [8-10]; MIN3P [11]). Developments have continued over the last decade with increasing capabilities added to existing simulators as well as new couplings between different transport and geochemical codes (e.g. HP1/HPx [12]; PHWAT [13]; RICH-PHREEQC [14]). Impetus to such advances was certainly provided by the release of modules such as IPhreeqc [15] and PhreeqcRM [16] devised to increase the flexibility in interfacing the widely used USGS's geochemical reaction package PHREEQC [17,18] with other codes. In particular, IPhreeqc is a C++ PHREEQC module designed for coupling PHREEQC's reaction capabilities (e.g., equilibrium reactions, ion exchange, surface complexation, solid solutions, mineral dissolution and precipitation, as well as kinetic reactions both abiotic and microbially mediated) to other software programs (for example, MATLAB®, Excel®, Visual Basic®) and/or programming and scripting languages (for instance, C, C++, FORTRAN, Python, R). IPhreeqc offers a wide range of extensive features to combine multidimensional transport simulators with comprehensive geochemistry packages including thermodynamic databases [19,20]. Recent reactive transport simulators that benefited from the IPhreeqc capabilities include the couplings with COMSOL Multiphysics® (e.g., [19]; [21,22]), OpenGeoSys [23,24] and UTCHEM [25].

In this study we also take advantage of the IPhreeqc capabilities to explore the coupling between a two-dimensional multicomponent ionic formulation of charged species advective-dispersive transport and reactive processes. Many studies have demonstrated the importance of electrostatic effects due to charge interactions and leading to multicomponent diffusion of ions in aqueous solutions. Experimental observations have shown the effects of Coulombic interactions on the diffusive mobility of major ions, heavy metals and radioactive tracers both at the laboratory [26,27] and at the field scale [28-31]. The description of such interactions in multicomponent diffusion models is usually treated by including an electromigration term in

addition to the classical Fickian diffusion term (e.g., [32-36]). In a series of recent laboratory flow-through experiments we have shown that the role of Coulombic effects is critical not only in diffusion-dominated systems but also in advection-dominated flow regimes [37-39]. In fact, the results of such experiments demonstrated that the displacement of ions in porous media is coupled and the electromigration effects do not vanish at high flow velocities. These experimental findings represent a challenge as well as an opportunity for further development of reactive transport codes. Only recently a dataset of multicomponent conservative ionic transport obtained under flow-through conditions in a homogeneous porous medium has been used to benchmark the multicomponent transport capabilities of the CrunchFlow and MIN3P codes [40]. However, to the best of our knowledge, the behavior and effects of Coulombic interactions for multidimensional conservative and reactive transport in physically and chemically heterogeneous porous media have not been investigated, yet. The purpose of this contribution is to present a reactive transport tool helping to address these issues in particular on the light of the increased recognition of the key role of molecular diffusion for solute transport from the pore to the field scale. Small scale diffusive processes have been shown to impact solute transport in flow-through systems not only at the laboratory (e.g., [41-45]) but also at the larger field scale (e.g., [46-54]). The impact of diffusion, which is the only true mixing process in groundwater [55], on solute transport indeed does not vanish at larger scales but propagates through scales also under flow-through conditions [53]. Models aiming at capturing these effects in heterogeneous flow fields need to implement improved and more realistic descriptions of local dispersion, linking the mechanical dispersion term to spatially-variable hydraulic conductivity values and avoiding using constant dispersivities that inevitably mask (or underestimate) the role of aqueous diffusion in porous media.

This work presents a two-dimensional reactive transport model that explicitly accounts for the Coulombic interactions coupled with geochemical reactions during multicomponent ionic transport in both homogeneous and heterogeneous flow-fields under transient transport conditions. The modeling approach is based on a charge-balanced multicomponent formulation and on the spatially variable description of local hydrodynamic dispersion that is of key importance for the coupling of the fluxes of the different ionic species in solution. Additionally, we couple the two-dimensional multicomponent ionic transport model with the widely used geochemical code PHREEQC (version 3, [18]) by using the reaction module IPhreeqc [15]. Thus, the proposed numerical reactive-transport model provides a comprehensive framework that is based on the novel combination of three specific features: (i) detailed description of spatially variable local hydrodynamic dispersion, (ii) multicomponent ionic formulation; and (iii) extensive reaction capabilities through the coupling with PHREEQC. These features represent distinctive and unique characteristics for a reactive

transport simulator and are particularly advantageous for performing transport simulations in physically and chemically heterogeneous domains. The 2-D multicomponent model is systematically benchmarked with the analytical solution of a 2-D transport problem, with experimental data, and with 1-D reactive transport scenarios solved in PHREEQC. Successively, application examples, with different levels of complexity, are presented to illustrate transient multicomponent ionic transport and the influence of charge interactions in both conservative and reactive systems in homogeneous and heterogeneous porous media.

5.2 Multicomponent Ionic Transport

The most distinguishing feature of aqueous diffusion of charged species compared to non-charged solutes is the electrostatic interactions between the dissolved charged species and/or with charged interfaces. Multicomponent ionic diffusion models are generally used to account for these inter-species interactions during diffusive movement of charged species at different scales (e.g., [27-29]; [32,33]; [35]; [56-59]). These models, based on Nernst-Planck formulations, are typically derived from the chemical potential expressions by following a pragmatic extension of Fick's law (e.g., [35,36,60]). Therefore, the multicomponent diffusive movement of a charged species in electrolyte systems can be expressed as [29,36]:

$$J_i = -D_i \nabla C_i - D_i C_i \nabla \ln \gamma_i - D_i \frac{z_i F}{RT} C_i \nabla \Phi \quad i = 1, 2, 3, ..., N \tag{5.1}$$

where D_i is the self-diffusion coefficient, C_i is the concentration of charged species i, γ_i is the activity coefficient, z_i is the charge number, F is the Faraday's constant, R is the ideal gas constant, T is the temperature, Φ is the electrostatic potential, and N is the number of species.

In dilute solutions and in the absence of strong ionic strength gradients, the gradient of the activity coefficients (second term of Eq. 5.1) can be neglected [33]. Thus, the above expression describing the multicomponent ionic diffusive fluxes reduces to:

$$J_i = -D_i \nabla C_i - D_i \frac{z_i F}{RT} C_i \nabla \Phi \tag{5.2}$$

This equation includes fluxes due to self-diffusion as well as electromigration, which is basically induced from the electrostatic interactions, for a particular mobile species. Following two physical constraints based on electroneutrality (i.e., (i) conservation of local charge balance, $\sum_{i=1}^{N} z_i C_i = 0$ and/or (ii) zero influx of electrical current, $\sum_{i=1}^{N} z_i J_i = 0$), the gradient of Φ can be expressed as:

$$\nabla\Phi = \frac{-\sum_{i=1}^{N}\left(z_i D_i \nabla C_i\right)}{\sum_{i=1}^{N}\left(z_i^2 F D_i C_i\right)/RT} \tag{5.3}$$

Therefore, the flux expression of Eq. (5.2) readily reduces to:

$$J_i = -D_i \nabla C_i + \frac{z_i D_i C_i}{\sum_{j=1}^{N}\left(z_j^2 D_j C_j\right)} \sum_{k=1}^{N}\left(z_k D_k \nabla C_k\right) \tag{5.4}$$

This formulation directly describes the movement of a particular charged species as a function of concentration gradients, self-diffusion coefficients, and charge numbers not only of that ion but also of all ionic species in the electrolyte system. Eq. (5.4) can also be further rearranged in a more compact notation that takes the form:

$$J_i = -\sum_{j=1}^{N}\left(D_{ij} \nabla C_j\right) \tag{5.5}$$

where D_{ij} are the inter-diffusion coefficients that include both the pure diffusive (first term, Eq. 5.4) and the electromigration (second term, Eq. 5.4) fluxes. The cross-coupled inter-diffusion coefficients are defined as:

$$D_{ij} = \delta_{ij} D_i - \frac{z_i z_j D_i D_j C_i}{\sum_{k=1}^{n}(z_k^2 D_k C_k)} \tag{5.6}$$

where δ_{ij} is the Kronecker delta that is equal to 1 when $i=j$ and equal to 0 if $i \neq j$.

In flow-through systems an analogous set of equations (Eqs. 5.1-5.6) can be derived by following the above steps and replacing the pure self-diffusion coefficients by the hydrodynamic dispersion coefficients [37,38].

5.3 Modeling Approach

The proposed model is implemented in MATLAB® and allows for steady-state flow, transient multicomponent advective-dispersive transport and geochemical reactions, the latter performed with the IPhreeqc coupling. Fig. 5.1 schematically illustrates the structure of the multicomponent reactive transport code. Details on the model capabilities, in particular the multicomponent ionic transport features and the coupling with the geochemical reaction package, are discussed in the sections below.

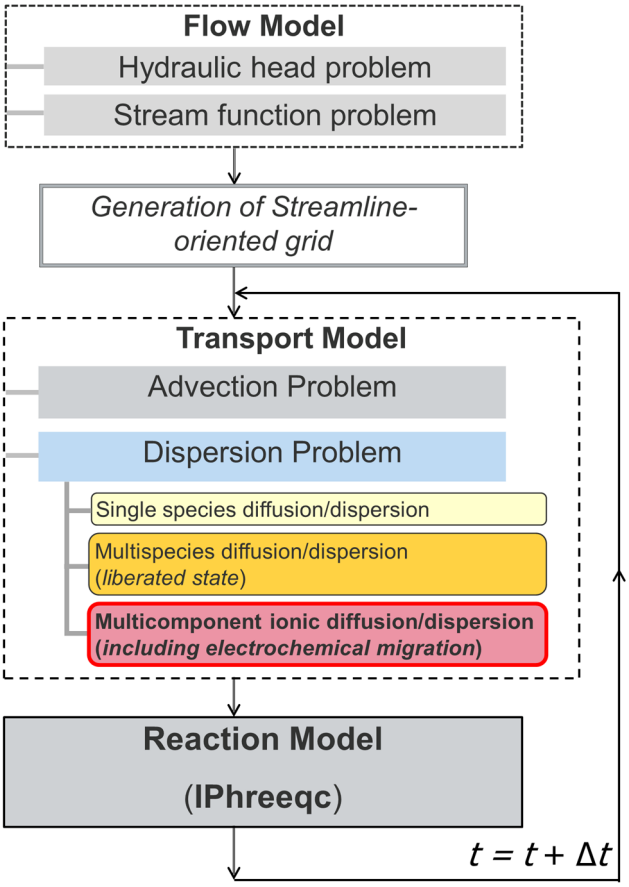

Figure 5.1. Schematic diagram of the structure of the multicomponent reactive transport model.

5.3.1 Solution of Flow and Transport Equations

The governing equation for steady-state groundwater flow in a two-dimensional domain is expressed as [61]:

$$\nabla \cdot \left(\mathbf{K} \nabla h \right) = 0$$
$$\nabla \cdot \left(\mathbf{K}^{-1} \nabla \psi \right) = 0 \qquad (5.7)$$

where h, ψ and $\mathbf{K}$ are hydraulic head, stream function and hydraulic conductivity tensor, respectively. The groundwater flow problem (Eq. 5.7) is solved numerically by bilinear finite elements on rectangular grid.

The governing equation for multicomponent ionic transport problem coupled with reactive processes in two-dimensional saturated porous media reads as:

$$\frac{\partial C_i}{\partial t} = -\boldsymbol{v}\cdot\nabla C_i + \nabla\cdot\left(\sum_{j=1}^{N}\mathbf{D}_{ij}\nabla C_j\right) - R_i \tag{5.8}$$

where t is time, $\boldsymbol{v}$ is the seepage velocity vector, $\mathbf{D}_{ij}$ is the tensor for cross-coupled dispersion coefficients, R_i is the reactive source/sink term. For charged compounds the entries of $\mathbf{D}_{ij}$ in a two-dimensional local coordinate system, referencing along the directions parallel and orthogonal to flow, are described as:

$$\mathbf{D}_{ij} = \begin{bmatrix} \mathbf{D}_{ij}^{L} & 0 \\ 0 & \mathbf{D}_{ij}^{T} \end{bmatrix} \tag{5.9}$$

in which $\mathbf{D}_{ij}^{L}$ and $\mathbf{D}_{ij}^{T}$ are the matrices of longitudinal and transverse cross-coupled dispersion coefficients [38], respectively. These cross-coupled terms, which allow accounting for the flux of a charged species driven by both its own concentration gradient and the electrical field created by the movement of other ions present in solution, are in fact analogous to inter-diffusion coefficients in Eq. (5.6) and can be expressed as:

$$\begin{aligned} \mathbf{D}_{ij}^{L} &= \delta_{ij}D_i^{L} - \frac{z_i z_j D_i^{L} D_j^{L} C_i}{\sum_{k=1}^{N}\left(z_k^2 D_k^{L} C_k\right)} \\ \mathbf{D}_{ij}^{T} &= \delta_{ij}D_i^{T} - \frac{z_i z_j D_i^{T} D_j^{T} C_i}{\sum_{k=1}^{N}\left(z_k^2 D_k^{T} C_k\right)} \end{aligned} \tag{5.10}$$

where D_i^{L} and D_i^{T} are the longitudinal and transverse hydrodynamic self-dispersion coefficient of species i (i.e., when a particular ion is "liberated" from the other charged species in solution). The hydrodynamic dispersion coefficients, which are important parameters for the realistic description of dispersive transport, are parameterized by using the linear relationship proposed by Guedes de Carvalho and Delgado [62] for longitudinal dispersion and a non-linear compound-specific relationship [50,63] for the transverse component:

$$\begin{aligned} D_i^{L} &= D_i^{P} + \frac{1}{2}vd \\ D_i^{T} &= D_i^{P} + D_i^{aq}\left(\frac{Pe_i^2}{Pe_i + 2 + 4\delta^2}\right)^{\beta} \end{aligned} \tag{5.11}$$

where D_i^{aq} is the aqueous diffusion coefficient, $D_i^{P} = D_i^{aq}/\tau$ is the pore diffusion coefficient and τ the tortuosity of the porous medium. Since the latter is difficult to determine, the pore diffusion coefficient is typically described as a function of the porosity (θ) and a common approximation for unconsolidated material is $D_i^{P} \approx \theta D_i^{aq}$ (e.g., Archie [64]; Boving and Grathwohl [65]). d is the average grain size diameter and Pe_i ($= vd / D_i^{aq}$; with v being the

flow velocity) is the grain Péclet number of species *i*. δ denotes the ratio between the length of a pore channel to its hydraulic radius. β is an empirical exponent that accounts for the effects of incomplete mixing in the pore channels. The parameterizations of D_i^L and D_i^T in Eq. 5.11 were selected because they have been validated and extensively supported by experimental data from controlled flow-through experiments. Other parameterizations such as the classic model of Scheidegger [66] as well as more complex models of local dispersion obtained for instance from pore-scale analysis and suggesting a weak non-linearity also of the longitudinal component [67] can be readily implemented. An important feature for high-resolution transport simulations in heterogeneous porous media is to take into account that the grain diameter (d) in Eq. (5.11) is spatially variable and should be linked to the local hydraulic conductivity value. We use the simple approximation of Hazen [68], which was adopted in previous studies (e.g., [51,69]), as a relationship between the grain diameter and hydraulic conductivity:

$$d \approx c\sqrt{K} \tag{5.12}$$

with the empirical proportionality constant c = 0.01 $m^{0.5}s^{0.5}$. This approach ensures a greatly improved representation of local dispersion compared to the common practice of considering constant dispersivities even in highly heterogeneous formations. The spatially variable hydrodynamic self-dispersion coefficients are of critical importance in the electrostatic cross-coupling between charged species and allow providing a detailed description of multicomponent ionic transport in heterogeneous formations.

The multicomponent transport problem (Eq. 5.8) is solved numerically on streamline-oriented grids following the method of Cirpka et al. [61]. The use of such grids, constructed based on the results of the flow simulation, reduces numerical errors by minimizing artificial dispersion. The advective-dispersive term is computed with the cell-centered finite volume method (FVM) [70]. We use a sequential non-iterative operator splitting approach to decouple the transport and reaction terms. For the advection problem, we use upwind differentiation for spatial discretization and the explicit Euler method for time integration. The dispersive fluxes are computed by the implicit Euler method for integration in time. The resulting system of equations for the dispersion problem is solved by using the direct matrix solver UMFPACK [71]). In multicomponent ionic transport problems, the system of equations becomes nonlinear due to the electrostatic interactions between the dispersive fluxes of different charged species. Therefore, we use an iterative scheme with a Picard loop to linearize the coupled non-linear set of equations in each temporal step. The detailed computational steps for the multicomponent transport and reaction calculations are summarized in Table 5.1.

For each time step, *dt*, we consider the concentration vector from the advection step (i.e., after the advective shift of concentration) as an initial guess of the Picard iteration to determine the cross-coupled dispersion coefficients (Eqs. 5.9-5.10). Afterwards, we determine the mobility matrix $\mathbf{M}_{\mathrm{MOB},i}^{\mathrm{disp}}$ which results from the spatial discretization on streamline-oriented grids and contains the divergence of dispersive fluxes defined by the finite volume method (*Step 2*). The newly computed $\mathbf{D}_{ij}^{L}, \mathbf{D}_{ij}^{T}$ and $\mathbf{M}_{\mathrm{MOB},i}^{\mathrm{disp}}$ are then used to calculate the new concentration vector, $\boldsymbol{C}_i^{\mathrm{disp}}$ (*Step 3*). Here, $\mathbf{M}_{\mathrm{STORE},i}$ denotes the storage matrix resulting from the spatial discretization and describes the discrete cell-area of each cell of the domain. $\boldsymbol{C}_i^{\mathrm{adv}}$ represents the concentration vector after the advection step. At each time step, the iteration in the dispersion step repeats until the concentration vector reaches a constant value: i.e., when the norm of the differences among the concentration values in two consecutive iterations (κ and κ+1) converges to a very small user-defined threshold value (ε).

Table 5.1: Algorithm for transient multicomponent ionic transport and reaction computation.

Discretization:

$$\frac{\partial C_i}{\partial t} + \boldsymbol{v}\cdot\nabla C_i - \nabla\cdot\left(\sum_{j=1}^{N}\mathbf{D}_{ij}\nabla C_j\right) \Rightarrow \mathbf{M}_{\mathrm{STORE},i}\frac{\partial \boldsymbol{C}_i}{\partial t} + \mathbf{M}_{\mathrm{MOB},i}^{\mathrm{adv}}\boldsymbol{C}_i + \mathbf{M}_{\mathrm{MOB},i}^{\mathrm{disp}}\boldsymbol{C}_i$$

Advection step:

$$\boldsymbol{C}_i^{\mathrm{adv},\,t+dt} = \boldsymbol{C}_i^{\,t} + \left(\mathbf{M}_{\mathrm{STORE},\,i}/dt\right)^{-1}\left(-\mathbf{M}_{\mathrm{MOB},i}^{\mathrm{adv},\,\kappa}\boldsymbol{C}_i^{\,t} + \boldsymbol{b}_i\right)$$

Dispersion step:

while $\mathrm{norm}\left(\boldsymbol{C}_i^{\mathrm{disp},\,t+dt\,(\kappa+1)} - \boldsymbol{C}_i^{\mathrm{disp},\,t+dt\,(\kappa)}\right) > \varepsilon$

Step 1: Calculate the cross-coupled dispersion coefficients in each cell,

$$\mathbf{D}_{ij}^{L,\,t+dt(\kappa)} = \delta_{ij}D_{ij}^{L} - \frac{z_i z_j D_i^L D_j^L C_i^{\mathrm{disp},\,t+dt(\kappa)}}{\sum_{k=1}^{N}\left(z_k^2 D_k^L C_k^{\mathrm{disp},\,t+dt(\kappa)}\right)}$$

$$\mathbf{D}_{ij}^{T,\,t+dt(\kappa)} = \delta_{ij}D_{ij}^{T} - \frac{z_i z_j D_i^T D_j^T C_i^{\mathrm{disp},\,t+dt(\kappa)}}{\sum_{k=1}^{N}\left(z_k^2 D_k^T C_k^{\mathrm{disp},\,t+dt(\kappa)}\right)}$$

Step 2: Calculate mobility matrix for dispersion problem, $\mathbf{M}_{\mathrm{MOB},i}^{\mathrm{disp},\,t+dt(\kappa)}$

Step 3: Solve for the concentration,

$$\boldsymbol{C}_i^{\mathrm{disp},\,t+dt(\kappa)} = \left(\mathbf{M}_{\mathrm{STORE},\,i}/dt + \mathbf{M}_{\mathrm{MOB},i}^{\mathrm{disp},\,t+dt(\kappa)}\right)^{-1}\left(\mathbf{M}_{\mathrm{STORE},\,i}\boldsymbol{C}_i^{\mathrm{adv},\,t+dt}/dt\right)$$

Step 4: Next iteration: $\kappa = \kappa + 1$

end

Reaction step:

$$\boldsymbol{C}_i^{\mathrm{disp},\,t+dt} \rightarrow \left[\mathbf{PHREEQC}\right] \rightarrow \boldsymbol{C}_i^{\mathrm{reac},\,t+dt}$$

5.3.2 Reaction Calculations and IPhreeqc Coupling

After the advection and dispersion steps, we perform reaction calculations with PHREEQC-3 [18] by using the IPhreeqc module [15]. In our calculations, we use the COM (component object model) version of IPhreeqc which allows all reaction capabilities of PHREEQC to be used by any software and scripting language that can interface with a Microsoft COM server, e.g., Excel®, Visual Basic®, Python, or MATLAB® [14,15]. After updating the species concentration within the transport step, the concentration vector is sequentially passed to IPhreeqc for reaction calculations. In the reaction step, the simulation is performed by considering a batch reactor in each cell of the 2-D model domain that contains user-defined physical and chemical properties representing the reactive processes of interest. After the reaction calculations, the newly updated concentration values in each cell are passed back to the transport model. Besides all dissolved species, the transport calculations also include elemental oxygen (O), hydrogen (H) and charge imbalance (CB) as extra solution components. These parameters allow PHREEQC recognizing the liquid phase (water) and tracking the charge balance which is important in various geochemical calculations [19] as well as for multicomponent ionic transport.

The formulation described above allows performing multicomponent ionic transport calculations in a rigorous way that collectively includes both the electrostatic coupling of dispersive fluxes and the full aqueous speciation computed by PHREEQC.

5.4 Benchmark Problems

The proposed multicomponent reactive transport model is benchmarked by comparing the model outcomes with: (a) the analytical solution of a 2-D transport problem, (b) a high-resolution experimental dataset, (c) a classical 1-D ion-exchange problem solved with PHREEQC-3 and (d) 1-D ion exchange considering multicomponent ionic transport. For the sake of brevity, we present in the following sections the benchmark cases (a) and (d), whereas the examples (b) and (c) can be found in the Supplementary Material.

5.4.1 Benchmark of Transient Multicomponent Ionic Transport

In order to test the performance of our transient multicomponent ionic transport code in a two-dimensional flow-through domain, we compare the simulation outcomes with an analytical solution of the classical 2-D advection-dispersion equation:

$$\frac{\partial C}{\partial t} = -v\frac{\partial C}{\partial x} + D_L\frac{\partial^2 C}{\partial x^2} + D_T\frac{\partial^2 C}{\partial z^2} \tag{5.13}$$

The analytical solution of the advection-dispersion equation in a semi-infinite two-dimensional perfectly homogeneous domain ($0<x<\infty$ and $-\infty<z<\infty$), considering transient transport of a solute initially distributed in a rectangular region with zero influx of solute mass at the upstream boundary (Eqs. 5.15-5.18), is given by [72,73]:

$$\begin{aligned} C(x,z,t) = \frac{C_0}{4}\Bigg[&\operatorname{erfc}\left(\frac{x-x_2-vt}{\sqrt{4D_i^L t}}\right) - \operatorname{erfc}\left(\frac{x-x_1-vt}{\sqrt{4D_i^L t}}\right) \\ &+ \exp\left(\frac{vx}{D_i^L}\right)\left\{\operatorname{erfc}\left(\frac{x+x_2+vt}{\sqrt{4D_i^L t}}\right) - \operatorname{erfc}\left(\frac{x+x_1+vt}{\sqrt{4D_i^L t}}\right)\right\}\Bigg] \cdot \left[\operatorname{erfc}\left(\frac{z-a}{2\sqrt{D_i^T t}}\right) - \operatorname{erfc}\left(\frac{z+a}{2\sqrt{D_i^T t}}\right)\right] \end{aligned} \tag{5.14}$$

The initial and boundary conditions are defined as:

$$C(x,z,0) = \begin{cases} C_0 & x_1 < x < x_2 \quad \text{and} \quad -a < z < a \\ 0 & \text{otherwise} \end{cases} \tag{5.15}$$

$$vC\big|_{x=0^+} = 0 \tag{5.16}$$

$$\frac{\partial C}{\partial x}(\infty, z, t) = 0 \tag{5.17}$$

$$\frac{\partial C}{\partial z}(x, \pm\infty, t) = 0 \tag{5.18}$$

where x_1 and x_2 are the longitudinal positions delimiting the initial location of the solute source. In the transverse direction, the solute is initially located between $-a$ and a.

We consider a two-dimensional homogeneous domain of 100 cm × 12 cm, which is discretized into 100 (Δx = 1 cm) and 240 (Δz = 0.5 mm) cells along the longitudinal and transverse dimension, respectively. The transport simulations are run for a total simulation time of t = 18 hours with a uniform horizontal velocity of v = 1.0 m/day. The porosity of the flow-through system is 0.41. We consider a rectangular solute source, with dimensions of 2 cm × 2 cm, initially located 2 cm downstream of the inlet boundary, between 5 and 7 cm along the vertical dimension (Fig. 5.2).

The simulation is performed for the transport of a single 1:1 electrolyte (NaCl) in pure ambient water. In such ionic systems, the electrostatic interactions couple the movement of the cation

(Na^+) and the anion (Cl^-) and lead to an identical displacement of the two species. As a result, although the strong electrolyte (NaCl) fully ionizes in the aqueous solution and the two ions (Na^+ and Cl^-) are characterized by different mobility, they travel as a single species in order to maintain electroneutrality. Hence, for this particular case, the diffusion (and dispersion) of these two ions can be characterized by a single diffusion coefficient (e.g., [36]):

$$D_{NaCl} = \frac{\left|z_{Na^+}\right| + \left|z_{Cl^-}\right|}{\left|z_{Na^+}\right| / D_{Cl^-}^{aq} + \left|z_{Cl^-}\right| / D_{Na^+}^{aq}} \tag{5.19}$$

where D_{NaCl} represents the combined diffusion coefficient of the electrolyte. z_{Na^+}, z_{Cl^-} and $D_{H^+}^{aq}$, $D_{Cl^-}^{aq}$ are the charge and the aqueous diffusion coefficients of Na^+ and Cl^-, respectively. Self-diffusion coefficients of sodium and chloride as well as of other ions used in the following sections are reported in Table 5.2. The value obtained combining diffusion coefficients of Na^+ and Cl^- (Eq. 5.19) for the salt is $D_{NaCl} = 1.44 \times 10^{-9}$ m^2/s. Therefore, the electrostatic ionic interactions reduce the multicomponent ionic transport problem into a single-species conservative transport problem. Thus, for this special case, the outcomes of the 2-D transient multicomponent ionic transport model can be directly compared with the results of the analytical solution (Eq. 5.14). In order to simulate transport in flow-through systems the hydrodynamic dispersion coefficients (Eq. 5.11) are calculated using the combined salt diffusion coefficient (Eq. 5.19) for the analytical solution (Eq. 5.14) and the self-diffusion coefficients of the individual ions for the numerical model. The latter takes into account the electrostatic interactions between Na^+ and Cl^- in the pore water by coupling their dispersive fluxes as explained in Section 5.2 and Section 5.3.

Table 5.2: Aqueous diffusion coefficients of different ions.

Diffusion coefficients	D^{aq} [m^2/s][a]
H^+	8.65×10^{-9}
Mg^{2+}	0.63×10^{-9}
Cl^-	1.81×10^{-9}
Na^+	1.20×10^{-9}
Br^-	1.86×10^{-9}
K^+	1.77×10^{-9}
Ca^{2+}	0.71×10^{-9}
NO_3^-	1.70×10^{-9}

[a] values from Lasaga [74], corrected for temperature and viscosity changes at 20°C

The comparison between the multicomponent ionic transport model and the analytical solution at the end of t = 18 hours of simulation is shown in Fig. 5.2. The instantaneous rectangular slug source spreads and approaches a Gaussian elliptical shape during the transport through the homogeneous porous medium (Fig. 5.2a-c). It is evident from the two-dimensional concentration distributions that the concentrations both from the multicomponent ionic transport simulations (Fig. 5.2a-b) and from the analytical solution (Eq. 5.14, Fig. 5.2c) are very similar. Fig. 5.2 also shows the longitudinal (panel d) and transverse (panel e) concentration profiles along the longitudinal and transverse axes through the center of the plume. The coupled displacement of the Na^+ and Cl^- ions results in overlapping concentration of these species both in the longitudinal and in the transverse direction. These profiles perfectly match with the concentration profiles of the combined electrolyte (i.e., NaCl salt as a single uncharged species) computed with the analytical solution. Thus, these results validate the accuracy of the transient multicomponent ionic transport simulations in conservative two-dimensional systems.

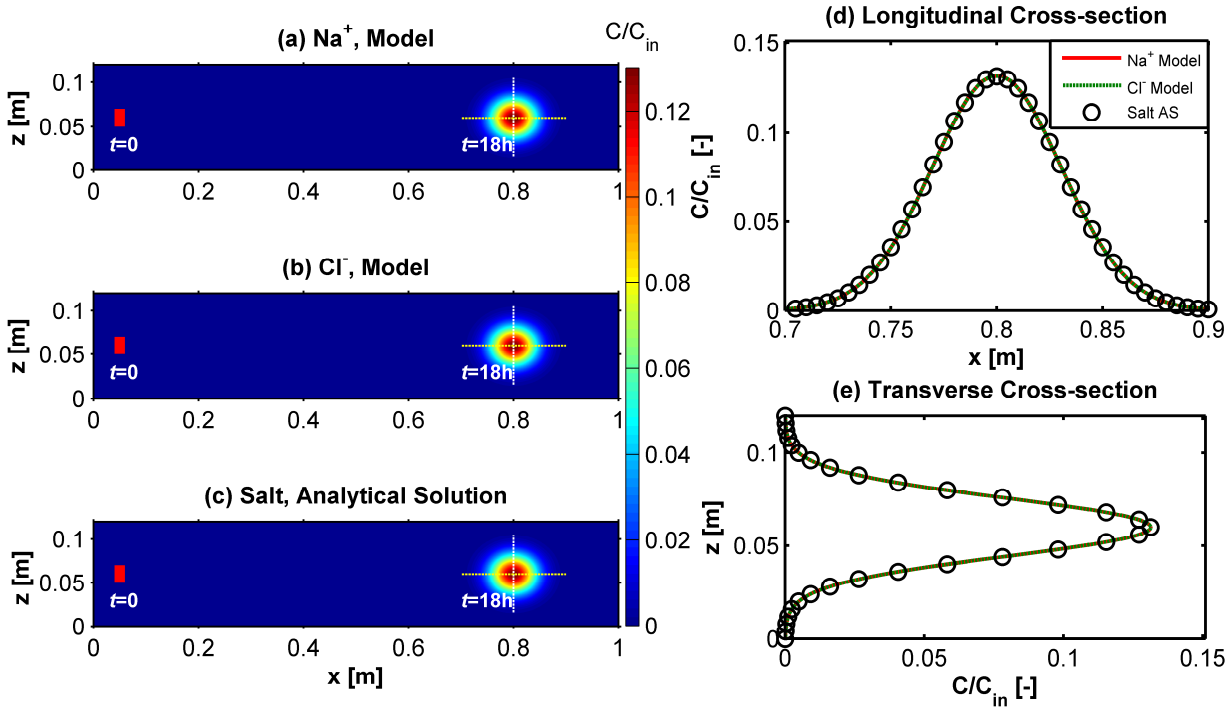

Figure 5.2. Comparison of the multicomponent ionic transport model and 2-D analytical solution for the transport of NaCl in pure water at v = 1 m/day: 2-D concentration distributions after t = 18 hours (a-c); longitudinal cross sectional profiles at z = 6 cm (d); transverse cross sectional profiles at x = 80 cm (e).

5.4.2 Benchmark of IPhreeqc Coupling: Ion-Exchange with Multicomponent Ionic Transport and Charge Interactions

In order to validate the coupling of our transport code with the geochemical code PHREEQC, we consider the example problem 11 of the PHREEQC-3 manual [18]. This example includes the advective-dispersive transport of ionic species in a one-dimensional, 8 cm long column containing a cation exchanger. The exchanger column, initially in equilibrium with a solution containing Na^+, K^+ and NO_3^-, is continuously flushed with a $CaCl_2$ solution. As a consequence, the cations (Na^+, K^+ and Ca^{2+}) undergo ion-exchange reactions with the exchanger and new equilibrium compositions of the exchanger and the pore water are established. The comparison between the 1D PHREEQC simulation and the 2D simulation carried out with the proposed code is presented in the Supplementary Material. The ion-exchange problem was also extended to the case of transient multicomponent ionic transport. In this example, we specifically focus on multicomponent diffusion (with charge effects) and ion-exchange problem. In order to focus on the multicomponent effects, we consider diffusion-dominated transport in the virtual column setup, by decreasing of a factor of ten the value of the seepage velocity (v = 0.024 m/day). The column geometry, the exchanger properties and the involved ions and concentrations are kept the same as in the original example described above. Instead of a single diffusion coefficient for all ionic species, species-specific aqueous diffusion coefficients are used for different ions. The self-diffusion coefficients used for different species are reported in Table 5.2. For the sake of simplicity, dispersivity is neglected and thus is set to zero and the pore diffusion coefficients are assumed to be identical to the aqueous diffusion coefficients (i.e., porosity, θ = 1). The 1-D PHREEQC simulations are conducted by using the keyword **multi_d**, which allows accounting for multicomponent ionic transport [29]. On the other hand, in our two-dimensional transport code coupled with PHREEQC, multicomponent ionic transport calculations are performed by solving Eqs. (5.7-5.10) as illustrated in Section 5.3 and Table 5.1.

Fig. 5.3 represents the simulated effluent breakthrough curves of different ionic species. Notice that, due to a smaller advective velocity, diffusion becomes more dominant in this case compared to the advection-dominated ion-exchange problem (Fig. S5.5, Supplementary Material). This is reflected in the smoother temporal concentration profiles of the ionic species. The evolution of Cl^- front shows an interesting pattern, with a sudden increase of Cl^- concentration, after ~1.75 PV when Ca^{2+} breakthrough starts. Such behavior is due to the multicomponent ionic transport through the exchanger column and the requirement of maintaining charge balance throughout the domain. Furthermore, the two simulations, using PHREEQC alone in a 1-D domain and using the 2-D multicomponent ionic transport code

combined with PHREEQC in a uniform 2-D domain (equivalent to 1-D), have the same outcome which, therefore, validates the transient multicomponent ionic transport calculations coupled with chemical reactions.

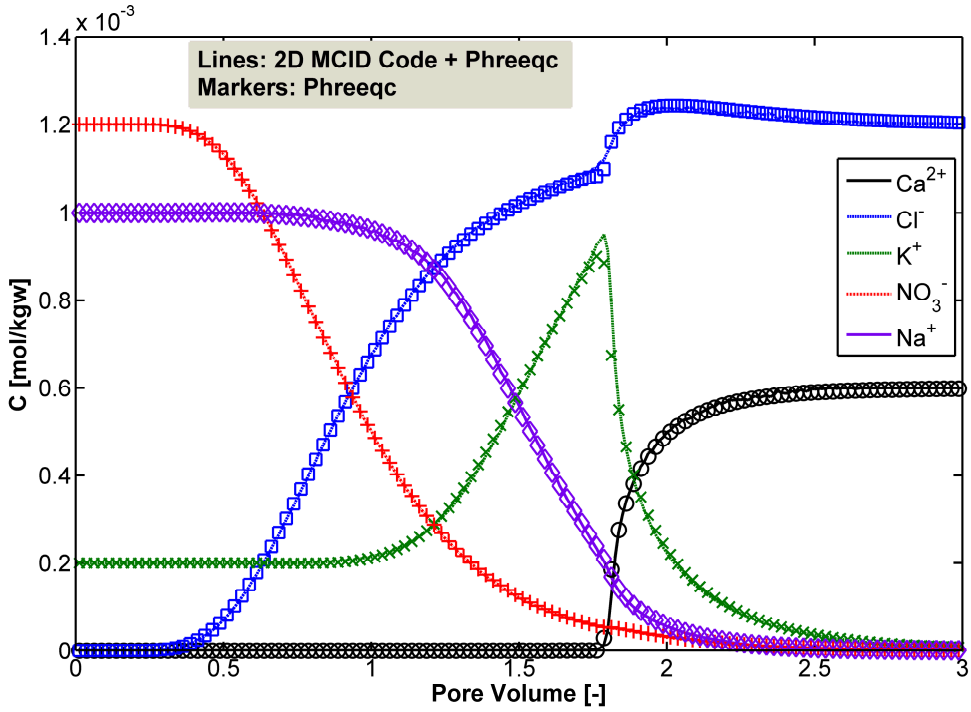

Figure 5.3. Benchmark of IPhreeqc coupling with the 2-D transport code for an example of ion-exchange coupled to multicomponent ionic transport with electrochemical migration.

5.5 Examples of Multicomponent Ionic Transport Simulations

In this section we present scenarios of multicomponent transport of ionic solutes in both homogeneous and heterogeneous domains. Section 5.5.1 focuses on conservative multicomponent transport of electrolyte systems. The impact of charge effects on breakthrough curves and plume dilution of the different ionic species during conservative transport are analyzed. Section 5.5.2 illustrates multicomponent transport of charged species undergoing ion-exchange reactions. We present scenarios with increasing level of complexity in terms of physical heterogeneity (i.e., spatially variable hydraulic conductivity) and chemical heterogeneity (i.e., spatially variable ion-exchange capacity).

5.5.1 Conservative Transport

5.5.1.1 Simulations in Homogeneous Domain

The simulations were performed to show the influence of charge interactions on transient multicomponent ionic transport. We consider two different domains, a homogeneous porous

medium and a heterogeneous formation, at two different scales. For the homogeneous case, we select a 2-D domain with dimensions of 100 cm × 20 cm (L × W), similar to the laboratory setup recently used to investigate multicomponent ionic transport [37-39], and with a uniform distribution of hydraulic conductivity and flow-velocity. Such simulation domain is representative of typical laboratory bench-scale quasi two-dimensional flow-through chambers packed with uniform grain sized material (e.g., [39,43,75]). The simulations were run, by considering a rectangular slug of electrolytes as initial condition, at two different horizontal flow velocities of 0.1 m/day and 1.0 m/day. At each flow velocity, three different combinations of electrolyte scenarios are considered: (i) transport of a single electrolyte (HCl) in pure water; (ii) transport of a single electrolyte (HCl) in a background electrolyte solution (NaBr); and (iii) transport of mixed electrolytes (H^+, Mg^{2+} and Cl^-) in pure water. The selection of this particular set of electrolytes is based on the variability of their aqueous diffusion coefficients (Table 5.2) and demonstrates the multicomponent charge coupling effects on ions undergoing conservative transport. The geometry, hydraulic and transport properties of different simulation domains are summarized in Table 5.3. It should be noted that these simulations are run by considering the assumption that the transported ionic species do not interact with the solid matrix and perfect conservative conditions exist.

Fig. 5.4 summarizes the breakthrough curves and transient flux-related dilution index for different electrolyte cases at the outlet end of the homogeneous meter-scale domain. The flux-related dilution index is a metric of mixing, originally developed for steady-state plumes [76], that expresses dilution as the act of distributing a given solute mass flux over a larger water flux and determines an effective volumetric discharge transporting the solute flux at a given longitudinal cross section. For the transient multicomponent transport of ionic species in flow-through domains, the flux-related dilution index of an ion "*i*" can be defined as [77]:

$$E_{Q,i}(x,t) = \exp\left(-\int_{\Omega} p_{Q,i}(x,t) \ln p_{Q,i}(x,t) q_x(x,t) d\Omega \right) \tag{5.20}$$

where $q_x = v\theta$ is the longitudinal component of specific discharge, Ω is the cross-sectional area, θ is the porosity, and $p_{Q,i}$ is the flux-related probability density function of the charged species "*i*" at time *t*:

$$p_{Q,i}(x,t) = \frac{C_i(x,t)}{\int_{\Omega} C_i(x,t) q_x(x,t)} \tag{5.21}$$

The simulation outcomes at velocity of 0.1 m/day and 1 m/day are shown in Figs. 5.4a-f and 5.4g-l, respectively. For the transport of a single electrolyte (HCl) in pure water, despite having very different diffusivities (Table 5.2), the breakthrough curves of the cation (H^+) and anion

(Cl^-) are identical at both flow velocities (Fig. 5.4a and 5.4g). On the other hand, during transport in the presence of a background electrolyte, their breakthrough profiles are significantly different, with the faster ion (H^+) having more spread profiles and lower peak concentrations compared to the slower one (Cl^-) (Fig. 5.4b and 5.4h). The profiles of flux-related dilution index show identical values for transport in pure water (Fig. 5.4d and 5.4j); whereas in the case of background electrolyte the cation (H^+) plume is considerably more diluted (approximately 2 times) than the anion (Cl^-) plume (Fig. 5.4e and 5.4k). This behavior is induced by the charge interactions between positively and negatively charged species. During transport in pure water the cation and anion travel together in order to fulfill the local charge balance and thus they are electrostatically coupled. On the other hand, when the same ions are transported through a background electrolyte solution, the domain is locally charge balanced by the background ions and, consequently, the cation and anion in the solute plume can travel and subsequently dilute according to their self-diffusive/dispersive properties. However, in both cases the $E_{Q,i}$ profiles for different ions show a monotonic increase over time at the outlet cross-section of the domain (Fig. 5.4e and 5.4f).

For the transport of mixed electrolytes in pure water (H^+, Mg^{2+} and Cl^-), the breakthrough curves show a distinct pattern which follows the same order as suggested by their self-diffusivities (Table 5.2): where H^+ has the most spread profile with the lowest peak concentration and Mg^{2+} shows the least spread profile and the highest peak concentration (Fig. 5.4c). The Cl^- profile lies in between those of the cations. Due to the electrostatic interaction during the displacement of the different ions, the profiles are also different compared to those of transport under "liberated" conditions (i.e., when they are transported as uncharged species). The behavior of the flux-related dilution index profiles of the ionic species for this scenario is quite interesting. The cation dilution profiles show a bulge-shape resembling a concave function. The cations have an increasing pattern of dilution reaching a maximum, and afterwards decreasing again (red and blue solid lines; Fig. 5.4f). The pattern is opposite (convex shaped) for the anion (Cl^-) for which the E_Q profile decreases and reaches a minimum at around mean breakthrough time and afterwards it starts increasing again (green lines; Fig. 5.4f). Such dilution behavior is significantly different compared to the monotonic increase at their "liberated" state (dotted lines; Fig. 5.4f) and can be explained considering the ionic interactions between the transported species. In fact, at early breakthrough times, when the fringe of the plume arrives at the outlet boundary, H^+ is more enriched compared to Mg^{2+} because of the higher diffusive/dispersive properties of H^+. As a consequence, H^+ is mainly responsible for counterbalancing the negative charge of Cl^- in the fringe area. Therefore, at the edge of the plume, the dilution of H^+ and Cl^- are similar, as reflected in their very early and late time $E_{Q,i}$ values, and these ions tend to be electrostatically coupled.

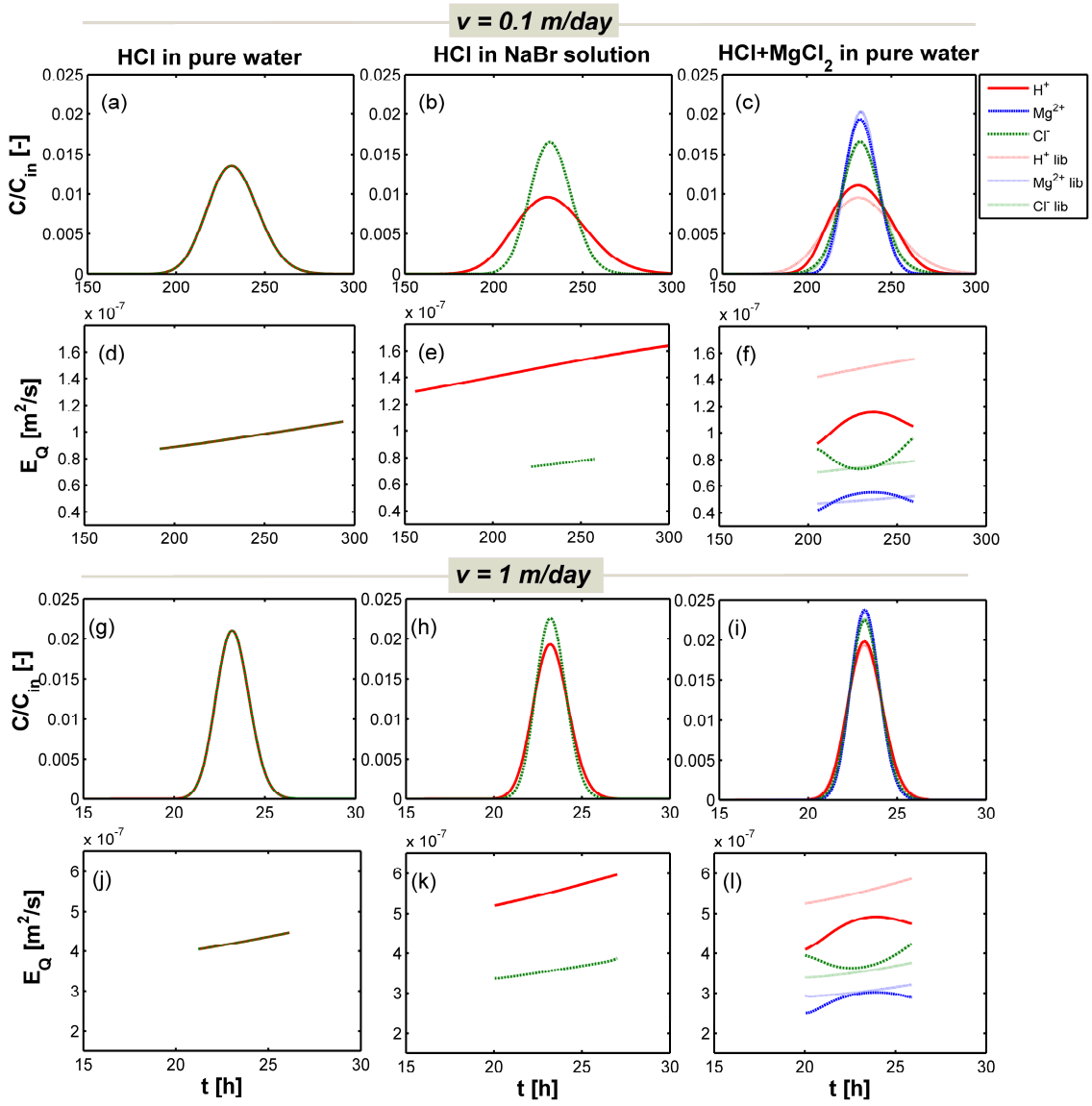

Figure 5.4. Breakthrough curves (a-c and g-i) and flux-related dilution indices (d-f and j-l) for simulations at v = 0.1 m/day (a-f) and v = 1 m/day 1 (g-l) in a homogeneous domain. $E_{Q,i}$ values are calculated for a concentration threshold equal to 10^{-6} of the peak concentration for each species.

Thus, among these two abundant species in the fringe zone, the diffusivity of H^+ decreases and the one of Cl^- increases compared to their true "liberated states" in order to maintain charge balance. On the other hand, in the center of the plume, Mg^{2+} has a higher relative concentration and hence higher contribution to counter the negative charge of Cl^-. So, in this case, E_{Q,Cl^-} decreases due to a stronger coupling to a slower positive ion (Mg^{2+}), and for the same reason Mg^{2+} dilution increases compared to its liberated values (Fig. 5.4f). The differences between the actual dilution of the ions' plumes compared to their theoretical displacements at "liberated

state" are notable for all the reported ions, as shown by the different patterns of the corresponding lines in Fig. 5.4f.

Similar patterns of concentration and dilution breakthrough curves are obtained at higher velocity (v = 1 m/day) (Figs. 5.4g-l). Due to the advection-dominated transport, breakthrough curves are less spread (narrow profiles with higher peak concentrations) compared to their respective cases at slow velocity (v = 0.1 m/day). Interestingly, because of the higher Péclet numbers (i.e., higher values of dispersion coefficients) at v = 1 m/day the absolute values of dilution indices ($E_{Q,i}$) are considerably higher (approximately 5 times) with respect to the ones obtained at slow velocity (Figs. 5.4j-l, 5.4d-f). This implies that, even though the breakthrough curves and the concentration distribution are less spread, the plumes are in fact more diluted at higher seepage velocity, since the mass fluxes of the different ions are distributed over larger water fluxes.

5.5.1.2 Simulations in Heterogeneous Domain

The analogous set of simulations was also performed in a heterogeneous domain to investigate the large-scale effects and the influence of heterogeneity on breakthrough and dilution during conservative multicomponent ionic transport. The simulations were run in a randomly generated two-dimensional flow-field (20 m × 2.5 m) representing a vertical cross-section of a mildly heterogeneous aquifer. The hydraulic conductivity statistics are consistent with those reported for the Borden aquifer [78] and the mean hydraulic gradient was adjusted to produce average flow velocities of 0.1 and 1 m/day. The domain is discretized into 200 cells (Δx = 10 cm) in the horizontal direction and 250 cells (Δz = 1 cm) in the vertical direction. The heterogeneous conductivity field is generated with an exponential covariance model and by using the spectral approach described by Dykaar and Kitanidis [79]. The summary of hydraulic and transport parameters used in the simulations are given in Table 5.3.

Fig. 5.5 shows the results of conservative transport simulation of mixed electrolytes in the generated 2-D random fields for an average flow velocity of 1 m/day, using spatially-variable local hydrodynamic dispersion coefficients in which the mechanical dispersion term is linked to the hydraulic conductivity through the average grain size (Eq. 5.12). The simulated velocities and streamlines are shown in Fig. 5.5a. The concentration distribution of the plume containing mixed electrolytes (HCl and $MgCl_2$) after 7 days of simulation is depicted in Fig. 5.5b-d. It is evident that due to heterogeneity and flow variability, the shapes of the different ionic plumes are irregular.

Table 5.3: Summary of geometry, flow and transport parameters of the homogeneous and heterogeneous domains.

Parameters	Homogeneous[a]	Heterogeneous[b]
Domain size (L×H) [m]	1 × 0.2	20 × 2.5
Discretization, $\Delta x/\Delta z$ [cm]	0.5/0.1	10/1
Slug size [m]	0.02 × 0.02	0.4 × 0.2
Average hydraulic conductivity [m/s]	1.27×10^{-2}	9.75×10^{-5}
$\sigma^2_{\ln K}$	-	0.29
Average horizontal flow velocity [m/day]	0.1; 1	0.1; 1
Average porosity [-]	0.41	0.34

[a]Data consistent with the experimental setup of Rolle et al. [37]
[b]Data consistent with the characterization of the Borden aquifer (Sudicky [78])

It is interesting to notice that even in this spatially variable domain and under an advection-dominated regime (average v = 1 m/day), the compound-specific behavior of the different ions is still significant as shown by the different distributions of the two cations and of the anion concentration. Due to a higher diffusivive/dispersive properties, the H^+ plume is evidently more diluted and shows a lower peak concentration compared to the other two ions (Fig. 5.5b). On the other hand, the Mg^{2+} plume is more affected by the spatial variability of the velocity distribution and consequently results in a more stretched but less diluted plume with a higher peak concentration (Fig. 5.5c). The shape of the anion (Cl^-) plume appears to be in-between those of the cations.

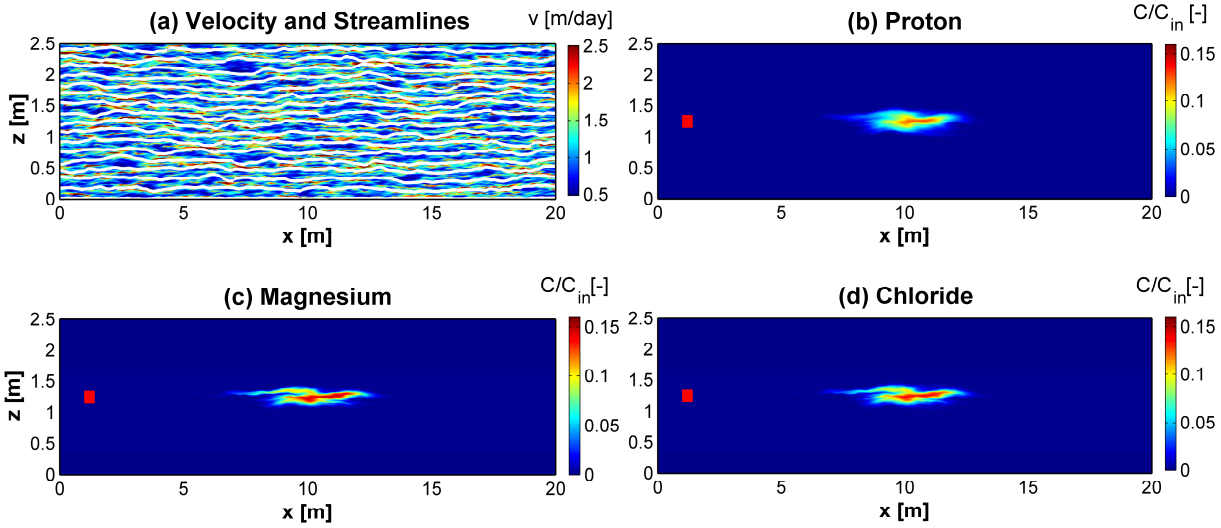

Figure 5.5. Seepage velocity distribution and streamlines (a); 2-D concentration maps (b-d) for mixed electrolyte case at v = 1 m/day after t = 7 days. The red rectangle represents the initial location of the solute slug (b-d).

The breakthrough curves of concentration and flux-related dilution index ($E_{Q,i}$), at the end of the domain, are illustrated in Fig. 5.6 for different simulations. Although the shape of the 2-D concentration distribution for different ions looks very irregular (non-Gaussian; Fig. 5.5b-d), their depth-integrated breakthrough curves have almost regular shape (Figs. 5.6a-c, g-i) in this mildly-heterogeneous domain.

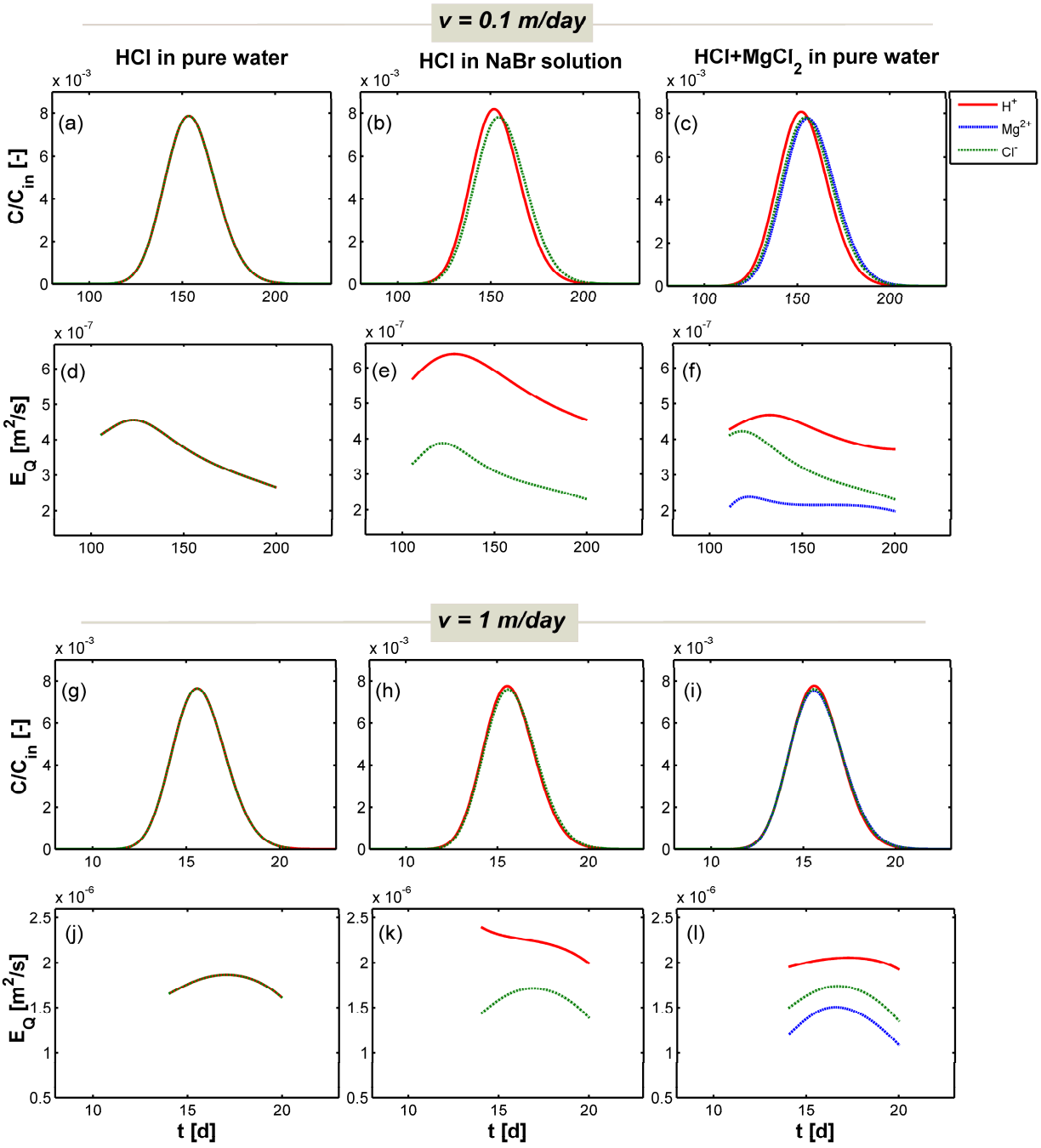

Figure 5.6. Breakthrough curves (a-c and g-i) and flux-related dilution indices (d-f and j-l) for simulations at v = 0.1 m/day (a-f) and 1 m/day (g-l) in a heterogeneous domain. $E_{Q,i}$ values are calculated for a concentration threshold equal to 10^{-6} of the peak concentration for each species.

For the transport of both HCl in a background electrolyte (Fig. 5.6b,h) as well as for the case of mixed electrolyte in pure water (Fig. 5.6c,i), the differences among the ionic temporal profiles are smaller compared to those observed in homogeneous domain. However, the differences in dilution between the ions are still significant as shown by the computed trends of $E_{Q,i}$. Unlike the regular increase of $E_{Q,i}$ in the homogeneous domain, the dilution breakthroughs in the heterogeneous flow field have a non-monotonic pattern. As observed in pore-scale domains [77], also for these continuum simulations such behavior can be attributed to the spatial variability of the velocity field and mass transfer limitations in the low-permeability zones of the heterogeneous flow field. Despite the different and irregular shape of the dilution breakthroughs compared to a homogeneous domain, the computed values of $E_{Q,i}$ at both flow velocities show the clear and persistent effect of the electrostatic coupling also in the heterogeneous flow field. This important feature can also be clearly appreciated from the maps of the ion concentration distributions (Fig. 5.5) but would be missed if one were to analyze exclusively flux-averaged concentration breakthrough curves at the outlet of the domain (Fig. 5.6 a-c and g-i).

The effect of electrostatic coupling is also evident from the maps of the dispersive flux components. As an example, Fig. 5.7 shows the results of transverse dispersive fluxes for the case of mixed electrolytes at v = 0.1 m/day. It is interesting to notice the interplay between the pure dispersive and the electrochemical migration components. For instance, considering H^+ it can be clearly observed that the electromigration component can have both a positive and a negative contribution to the total dispersive flux (Fig. 5.7g). Thus, the displacement of the ion can be increased or decreased in different locations within the plume. Similar considerations are valid for the other cation and for the anion. The latter shows an inversely correlated behavior with respect to H^+, with displacement of Cl^- ions enhanced in the plume fringe, where they are mostly coupled to H^+, and decreased in the plume core, where the charge interaction is stronger with Mg^{2+}. Mapping of the ionic flux components helps understanding and visualizing the coupling between the transport of charged species and confirms a similar behavior as noticed in the small scale homogeneous domain by analyzing the dilution breakthrough curves (Fig. 5.4f and 5.4l).

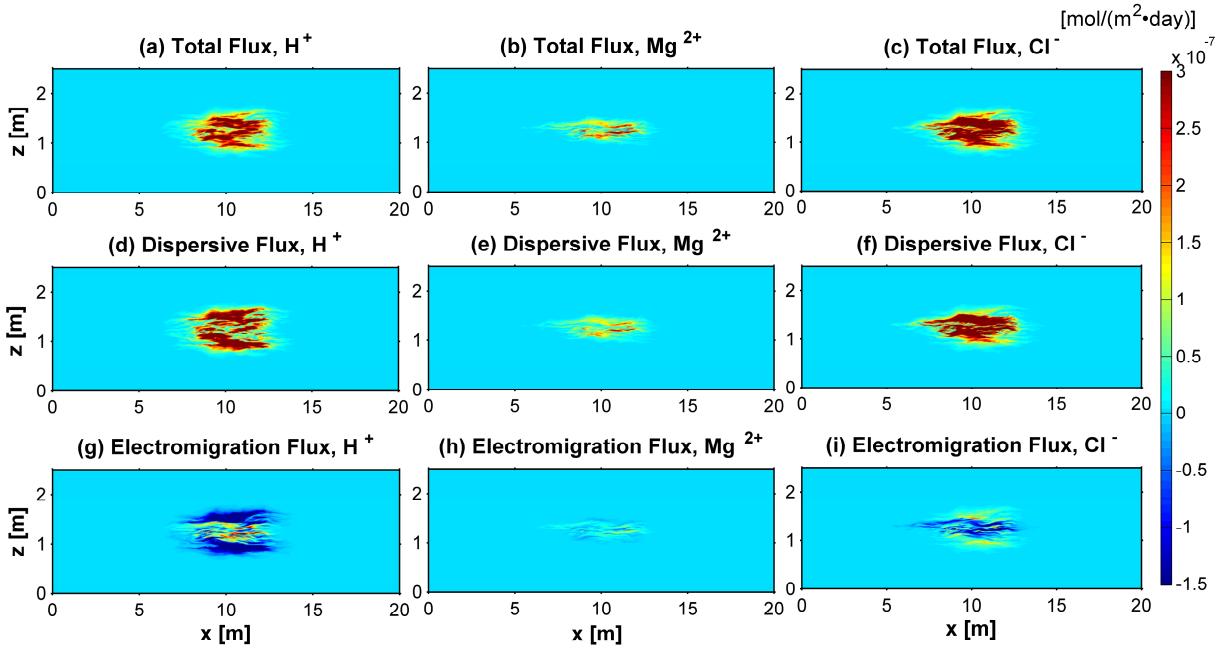

Figure 5.7. Maps of multicomponent ionic transverse fluxes for the transport of mixed electrolytes after 70 days (v = 0.1 m/day): Total fluxes (a, b, c), Dispersive fluxes (d, e, f) and Electrochemical migration fluxes (g, h, i). The direction from the core to the fringe of the plume is considered positive for the calculated fluxes.

5.5.2 Multicomponent Reactive Transport

In this section we present examples of two-dimensional multicomponent ionic transport coupled to chemical reactions in physically and chemically heterogeneous domains. We consider ion-exchange reactions and, similarly to a previous study [80], we extend a 1-D example problem (Section 5.4.2) to two-dimensional spatially-variable domains. We focus on multicomponent ionic transport and we consider a slug release of $CaCl_2$ in a 2-D domain containing Na^+, K^+ and NO_3^- as initial and ambient solution. The simulations are run in heterogeneous domains with different distributions of key physical and chemical parameter such as the hydraulic conductivity and the cation exchange capacity (Table 5.4).

Table 5.4: Description of the multicomponent reactive transport scenarios.

Scenario	*K* distribution	*CEC* distribution	Domain size	Slug size
A	heterogeneous	homogeneous	20 m × 2.5 m	4 m × 0.3 m
B	heterogeneous	heterogeneous	20 m × 2.5 m	4 m × 0.3 m

The simulations were run in the randomly generated 2-D fields with the same geometry and hydraulic properties of those used in Section 5.1.2. Fig. 5.8 shows distributions of the controlling physical and chemical parameters. In both scenarios, we consider solute slugs of $CaCl_2$ (6 mM), initially placed 1 m downstream of the inflow boundary and with dimensions of 4 m × 0.3 m, that were transported through the heterogeneous domains. The inflow and initial solutions contain $NaNO_3$ (1 mM) and KNO_3 (0.2 mM).

Scenario A considers the effects of physical heterogeneity on the reactive transport problem. In this particular scenario, a uniform value of *CEC* (1.1 meq/L; same as [18]) was used throughout the entire physically heterogeneous domain.

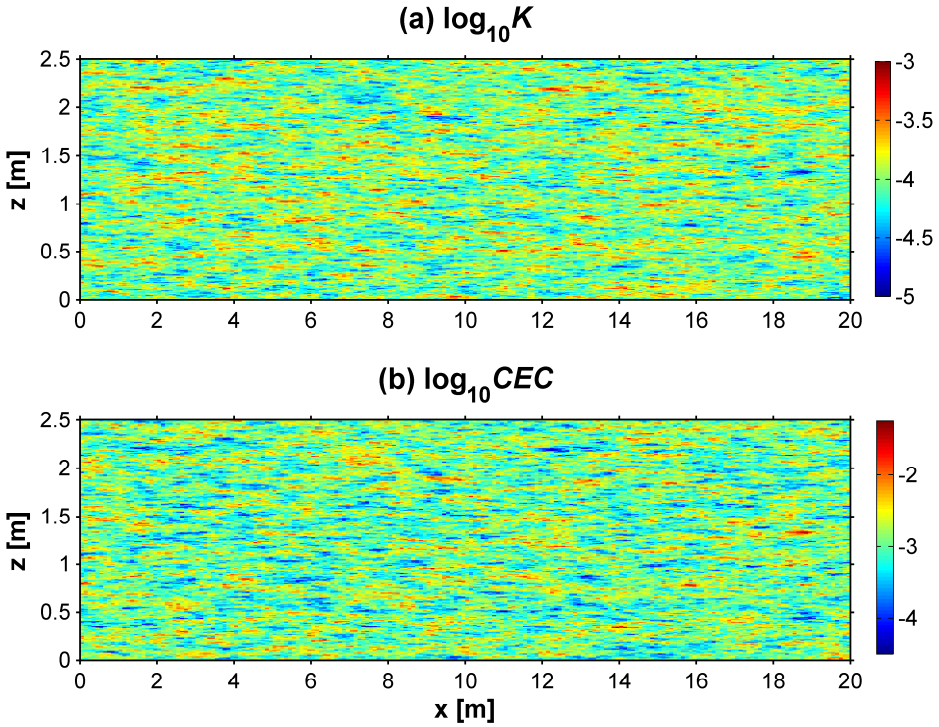

Figure 5.8. (a) Spatial distribution of hydraulic conductivity *K* (m/s) used in the simulated reactive transport scenarios A and B. (b) Spatial distribution of cation exchange capacity, CEC (eq/L) used in Scenario B.

In Scenario B, *CEC* values (Fig. 5.8b) were attributed to each cell of the domain considering a negative correlation with hydraulic conductivity as suggested in previous studies (e.g., [80-83]):

$$\ln CEC = a \ln K + b \tag{5.22}$$

where *a* and *b* are coefficients relating the hydraulic conductivity, *K* and the cation exchange capacity, *CEC*. In a field study, Christiansen et al. [81] identified a negative correlation between *K* and *CEC* in an aquifer (*a* = -0.59) composed of calcareous and non-calcareous

layers. We base our simulations on the negative correlation proposed in that study, implying that the low-permeability regions have higher cation exchange capacity than the high-permeability zones (and vice versa).

Fig. 5.9 summarizes the results of the multicomponent reactive transport simulations performed in scenarios A and B. The top row of panels depict the 2-D concentration distribution of the cation plumes (Ca^{2+}; Fig. 5.9a,e) and the lower two rows of panels show the distribution of the background cations (Na^+ and K^+) after 75 days of simulation. All simulations are run at an average seepage velocity of 0.1 m/day. Fig. 5.9a-c shows the spatial distribution of different cations plumes in Scenario A. In this domain, the solute slug $CaCl_2$ moves with groundwater along the 2-D random flow-field containing homogeneous cation-exchange properties. All the ionic plumes show irregularities because of the spatially variable hydraulic conductivity and velocity distributions. The displacing cation, Ca^{2+}, shows a tailing in the upstream front and a sharper interface in the downstream front of the plume. As it propagates through the domain, Ca^{2+} reacts with the exchanger and displaces the background cations (K^+ and Na^+) from the solid. Because of different affinities towards the solid phase, a chromatographic sequence is clearly observed among the positive ions: with Na^+ (lowest affinity, Fig. 5.9c) being the first species released from the solid phase, followed by K^+ (Fig. 5.9b) and, finally, by the displacing species Ca^{2+} (highest affinity, Fig. 5.9a).

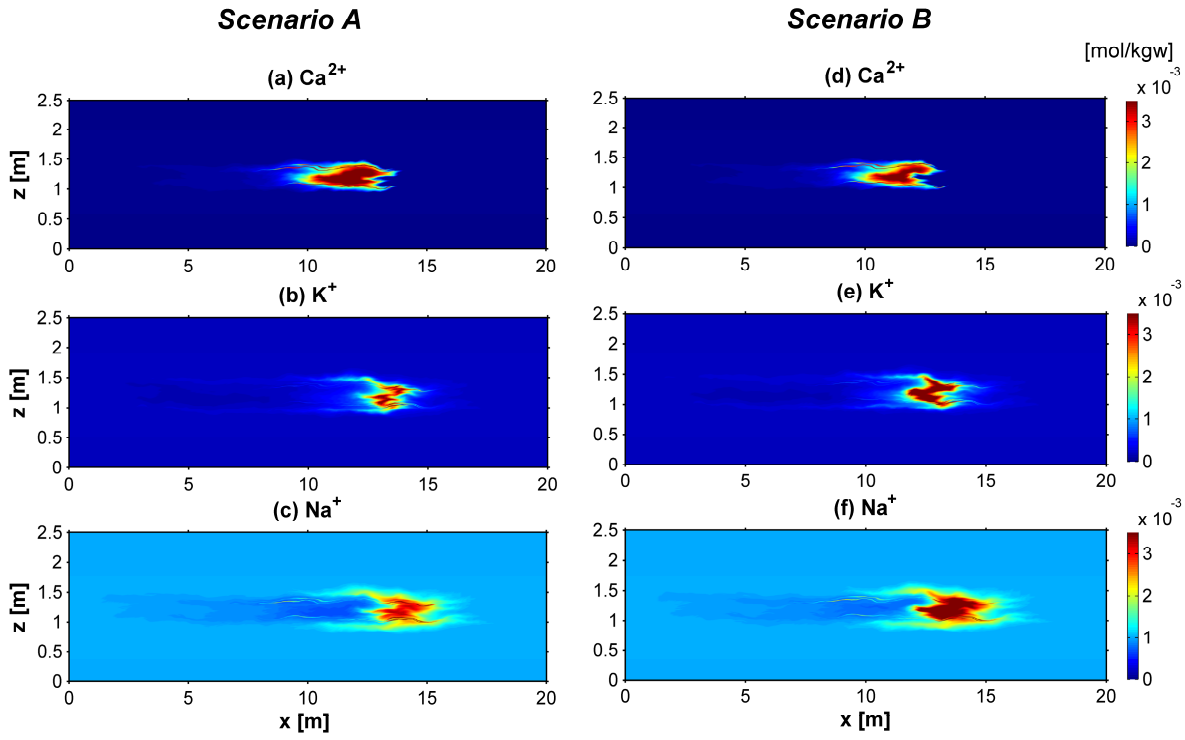

Figure 5.9. 2-D concentration distribution of cations in Scenario A (a-c) and B (d-f) after 75 days of simulation.

The effect of K^+ and Na^+ displacement from the solids is also reflected from the fact that these background cations show a surplus of dissolved concentration relative to their initial values (Fig. 5.9b-c). The center of mass of the cation plumes also moves with different apparent velocities: with Na^+ being the fastest species and Ca^{2+} being the slowest one.

In Scenario B, the solute slug migrates with groundwater along random flow paths and in a geochemically heterogeneous domain. The concentration and spreading of cation plumes (Fig. 5.9d-f) are quite different compared to the previous scenario. The background ions (K^+ and Na^+) contain relatively higher concentration in the dissolved phase compared to Scenario A (relative differences in the peak concentrations are ~32% for K^+ and ~11% for Na^+). Conversely, Ca^{2+} shows a distribution that has smaller peak concentration (approximately 22%) relative to the plume in Scenario A (Fig. 5.9a,d). This implies that the spatially correlated random distribution of geochemical properties leads to an enhancement of ion-exchange reactions and more effective retention of Ca^{2+}. After 75 days of simulation, the total mass of Ca^{2+} in the dissolved phase is ~34% smaller in the chemically heterogeneous domain with respect to Scenario A. This behavior can also be further confirmed from the depth-integrated breakthrough curves of Ca^{2+} at the end of the heterogeneous domains (Fig. 5.10a). The depth-integrated peak concentration of Ca^{2+} in Scenario B (red solid line) is significantly smaller (approximately ~5 times) compared to Scenario A (black solid line). The mean arrival of breakthrough in Scenario B is also considerably delayed (~20 days) compared to Scenario A. The dotted lines represent the breakthrough curves of respective scenarios by ignoring the charge interactions (i.e., as "liberated state"); while keeping the other hydraulic, transport and geochemical conditions identical in the simulations. Scenarios A and B were constructed using the same average *CEC*. However, the total cation exchange capacity in the two systems is different and this has an important effect on the breakthrough of calcium in the two setups. Therefore, we considered an additional case in which not the average, but the total *CEC* is the same in the two cases. The results of this additional simulation are reported in Fig. 5.10b and show a closer behavior in terms of both arrival time and peak concentration between scenario A and scenario B. It is interesting to notice that in all cases a contribution due to electrochemical migration can be appreciated even in the integrated profiles. Such contribution, in the considered physically and/or chemically heterogeneous realizations, tends to cause an additional retardation of the calcium plumes. We attribute this observation to the enhancement of Ca^{2+} dispersion fluxes through the electrostatic coupling with the more mobile anions present in the domain. This results in lower peak concentrations and more spread Ca^{2+} profiles. Such differences in displacement do not only influence the breakthrough of calcium but also the mass recovered at the outlet. In fact, the electromigration contribution to the dispersive fluxes causes enhanced displacement of calcium at the outer fringe of the plume. In

these regions calcium comes into contact with solid with available *CEC* and, thus, it is retained more effectively in the solid phase. As a consequence, a lower portion of the mass is recovered at the outlet.

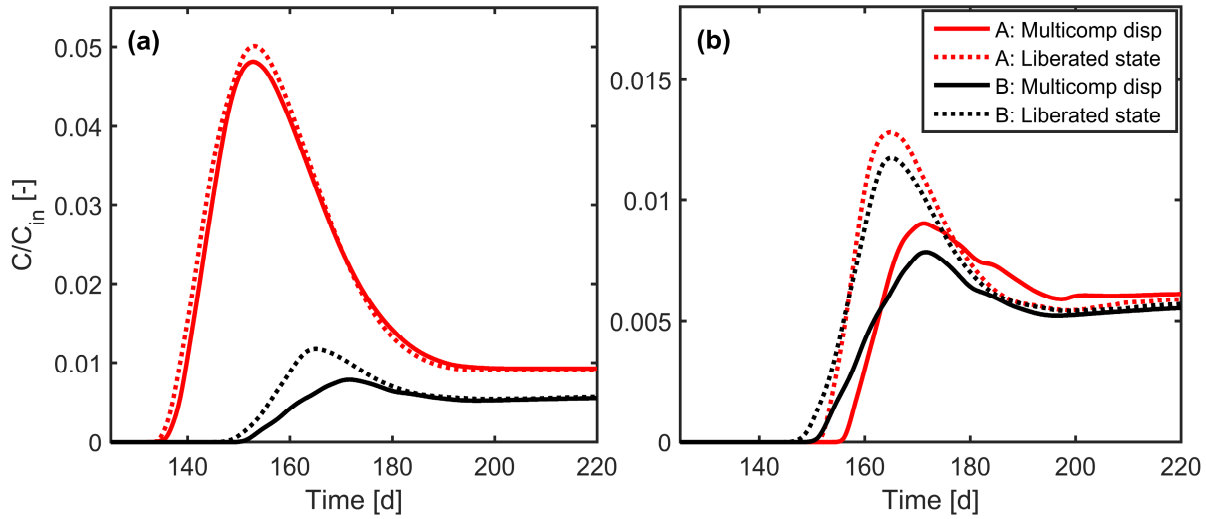

Figure 5.10. Depth-integrated breakthrough curves of Ca^{2+} at the end of the heterogeneous domain in Scenario A and B, considering multicomponent ionic transport (solid lines) as well as transport in "liberated" state (dotted lines). (a) Simulations with same average *CEC* between Scenario A and B; (b) Simulations with same total *CEC* between Scenario A and B.

5.6 Summary and Conclusions

In this paper, we presented a two-dimensional multicomponent reactive transport model which is capable of taking into account the electrochemical migration effects during ionic transport as well as a wide range of geochemical reactions. The modeling framework is based on a multicomponent formulation of diffusive/dispersive fluxes and on the compound-specific and spatially variable description of local hydrodynamic dispersion. The proposed approach allows a detailed description of physical and electrochemical processes during multicomponent ionic transport in both homogeneous and heterogeneous formations. Additionally, the multicomponent ionic transport model is coupled with the geochemical code PHREEQC, thus providing the flexibility of simulating a wide variety geochemical reactions included in the PHREEQC package. Two-dimensional conservative and reactive (ion-exchange) transport scenarios were presented to demonstrate the capability of the developed model to simulate multicomponent ionic transport in physically and chemically heterogeneous formations. The simulations were performed in a homogeneous porous medium at laboratory scale, as well as in heterogeneous porous media at the field scale. The simulation outcomes show that the

micro-scale physical (diffusion/dispersion) and/or electrochemical processes (Coulombic interactions) significantly affect the macro-scale transport and dilution both in the homogeneous and in the heterogeneous domains. For conservative transport, the results of this study show that the coupling effects of charge interactions can be appreciated from the 2-D distribution of the different ions and quantified using metrics of mixing such as the flux-related dilution index. However, such effects might be overlooked by only analyzing flux-averaged concentration breakthrough curves. Furthermore, mapping the different components of the dispersive fluxes is also very useful to understand and visualize the Coulombic coupling between the different ions and the effects of electrochemical migration. The impact of electrostatic interactions is also shown to be significant for the evolution of reactive plumes undergoing cation exchange in physically and geochemically heterogeneous domains. For these scenarios we found that the two-dimensional concentration distributions of the transported ions, as well as their integrated breakthrough curves at the outlet, are affected by the electrochemical migration terms coupling the transport of the charged species. Such effects influence the displacement of the dissolved ions in the pore water as well as their interaction with the solid matrix, since a different displacement compared to the "liberated state" causes the ions to interact with different reactive zones of the porous medium.

Besides the specific scenarios investigated in this study, the proposed multicomponent ionic transport code can be used to explore the effects of Coulombic interactions in porous media in a wide variety of reactive transport problems. This can include mineral precipitation and dissolution, sorption and surface complexation reactions, propagation of pH fronts, mobilization of heavy metals and metalloids and biodegradation reactions (e.g., [84-90]). We think that the code offers particular advantages for the study of transport and Coulombic interactions in flow-through systems when the aim is to provide a detailed description of the effects of physical and chemical heterogeneity. The current model formulation is limited to multicomponent ionic transport of dilute solutions in two-dimensional formations. Further work is required to extend the framework to systems with strong gradients of ionic strength and to three-dimensional transport problems. For fully 3-D transport, recent experimental studies have shown a more pronounced effect of diffusion and compound-specific dispersion on solute displacement and plume dilution [45]. Therefore, under these conditions, the effects of Coulombic interactions on the displacement of charged species are expected to be more pronounced compared to two-dimensional systems. Furthermore, in fully three-dimensional anisotropic heterogeneous porous media, the topology of the flow field and the possible development of twisting streamlines may play a major role on solute transport [91-93] and, thus, will also be of interest for multicomponent ionic transport problems.

Acknowledgments

This work was supported by the Baden-Württemberg Stiftung under the Eliteprogram for Postdocs. We would like to thank Prof. O. A. Cirpka (University of Tübingen) for discussion and for providing an early version of the streamline oriented code.

References

[1] Steefel CI, Appelo CAJ, Arora B, Jacques D, Kalbacher T, Kolditz O,Yeh GT. Reactive transport codes for subsurface environmental simulation. Computat Geosci 2015; 19:445-78. doi: 10.1007/s10596-014-9443-x.

[2] Barry DA, Prommer H, Miller CT, Engesgaard P, Brun A, Zheng C. Modelling the fate of oxidisable organic contaminants in groundwater. Adv Water Resour 2002;25: 945-83. doi: http://dx.doi.org/10.1016/S0309-1708(02)00044-1.

[3] Steefel CI, Lasaga AC. A coupled model for transport of multiple chemical-species and kinetic precipitation dissolution reactions with application to reactive flow in single-phase hydrothermal systems. Am Journal Sci 1994;294:529-92.

[4] Bethke C. Modelling transport in reacting geochemical systems. CR Acad Sci Ii A 1997;324:513-28.

[5] Prommer H, Barry DA, Zheng C. MODFLOW/MT3DMS-based reactive multicomponent transport modeling. Ground Water 2003, *41*, 247–257.

[6] Parkhurst DL, Kipp KL, Engesgaard P, Charlton SR. PHAST - A program for simulating ground-water flow, solute transport, and multicomponent geochemical reactions. Geochim Cosmochim Acta 2005; 69.

[7] Yeh GT, VS Tripathi. HYDROGEOCHEM: A coupled model HYDROlogical transport and GEOCHEMical equilibrium of multi component systems. ORNL 6371, Oak Ridge National Laboratory 1990.

[8] Xu T, Pruess K. Modeling multiphase non-isothermal fluid flow and reactive geochemical transport in variably saturated fractured rocks 1: Methodology. Am J Sci 2001;301:16-33, doi: 10.2475/ajs.301.1.16.

[9] Xu T, Sonnenthal E, Spycher N, Pruess K. TOUGHREACT—A simulation program for non-isothermal multiphase reactive geochemical transport in variably saturated geologic media: Applications to geothermal injectivity and CO2 geological sequestration. Comput Geosci 2006;32:145-65. doi: http://dx.doi.org/10.1016/j.cageo.2005.06.014.

[10] Xu T, Spycher N, Sonnenthal E, Zhang G, Zheng L, Pruess K. TOUGHREACT Version 2.0: A simulator for subsurface reactive transport under non-isothermal multiphase flow conditions. Comput Geosci 2011;37:763-74. doi: http://dx.doi.org/10.1016/j.cageo.2010.10.007.

[11] Mayer KU, Frind EO, Blowes DW. Multicomponent reactive transport modeling in variably saturated porous media using a generalized formulation for kinetically controlled reactions. Water Resour Res 2002;38:1301-21. doi: 10.1029/2001WR000862.

[12] Šimunek J, Jacques D, Šejna M, Van Genuchten MT. The HP2 program for HYDRUS (2D/3D): A coupled code for simulating two-dimensional variably-saturated water flow, heat

transport, and biogeochemistry in porous media, Version 1.0. PC Progress, Prague, Czech Republic 2012:76.

[13] Mao X, Prommer H, Barry DA, Langevin CD, Panteleit B, Li L. Three-dimensional model for multi-component reactive transport with variable density groundwater flow. Environ Model Softw 2006;21:615-28. doi: http://dx.doi.org/10.1016/j.envsoft.2004.11.008.

[14] Wissmeier L, Barry DA. Implementation of variably saturated flow into PHREEQC for the simulation of biogeochemical reactions in the vadose zone. Environ Model Softw 2010;25:526-38. doi: http://dx.doi.org/10.1016/j.envsoft.2009.10.001.

[15] Charlton SR, Parkhurst DL. Modules based on the geochemical model PHREEQC for use in scripting and programming languages. Comput Geosci 2011;37:1653-63. doi: http://dx.doi.org/10.1016/j.cageo.2011.02.005.

[16] Parkhurst DL, Wissmeier L. PhreeqcRM: A reaction module for transport simulators based on the geochemical model PHREEQC. Adv Water Resour 2015;83:176-89. doi: http://dx.doi.org/10.1016/j.advwatres.2015.06.001.

[17] Parkhurst DL, Appelo CAJ. User's guide to PHREEQC (Version 2) - A computer program for speciation, batch-reaction, one-dimensional transport, and inverse geochemical calculations. U.S. Geological Survey Water Resources Investigations Report 1999; 99-4259.

[18] Parkhurst DL, Appelo CAJ. Description of input and examples for PHREEQC version 3-A computer program for speciation, batch-reaction, one dimensional transport, and inverse geochemical calculations. U.S. Geological Survey Techniques and Methods 2013;6-A43:497. available only at http://pubs.usgs.gov/tm/06/a43/.

[19] Wissmeier L, Barry DA. Simulation tool for variably saturated flow with comprehensive geochemical reactions in two- and three-dimensional domains. Environ Model Softw 2011;26:210-8. doi: http://dx.doi.org/10.1016/j.envsoft.2010.07.005.

[20] Müller M, Parkhurst DL, Charlton SR. Programming PHREEQC calculations with C++ and Python - A comparative study. In: Maxwell R, Poeter E, Hill M, Zheng C, MODFLOW and More 2011 - Integrated Hydrological Modeling Proceedings 2011:632-636.

[21] Nardi A, Idiart A, Trinchero P, de Vries LM, Molinero J. Interface COMSOL-PHREEQC (iCP), an efficient numerical framework for the solution of coupled multiphysics and geochemistry. Comput Geosci 2014;69:10-21. doi: http://dx.doi.org/10.1016/j.cageo.2014.04.011.

[22] Nasir O, Fall M, Evgin E. A simulator for modeling of porosity and permeability changes in near field sedimentary host rocks for nuclear waste under climate change influences. Tunn Undergr Sp Tech 2014;42:122-35. doi: http://dx.doi.org/10.1016/j.tust.2014.02.010.

[23] Kolditz O, Bauer S, Bilke L, Böttcher N, Delfs JO, Fischer T, Zehner B. OpenGeoSys: An open-source initiative for numerical simulation of thermo-hydro-mechanical/chemical (THM/C) processes in porous media. Environ Earth Sci 2012;67:589-99. doi: 10.1007/s12665-012-1546-x.

[24] He W, Beyer C, Fleckenstein JH, Jang E, Kolditz O, Naumov D, Kalbacher T. A parallelization scheme to simulate reactive transport in the subsurface environment with OGS#IPhreeqc 5.5.7-3.1.2. Geosci Model Dev 2015;8:3333-48. doi: 10.5194/gmd-8-3333-2015.

[25] Korrani AKN, Sepehrnoori K, Delshad M. Coupling IPhreeqc with UTCHEM to model reactive flow and transport. Comput Geosci 2015;82:152-69, doi: http://dx.doi.org/10.1016/j.cageo.2015.06.004.

[26] Vinograd JR, McBain JW. Diffusion of electrolytes and of the ions in their mixtures. J Am Chem Soc 1941;63:2008-15. doi: 10.1021/ja01852a063.

[27] Liu CX, Shang JY, Zachara JM. Multispecies diffusion models: A study of uranyl species diffusion. Water Resour Res 2011; 47: W12514. http://dx.doi.org/10.1029/2011WR010575.

[28] Giambalvo ER, Steefel CI, Fisher AT, Rosenberg ND, Wheat CG. Effect of fluid-sediment reaction on hydrothermal fluxes of major elements, eastern flank of the Juan de Fuca Ridge. Geochim Cosmochim Acta 2002;66:1739-57. doi: 10.1016/S0016-7037(01)00878-X.

[29] Appelo CAJ, Wersin P. Multicomponent diffusion modeling in clay systems with application to the diffusion of tritium, iodide, and sodium in opalinus clay. Environ Sci Tech 2007;41:5002-7. doi: Doi 10.1021/Es0629256.

[30] Appelo CAJ, Vinsot A, Mettler S, Wechner S. Obtaining the porewater composition of a clay rock by modeling the in- and out-diffusion of anions and cations from an in-situ experiment. J Contam Hydrol 2008;101:67-76. doi: DOI 10.1016/j.jconhyd.2008.07.009.

[31] Appelo CAJ, Van Loon LR, Wersin P. Multicomponent diffusion of a suite of tracers (HTO, Cl, Br, I, Na, Sr, Cs) in a single sample of Opalinus Clay. Geochim Cosmochim Acta 2010;74:1201-19. doi: 10.1016/j.gca.2009.11.013.

[32] Ben-Yaakov S. Diffusion of sea water ions—I. Diffusion of sea water into a dilute solution. Geochim Cosmochim Acta 1972;36:1395-406. doi: 10.1016/0016-7037(72)90069-5.

[33] Lasaga AC. The treatment of multi-component diffusion and ion pairs in diagenetic fluxes. Am J Sci 1979;279:324-46. doi: 10.2475/ajs.279.3.324.

[34] Felmy AR, Weare JH. Calculation of multicomponent ionic-diffusion from zero to high-concentration 1. The System Na-K-Ca-Mg-Cl-SO_4-H_2O at 25-degrees-C. Geochim Cosmochim Acta 1991;55:113-31. doi: Doi 10.1016/0016-7037(91)90405-T.

[35] Boudreau BP, Meysman FJR, Middelburg JJ. Multicomponent ionic diffusion in porewaters: Coulombic effects revisited. Earth Planet Sci Lett 2004;222:653-66. doi: 10.1016/j.epsl.2004.02.034.

[36] Cussler EL. Diffusion : Mass transfer in fluid systems. 3rd ed. Cambridge University Press, Cambridge, New York 2009.

[37] Rolle M, Muniruzzaman M, Haberer CM, Grathwohl P. Coulombic effects in advection-dominated transport of electrolytes in porous media: Multicomponent ionic dispersion. Geochim Cosmochim Acta 2013;120:195-205. doi: http://dx.doi.org/10.1016/j.gca.2013.06.031.

[38] Muniruzzaman M, Haberer CM, Grathwohl P, Rolle M. Multicomponent ionic dispersion during transport of electrolytes in heterogeneous porous media: Experiments and model-based interpretation. Geochim Cosmochim Acta 2014;141:656-69. doi: http://dx.doi.org/10.1016/j.gca.2014.06.020.

[39] Muniruzzaman M, Rolle M. Impact of multicomponent ionic transport on pH fronts propagation in saturated porous media. Water Resour Res 2015;51:6739-55. doi: 10.1002/2015WR017134.

[40] Rasouli P, Steefel CI, Mayer KU, Rolle M. Benchmarks for multicomponent diffusion and electrochemical migration. Computat Geosci 2015;19:523-33. doi: 10.1007/s10596-015-9481-z.

[41] Bauer RD, Rolle M, Bauer S, Eberhardt C, Grathwohl P, Kolditz O, Griebler C. Enhanced biodegradation by hydraulic heterogeneities in petroleum hydrocarbon plumes. J Contam Hydrol 2009;105:56-68. doi: 10.1016/j.jconhyd.2008.11.004.

[42] Rolle M, Chiogna G, Bauer R, Griebler C, Grathwohl P. Isotopic fractionation by transverse dispersion: Flow-through microcosms and reactive transport modeling study. Environ Sci Tech 2010;44:6167-73. doi: 10.1021/es101179f.

[43] Haberer CM, Rolle M, Cirpka OA, Grathwohl P. Oxygen transfer in a fluctuating capillary fringe. Vadose Zone J 2012;11. doi: 10.2136/Vzj2011.0056.

[44] Hochstetler DL, Rolle M, Chiogna G, Haberer CM, Grathwohl P, Kitanidis PK. Effects of compound-specific transverse mixing on steady-state reactive plumes: Insights from pore-scale simulations and Darcy-scale experiments. Adv Water Resour 2013;54:1-10. doi: 10.1016/j.advwatres.2012.12.007.

[45] Ye Y, Chiogna G, Cirpka OA, Grathwohl P, Rolle M. Enhancement of plume dilution in two-dimensional and three-dimensional porous media by flow focusing in high-permeability inclusions. Water Resour Res 2015;51:5582-602. doi: 10.1002/2015WR016962.

[46] Fiori A, Jankovic I, Dagan G. The impact of local diffusion upon mass arrival of a passive solute in transport through three-dimensional highly heterogeneous aquifers. Adv Water Resour 2011;34:1563-73. doi: 10.1016/j.advwatres.2011.08.010.

[47] Hadley PW, Newell C. The new potential for understanding groundwater contaminant transport. Groundwater 2014;52:174-86. doi: 10.1111/gwat.12135.

[48] LaBolle EM, Fogg GE. Role of molecular diffusion in contaminant migration and recovery in an alluvial aquifer system. Trans Porous Med 2001;42:155-79. doi: 10.1023/A:1006772716244.

[49] Liu CX, Ball WP. Back diffusion of chlorinated solvent contaminants from a natural aquitard to a remediated aquifer under well-controlled field conditions: Predictions and measurements. Ground Water 2002;40:175-84. doi: 10.1111/j.1745-6584.2002.tb02502.x.

[50] Chiogna G, Eberhardt C, Grathwohl P, Cirpka OA, Rolle M. Evidence of compound-dependent hydrodynamic and mechanical transverse dispersion by multitracer laboratory experiments. Environ Sci Tech 2010;44:688-93. doi: 10.1021/Es9023964.

[51] Chiogna G, Cirpka OA, Grathwohl P, Rolle M. Relevance of local compound-specific transverse dispersion for conservative and reactive mixing in heterogeneous porous media. Water Resour Res 2011;47:W07540. doi: 10.1029/2010wr010270.

[52] Rasa E, Chapman SW, Bekins BA, Fogg GE, Scow KM, Mackay DM. Role of back diffusion and biodegradation reactions in sustaining an MTBE/TBA plume in alluvial media. J Contam Hydrol 2011;126:235-47. http://dx.doi.org/10.1016/j.jconhyd.2011.08.006.

[53] Rolle M, Chiogna G, Hochstetler DL, Kitanidis PK. On the importance of diffusion and compound-specific mixing for groundwater transport: An investigation from pore to field scale. J Contam Hydrol 2013;153:51-68. http://dx.doi.org/10.1016/j.jconhyd.2013.07.006.

[54] Van Breukelen BM, Rolle M. Transverse hydrodynamic dispersion effects on isotope signals in groundwater chlorinated solvents' plumes. Environ Sci Tech 2012;46:7700-8. doi: 10.1021/es301058z.

[55] Kitanidis PK. The concept of the Dilution Index. Water Resour Res 1994;30:2011-26. doi: 10.1029/94WR00762.

[56] Van Cappellen P, J-F Gaillard. Biogeochemical dynamics in aquatic sediments. Reviews in Mineralogy and Geochemistry. 34 (1996) 335-76.

[57] Liu CX, Zachara JM, Felmy AR, Gorby Y. An electrodynamics-based model for ion diffusion in microbial polysaccharides. Colloids Surf A and B 2004:38:55-65. doi: 10.1016/j.colsurfb.2004.08.003.

[58] Alizadeh A, Zhang L, Wang MR. Mixing enhancement of low-Reynolds electro-osmotic flows in microchannels with temperature-patterned walls. J Colloid Interface Sci 2014;431:50-63. doi: 10.1016/j.jcis.2014.05.070.

[59] Zhang L, Wang MR. Modeling of electrokinetic reactive transport in micropore using a coupled lattice Boltzmann method. J Geophys Res-Sol Ea 2015;120:2877-90. doi: 10.1002/2014JB011812.

[60] Bard AJ, Faulkner LR. Electrochemical methods fundamentals and applications. (2nd ed.). John Wiley, New York 2001:718.

[61] Cirpka OA, Frind EO, Helmig R. Streamline-oriented grid generation for transport modelling in two-dimensional domains including wells. Adv Water Resour 1999;22:697-710. doi: 10.1016/s0309-1708(98)00050-5.

[62] Guedes de Carvalho JRF, Delgado JMPQ. Overall map and correlation of dispersion data for flow through granular packed beds. Chem Eng Sci 2005;60:365-75. doi: http://dx.doi.org/10.1016/j.ces.2004.07.121.

[63] Rolle M, Hochstetler DL, Chiogna G, Kitanidis PK, Grathwohl P. Experimental investigation and pore-scale modeling interpretation of compound-specific transverse dispersion in porous media. Trans Porous Med 2012;93:347-62. doi: 10.1007/s11242-012-9953-8.

[64] Archie GE. The electrical resistivity log as an aid in determining some reservoir characteristics. Trans AIME; 146.

[65] Boving TB, P Grathwohl. Tracer diffusion coefficients in sedimentary rocks: correlation to porosity and hydraulic conductivity. J Contam Hydrol 2001; 53:85-100. doi: Doi 10.1016/S0169-7722(01)00138-3.

[66] Scheidegger AE. General theory of dispersion in porous media. Journal of Geophys Res 1961;66:3273-8. doi: 10.1029/JZ066i010p03273.

[67] Bijeljic B, Muggeridge AH, Blunt MJ. Pore-scale modeling of longitudinal dispersion. Water Resour Res 2004;40:W11501. doi: 10.1029/2004wr003567.

[68] Hazen A. Some physical properties of sands and gravels: with special reference to their use in filtration. Ann Rep State Board of Health Mass 1892;24:541-556.

[69] Eckert D, Rolle M, Cirpka OA. Numerical simulation of isotope fractionation in steady-state bioreactive transport controlled by transverse mixing. J Contam Hydrol 2012;140–141:95-106. doi: http://dx.doi.org/10.1016/j.jconhyd.2012.08.010.

[70] Cirpka OA, Frind EO, Helmig R. Numerical methods for reactive transport on rectangular and streamline-oriented grids. Adv Water Resour 199;22:711-28. http://dx.doi.org/10.1016/S0309-1708(98)00051-7.

[71] Davis T, Duff I. An unsymmetric-pattern multifrontal method for sparse LU factorization. SIAM J Matrix Anal 1997;18:140-58. doi: 10.1137/S0895479894246905.

[72] Leij FJ, Skaggs TH, van Genuchten MT. Analytical solutions for solute transport in three-dimensional semi-infinite porous media. Water Resour Res 1991;27:2719-33. doi: 10.1029/91WR01912.

[73] van Genuchten MT, Leij FJ, Skaggs TH, Toride N, Bradford SA, Pontedeiro EM. Exact analytical solutions for contaminant transport in rivers 1. The equilibrium advection-dispersion equation. J Hydrol Hydromech 2013;61:146-60. doi: 10.2478/johh-2013-0020.

[74] Lasaga AC. Kinetic theory in the earth sciences. Princeton University Press, Princeton, N.J 1998.

[75] Tartakovsky AM, Redden G, Lichtner PC, Scheibe TD, Meakin P. Mixing-induced precipitation: Experimental study and multiscale numerical analysis. Water Resour Res 2008;44:W06s04. doi: 10.1029/2006wr005725.

[76] Rolle M, Eberhardt C, Chiogna G, Cirpka OA, Grathwohl P. Enhancement of dilution and transverse reactive mixing in porous media: Experiments and model-based interpretation. J Contam Hydrol 2009;110:130-42. doi: 10.1016/j.jconhyd.2009.10.003.

[77] Rolle M, Kitanidis PK. Effects of compound-specific dilution on transient transport and solute breakthrough: A pore-scale analysis. Adv Water Resour 2014;71:186-99. http://dx.doi.org/10.1016/j.advwatres.2014.06.012.

[78] Sudicky EA. A natural gradient experiment on solute transport in a sand aquifer: Spatial variability of hydraulic conductivity and its role in the dispersion process. Water Resour Res 1986;22:2069-82. doi: 10.1029/WR022i013p02069.

[79] Dykaar BB, Kitanidis PK. Determination of the effective hydraulic conductivity for heterogeneous porous media using a numerical spectral approach: 1. Method. Water Resour Res. 1992;28:1155-66. doi: 10.1029/91WR03084.

[80] Yang C, J Samper. Numerical evaluation of multicomponent cation exchange reactive transport in physically and geochemically heterogeneous porous media. Computat Geosci 2009;13:391-404. doi: 10.1007/s10596-009-9127-0.

[81] Christiansen JS, Engesgaard PK, Bjerg PL. A physically and chemically heterogeneous aquifer: field study and reactive transport modelling. In: Groundwater Quality: Remediation and Protection, Proceedings of the GQ'98 Conference, IAHS Press, Wallingford 1998:329-36.

[82] Jacques D, Mouvet C, Mohanty B, Vereecken H, Feyen J. Spatial variability of atrazine sorption parameters and other soil properties in a podzoluvisol. J Contam Hydrol 1999;36:31-52. http://dx.doi.org/10.1016/S0169-7722(98)00141-7.

[83] Samper J, Yang C. Stochastic analysis of transport and multicomponent competitive monovalent cation exchange in aquifers. Geosphere 2006;2:102-12. doi: 10.1130/ges00030.1.

[84] Kjøller C, Postma D, Larsen F. Groundwater acidification and the mobilization of trace metals in a sandy aquifer. Environ Sci Tech 2004;38:2829-35. doi: 10.1021/es030133v.

[85] Prigiobbe V, Bryant SL. pH-dependent transport of metal cations in porous media. Environ Sci Tech 2014;48:3752-9. doi: 10.1021/es403695r.

[86] Li L, Salehikhoo F, Brantley SL, Heidari P. Spatial zonation limits magnesite dissolution in porous media. Geochim Cosmochim Acta 2014;126:555-73. http://dx.doi.org/10.1016/j.gca.2013.10.051.

[87] Molins S, Trebotich D, Steefel CI, Shen CP. An investigation of the effect of pore scale flow on average geochemical reaction rates using direct numerical simulation. Water Resour Res 2012;48:W03527. doi: 10.1029/2011wr011404.

[88] Haberer CM, Muniruzzaman M, Grathwohl P, Rolle M. Diffusive/Dispersive and reactive fronts in porous media: Fe (II)-Oxidation at the unsaturated/saturated interface. Vadose Zone J 2015;14(5). doi: http://dx.doi.org/10.2136/vzj2014.07.0091.

[89] Fakhreddine S, Lee J, Kitanidis PK, Fendorf S, Rolle M. Imaging geochemical heterogeneities using inverse reactive transport modeling: An example relevant for characterizing arsenic mobilization and distribution. Adv Water Resour 2016;88: 186-97. http://dx.doi.org/10.1016/j.advwatres.2015.12.005.

[90] Redden G, Fox D, Zhang C, Fujita Y, Guo L, Huang H. $CaCO_3$ precipitation, transport and sensing in porous media with in situ generation of reactants. Environ Sci Tech 2014;48:542-9. doi: 10.1021/es4029777.

[91] Chiogna G, Rolle M, Bellin A, Cirpka OA. Helicity and flow topology in three-dimensional anisotropic porous media. Adv Water Resour 2014;73:134-43. http://dx.doi.org/10.1016/j.advwatres.2014.06.017.

[92] Ye Y, G Chiogna, OA Cirpka, P Grathwohl, M Rolle. experimental evidence of helical flow in porous media. Phys Rev Lett 2015;115:194502. doi: 10.1103/Physrevlett.115.194502.

[93] Cirpka OA, Chiogna G, Rolle M, Bellin A. Transverse mixing in three-dimensional nonstationary anisotropic heterogeneous porous media. Water Resour Res 2015;51:241-60. doi: 10.1002/2014WR015331.

S5. Supplementary Material

S5.1 Introduction

This document provides two additional benchmark examples of the 2-D multicomponent ionic transport model proposed in this study. The first benchmark problem validates the multicomponent ionic transport calculations against measured experimental data in a quasi 2-D laboratory setup, as well as with the outcomes from simplified 1-D PHREEQC simulations for the case of conservative transport of mixed electrolytes in porous media under steady-state flow and transport conditions. The second example shows the performance of the coupling of the proposed transport code with the geochemical code PHREEQC using IPhreeqc module for an ion exchange problem.

S5.2 Benchmark of multicomponent ionic transport with an experimental dataset

In addition to the benchmark examples presented in Section 5.4, we consider an example involving the transport of mixed electrolyte species in pure water under steady-state flow and transport conditions. This scenario corresponds to one of the experiments performed by Rolle et al. (2013) and considers a mixed electrolyte solution (KCl and $MgCl_2$) that is continuously injected through a line source located at the center of the inlet boundary of a 2-D saturated porous media.

Fig. S5.1 shows the steady-state concentration distributions of different ionic plumes (K^+, Mg^{2+}, and Cl^-) obtained from the simulations using our proposed 2-D multicomponent ionic transport code.

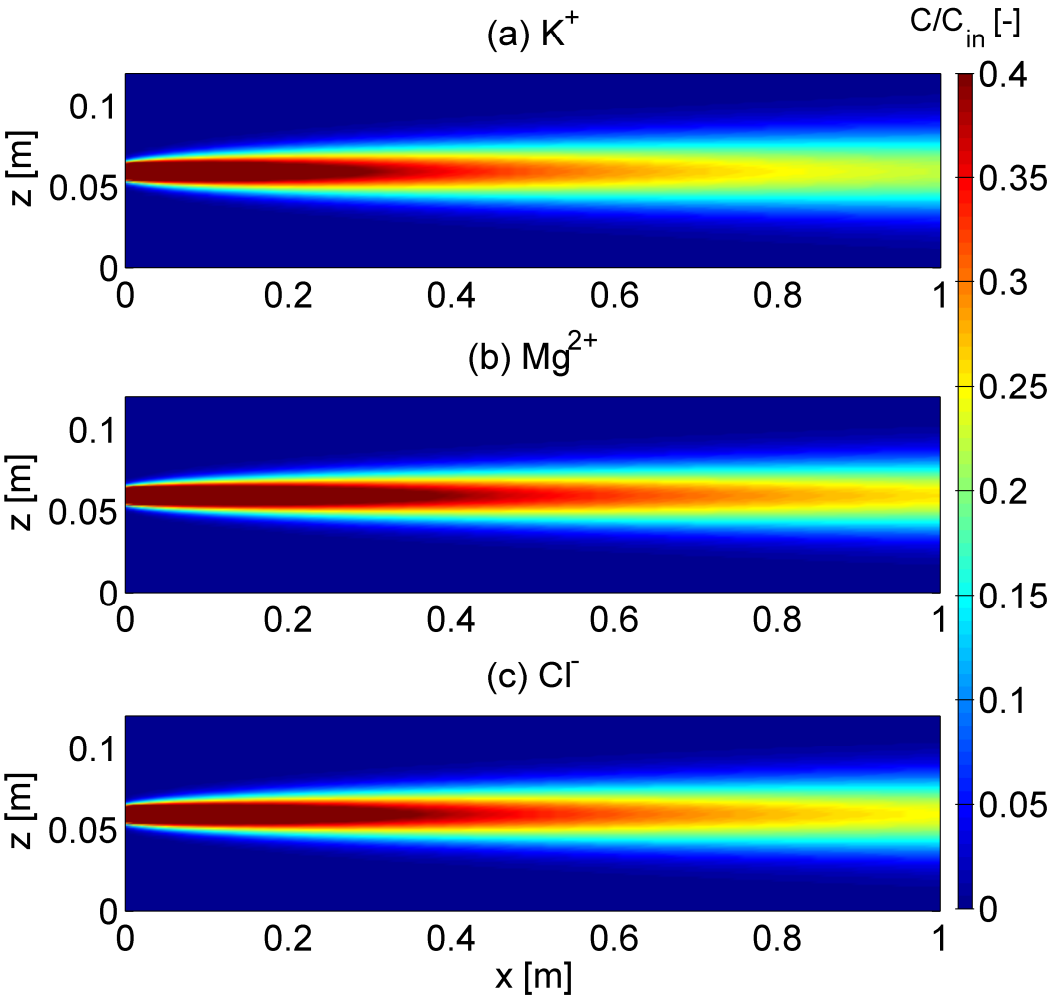

Figure S5.1. 2-D steady-state plumes for different ionic species obtained from the simulation of the transport of KCl and $MgCl_2$ in pure water using the proposed 2-D multicomponent ionic transport code.

The experimental data were provided by Rolle et al. (2013), who performed such laboratory bench-scale flow-through experiments at a seepage velocity of 1.5 m/day. The experiments were conducted in a quasi 2-D water saturated domain (100 cm × 12 cm) with high resolution concentration measurements at the outlet (5 mm spacing) of the flow-through system. Additionally, this particular example was also considered in the benchmark study of Rasouli et al. (2015) where MIN3P (Mayer et al. 2002) and CrunchFlow (Steefel and Lasaga, 1994) codes were compared with the PHREEQC calculations. Figs. S5.2 and S5.3 demonstrate that our simulation results agree very well with the experimental data, showing a different lateral displacement of the ions due to the electrostatic interactions, as well as with the simplified (i.e., no explicit consideration of the flow) 1-D PHREEQC simulations.

(i) Verification with experimental data

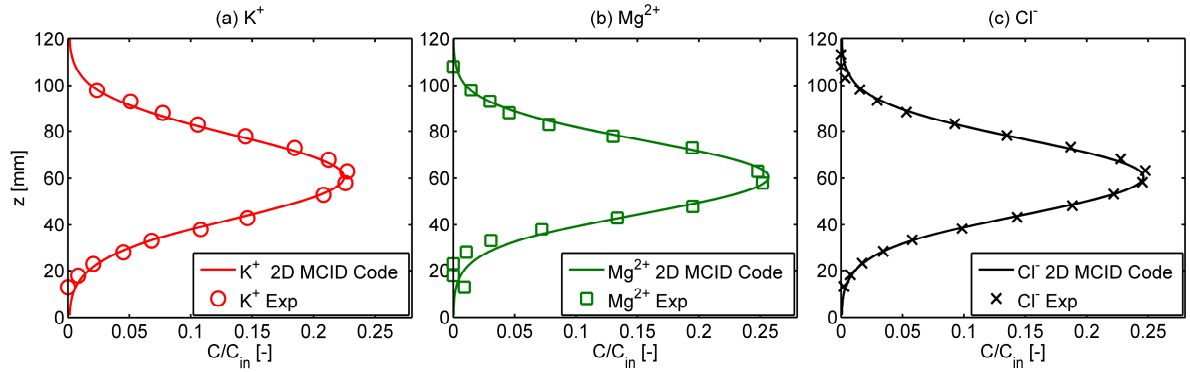

Figure S5.2. Comparison between the experimental data (markers) obtained from the 2-D flow-through system (Rolle et al., 2013) and the simulation outcomes (solid lines) of the proposed multicomponent ionic dispersion model.

(ii) Verification with PHREEQC calculations

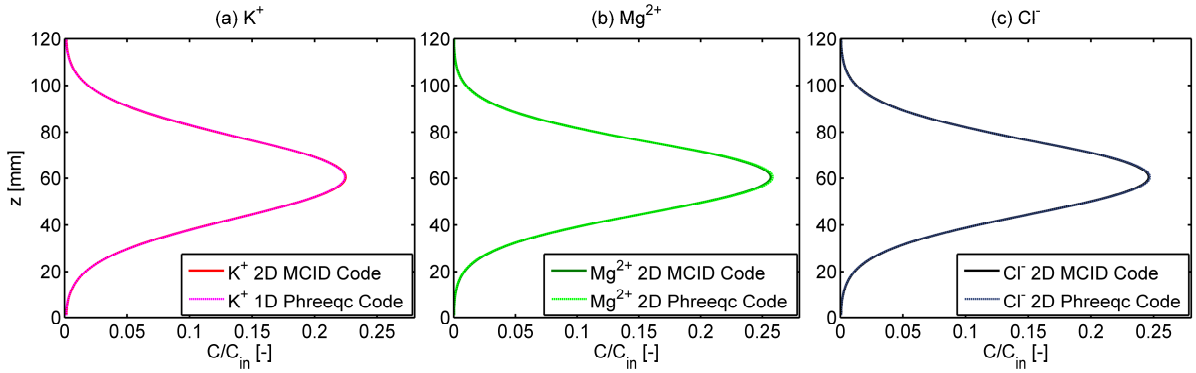

Figure S5.3. Comparison between the outcomes of the proposed 2-D multicomponent ionic dispersion code (solid lines) and 1-D PHREEQC simulations (dashed lines).

S5.3 Benchmark of IPhreeqc coupling for an ion-exchange problem

As mentioned in Section 5.4.2, we consider the example problem 11 of the PHREEQC-3 manual to validate the coupling of our 2-D multicomponent ionic transport code with the geochemical code PHREEQC. This example includes the advective-dispersive transport of ionic species in a one-dimensional, 8 cm long column containing a cation exchanger (Fig. S5.4). The initial solution of the column contains 1.0 mmol Na^+, 0.2 mmol K^+ and 1.2 mmol NO_3^- per kilogram of water. The inlet solution has a composition of 0.6 mmol Ca^{2+}/kg water and 1.2 mmol Cl^-/kg water. Further details and PHREEQC input files can be found in the manual of PHREEQC (Parkhurst and Appelo, 2013).

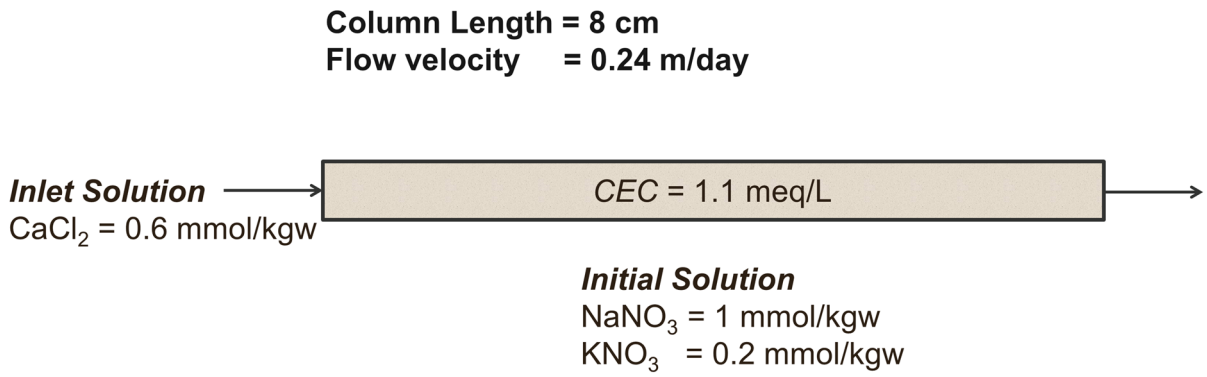

Figure S5.4. Schematic diagram of the transport and ion-exchange problem of Example 11 in PHREEQC manual.

This example was simulated in 1-D using PHREEQC, as well as a 2-D problem with the proposed code in an equivalent domain with a two-dimensional discretization (8 cm × 2 cm; grid size: Δx = 2 mm, Δz = 2 mm). The comparison of the results shows an excellent agreement (Fig. S5.5), which validates the performance of the coupling between the 2-D transport code implemented in MATLAB® and the geochemical reaction engine (PHREEQC).

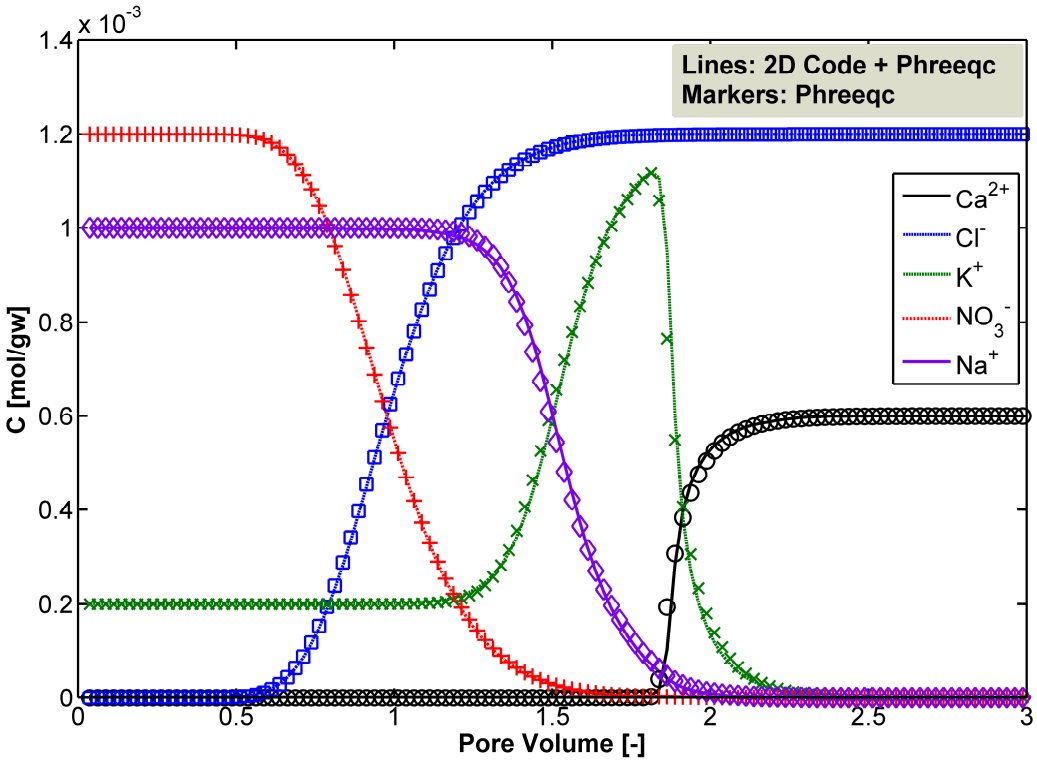

Figure S5.5: Benchmark of IPhreeqc coupling with the 2-D transport code for a classical transport and ion-exchange problem presented in the PHREEQC manual (Example 11).

Chapter 6

Experimental investigation of the impact of compound-specific dispersion and electrostatic interactions on transient transport and solute breakthrough[¥]

Abstract

This study investigates the effects of compound-specific diffusion/dispersion and electrochemical migration on transient solute transport in saturated porous media. We conducted laboratory bench-scale experiments, under advection-dominated regimes (seepage velocity: 0.5, 5, 25 m/day), in a quasi two-dimensional flow-through setup using pulse injection of multiple tracers (both uncharged and ionic species). Extensive sampling and measurement of solutes' concentrations (~1500 samples; >3000 measurements) were performed at the outlet of the flow-through setup, at high spatial and temporal resolution. The experimental results show that the compound-specific effects and charge-induced Coulombic interactions are important not only at low velocities and/or in steady-state plumes but also for transient transport under high flow velocities. Such effects can lead to remarkably different behaviors of measured breakthrough curves also at very high Péclet numbers. To quantitatively interpret the experimental results, we used four modeling approaches: classical advection-dispersion equation (ADE), continuous time random walk (CTRW), dual domain mass transfer model (DDMT), and a multicomponent ionic dispersion model. The latter is based on the multicomponent formulation of coupled diffusive/dispersive fluxes and was used to describe and explain the electrostatic effects of charged species. Furthermore, we determined experimentally the temporal profiles of the flux-related dilution index. This metric of mixing, used in connection with the traditional solute breakthrough curves, proved to be useful to correctly distinguish between plume spreading and mixing, particularly for the cases in which the sole analysis of spatially-integrated concentration breakthrough curves may lead to erroneous interpretation of plume dilution.

[¥] Reproduced from: Muniruzzaman, M., and M. Rolle (2017), Experimental investigation of the impact of compound-specific dispersion and electrostatic interactions on transient transport and solute breakthrough, *Water Resources Research*, 53, doi:10.1002/2016WR019727.

6.1 Introduction

Conservative transport in porous media is determined by fundamental physical (e.g., aqueous diffusion, advection) and/or electrochemical (e.g., Coulombic effects, ion-pairing, charge coupling) processes (e.g., Kitanidis, 1994; Haggerty and Gorelick, 1995, Wang and Van Cappellen, 1996; Boudreau, 1997; Thullner et al., 2005; Appelo and Wersin, 2007; Steefel and Maher, 2009). In particular, dilution and mixing of solute plumes are ultimately controlled by small-scale processes such as diffusion and local scale dispersion (e.g., Chiogna et al., 2011; Cirpka et al., 2011). Numerous studies focusing on experimental and numerical investigations have contributed to the increased recognition that aqueous diffusion, which is the only true mixing mechanism in groundwater (Kitanidis, 1994), quantitatively plays an important role on macroscale solute transport in porous media (e.g., Carrera et al., 1998; LaBolle and Fogg, 2001; Chiogna et al., 2010; Zhang et al., 2010; Fiori et al., 2011; Haberer et al., 2011; Molins et al., 2012 Rolle et al., 2013a; Hadley and Newell, 2014). Recent experiments and pore-scale simulations showed the key effects of diffusion-limited incomplete mixing in the pore channels on the observed macroscopic transport behavior (e.g., Gramling et al., 2002; Raje and Kapoor, 2000; Tartakovsky et al., 2009) and have triggered the development of new transport theories and formulations (e.g., Edery et al., 2009; Sanchez-Vila et al., 2010; Chiogna and Bellin, 2013; Porta et al., 2015). In the study of transverse mixing, such effects were found to be responsible for the nonlinear dependence of the mechanical dispersion term on the average flow velocity, as well as on its direct dependence on the solute diffusivity also in advection-dominated regimes (e.g., Chiogna et al., 2010; Rolle et al., 2012; Scheven et al., 2014; Hochstelter et al., 2013).

An aspect that has been investigated in the geochemical studies (Vinograd and McBain, 1941; Felmy and Weare, 1991; Van Cappellen and Gaillard, 1996; Giambalvo et al., 2002; Liu, 2007; Appelo et al., 2008; Steefel and Maher, 2009), but that is not typically considered in the subsurface hydrology literature is that, besides diffusion, also electrostatic interactions affect the movement of charged solutes (e.g., major ions and many inorganic and organic contaminants) in groundwater. The capability to capture, accurately describe and properly upscale the effects of controlling small-scale processes on macroscopic transport is of primary importance to further develop and advance the current descriptions and formulations of solute transport in porous media. To this end, controlled laboratory experiments are instrumental to provide high-resolution data necessary to test and validate different modeling approaches. Despite a wealth of experimental data have been collected over decades in laboratory flow-through systems and particularly in 1-D column setups (e.g. Delgado 2006), multidimensional and multi-tracer transient experiments with depth-resolved measurements are rare. Although it

might be argued that depth-integrated measurements are more convenient and representative of common practice, they are not ideal to understand transport and mixing processes (Cirpka and Kitanidis, 2000). In particular, if the goal is to characterize the effects of small-scale diffusive processes on transient solute transport, depth-resolved measurements of solute concentrations (and volumetric fluxes) are necessary.

The main objective of this study is to provide a detailed experimental investigation of transient transport in saturated porous media. We perform laboratory bench-scale experiments in homogeneously packed quasi 2-D setups under advection-dominated regimes. In particular, we use the simultaneous injection of multiple tracers (both "charge-neutral" and "charged" species) to identify the effects of compound-specific diffusion/dispersion, pore-scale incomplete mixing, and electrostatic interactions on plume dilution and spreading. The injection of a small pulse facilitates establishing "fully 2-D" transient plumes. The plumes mix with the surrounding ambient water and their breakthrough at the outlet is measured at high spatial and temporal resolution. Such sampling approach allows characterizing both longitudinal and transverse evolution of the tracer plumes. We determined experimentally the entropy based flux-related dilution index from concentrations and flow rates measurements. Temporal profiles of this metric of mixing were helpful for the interpretation of the integrated flux-weighted breakthrough curves and to help distinguishing between plume spreading and dilution. The concentration breakthrough curves were quantitatively analyzed with different transport models: classical advection-dispersion model (ADE), continuous time random walk (CTRW), and dual-domain mass transfer model (DDMT). The electrostatic behavior of multicomponent ionic tracers was explained by using a forward model based on a Nernst-Planck formulation including the coupling of dispersive fluxes. Both experimental and model outcomes show that the aqueous diffusion and the electrostatic interactions can significantly impact the macroscale transient transport and can lead to remarkably different behaviors under strongly advection-dominated regimes. Our experimental dataset also represents a challenge, as well as an opportunity of further development, for the different models. In fact, despite individual fits could reproduce the measured concentrations, generalized formulations able to consistently capture all experimental conditions will need to be developed.

6.2 Experimental Setup

Laboratory experiments were performed to investigate the transient solute transport as well as plume dilution in a quasi 2-D flow-through system. The experimental setup consists of an acrylic-glass chamber which has inner dimensions of 100 cm × 19 cm × 1 cm (L × H × W).

The flow-through chamber is equipped with 24 equally-spaced (5 mm apart) ports at both inlet and outlet ends (Fig. 6.1). At each end, these injection (inlet) and extraction (outlet) ports are directly connected to a 24-channel high-precision peristatic pump (ISMATEC IPC-N24, Ismatec, Glattburg, Switzerland) through Fluran HCA pump tubings (ID 0.64 mm; Ismatec, Glattburg, Switzerland). The flow-through setup was homogeneously packed with glass beads with a grain size diameter of 1.00-1.50 mm (Sartorius AG, Göttingen, Germany). In order to avoid possible air entrapment in the water-saturated porous medium, a wet-packing procedure is followed in the packing step (e.g., Haberer et al., 2012). The peristaltic pumps were used to obtain a uniform horizontal fluid flow in the porous medium. Before each experiment, both inlet and outlet pumps were calibrated and the experiments were performed in a temperature controlled room (T = 20 °C). Figure 6.1 illustrates the experimental setup, as well as an example of high-resolution sampling at the outlet ports.

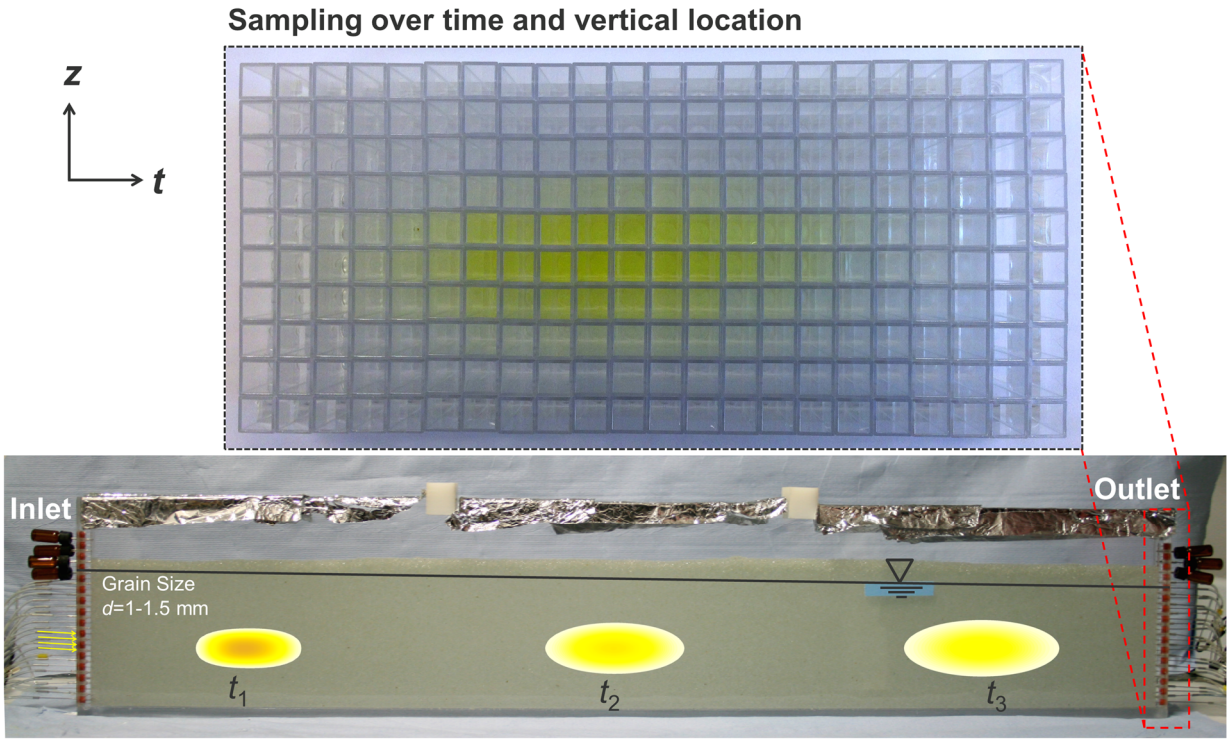

Figure 6.1. Laboratory flow-through setup. The yellowish-shaded areas represent the schematic illustration of the temporal evolution of the tracer plumes injected from the four central inlet ports. The inset shows a photograph of fluorescein samples collected at different vertical locations at the outlet as a function of time.

The experiments were initiated by establishing a steady water flow by flushing the domain with at least two pore volumes. When the flow-condition was completely stable over time, we

started the transport experiments by injecting the tracer solutions through the four central inlet ports (port no. 10, 11, 12 and 13; corresponding to the vertical location of 5, 5.5, 6 and 6.5 cm from the bottom of the chamber, respectively). All tracer experiments were performed by applying a pulse type input at the inlet boundary for a finite duration. In order to maintain the same size of the tracer pulses in different experiments with different seepage velocities, we inject the tracer solutions for the duration of ~0.05 pore volumes. Afterwards, samples were taken at all the outlet extraction ports at regular time intervals. Such sampling strategy enables measuring both high-resolution temporal and spatial profiles at the outlet of flow-through system. Additionally, we determined the volumetric water flux in each extraction port by collecting and weighing the effluent for a given period of time. Details of the experimental settings are reported in Table 6.1.

Table 6.1: Summary of geometry and transport parameters of the experimental system.

Experimental settings	
Flow-through chamber dimensions (L×H×W) [cm]	100×19×1
Number of inlet/outlet ports used	23/24
Port spacing [mm]	5
Grain diameter of porous matrix [mm]	1.00-1.50
Average horizontal velocity [m/day]	0.5, 5, 25
Average porosity [-]	0.41
Diffusion coefficients	D^{aq} [m^2/s][a]
Na^+	1.20×10^{-9}
K^+	1.77×10^{-9}
Mg^{2+}	0.63×10^{-9}
Cl^-	1.81×10^{-9}
Br-	1.86×10^{-9}
Fluorescein[b]	0.45×10^{-9}

[a] values from Lasaga (1998) at 18°C, and corrected for temperature and viscosity changes at 20°C (experimental conditions)
[b]calculated after Worch (1993)

In this work, we performed two types of experiments targeting on different tracer behavior: (i) multi-tracer experiments, and (ii) multicomponent ionic experiments. Multi-tracer experiments were conducted at three distinct seepage velocities: $v \approx 0.5$, 5 and 25 m/day. Solutions containing potassium chloride (30-136 mg/L) and sodium fluorescein (27-102 mg/L) were used as tracer solution; whereas ultra-pure Milli-Q water (Labostar 1-DI, Evoqua, USA) was used as ambient solution. The aqueous diffusivities of the different solutes vary considerably and are reported in Table 6.1. Multicomponent ionic experiments were performed to show the relevance of electrostatic effects during transient transport in multi-ionic environments. In these experiments, a pulse of 1:2 electrolyte solution (magnesium chloride; 0.80 mM) was

injected into the saturated porous medium. As ambient solution, either Milli-Q water or NaBr solution (1:1 electrolyte; 4.04 mM) was used for these experiments (Table 6.2). The multicomponent ionic experiments were performed at a flow velocity of ~5 m/day.

The samples collected at the outlet ports were analyzed to determine the concentration of the different solutes. Fluorescein concentration was measured by using a UV-spectrophotometer (DR 2800, Hach, Germany). The extinction and emission wavelengths were 483 and 515 nm, respectively. The anion concentrations (Cl^-, Br^-) were measured by ion-chromatography (Dionex ICS-1500, Thermo Scientific, USA); whereas the cations (Mg^{2+} and Na^+) were measured by ICP-MS (Agilent 7700 Series, Agilent Technologies, Japan). Table 6.2 summarizes important experimental conditions, as well as details on the sampling procedure.

Table 6.2: Tracers' inlet concentrations, pulse duration, sampling intervals and number of samples

Experiments	**Tracer concentrations [mg/L]**		**Pulse duration [min]**	**Sampling intervals [min]**	**No. of Samples**	**No. of Measurements**
Multi-tracer experiments						
	Fluorescein	*KCl*				
$v \approx 0.5$ m/day	27	30	165	50	260	520
$v \approx 5$ m/day	101.6	136.2	15	5	300	600
$v \approx 25$ m/day	35.9	40.7	3	1	270	540
Multicomponent ionic experiments ($v \approx 5$ *m/day*)						
	Tracer ($MgCl_2$)	*Ambient Solution*				
(a) in pure water	0.80 mM	Milli-Q water	15	5	300	600
(b) in a buffer electrolyte solution	0.80 mM	NaBr (4.04 mM)	15	5	300	1200

6.3 Modeling Approach and Data Evaluation

Four different solute transport models were used to interpret the results of the multi-tracer experiments. This section provides a brief overview of the models and of the data evaluation approaches.

6.3.1 Analysis of Breakthrough Curves (BTC)

6.3.1.1 Advection-dispersion Equation (ADE)

The classical advection-dispersion equation, based on hydrodynamic dispersion theory (Bear, 1972), is the most commonly used model to describe solute transport in porous media. In a 2-D flow-through domain, representing our experimental setup, the transport of a conservative solute species is described as:

$$\frac{\partial C}{\partial t} = -v\frac{\partial C}{\partial x} + D_L\frac{\partial^2 C}{\partial x^2} + D_T\frac{\partial^2 C}{\partial z^2} \tag{6.1}$$

where C [mol/m^3] is the concentration of the solute, v [m/s] is the seepage velocity along the main flow, D_L [m^2/s] and D_T [m^2/s] are longitudinal and transverse hydrodynamic dispersion coefficients, respectively, x [m] and z [m] are the spatial coordinates in the directions parallel and orthogonal to principal flow direction, respectively, and t [s] denotes time. Closed-form analytical solutions of the above partial differential equation exist in the literature for simplified boundary and/or initial conditions (e.g., Carslaw and Jaeger, 1959; Crank, 1975). In our experiments, we used a pulse input of tracers along a line source for a finite duration, for which the boundary ($f(x)$) and initial ($g(z,t)$) conditions in a semi-infinite ($0<x<\infty$ and $-\infty<z<\infty$) 2-D domain read as:

Boundary condition:
$$g(z,t) = \begin{cases} C_0 & |z| < w/2 \quad \text{and} \quad 0 < t \le t_0 \\ 0 & \text{otherwise} \end{cases} \tag{6.2}$$

Initial condition:
$$f(x) = 0 \tag{6.3}$$

with,
$$C(x,z,0) = f(x) \tag{6.4}$$

$$C(0,z,t) = g(z,t) \tag{6.5}$$

$$\frac{\partial C}{\partial x}(\infty,z,t) = 0 \tag{6.6}$$

$$\frac{\partial C}{\partial z}(x,\pm\infty,t) = 0 \tag{6.7}$$

in which, w [m] denotes the source width at the inflow, C_0 [mol/m^3] is the inflow concentration, and t_0 [s] is time duration of the pulse. Considering uniform transport coefficients and a perfectly homogeneous, isotropic semi-infinite domain, the analytical solution of the 2-D transient transport problem subjected to the above boundary and initial conditions is given by (e.g., Leij et al., 1991; van Genuchten et al., 2013),

$$C(x,z,t)=\frac{C_0}{2}\int_{P(t)}^{t}\frac{x}{\tau}\left[\left\{\frac{1}{\sqrt{4\pi D_L\tau}}\exp\left(-\frac{(x-v\tau)^2}{4D_L\tau}\right)\right\}\cdot\left\{erfc\left(\frac{z-w/2}{\sqrt{4D_T\tau}}\right)-erfc\left(\frac{z+w/2}{\sqrt{4D_T\tau}}\right)\right\}\right]d\tau$$

where, (6.8)

$$P(t)=\begin{cases}0 & \text{when} \quad 0<t\le t_0\\ t-t_0 & \text{when} \quad t>t_0\end{cases}$$

The above equation (Eq. 6.8) is a simplified macroscopic description of our experimental system and can be used for the 2-D interpretation of the measured results. However, for the analysis of breakthrough curves a 1-D model is convenient and it is necessary when only vertically integrated measurements are available. Under these conditions the governing equation reads as:

$$\frac{\partial C}{\partial t}=-v\frac{\partial C}{\partial x}+D_L\frac{\partial^2 C}{\partial x^2} \tag{6.9}$$

The analytical solution for 1-D ADE for equivalent boundary and initial conditions as described in Eqs (6.2-6.7) is given by (e.g., van Genuchten et al., 2013),

$$\begin{aligned}C(x,t)=\frac{C_0}{2}\Bigg[&\left\{erfc\left(\frac{x-vt}{\sqrt{4D_Lt}}\right)-erfc\left(\frac{x-v(t-t_0)}{\sqrt{4D_L(t-t_0)}}\right)\right\}\\&+\exp\left(\frac{vx}{D_L}\right)\left\{erfc\left(\frac{x+vt}{\sqrt{4D_Lt}}\right)-erfc\left(\frac{x+v(t-t_0)}{\sqrt{4D_L(t-t_0)}}\right)\right\}\Bigg]\end{aligned} \tag{6.10}$$

This simplified 1-D analytical solution agrees very well with the full 2-D analytical solution of Eq. (6.8) when the mass-fluxes at a specific cross-section are vertically integrated and normalized by the integrated mass-flux at the inflow boundary. We term this spatially integrated quantities as "boundary-normalized integrated breakthrough curves" or just "integrated BTCs" $\left(\hat{C}(x,t)\Big|_{BN}^{BTC}\right)$,

$$\hat{C}(x,t)\Big|_{BN}^{BTC}=\frac{\int_{-\infty}^{\infty}C(x,z,t)q_x(z)dz}{\int_{-\infty}^{\infty}g(z,t)q_x(z)dz} \tag{6.11}$$

where q_x [m/s] denotes the specific discharge in the longitudinal direction. So, for simplicity, we used this 1-D solution (Eq. 6.10) to fit the breakthrough curves measured at each individual outlet ports (local BTC) as well as their integrated quantities (Eq. 6.11).

6.3.1.2 Continuous Time Random Walk Formulation (CTRW)

In addition to the fitting of ADE model, we also used a continuous time random walk (CTRW) formulation to interpret the measured breakthrough curves and, in particular, to investigate the "non-Fickian" or "anomalous" behavior of tracer plumes studied in our experiments. The CTRW framework, which describes the solute transport mechanisms as particles undergoing a series of transition steps over space, $\boldsymbol{s}$ and time, t, is able to capture non-Fickian transport phenomena with long-term tailings in breakthrough curves where conventional ADE fails (e.g., Berkowitz and Scher, 1997; Berkowitz et al., 2000; 2006; Hatano and Hatano et al., 1998; Kosakowski et al., 2001; Levy and Berkowitz, 2003; Dentz et al., 2011). Usually, these transition steps are described by a joint probability density function $\psi(\boldsymbol{s}, t)$. In many applications of transport in porous media, a decoupled form of $\psi(\boldsymbol{s}, t)$ is often used with $\psi(\boldsymbol{s}, t) = p(\boldsymbol{s})\ \psi(t)$: where $p(\boldsymbol{s})$ denotes the probability distribution of the length of jumps, and $\psi(t)$ is the rate of probability for a transition time, t between sites (Berkowitz, et al., 2006; Berkowitz and Scher, 2009; 2010). The CTRW transport equation in partial differential equation form reads as:

$$\frac{\partial c(\mathbf{s},t)}{\partial t} = -\int_0^t M(t-t')\left[\mathbf{v}_\psi \cdot \nabla c(\mathbf{s},t') - \mathbf{D}_\psi : \nabla\nabla c(\mathbf{s},t')\right]dt' \tag{6.12}$$

in which $c(\mathbf{s}, t)$ is the concentration, $\mathbf{v}_\psi$ and $\mathbf{D}_\psi$ are the transport velocity and generalized dispersion coefficient, respectively. $M(t)$ is a memory function which accounts for the unknown, small-scale heterogeneities beyond the level of experimental detection (Cortis, et al., 2004).

In Laplace transformed form, the above CTRW transport equation takes the form:

$$u\tilde{c}(\mathbf{s},u) - c_0(\mathbf{s}) = -\tilde{M}(u)\left[\mathbf{v}_\psi \cdot \nabla\tilde{c}(s,u) - \mathbf{D}_\psi : \nabla\nabla\tilde{c}(\mathbf{s},u)\right] \tag{6.13}$$

where $\tilde{c}(\mathbf{s},u)$ is the Laplace transformed concentration, u is the Laplace variable, and $\tilde{M}(u)$ is the memory function in Laplace space.

$$\tilde{M}(u) \equiv \bar{t}u\frac{\tilde{\psi}(u)}{1-\tilde{\psi}(u)} \tag{6.14}$$

in which $\bar{t}$ is a characteristic transition time, and $\tilde{\psi}(u)$ is the Laplace transform of probability rate for transition time, $\psi(t)$. Depending on the expression of $\tilde{\psi}(u)$, this memory function, $\tilde{M}(u)$ can take any possible form. Therefore, the functional form of $\tilde{\psi}(u)$ is of utmost importance in approximating the nature of solute transport in CTRW formulation. We use the truncated power law (TPL) form of $\tilde{\psi}(u)$ which has been found to be successfully used by numerous authors in interpreting solute transport observed in laboratory and field scales (e.g., Berkowitz et al., 2006; 2009; Bijeljic and Blunt, 2006; Deng et al., 2008; Heidari and Li,

2014). The TPL model, which allows the identification of the beginning and ending of the non-Fickian behavior, is written as:

$$\tilde{\psi}(u) \equiv (1+\tau_2 u t_1)^{\beta} \exp(t_1 u) \frac{\Gamma(-\beta, \tau_2^{-1} + t_1 u)}{\Gamma(-\beta, \tau_2^{-1})} \qquad 0 < \beta < 2 \qquad (6.15)$$

where t_1 and t_2 (with $\tau_2 \equiv t_2/t_1$) are the lower and upper limits of power law behavior respectively, and Γ is incomplete gamma function. Therefore, in the TPL formulation, the solution for tracer concentrations, $c(\boldsymbol{s}, t)$ requires three input parameters (β, t_1 and t_2) in connection with the transport coefficients (v_ψ and D_ψ). The parameter β is a measure of the extent of "non-Fickian" or "anomalous" nature of transport with values between 0 and 2 representing the non-Fickian behavior: where $\beta = 0 - 1$ indicates more pronounced anomalous behavior compared to those of $\beta = 1 - 2$; and the formulation reduces to the classical ADE form (Fickian behavior) when $\beta > 2$. Thus, the use of TPL form allows the identification of transition from Fickian to anomalous behavior. We used CTRW MATLAB Toolbox (Cortis et al., 2005) to fit our experimental breakthrough curves with the model.

6.3.1.3 Dual-domain Mass Transfer Model (DDMT)

The dual-domain mass transfer (DDMT) model is also often used to reproduce concentration measurements, showing deviations from the conventional ADE model, during transport in porous media (e.g., van Genuchten and Wierenga, 1976). This model considers solute migration in a porous medium represented with two distinct domains: a mobile domain (a certain fraction of the total porosity) where transport follows advection-dispersion behavior; and a stagnant immobile domain (the remaining fraction of the total porosity), which does not experience advection or dispersion and mass-exchange only takes place due to the concentration variation between mobile and immobile domain. The transport equations for DDMT for a first-order exchange in 1-D domain are given by:

$$\eta_m \frac{\partial C_m}{\partial t} + \eta_{im} \frac{\partial C_{im}}{\partial t} + q \frac{\partial C_m}{\partial x} - \eta_m \frac{\partial}{\partial x}\left(D_L^m \frac{\partial C_m}{\partial x} \right) = 0 \qquad (6.16)$$

$$\eta_{im} \frac{\partial C_{im}}{\partial t} = \xi (C_m - C_{im}) \qquad (6.17)$$

where the indices m and im refer to the mobile and immobile domains, respectively. C_m [mol/m^3] and C_{im} [mol/m^3] are the concentrations in mobile and immobile domain; η_m [-] and η_{im} [-] are, respectively, the mobile and immobile porosities; q [m/s] denotes the specific discharge; and ξ [1/s] is the mass transfer coefficient. Although this model was originally developed to describe solute transport in fractured/aggregated or non-equilibrium sorbing

media (e.g., Gerke and van Genuchten, 1993; Gorelick et al., 2005; Luo et al., 2005; Valocchi, 1985), it is often applied also to porous media systems where a "physical dual-domain" network is not explicitly identifiable (e.g., Luo et al., 2007; Ronayne et al., 2010; Liu and Kitanidis, 2012). We applied this model as an extension of ADE model to match our concentration measurements obtained from the experimental system.

6.3.2 Quantification of Transverse Dispersion

In order to identify the transverse displacement of the injected plumes in our quasi 2-D flow-through systems, we match the experimentally measured concentrations with the ADE model to obtain transverse dispersion coefficient, D_T. This can be done by fitting the 2-D analytical solution of Eq. (6.8) with the locally measured breakthrough curves at all individual outlet ports. Alternatively, following a similar approach to the one described in Eq. (6.11), we can further simplify the treatment by "decoupling" the transverse problem from the longitudinal one. The simplification is done by integrating the outlet concentrations over time at each vertical location. Thus, we consider only the plumes' displacement in the transverse direction. As done in Eq. (6.11), these time-integrated concentrations are normalized by the time-integrated inflow boundary condition and we term this quantity as "boundary normalized integrated spatial profiles" or just "integrated spatial profiles" $\left(\hat{C}(x,z)\Big|_{BN}^{SP}\right)$,

$$\hat{C}(x,z)\Big|_{BN}^{SP} = \frac{\int_0^\infty C(x,z,t)dt}{\int_0^\infty g(z,t)dt} \tag{6.18}$$

Once again, along a specific cross-section, the above time-integrated quantity of Eq. (6.18) produces the same outcome as the analytical solution for 2-D steady-state transport subjected to a line source at the inlet (Domenico and Palciauskas, 1982):

$$C(x,z) = \frac{C_0}{2}\left\{erfc\left(\frac{z-w/2}{\sqrt{4D_T x/v}}\right) - erfc\left(\frac{z+w/2}{\sqrt{4D_T x/v}}\right)\right\} \tag{6.19}$$

Therefore, we fit Eq. (6.19) to the time-integrated spatial profiles $\left(\hat{C}(x,z)\Big|_{BN}^{SP}\right)$, calculated from our measured data, to characterize the transverse evolution (D_T) of the injected tracers at the outlet of the domain.

6.3.3 Evaluation of Plume Dilution

As a metric of dilution, we use the flux-related dilution index. This quantity describes dilution as the "act of distributing a given solute mass flux over a larger water flux" and represents the effective volumetric water flux carrying the solute mass flux at a given longitudinal cross-section (Rolle et al., 2009). For transient transport in porous media, the flux-related dilution index can be written as (Rolle and Kitanidis, 2014):

$$E_Q(x,t) = \exp\left(-\int_{\Omega} p_Q(x,t) \ln p_Q(x,t) q_x(x,t) d\Omega \right) \tag{6.20}$$

where $q_x = v\theta$ is the longitudinal component of specific discharge, Ω [m^2] is the cross-sectional area perpendicular to the main flow, θ [-] is the total porosity, and p_Q [s/m^3] is the flux-related probability density function at time t:

$$p_Q(x,t) = \frac{C(x,t)}{\int_{\Omega} C(x,t) q_x(x,t)} \tag{6.21}$$

6.3.4 Modeling Multicomponent Ionic Dispersion

The transport mechanism of charged solutes in a multi-ionic environment is conceptually different compared to the charge-neutral species due to the additional contribution of electrostatic interactions. Mathematically, transport processes of such charged species are commonly described by the Nernst-Planck formulations by explicitly accounting for electrochemical potential gradients (e.g., Bard and Faulkner, 2001; Cussler, 2009). For the multicomponent transport of dilute electrolyte solutions under the simplified condition of negligible ionic strength gradients, the total diffusive flux of ionic species is expressed as the additional contribution of a purely diffusive flux (Fick's law) and an electrochemical migration term (e.g., Lasaga, 1978; Boudreau et al., 2004; Appelo and Wersin, 2007):

$$J_i = -D_i \nabla C_i - D_i \frac{z_i F}{RT} C_i \nabla \Phi \tag{6.22}$$

where C_i [mol/m^3] is the concentration of a mobile charged species i (i = 1,2,3,…,N), D_i [m^2/s] is the "self-diffusion" coefficient (i.e., diffusion at its "liberated" state), z_i [-] denotes the charge, F [C/equiv] is the Faraday's constant, R [J/(mol·K)] is the ideal gas constant, T [K] is the temperature, and Φ [J] is the electrostatic potential.

By considering the electroneutrality constraints of the solution: i.e., (i) condition of local charge-balance $\sum_{i=1}^{N} z_i C_i = 0$ and/or (ii) condition of maintaining zero electrical current, $\sum_{i=1}^{N} z_i J_i = 0$, the electrostatic potential gradient $(\nabla\Phi)$ can be expressed as:

$$\nabla\Phi = \frac{-\sum_{i=1}^{N}\left(z_i D_i \nabla C_i\right)}{\sum_{i=1}^{N}\left(z_i^2 F D_i C_i\right)/RT} \tag{6.23}$$

As a result, the flux expression of Eq. (6.23) takes the form,

$$J_i = -D_i \nabla C_i + \frac{z_i D_i C_i}{\sum_{j=1}^{N}\left(z_j^2 D_j C_j\right)} \sum_{k=1}^{N}\left(z_k D_k \nabla C_k\right) \tag{6.24}$$

This formulation enables accounting for both the movements due to the self-diffusion as well as the concentration gradients of other dissolved charged species. Key steps regarding the detailed derivation of the above equations can be found in the works of Ben-Yaakov, 1972; Lasaga, 1979, Van Cappellen and Gaillard, 1996; Boudreau et al, 2004; Appelo and Wersin, 2007; Liu et al., 2011 among others. Under flow-through conditions, self-diffusion coefficients in Eq. (6.22-6.24) should be replaced by hydrodynamic dispersion coefficients since the transport is also influenced by the fluid flow (Rolle et al., 2013b; Muniruzzaman et al., 2014; Muniruzzaman and Rolle, 2015). Therefore, using the above flux expression, the governing multicomponent transport equation for ionic solutes in 2-D saturated porous media reads as:

$$\frac{\partial C_i}{\partial t} = -v\frac{\partial C_i}{\partial x} + \frac{\partial}{\partial x}\left(\sum_{j=1}^{N} \mathbf{D}_L^{ij} \frac{\partial C_i}{\partial x}\right) + \frac{\partial}{\partial z}\left(\sum_{j=1}^{N} \mathbf{D}_T^{ij} \frac{\partial C_i}{\partial z}\right) \tag{6.25}$$

in which $\mathbf{D}_L^{ij}$ and $\mathbf{D}_T^{ij}$ are the matrices of longitudinal and transverse cross-coupled dispersion terms (Muniruzzaman et al., 2014), respectively. These inter-dispersion coefficients are defined as,

$$\begin{aligned} \mathbf{D}_L^{ij} &= \delta_{ij} D_L^i - \frac{z_i z_j D_L^i D_L^j C_i}{\sum_{k=1}^{N}\left(z_k^2 D_L^k C_k\right)} \\ \mathbf{D}_T^{ij} &= \delta_{ij} D_T^i - \frac{z_i z_j D_T^i D_T^j C_i}{\sum_{k=1}^{N}\left(z_k^2 D_T^k C_k\right)} \end{aligned} \tag{6.26}$$

with D_L^i and D_T^i being the longitudinal and transverse "self-dispersion coefficient" (i.e., when a particular ion, i is "liberated" from the other charged species in solution) and δ_{ij} being the Kronecker delta that is equal to 1 when $i=j$ and equal to 0 if $i\neq j$. The multicomponent ionic

transport model is solved using a finite volume scheme (FVM) on streamline-oriented grids with the approach of Cirpka et al. (1999a; 199b). We use a discretization of Δx = 5 mm and Δz = 1 mm to simulate the outcomes obtained in our multicomponent ionic transport experiments. The simulations are performed using a pulse type boundary at the inlet and zero dispersive flux at the remaining boundaries. In order to linearize the non-linearity induced from the coupled dispersive fluxes in the transport equations (Eq. 6.25-6.26), we use a Picard iterative scheme to solve the system of equations. The concentration matrix is solved with the direct matrix solver UMFPACK (Davis and Duff, 1997) and the all relevant calculations are performed in MATLAB®. Further information regarding model development and benchmarks can be found in Muniruzzaman et al. (2014) and Muniruzzaman and Rolle (2016; *under review*).

6.4 Results and Discussion

We performed experiments with two distinct sets of tracers: (i) multi-tracer experiments (with "non-interacting" tracers: fluorescein and chloride), and (ii) multicomponent ionic experiments (with electrostatically interacting $MgCl_2$ solutions in different ambient solutions).

6.4.1 Multi-tracer Experiments

6.4.1.1 Integrated Breakthrough Curves

The experiments were performed at three distinct average velocities of 0.5, 5 and 25 m/day with the pulse durations of 165, 15 and 3 minutes, respectively (Table 6.2). Chloride and fluorescein were used as tracers and measured at the outlet. Chloride has significantly higher (approximately fourfold) diffusivity compared to that of fluorescein (Table 6.1). Figure 6.2 summarizes the integrated breakthrough curves (Eq. 6.11) along with the flux-related dilution indices (Eq. 6.20) measured in the experiments at different seepage velocities at the outlet of the flow-through setup. The breakthrough of the tracers was observed with no retardation for chloride and with a slight retardation for fluorescein (linear retardation factor of ~1.04) due to weak sorptive interactions with the porous matrix. The breakthrough curves of the two tracers are reported as function of the pore volumes for direct comparison. Examining the temporal trend of the concentration profiles, integrated over the entire cross-section, approximately bell-shaped curves for different velocities can be observed (Fig. 6.2a-c). However, the breakthrough curves for the two different tracers, chloride (black circles) and fluorescein (black crosses), show remarkably different spreads and peak concentrations at all velocities. The curves for chloride (solute with higher diffusivity, D_{aq} = 1.81×10^{-9} m^2/s) exhibit higher peak

concentrations and have less spread profiles than the ones of fluorescein (solute with lower diffusivity, $D_{aq} = 0.45\times10^{-9}$ m^2/s).

The lines indicate the best fitted modeled curves to the measured concentrations for three different transport models: ADE (red solid lines), CTRW (blue dash-dotted lines), and DDMT (green dashed lines) (Fig. 6.2a-c). Table 6.3 lists the best fitted parameters obtained from the different models at different velocities. The fitted values of D_L, which is basically an indicator of the macroscopic spreading of the solute plumes in the longitudinal direction, also show consistent outcomes where longitudinal dispersion of fluorescein is approximately double compared to the ones of chloride in all experiments. Such separations in tracers' concentration profiles and spreading are quite remarkable especially the cases with very high velocities ($v \approx 5$ and 25 m/day), where the transport is strongly advection-dominated.

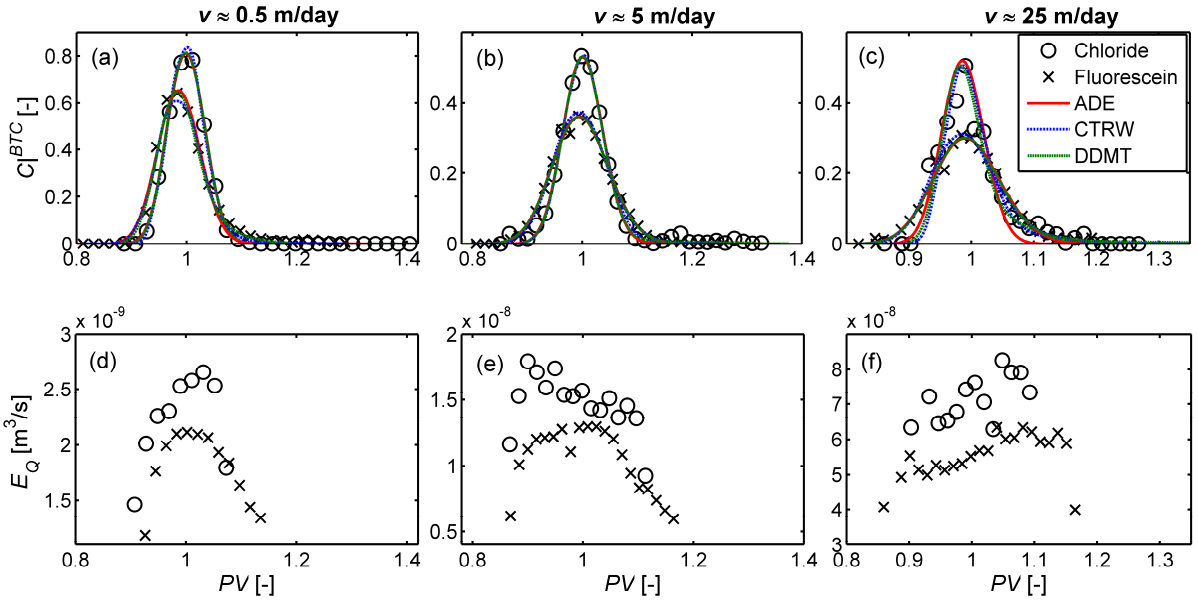

Figure 6.2. Breakthrough curves of the flux-weighted integrated-concentrations normalized by the flux-weighted inflow boundary conditions (a-c), and flux-related dilution indices (d-f) at the outlet cross-section for the seepage velocity of $v \approx 0.5$ m/day (a,d), 5 m/day (b,e) and 25 m/day (c,f).

Although, the compound-specific trends in these solute profiles are quite evident, such behavior may convey the counterintuitive impression that the compound with higher diffusion coefficient (chloride) results in the less spread profile with significantly higher peak concentration compared to the compound with lower diffusivity (fluorescein). In fact, based on the exclusive analysis of these integrated breakthrough curves one may come to the erroneous conclusion that the more spread and less peaked fluorescein profiles correspond to the more diluted plumes. A similar behavior was observed in the pore-scale modeling study of Rolle and

Kitanidis (2014), who explained that this behavior is due to the fact that, in advection-dominated regimes, the transport departs from being close to physical equilibrium and spreading ceases to be a good proxy for plume dilution and mixing. This was the case in all experimental setups, in fact, even the experiment with the lowest seepage velocity ($v \approx 0.5$ m/day), which lies in the upper limit of typical natural groundwater flow, is characterized by a grain Péclet number of ~4.96 for chloride and ~19.76 for fluorescein. A metric such as the flux-related dilution index is helpful to distinguish spreading and mixing from the outlet measurements. We computed the flux-related dilution index of the tracer plumes at the outlet at different time points by using the concentrations and volumetric fluxes measured at each individual outlet port (Eq. 6.20). The results show an opposite pattern compared to the concentration breakthrough curves and suggest that the chloride (tracer with higher D_{aq}) plume is remarkably more diluted compared to fluorescein plume at all velocities (Fig. 6.2d-f). Therefore, despite the more spread integrated breakthrough curves, the water fluxes carrying the fluorescein plumes are, in fact, ~40%, ~33%, and ~20% smaller compared to the ones transporting the chloride plume at the flow velocity of 0.5, 5, and 25 m/day, respectively. The fact that the chloride plumes are more diluted than those of fluorescein directly stems from the higher diffusivity of chloride. Consequently, even though the different tracer pulses were simultaneously injected in the macroscopically homogeneous domain, the tracer compounds evolve differently through the pore-channels because of the different diffusivity and the different extent of incomplete mixing in the pores at these high flow velocities. The macroscopic result of these small scale processes is that the solute with higher diffusivity is distributed over larger volumes and water fluxes. Notice that, although rather intuitive, these results cannot be explained by classical dispersion theory using the common linear parameterization, $D = D_P + \alpha v$ (Scheidegger, 1961). According to this parameterization, diffusion only acts through the velocity-independent pore diffusion term (D_P) and, thus, should only play a minor or negligible role in advection- and strongly advection-dominated regimes. Therefore, in contrast to what was observed in the experiments, the same distribution of different solutes at high flow velocity would be expected, due to the fact that in these conditions the mechanical dispersion term dominates. The latter term is described as the product of the seepage velocity and a dispersivity coefficient (α), typically assumed to be a property of the porous medium.

The trends of E_Q (x,t) profiles for different solutes at the outlet are also quite interesting (Fig. 6.2d-f). Instead of a monotonically increasing pattern as expected from the Gaussian plume (i.e., complete mixing or physical equilibrium in the pore-channels), the dilution profiles have a tendency to either level off or decrease after the mean arrival time. Rolle and Kitanidis

(2014) pointed out that this behavior is basically determined by two competing factors: the tendency of increasing dilution with travel time and/or travel distance, and the incomplete-mixing induced pore-scale mass transfer limitations occurring at these rather high flow velocities leading to an effect of "undiluteness" for the different solute plumes. The absolute values of flux-related dilution indices (E_Q) also increase with increasing average seepage velocity (Fig. 6.2d-f). The incomplete mixing and "undiluteness" effect is also visible in the breakthrough curves, especially at high flow velocities ($v \approx 5$ and 25 m/day), with the presence of a tailing at late times (Fig. 6.2b-d). Such effects are indicative of "non-Fickian" or "anomalous" transport behavior. As an example, this behavior is illustrated in Figure 6.3 by plotting the concentration profiles of the experiment at $v \approx 25$ m/day in log-scale in order to specifically focus on the long-term tailings. In the logarithmic plots it is evident that both tracer compounds show considerable extent of tailing where the ADE model (red solid lines) shows deviation from the data (Fig. 6.3a-b).

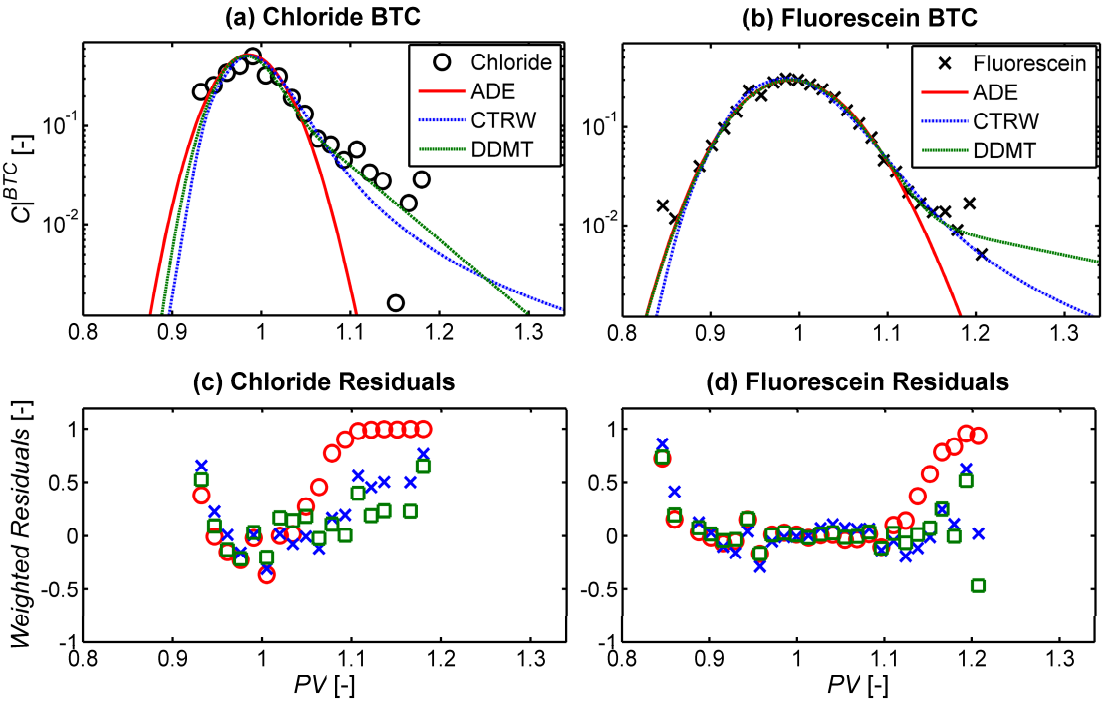

Figure 6.3. Breakthrough curves of the flux-weighted integrated-concentrations normalized by the flux-weighted inflow boundary conditions in logarithmic scale (a,b), and the model fitted weighted residuals (c,d) at the seepage velocity of $v \approx 25$ m/day.

On the other hand, the CTRW (blue dashed-dotted lines) and the DDMT (green dashed lines) model are able to effectively capture the plume tails. The residuals between the data points and the best fitted modeled values, weighted by the measured values, also confirm consistent outcomes where both CTRW (blue crosses) and DDMT (green squares) model show smaller magnitudes of the weighted residuals at late times (Fig. 6.3c-d). This feature evidently

indicates the better performance of these two models over the ADE model (red circles) in reproducing the late-time behaviors (PV>1.1) for both tracer plumes. The characteristics of anomalous nature of the transport are also appreciable from the fitted parameters obtained from the CTRW and DDMT models (Table 6.3). In CTRW, β is the parameter that determines the extent of anomalous transport with $0<\beta<2$ indicating the existence of non-Fickian behavior. For $\beta>2$, the transport reduces to classical Fickian form.

For $v \approx 0.5$ and 5 m/day, the best fitted β values for chloride are 2.364 and 2.006, respectively; whereas for fluorescein the obtained values of β are 1.781 and 1.957, respectively. These values suggest that, while the chloride transport stays in the Fickian regime, the transport of fluorescein becomes "weakly" anomalous even in this homogeneously packed quasi 2-D flow-through setup. These values and their interpretation appear to be reasonable also with respect to the fundamental physical processes in the pore channels and with the compound-specific behavior resulting in fluorescein (lower diffusivity) being relatively more influenced by the incomplete-mixing in the pores than chloride (higher diffusivity). Conversely, at the highest velocity tested ($v \approx 25$ m/day), a $\beta<2$ is obtained for both tracer compounds demonstrating that at such high advective velocity both tracers show anomalous behavior.

The parameters obtained by fitting the DDMT model can also be used to explain the observed behavior of the different tracer plumes. For the first two experiments ($v \approx 0.5$ and 5 m/day), the fitted mobile fraction (η_m) of total porosity (θ=0.41) for chloride is slightly higher compared to the values obtained for fluorescein. On the other hand, practically identical results were obtained for the experiments at the highest Péclet number ($v \approx 25$ m/day). As observed for the ADE and the CTRW models, also for the DDMT non-unique and compound-specific fitting parameters were obtained at the different flow velocities. In particular, the higher mass-transfer coefficients obtained for chloride depends the higher diffusivity of this species.

6.4.1.2 Port-resolved Breakthrough Curves

Figure 6.4 depicts the maps of the concentration measurements performed at different locations along the outlet of our 2-D experimental domain at different times. The measurements are shown as concentrations normalized by the corresponding inlet concentrations for each tracer. The top two rows of panels denote the measured data points plotted with vertical locations (z) and data collection time (PV) for different velocities (Fig. 6.4a-f). Each grid block in these plots indicates a measurement point across the time and space; whereas the respective concentration value is shown with the color. The lower two rows of panels represent the cubic

interpolation of the measured concentration values (Fig. 6.4g-l). The white dots delineate the contours of the interpolated normalized concentrations, whereas the solid lines represent the corresponding ADE predicted contours shown at levels 0.02 and 0.1. This representation helps visualizing the overall shape of the tracer plumes arriving at the outlet cross-section. In fact, assuming a macroscopically homogeneous domain and a constant advective velocity, the time axis can be translated into space with $x = vt$. So, these concentration distributions can be viewed as analogous to a snapshot of the spatial distribution of the tracer plume at the mean breakthrough time.

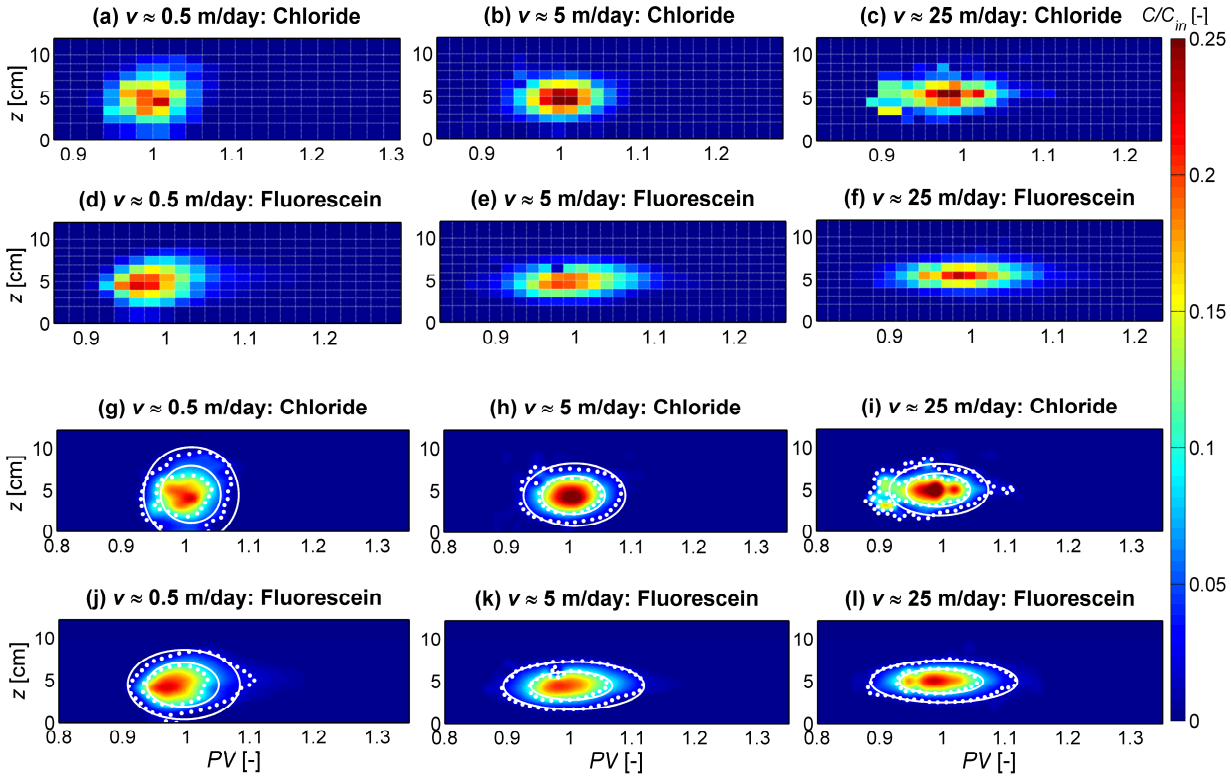

Figure 6.4. 2-D maps of concentration measurements performed at each individual outlet port as a function of time for different flow velocities: measured data points (a-f), and cubic interpolation of the measured values (g-l). The contour lines are shown for normalized concentration values of 0.02 and 0.1 with dots representing the interpolated measured values and the solid lines being the ADE predicted values.

As pointed out earlier from the analysis of the integrated temporal profiles, there are significant differences in the shape and spreading between the two tracer compounds. At lower Péclet number ($v \approx 0.5$ m/day), the shape of a particular compound's plume tend to be more "circular" (left column; Fig. 6.4); whereas with the increasing seepage velocity ($v \approx 5$ and 25 m/day), the plume becomes more stretched and elongated along the longitudinal/time axis (middle and

right columns in Fig. 6.4). This is expected since the at high flow velocity, the small characteristic advective time does not allow enough time for diffusion to act. This limits the macroscopic transverse migration of the tracer plume, and at the pore scale, it results in incomplete mixing in the pore channels in highly advection-dominated systems. It is interesting to note that fluorescein (Fig. 6.4d-f,j-l) has a much longer and stretched plume compared to chloride (Fig. 6.4a-c,g-i) in all cases including the one at $v \approx 25$ m/day. This implies that following the simultaneous injection (with same initial size and shape), the tracer compounds undergo significantly different extents of spreading and mixing. These differences are attributed to their diffusive mobilites because both tracers are simultaneously transported under identical hydraulic and transport conditions and through the same pore network. Such behavior is remarkable and confirms that the compound-specific effect does not vanish even at high pore-water velocities and can lead to significant differences in multispecies transport.

Figure 6.5 summarizes the breakthrough curves measured at different vertical locations (z) for the specific case of $v \approx 5$ m/day. The profiles measured at the central outlet ports of the vertical cross-section correspond to the core of the plumes and look similar to the integrated profiles of Fig. 6.2 (Fig. 6.5c-f). At the top and bottom locations (i.e., plume fringe area), the differences between the peak concentrations of the two tracer compounds tend to increase (Fig. 6.5a-b,g-i). Such discrepancies arise from the differences in diffusion coefficients; where the higher D_{aq} of chloride leads to further transverse displacement. Hence, considerably higher peak concentrations of chloride are observed in the upper and lower plume fringe compared to the ones of fluorescein (Fig. 6.5a,i). The measured data were fitted with different transport models (ADE, CTRW and DDMT) for all "locally" measured profiles. In each port, the fitting was performed as 1-D transport problem (Eq. 6.9) by considering the transport occurring along a "stream-tube" from the point of injection to the point of observation (i.e., as if we consider each stream-tube as an independent 1-D column).

It is important to mention that, the fitted longitudinal dispersion (D_L) values determined in different vertical locations show variability for both tracers (listed in Table 6.4). While the central ports show the values similar to the one obtained from the integrated profiles, D_L has a decreasing trend especially from the core to the fringe of the plume. Also notice that at the outer fringe the quality of the fits decreases due to the considerably lower and more scattered values of measured concentrations. Fluorescein plumes typically show a higher dispersion coefficient, indicating more extent of spreading along the stream-tube (Table 6.4).

Table 6.3: Summary of the fitted parameters for the breakthrough curves integrated over the outlet cross-section.

Model	Parameters	$v \approx 0.5$ m/day				$v \approx 5$ m/day				$v \approx 25$ m/day			
		Chloride		Flourescein		Chloride		Flourescein		Chloride		Flourescein	
		Best fit (p)	Std. dev. (σ_p)	Best fit (p)	Std. dev. (σ_p)	Best fit (p)	Std. dev. (σ_p)	Best fit (p)	Std. dev. (σ_p)	Best fit (p)	Std. dev. (σ_p)	Best fit (p)	Std. dev. (σ_p)
ADE	v [m/day]	0.62	3.80×10^{-4}	0.57	4.66×10^{-4}	4.83	2.77×10^{-3}	4.60	2.32×10^{-3}	21.78	2.62×10^{-2}	20.57	1.76×10^{-2}
	D_L [m^2/s]	2.64×10^{-9}	1.23×10^{-10}	4.04×10^{-9}	1.69×10^{-9}	3.21×10^{-8}	8.92×10^{-10}	6.86×10^{-8}	9.54×10^{-10}	1.30×10^{-7}	8.18×10^{-9}	3.44×10^{-7}	7.88×10^{-9}
	D_T [m^2/s]	2.16×10^{-9}	3.41×10^{-10}	9.19×10^{-10}	3.66×10^{-11}	6.67×10^{-9}	2.97×10^{-10}	3.45×10^{-9}	1.50×10^{-10}	1.74×10^{-8}	8.27×10^{-10}	1.10×10^{-8}	6.44×10^{-10}
CTRW	v_ψ [m/day]	0.45	6.78×10^{-9}	0.73	4.46×10^{-6}	4.78	3.52×10^{-5}	4.79	2.24×10^{-4}	38.88	5.16E-04	26.64	1.49×10^{-3}
	D_ψ [m^2/s]	2.76×10^{-10}	1.23×10^{-13}	2.57×10^{-9}	5.22×10^{-11}	1.60×10^{-8}	1.91×10^{-10}	4.37×10^{-8}	3.43×10^{-10}	1.83×10^{-8}	1.01×10^{-9}	1.69×10^{-7}	2.14×10^{-9}
	β [-]	2.364	4.40×10^{-10}	1.781	2.08×10^{-8}	2.006	2.15×10^{-9}	1.957	4.29×10^{-9}	1.549	5.18×10^{-7}	1.768	7.31×10^{-8}
	t_1 [min]	4.38×10^{-1}	7.34×10^{-9}	7.90×10^{-2}	2.96×10^{-9}	2.20×10^{-2}	3.70×10^{-10}	2.43×10^{-2}	6.20×10^{-10}	6.92×10^{-4}	4.8×10^{-9}	6.28×10^{-3}	5.88×10^{-9}
	t_2 [min]	9.16×10^{7}	0.13	7.53×10^{9}	243.12	1.81×10^{8}	1.94	1.41×10^{8}	25.15	1.41×10^{8}	292.98	1.41×10^{8}	14.467
DDMT	v_m [m/day]	0.62	0.0005	0.58	0.0005	4.84	0.0039	4.60	0.0730	21.95	0.02226	20.61	0.1755
	D_m [m^2/s]	2.23×10^{-9}	4.10×10^{-10}	2.74×10^{-9}	4.34×10^{-10}	3.03×10^{-8}	9.21×10^{-10}	6.77×10^{-8}	1.36×10^{-9}	8.08×10^{-8}	1.18×10^{-8}	3.21×10^{-7}	1.08×10^{-8}
	η_m [-]	0.4070	0.0020	0.4038	0.0011	0.4056	0.0002	0.4034	0.0063	0.4015	0.0006	0.4018	0.0031
	ξ [1/s]	2.46×10^{-6}	3.61×10^{-6}	1.16×10^{-6}	2.97×10^{-7}	1.25×10^{-6}	1.64×10^{-8}	4.77×10^{-7}	9.47×10^{-8}	4.37×10^{-5}	6.24×10^{-6}	8.20×10^{-6}	4.76×10^{-7}

Table 6.4: Summary of local breakthrough curves fitting at $v \approx 5$ m/day

z	ADE								CTRW				DDMT							
	Chloride				Fluorescein				Chloride		Fluorescein		Chloride				Fluorescein			
	v	σ_v	D_L	σ_{D_L}	v	σ_v	D_L	σ_{D_L}	β	σ_β	β	σ_β	η_m	σ_{η_m}	ξ	σ_ξ	η_m	σ_{η_m}	ξ	σ_ξ
[cm]	[m/day]		[m^2/s] $\times10^8$		[m/day]		[m^2/s] $\times10^8$		[-]		[-]		[-]		[1/s] $\times10^6$		[-]		[1/s] $\times10^6$	
1.25	4.84	0.003	2.97	0.10	4.69	0.002	0.32	0.06	2.008	7.0×10^{-9}	1.989	1.4×10^{-9}	0.4062	0.0003	3.83	0.49	0.4014	0.0477	0.44	3.83
2.75	4.85	0.002	2.81	0.08	4.64	0.001	4.22	0.08	2.008	2.3×10^{-9}	1.979	2.5×10^{-9}	0.4069	0.0032	0.50	0.10	0.4080	0.0017	1.50	1.03
3.75	4.85	0.003	2.63	0.10	4.65	0.002	5.58	0.09	2.011	2.0×10^{-9}	1.949	1.0×10^{-8}	0.4070	0.0020	0.74	0.10	0.3960	0.0070	71.18	49.69
4.75	4.83	0.001	2.98	0.06	4.61	0.003	7.16	0.11	2.005	5.7×10^{-9}	1.849	1.2×10^{-8}	0.4068	0.0011	0.50	0.04	0.3936	0.0022	44.38	8.71
5.75	4.82	0.002	3.28	0.07	4.58	0.003	7.26	0.14	2.005	8.5×10^{-10}	1.908	1.2×10^{-8}	0.4058	0.0022	0.51	0.04	0.3898	0.0043	66.19	19.83
6.75	4.81	0.003	2.72	0.09	4.53	0.002	6.95	0.06	2.004	7.9×10^{-9}	1.879	6.3×10^{-8}	0.4066	0.0015	1.28	0.18	0.4075	0.0012	5.00	3.72
7.75	4.84	0.003	5.94	0.13	4.56	0.005	5.31	0.22	2.015	2.5×10^{-7}	1.979	2.3×10^{-8}	0.4000	0.0040	27.79	16.60	0.4089	0.0030	1.00	4.47
8.75	5.02	0.005	1.97	0.12	4.58	0.006	1.51	0.44	2.015	4.9×10^{-8}	1.979	1.2×10^{-6}	0.4069	0.0029	3.00	3.99	0.4085	0.0075	1.00	16.10
9.75	5.18	0.003	0.90	0.05	-	-	-	-	2.004	3.3×10^{-8}	-	-	0.4068	0.0005	2.06	0.45	-	-	-	-

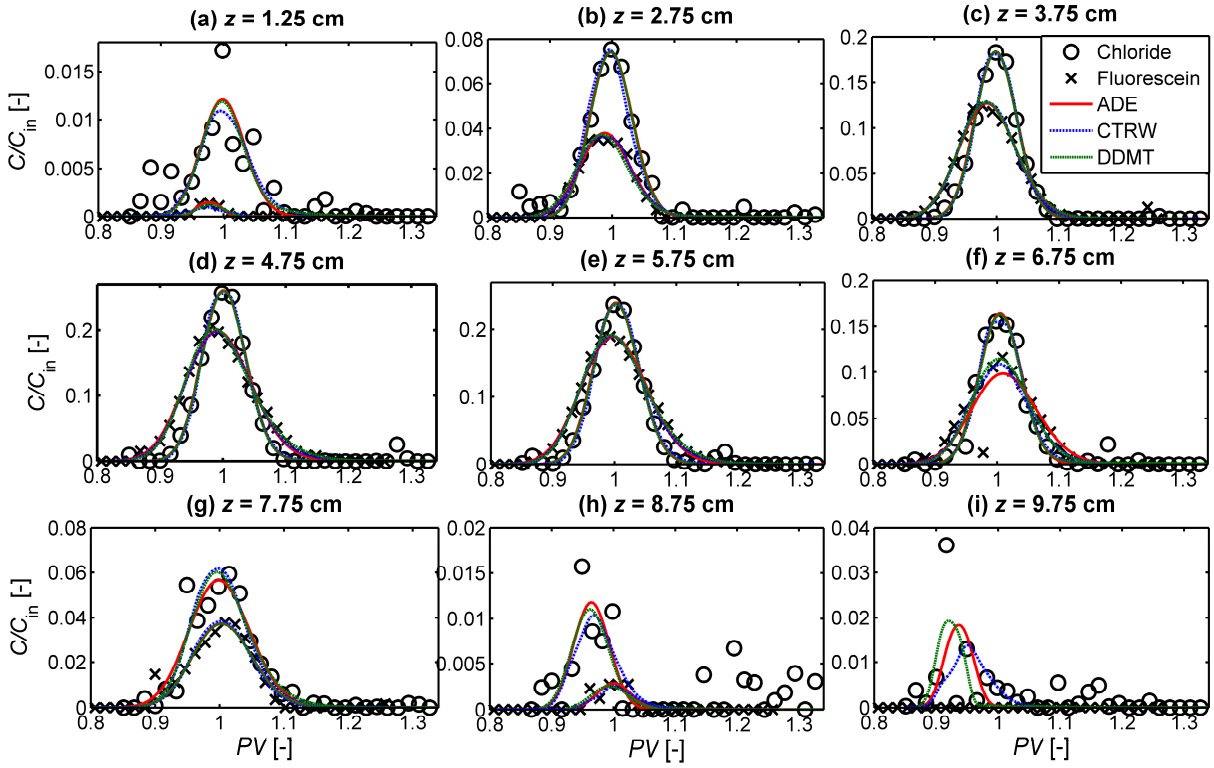

Figure 6.5. Breakthrough curves measured at each individual port for the seepage velocity of $v \approx 5$ m/day.

The calculated values of average seepage velocities (v) in each port are also consistent with the measured flow rates in the respective port. The degrees of anomalous behavior of these two compounds, interpreted based on the outcomes of the CTRW fits, are in the similar range as obtained from their integrated profiles. For chloride, $\beta = 2.004 - 2.015$ was found for different locations of the plume; whereas the fitted β for fluorescein stayed slightly below 2 (1.849 – 1.989) indicating the existence of "weak" non-Fickian behavior. The DDMT model fitting also suggest similar outcomes, as obtained from the CTRW model.

6.4.1.3 Transverse Spreading and Dispersion

We analyze the transverse displacement of the tracer plumes by integrating the concentration measurements along the time axis (Eq. 6.18). This temporal integration, basically, determines the fraction of total injected tracer mass (zeroth temporal moments) recovered at each outlet port. In particular, with this approach, we eliminate the longitudinal plume evolution/spreading by disregarding any concentration gradient along each advective travel path of our 2-D domain. Consequently, the transport of the 2-D tracer pulse reduces to a more simplified form,

which describes only the lateral concentration distribution in different longitudinal cross-sections. As explained in Section 6.3.2, these time-integrated vertical concentration profiles normalized by the temporal integral of the inflow boundary condition $\left(\hat{C}(x,z)\Big|_{BN}^{SP}\right)$ agree very well with the 2-D steady-state analytical solution of Eq. (6.19). We quantify the transverse dispersion coefficient (D_T) of different tracers by fitting Eq. (6.19) to the measurements by using the seepage velocities obtained from the integrated breakthrough profiles. For simplicity, we only fit the ADE model here to obtain the extent of transverse displacement.

Figure 6.6 represents the time-integrated spatial profiles for different cases at the end of our experimental domain. It is interesting to notice that the spreading and peak concentrations of the two tracers show a completely opposite behavior compared to the observations for the integrated breakthrough curves (Fig. 6.2). In fact, in the lateral direction, the compound-specific behavior is more intuitive and chloride (higher D_{aq}) has more spread profiles with lower peak concentrations compared to the ones of fluorescein (lower D_{aq}). Even in the case of strongly advection-dominated transport ($v \approx 25$ m/day, Fig. 6.6c), the compound-specific migration is significant and a considerable separation between the two tracer profiles exists. Therefore, as pointed out from the analysis of the flux-related dilution index profiles for the integrated breakthrough curves (Fig. 6.2d-f) and in the 2-D mapping of the plumes from the outlet measurements (Fig. 6.4), the more diluted chloride plume shows more significant lateral displacement at all flow velocities.

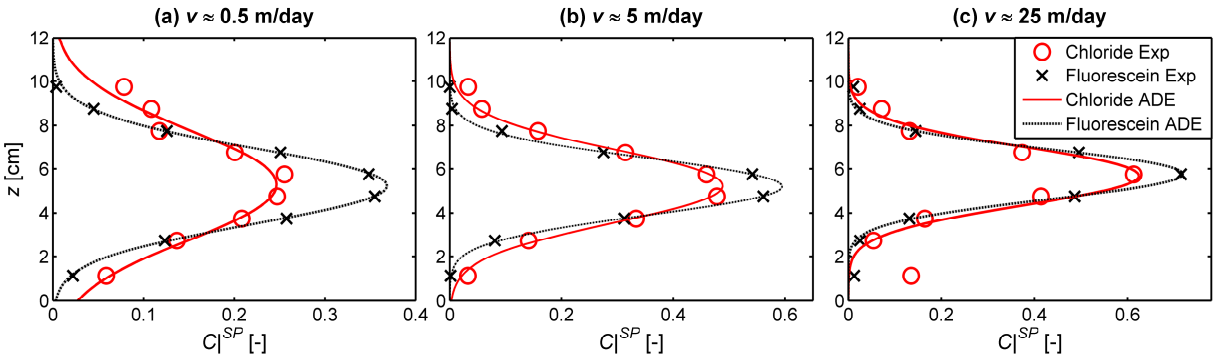

Figure 6.6. Time-integrated transverse profiles normalized by the temporal integral of inflow boundary condition for the seepage velocity of 0.5 (a), 5 (b), and 25 (c) m/day.

The fitted transverse dispersion coefficients (D_T) listed in Table 6.3 also show that the less mobile fluorescein has always a smaller value compared to chloride for all flow velocities. These D_T values are in very good agreement with the predictions from a non-linear compound-

specific transverse dispersion parameterization (Fig. 6.7). Such parameterization was inspired by an earlier statistical model of Bear and Bachmat (1967) and was developed based on steady-state flow-through experiments in the works of Chiogna et al. (2010) and Rolle et al. (2012). The parameterization reads as:

$$D_T = D_P + D_{aq}\left(\frac{Pe^2}{Pe + 2 + 4\delta^2}\right)^B \tag{6.27}$$

where D_P [m^2/s] is the pore diffusion coefficient; Pe [-] denotes the grain Péclet number, defined as $Pe = vd/D_{aq}$ (d [m] is the average grain size diameter); δ [-] is the ratio between the length of a pore channel to its hydraulic radius; and B [-] is an empirical exponent accounting for incomplete mixing in pore channels. It should be noted that, in order to avoid confusions with β in CTRW interpretations, we use a capital beta (B) in Eq. 6.27. By conducting a series of multi-tracer laboratory and pore-scale experiments across a wide range of flow velocity and in porous media with different grain sizes the values of δ and B were characterized (Rolle et al., 2012; Hochstelter et al., 2013; Ye et al., 2015a; 2015b). In our calculations we use $\delta = 6.2$ and B = 0.5, which are representative for the porous medium used in this study.

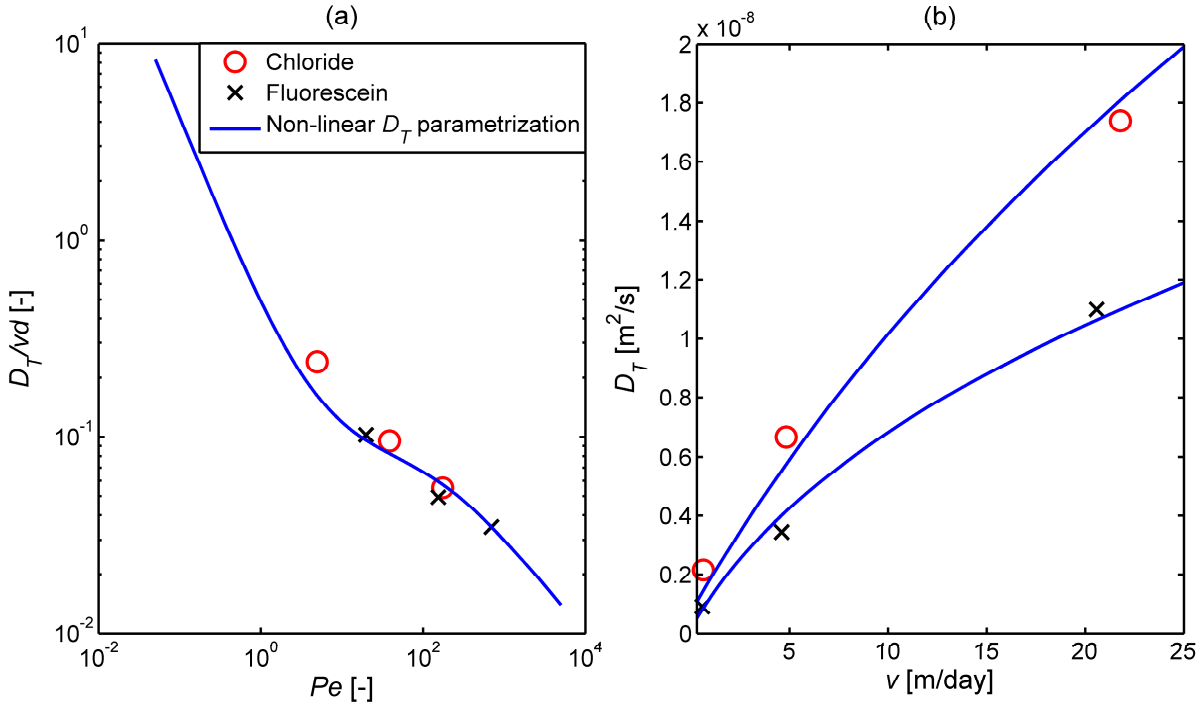

Figure 6.7. Comparison between the D_T values computed from the measurements performed in this study (markers) and the predictions from the non-linear compound-specific parameterization (lines).

Fig. 6.7a directly compares the experimentally determined D_T values (markers) with the computed ones according to Eq. (6.27) (continuous line) as a function of *Pe*; whereas Fig. 6.7b illustrates the pattern of D_T as a function of flow-velocity, v. It is remarkable to notice that the compound-specific effects on transverse dispersion are also relevant at high advective velocities, including at $v \approx 25$ m/day (Fig. 6.7b). In fact, the separation between the two tracer dispersion coefficients has an increasing trend with increasing seepage velocities. Eq. (6.27) captures this behavior by considering an explicit dependence of the mechanical dispersion term on the aqueous diffusion coefficients. Similarly to the compound-specific longitudinal spreading, also in this case the behavior observed in the experiments cannot be explained by the classical linear parameterization of transverse dispersion (e.g., Scheidegger, 1961). At the upper limit of our experimental seepage velocities ($v \approx 25$ m/day), the mechanical dispersion term is almost two orders of magnitudes higher relative to the pore diffusion term. Hence, applying a species-independent mechanical dispersion parameterization ($\alpha_T v$) would lead to practically identical hydrodynamic dispersion coefficients (D_T) for both tracer species under such flow conditions. Therefore, also the transient multitracer experiments performed in this study confirm the importance of considering the dependence of mechanical dispersion on both flow-velocity and species diffusivity for an accurate description of solute transport in flow-through systems.

6.4.2 Multicomponent Ionic Experiments

As summarized in Table 6.2, experiments were also performed to identify the impact of Coulombic interactions during transient multicomponent ionic transport. Focusing on different settings of ionic tracers, we consider two distinct experiments, in which the first one includes the injection of a pulse of a 1:2 electrolyte ($MgCl_2$; 0.8 mM) solution in pure water. The second experiment was performed by injecting the same electrolyte solution ($MgCl_2$; 0.8 mM) but, this time, a NaBr solution (1:1 electrolyte; 4.04 mM) was used as the ambient solution. The concentration measurements were performed at different outlet ports and at different times, as done in the multi-tracer cases illustrated in the previous sections. Both multicomponent ionic transport experiments were performed at a seepage velocity of ~5 m/day, which is still representative of strongly advection-dominated regimes.

Figure 6.8 summarizes the spatially-integrated breakthrough curves as well as the time-integrated transverse profiles for the two cases of multicomponent ionic transport. The general shapes of these profiles are similar to the ones obtained for the multi-tracer experiments (Fig. 6.2 and 6.6). Notice that, although the same electrolyte species was used as tracer in both

experiments, the measured concentration profiles of the cation and the anion are significantly different because of the different ambient solutions. For the transport in pure water, Mg^{2+} and Cl^- plumes tend to travel together as indicated by their practically identical temporal and spatial profiles despite the two have distinct diffusion coefficients (Table 6.1; Fig. 6.8a-b). Since pure water (Milli-Q) is free of any major ions, the transported cation (Mg^{2+}) and anion (Cl^-) are electrostatically forced to travel together in order to fulfill the charge balance of the system. In this case, the electromigration term (Eqs. 6.22 and 6.24) will provide a positive contribution and "speed up" the displacement of the slower cation(Mg^{2+}) and a negative contribution, slowing down the displacement of the faster anion (Cl^-). The hydrodynamic dispersion coefficients (D_L, D_T) obtained by fitting the measured profiles for these two cases with the 1-D ADE model also provide very similar values for the two ions (for Mg^{2+}: D_L=4.33×10^{-8}; D_T=5.55×10^{-9} and for Cl^-: D_L=4.13×10^{-8}; D_T=5.55×10^{-9} m^2/s).

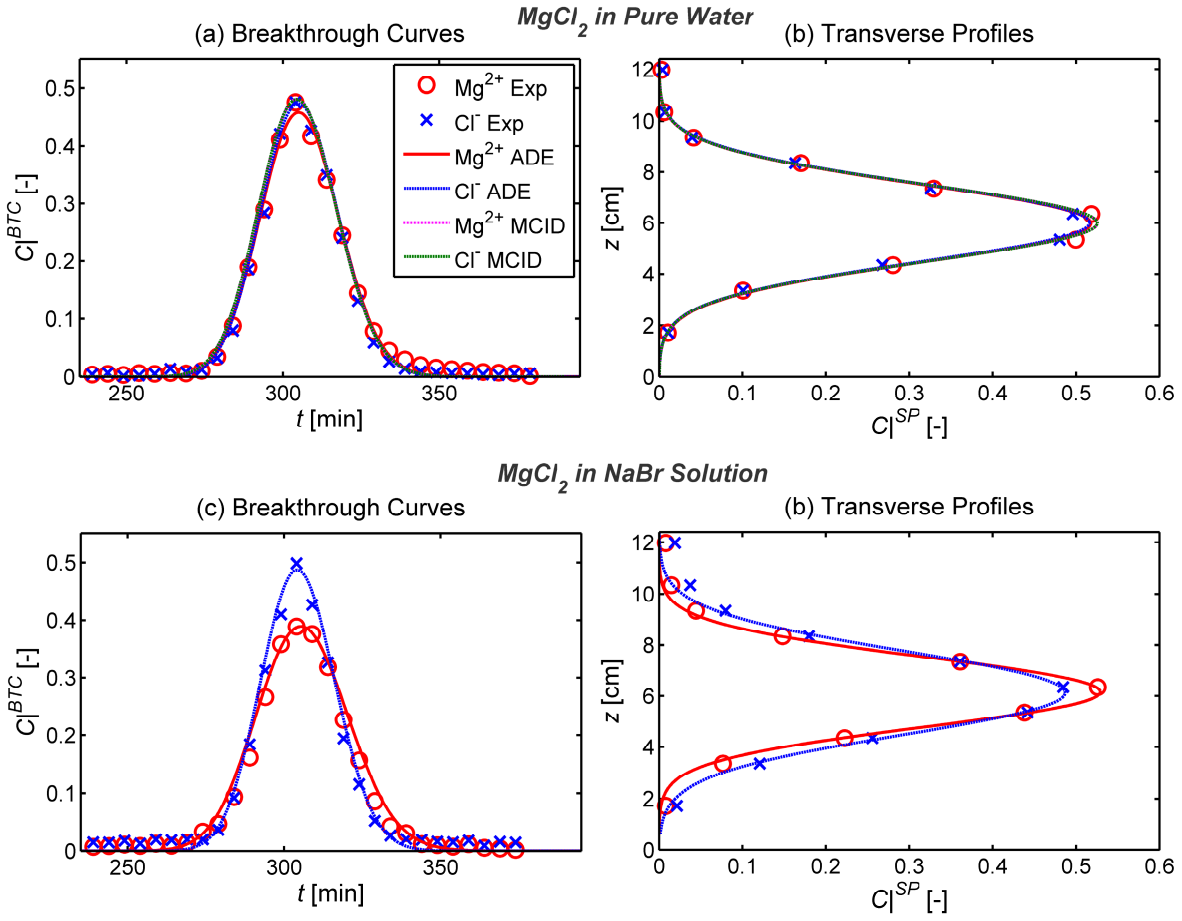

Figure 6.8. Integrated breakthrough curves (a,c) and vertical concentration profiles (b,d) during the transport of $MgCl_2$ in pure water (a-b) and in NaBr background solution (c-d). The markers indicate the measured quantities whereas the lines represent the fitted profiles with 1-D ADE model (solid lines) and the simulated profiles with the 2-D multicomponent ionic transport model (dotted lines).

In contrast, when $MgCl_2$ is injected in a NaBr ambient solution (with ~fourfold of the injected tracer concentration), the system is already charge-balanced by these background ions (Na^+ and Br^-). Hence, the plume ions (Mg^{2+} and Cl^-) can migrate with mobilities close to their "self-diffusive/dispersive" properties without experiencing any noticeable electrostatic interaction. This results in separated profiles of the measured concentrations of these ions at the outlet of the flow-through setup (Fig. 6.8c-d). Fitting these profiles also resulted in distinct values of longitudinal and transverse hydrodynamic dispersion coefficients D_L (for Mg^{2+}: D_L=6.05×10^{-8}; D_T=4.20×10^{-9} and for Cl^-: D_L=3.78×10^{-8}; D_T=6.48×10^{-9} m^2/s).

Notice that in the second multicomponent ionic experiment, in which both longitudinal and transverse profiles became distinct, the same patterns discussed in the previous sections were observed: more peaked and less spread breakthrough curves for the more mobile species (in this cases Cl^-), which, instead, show a more spread and less peaked profile in the lateral direction compared to the less mobile ion (Mg^{2+}).

Although, accurately capturing transport processes of these ionic species requires either a detailed pore-scale model or a continuum model, with correct dispersion parameterizations (both longitudinal and transverse) accounting for all the relevant processes (e.g., species diffusion, flow-velocity, and the extent of incomplete mixing in the pores), here we attempt to predict the multicomponent transport of $MgCl_2$ in pure water by using the overall dispersion parameters obtained from the case of transport in buffer electrolyte (NaBr). This treatment is based on the assumption that in the presence of NaBr ambient solution, Mg^{2+} and Cl^- travel exactly according to their self-diffusivities (i.e., as if charge-neutral species). Therefore, the values of D_L and D_T of these ions obtained from this case can be regarded as their "self-dispersion" coefficients. We inserted these fitted "bulk dispersion" values to the multicomponent ionic dispersion model (Eq. 6.25; Section 6.3.4) to predict the coupled transport of $MgCl_2$ in pure water. The magenta and cyan dotted lines in Fig. 6.8a-b refer to the predicted concentration profiles, which show a very good agreement with the measurements and the fitted profiles.

The multicomponent ionic transport model enables us to effectively visualize the electrostatic interactions by mapping the spatial distributions of different flux components (Eq. 6.22: $J_{tot} = J_{dis} + J_{mig}$). In Figure 6.9, we illustrate the behavior for the case of transport of $MgCl_2$ in pure water. The top two rows of panels represent the longitudinal flux components (Fig. 6.9a-f), whereas the remaining bottom panels refer to the transverse flux components (Fig. 6.9g-l) after t = 50, 150, and 250 minutes of simulation.

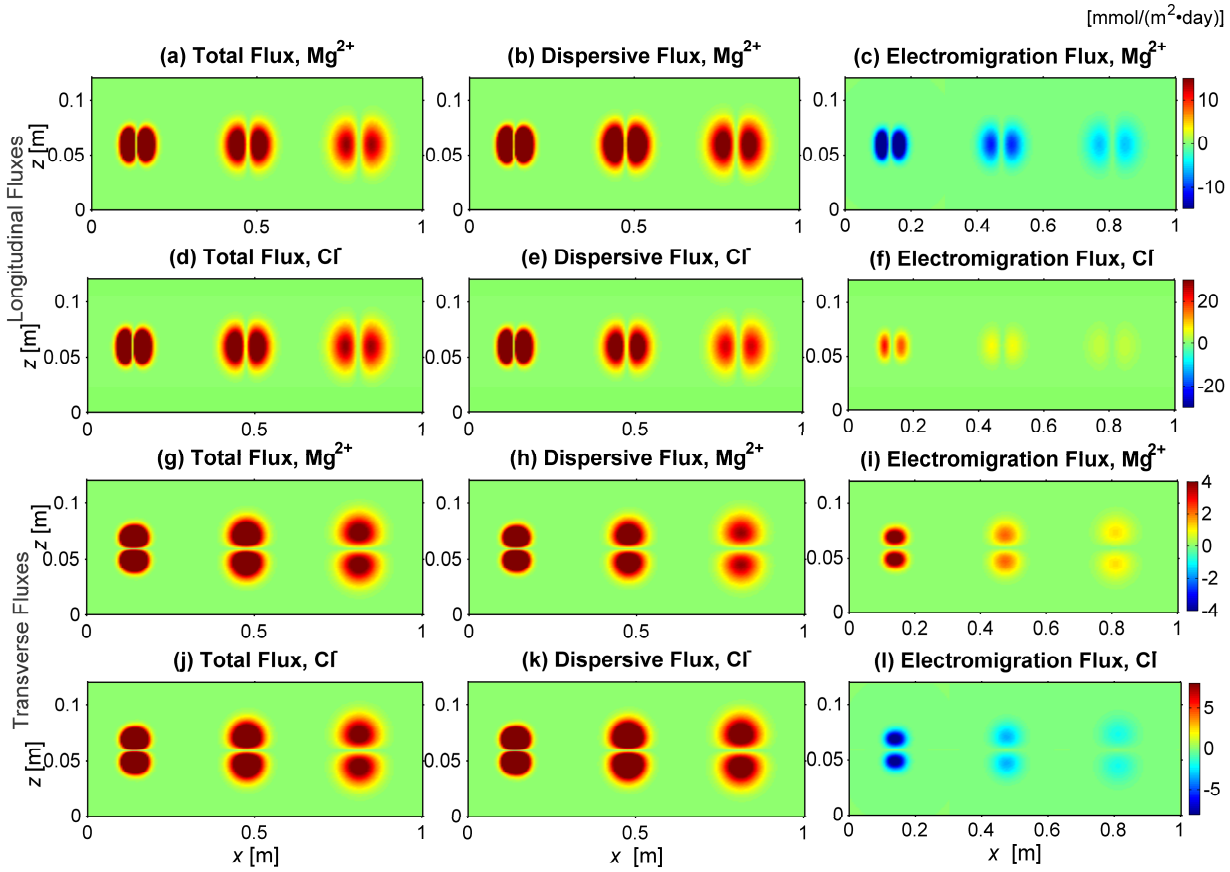

Figure 6.9. Maps of multicomponent ionic flux components in the longitudinal (a-f) and transverse (g-i) direction for the transport of $MgCl_2$ in pure water after t = 50, 150, and 250 minutes. The direction from the core to the fringe of the plume is considered positive in the flux calculations.

It is interesting to notice that, although both Mg^{2+} and Cl^- have identical overall distributions of total fluxes (J_{tot}) (left column panel), the different components of J_{tot} are distinct because of the variation in the "self-dispersion" coefficients of the different species. For transverse fluxes, J_{dis} values are higher for Cl^- compared to Mg^{2+} as Cl^- has higher D_T (Fig. 6.9h,k). The situation is opposite in the longitudinal J_{dis} distributions where Mg^{2+} apparently has a macroscopically higher D_L (Fig. 6.9b,e). The electrochemical migration flux components, J_{mig} have the most interesting distributions with the cation (Mg^{2+}) and anion (Cl^-) species showing similar pattern but opposite signs (right column panel). Such negative correlation facilitates an enhancement in the total flux for the slower species, and a reduction for the faster species, respectively. Thus, the electrostatic potential gradient couples the positively and negatively charged species leading to practically identical concentration profiles.

6.5 Summary and Conclusions

In this work, we experimentally show the critical role of small-scale physical and electrochemical processes on transient solute transport in porous media under advection dominated flow-regimes ($v \approx 0.5$–25 m/day). The experiments were performed in a quasi 2-D flow-through setup with measurements conducted at high spatial and temporal resolution (i.e., ~300 samples/experiment). The simultaneous injection of multiple tracer species enables quantifying the impact of compound-specific mixing and electrochemical migration during transport in porous media. The analysis of the obtained concentration profiles (breakthrough curves and spatial profiles) confirms that the small-scale compound-specific effects (e.g., aqueous diffusion, charge induced electromigration) do not vanish under strongly advection-dominated regimes, but propagates through the scales and lead to significantly distinct behaviors of spreading and plume dilution at the macroscopic Darcy scale. We provide first experimental evidence of compound-specific diffusion/dispersion effects, as well as Coulombic interactions during multispecies transient transport in porous media, under advection-dominated conditions.

Four different transport models have been used to quantitatively interpret the measured breakthrough curves. In addition to the conventional ADE model, we use CTRW (with TPL form) and DDMT models to analyze the non-Fickian behavior. Both the experimental and simulation outcomes show that non-Fickian or "anomalous" transport, highlighting the impact of unresolved pore-scale heterogeneity, is observed in most cases even though the experimental domain was macroscopically "homogeneous". However, the extent of "anomalous" behavior was dependent on both seepage velocity, as well as on compound-specific diffusion coefficients. For the multicomponent ionic transport, we reproduce the obtained concentration profiles and explain the specific charge-induced ionic interactions with a mechanistic forward model based on the multicomponent formulations of diffusive/dispersive fluxes. Our experiments show that the sole analysis of integrated breakthrough curves may not provide an adequate portrayal of actual transport processes and can even lead to erroneous conclusions regarding mixing and plume dilution, especially under high flow velocities. Such outcomes suggest that, at high flow velocities, the spreading of breakthrough curves cannot be used as a good proxy to assess the dilution state of solute plumes. We also show that experimentally-determined entropy-based metrics, such as the flux-related dilution index, are useful to help distinguishing plume spreading from mixing.

This experimental study was carried out to investigate the impact of diffusion and electrochemical interactions on macroscopic solute transport. Perhaps due to the perception of

the small scale at which these processes occur and/or the small numerical values of the related coefficients, the study of these phenomena has received only limited attention. Our results show that small-scale processes have an important influence on macroscopic transport problems in porous media. These findings are relevant for advancing the understanding of solute transport in groundwater, which is often, inherently, a multispecies (i.e., compound-specific) and/or a multicomponent ionic transport problem. In our view, the outcomes of these experiments provide also a valuable dataset for the development of modeling approaches. In fact, despite satisfactory results could be obtained by fitting different models to distinct experiment data, comprehensive frameworks able to consistently represent the macroscopic effects of small scale interactions through the different conditions of flow velocity, compound-specific properties and electrostatic interaction need to be developed.

Our investigation was carried out considering conservative transport under simplified physical and chemical conditions. The extrapolation of these outcomes to more complex physical and chemically heterogeneous natural or engineered systems remains an open challenge. Furthermore, these experiments were performed in 2-D setups and it is not clear, yet, how such effects will impact transient transport in fully 3-D domains, in which the role of diffusion and compound-specific mixing is quantitatively more significant (Ye al. 2015a) but also more complex flow topologies, resulting from physical heterogeneity and/or anisotropy (Ye et al. 2015b; Chiogna et al., 2014; Cirpka et al., 2015), may affect the behavior and magnitude of diffusive/dispersive mixing as well as electrochemical migration. The expected increase in the availability of high-resolution investigations at different scales from microfluidic experiments, to laboratory (as the present study) and field-scale investigations, will provide unprecedented capabilities to understand and quantify small scale subsurface processes. Furthermore, enhanced possibilities to resolve the small scale will lead to significant improvement in the description and properly upscaling the effects of diffusion and electromigration processes in multispecies, macroscopic transport in porous media.

Acknowledgments

The authors thank Jens Schaarup Sørensen for the assistance in establishing experimental setup and ion-chromatography measurements. We also thank Sinh Hy Nguyen and Mikael Emil Olsson for performing the ICP-MS measurements.

M.R. and M.M. acknowledge the Baden-Württemberg Stiftung for the financial support of this research project by the Eliteprogram for Postdocs.

References

Appelo, C. A. J., and P. Wersin (2007), Multicomponent diffusion modeling in clay systems with application to the diffusion of tritium, iodide, and sodium in opalinus clay, Environmental Science & Technology, 41(14), 5002-5007.

Appelo, C. A. J., A. Vinsot, S. Mettler, and S. Wechner (2008), Obtaining the porewater composition of a clay rock by modeling the in- and out-diffusion of anions and cations from an in-situ experiment, Journal of Contaminant Hydrology, 101(1-4), 67-76.

Bard, A. J., and L. R. Faulkner (2001), Electrochemical methods fundamentals and applications, 2. ed. ed., XXI, 833 S. pp., Wiley, New York Weinheim.

Bear, J. (1972), Dynamics of fluids in porous media, xvii, p-764, American Elsevier Pub. Co., New York.

Bear J., and Bachmat Y. (1967) A generalized theory on hydrodynamic dispersion in porous media. In IASH Symposium on Artificial Recharge and Management of Aquifers, Haifa, Israel,vol. 72, pp. 7–16.

Ben-Yaakov, S. (1972), Diffusion of sea water ions—I. Diffusion of sea water into a dilute solution, Geochimica et Cosmochimica Acta, 36(12), 1395-1406.

Berkowitz, B., and H. Scher (1997), Anomalous Transport in Random Fracture Networks, Phys Rev Lett, 79(20), 4038-4041.

Berkowitz, B., and H. Scher (2009), Exploring the nature of non-Fickian transport in laboratory experiments, Advances in Water Resources, 32(5), 750-755.

Berkowitz, B., and H. Scher (2010), Anomalous transport in correlated velocity fields, Physical review. E, Statistical, nonlinear, and soft matter physics, 81(1 Pt 1), 011128.

Berkowitz, B., H. Scher, and S. E. Silliman (2000), Anomalous transport in laboratory-scale, heterogeneous porous media, Water Resources Research, 36(1), 149-158.

Berkowitz, B., A. Cortis, M. Dentz, and H. Scher (2006), Modeling non-Fickian transport in geological formations as a continuous time random walk, Reviews of Geophysics, 44(2).

Berkowitz, B., A. Cortis, I. Dror, and H. Scher (2009), Laboratory experiments on dispersive transport across interfaces: The role of flow direction, Water Resources Research, 45(2).

Bijeljic, B., and M. J. Blunt (2006), Pore-scale modeling and continuous time random walk analysis of dispersion in porous media, Water Resources Research, 42(1).

Boudreau, B. P. (1997), Diagenetic models and their implementation: modelling transport and reactions in aquatic sediments; with 19 tables, XVI, 414 pp., Springer Berlin, Heidelberg.

Boudreau, B. P., F. J. R. Meysman, and J. J. Middelburg (2004), Multicomponent ionic diffusion in porewaters: Coulombic effects revisited, Earth and Planetary Science Letters, 222(2), 653-666.

Carrera, J., X. Sanchez-Vila, I. Benet, A. Medina, G. Galarza, and J. Guimera (1998), On matrix diffusion: formulations, solution methods and qualitative effects, Hydrogeol J, 6(1), 178-190.

Carslaw, H. S., and J. C. Jaeger (1959), Conduction of heat in solids, 2d ed., 510 p. pp., Clarendon Press, Oxford,.

Chiogna, G., and A. Bellin (2013), Analytical solution for reactive solute transport considering incomplete mixing within a reference elementary volume, Water Resour. Res., 49, 2589–2600, doi:10.1002/wrcr.20200.

Chiogna, G., O. A. Cirpka, P. Grathwohl, and M. Rolle (2011), Relevance of local compound-specific transverse dispersion for conservative and reactive mixing in heterogeneous porous media, Water Resour. Res., 47(7), W07540.

Chiogna, G., M. Rolle, A. Bellin, and O. A. Cirpka (2014), Helicity and flow topology in three-dimensional anisotropic porous media, Advances in Water Resources, 73, 134-143.

Chiogna, G., C. Eberhardt, P. Grathwohl, O. A. Cirpka, and M. Rolle (2010), Evidence of Compound-Dependent Hydrodynamic and Mechanical Transverse Dispersion by Multitracer Laboratory Experiments, Environmental Science & Technology, 44(2), 688-693.

Cirpka, O. A., and P. K. Kitanidis (2000), An advective-dispersive stream tube approach for the transfer of conservative-tracer data to reactive transport, Water Resources Research, 36(5), 1209-1220.

Cirpka, O. A., F. P. J. de Barros, G. Chiogna, M. Rolle, and W. Nowak (2011), Stochastic flux-related analysis of transverse mixing in two-dimensional heterogeneous porous media, Water Resour. Res., 47, W06515, doi:10.1029/2010WR010279.

Cirpka, O. A., E. O. Frind, and R. Helmig (1999a), Numerical methods for reactive transport on rectangular and streamline-oriented grids, Advances in Water Resources, 22(7), 711-728.

Cirpka, O. A., E. O. Frind, and R. Helmig (1999b), Streamline-oriented grid generation for transport modelling in two-dimensional domains including wells, Advances in Water Resources, 22(7), 697-710.

Cirpka, O. A., G. Chiogna, M. Rolle, and A. Bellin (2015), Transverse mixing in three-dimensional nonstationary anisotropic heterogeneous porous media, Water Resources Research, 51(1), 241-260.

Cortis, A., and B. Berkowitz (2005), Computing “Anomalous” Contaminant Transport in Porous Media: The CTRW MATLAB Toolbox, Ground Water, 43(6), 947-950.

Cortis, A., Y. Chen, H. Scher, and B. Berkowitz (2004), Quantitative characterization of pore-scale disorder effects on transport in ``homogeneous'' granular media, Physical Review E, 70(4), 041108.

Crank, J. (1975), The mathematics of diffusion, 2d ed., viii, 414 p. pp., Clarendon Press, Oxford, Eng.

Cussler, E. L. (2009), Diffusion : mass transfer in fluid systems, 3rd ed., xvii, 631 p. pp., Cambridge University Press, Cambridge ; New York.

Davis, T., and I. Duff (1997), An Unsymmetric-Pattern Multifrontal Method for Sparse LU Factorization, SIAM Journal on Matrix Analysis and Applications, 18(1), 140-158.

Delgado, J. M. P. Q. (2006), A critical review of dispersion in packed beds, Heat and Mass Transfer, 42(4), 279-310.

Deng, J., X. Jiang, X. Zhang, W. Hu, and J. W. Crawford (2008), Continuous time random walk model better describes the tailing of atrazine transport in soil, Chemosphere, 71(11), 2150-2157.

Dentz, M., T. Le Borgne, A. Englert, and B. Bijeljic (2011), Mixing, spreading and reaction in heterogeneous media: A brief review, Journal of Contaminant Hydrology, 120–121(0), 1-17.

Domenico, P. A., and V. V. Palciauskas (1982), Alternative Boundaries in Solid Waste Management, Ground Water, 20(3), 303-311.

Edery, Y., H. Sher, and B. Berkowitz (2009), Modeling bimolecular reactions and transport in porous media, Geophys. Res. Lett., 36, L02407, doi:10.1029/2008GL036381.

Felmy, A. R., and J. H. Weare (1991), Calculation of Multicomponent Ionic-Diffusion from Zero to High-Concentration .1. The System Na-K-Ca-Mg-Cl-So4-H2o at 25-Degrees-C, Geochimica Et Cosmochimica Acta, 55(1), 113-131.

Fiori, A., I. Jankovic, and G. Dagan (2011), The impact of local diffusion upon mass arrival of a passive solute in transport through three-dimensional highly heterogeneous aquifers, Advances in Water Resources, 34(12), 1563-1573.

Gerke, H. H., and M. T. van Genuchten (1993), A dual-porosity model for simulating the preferential movement of water and solutes in structured porous media, Water Resources Research, 29(2), 305-319.

Giambalvo, E. R., C. I. Steefel, A. T. Fisher, N. D. Rosenberg, and C. G. Wheat (2002), Effect of fluid-sediment reaction on hydrothermal fluxes of major elements, eastern flank of the Juan de Fuca Ridge, Geochimica Et Cosmochimica Acta, 66(10), 1739-1757.

Gorelick, S. M., G. Liu, and C. Zheng (2005), Quantifying mass transfer in permeable media containing conductive dendritic networks, Geophysical Research Letters, 32(18), n/a-n/a.

Gramling, C. M., C. F. Harvey, and L. C. Meigs (2002), Reactive transport in porous media: A comparison of model prediction with laboratory visualization, Environ. Sci. Technol., 36(11), 2508–2514.

Haberer, C. M., M. Rolle, S. Liu, O. A. Cirpka, and P. Grathwohl (2011), A high-resolution non-invasive approach to quantify oxygen transport across the capillary fringe and within the underlying groundwater, Journal of Contaminant Hydrology, 122(1–4), 26-39.

Hadley, P. W., and C. Newell (2014), The New Potential for Understanding Groundwater Contaminant Transport, Groundwater, 52(2), 174-186.

Haggerty, R., and S. M. Gorelick (1995), Multiple-Rate Mass-Transfer for Modeling Diffusion and Surface-Reactions in Media with Pore-Scale Heterogeneity, Water Resources Research, 31(10), 2383-2400.

Hatano, Y., and N. Hatano (1998), Dispersive transport of ions in column experiments: An explanation of long-tailed profiles, Water Resources Research, 34(5), 1027-1033.

Heidari, P., and L. Li (2014), Solute transport in low-heterogeneity sandboxes: The role of correlation length and permeability variance, Water Resources Research, 50(10), 8240-8264.

Hochstetler, D. L., M. Rolle, G. Chiogna, C. M. Haberer, P. Grathwohl, and P. K. Kitanidis (2013), Effects of compound-specific transverse mixing on steady-state reactive plumes: Insights from pore-scale simulations and Darcy-scale experiments, Advances in Water Resources, 54, 1-10.

Kitanidis, P. K. (1994), The concept of the Dilution Index, Water Resources Research, 30(7), 2011-2026.

Kosakowski, G. (2004), Anomalous transport of colloids and solutes in a shear zone, Journal of Contaminant Hydrology, 72(1–4), 23-46.

LaBolle, E. M., and G. E. Fogg (2001), Role of molecular diffusion in contaminant migration and recovery in an alluvial aquifer system, Transport in Porous Media, 42(1-2), 155-179.

Lasaga, A. C. (1979), The treatment of multi-component diffusion and ion pairs in diagenetic fluxes, American Journal of Science, 279(3), 324-346.

Lasaga, A. C. (1998), Kinetic theory in the earth sciences, x, 811 p. pp., Princeton University Press, Princeton, N.J.

Leij, F. J., T. H. Skaggs, and M. T. Van Genuchten (1991), Analytical Solutions for Solute Transport in Three-Dimensional Semi-infinite Porous Media, Water Resources Research, 27(10), 2719-2733.

Levy, M., and B. Berkowitz (2003), Measurement and analysis of non-Fickian dispersion in heterogeneous porous media, Journal of Contaminant Hydrology, 64(3–4), 203-226.

Liu, C. X. (2007), An ion diffusion model in semi-permeable clay materials, Environmental Science & Technology, 41(15), 5403-5409.

Liu, Y., and P. K. Kitanidis (2012), Applicability of the Dual-Domain Model to Nonaggregated Porous Media, Groundwater, 50(6), 927-934.

Luo, J., M. Dentz, O. A. Cirpka, and P. K. Kitanidis (2007), Breakthrough curve tailing in a dipole flow field, Water Resources Research, 43(9), n/a-n/a.

Luo, J., O. A. Cirpka, W. Wu, M. N. Fienen, P. M. Jardine, T. L. Mehlhorn, D. B. Watson, C. S. Criddle, and P. K. Kitanidis (2005), Mass-Transfer Limitations for Nitrate Removal in a Uranium-Contaminated Aquifer, Environmental Science & Technology, 39(21), 8453-8459.

Molins, S., D. Trebotich, C. I. Steefel, and C. P. Shen (2012), An investigation of the effect of pore scale flow on average geochemical reaction rates using direct numerical simulation, Water Resources Research, 48.

Muniruzzaman, M., and M. Rolle (2015), Impact of multicomponent ionic transport on pH fronts propagation in saturated porous media, Water Resources Research, 51(8), 6739-6755.

Muniruzzaman, M., C. M. Haberer, P. Grathwohl, and M. Rolle (2014), Multicomponent ionic dispersion during transport of electrolytes in heterogeneous porous media: Experiments and model-based interpretation, Geochimica et Cosmochimica Acta, 141(0), 656-669.

Porta, G. M., B. Bijeljic, M. J. Blunt, and A. Guadagnini (2015), Continuum-scale characterization of solute transport based on pore-scale velocity distributions, Geophys. Res. Lett., 42, 7537–7545, doi:10.1002/2015GL065423.

Raje, D. S., and V. Kapoor (2000), Experimental study of bimolecular reaction kinetics in porous media, Environ. Sci. Technol., 34, 1234–1239, doi:10.1021/es9908669

Rolle, M., and P. K. Kitanidis (2014), Effects of compound-specific dilution on transient transport and solute breakthrough: A pore-scale analysis, Advances in Water Resources, 71, 186-199.

Rolle, M., G. Chiogna, D. L. Hochstetler, and P. K. Kitanidis (2013a), On the importance of diffusion and compound-specific mixing for groundwater transport: An investigation from pore to field scale, Journal of Contaminant Hydrology, 153(0), 51-68.

Rolle, M., M. Muniruzzaman, C. M. Haberer, and P. Grathwohl (2013b), Coulombic effects in advection-dominated transport of electrolytes in porous media: Multicomponent ionic dispersion, Geochimica et Cosmochimica Acta, 120(0), 195-205.

Rolle, M., C. Eberhardt, G. Chiogna, O. A. Cirpka, and P. Grathwohl (2009), Enhancement of dilution and transverse reactive mixing in porous media: Experiments and model-based interpretation, Journal of Contaminant Hydrology, 110(3–4), 130-142.

Rolle, M., D. L. Hochstetler, G. Chiogna, P. K. Kitanidis, and P. Grathwohl (2012), Experimental Investigation and Pore-Scale Modeling Interpretation of Compound-Specific Transverse Dispersion in Porous Media, Transport in Porous Media, 93(3), 347-362.

Ronayne, M. J., S. M. Gorelick, and C. Zheng (2010), Geological modeling of submeter scale heterogeneity and its influence on tracer transport in a fluvial aquifer, Water Resources Research, 46(10), n/a-n/a.

Sanchez-Vila, X., D. Fernàndez-Garcia, and A. Guadagnini (2010), Interpretation of column experiments of transport of solutes undergoing an irreversible bimolecular reaction using a continuum approximation, Water Resour. Res., 46, W12510, doi:10.1029/2010WR009539

Scheidegger, A. E. (1961), General theory of dispersion in porous media, Journal of Geophysical Research, 66(10), 3273-3278.

Scheven, U. M., S. Khirevich, A. Daneyko, and U. Tallarek (2014), Longitudinal and transverse dispersion in flow through random packings of spheres: A quantitative comparison of experiments, simulations, and models, Physical Review E, 89(5), 053023.

Steefel, C. I., and K. Maher (2009), Fluid-Rock Interaction: A Reactive Transport Approach, Rev Mineral Geochem, 70, 485-532.

Tartakovsky, A. M., G. D. Tartakovsky, and T. D. Scheibe (2009), Effects of incomplete mixing on multicomponent reactive transport, Adv. Water Resour., 32(11), 1674–1679, doi:10.1016/j.advwatres.2009.08.012.

Thullner, M., P. Van Cappellen, and P. Regnier (2005), Modeling the impact of microbial activity on redox dynamics in porous media, Geochimica Et Cosmochimica Acta, 69(21), 5005-5019.

Valocchi, A. J. (1985), Validity of the Local Equilibrium Assumption for Modeling Sorbing Solute Transport Through Homogeneous Soils, Water Resources Research, 21(6), 808-820.

Van Cappellen, P., and J.-F. Gaillard (1996), Biogeochemical dynamics in aquatic sediments, Reviews in Mineralogy and Geochemistry, 34(1), 335-376.

van Genuchten, M. T., and P. J. Wierenga (1976), Mass Transfer Studies in Sorbing Porous Media I. Analytical Solutions1, Soil Science Society of America Journal, 40(4), 473-480.

van Genuchten, M. T., F. J. Leij, T. H. Skaggs, N. Toride, S. A. Bradford, and E. M. Pontedeiro (2013), Exact analytical solutions for contaminant transport in rivers 1. The equilibrium advection-dispersion equation, J Hydrol Hydromech, 61(2), 146-160.

Vinograd, J. R., and J. W. McBain (1941), Diffusion of Electrolytes and of the Ions in their Mixtures, Journal of the American Chemical Society, 63(7), 2008-2015.

Wang, Y. F., and P. VanCappellen (1996), A multicomponent reactive transport model of early diagenesis: Application to redox cycling in coastal marine sediments, Geochimica Et Cosmochimica Acta, 60(16), 2993-3014.

Ye, Y., G. Chiogna, O. A. Cirpka, P. Grathwohl, and M. Rolle (2015a), Experimental Evidence of Helical Flow in Porous Media, Phys Rev Lett, 115(19), 194502.

Ye, Y., G. Chiogna, O. Cirpka, P. Grathwohl, and M. Rolle (2015b), Experimental investigation of compound-specific dilution of solute plumes in saturated porous media: 2-D vs. 3-D flow-through systems, Journal of Contaminant Hydrology, 172, 33-47.

Zhang, C. Y., K. Dehoff, N. Hess, M. Oostrom, T. W. Wietsma, A. J. Valocchi, B. W. Fouke, and C. J. Werth (2010), Pore-Scale Study of Transverse Mixing Induced CaCO3 Precipitation and Permeability Reduction in a Model Subsurface Sedimentary System, Environmental Science & Technology, 44(20), 7833-7838.

Chapter 7

Conclusions

This work focuses on investigating the influence of electrochemical effects on multicomponent ionic transport especially under flow-through conditions. By performing laboratory experiments and numerical modeling, we present a detailed investigation to provide improved understanding of charge-induced Coulombic interactions during the multicomponent transport of ionic species in two-dimensional saturated porous media. The outcomes of this thesis offer new insights regarding the coupled diffusive/dispersive movement and establish the importance of small-scale electrostatic effects on macroscopic multicomponent ionic transport also when advection is the dominant mass-transfer process. In particular, the main conclusions of this work are summarized in the following points:

- *Relevance of electrostatic effects in advection-dominated regimes.* As shown in Chapter 2, the Coulombic interactions are relevant not only in diffusion-dominated but also in advection-dominated systems. Laboratory bench-scale experiments were performed with different combinations of charged solutes in a controlled quasi 2-D flow-through setup applying advection-dominated flow-through regimes (flow velocities: ~1.5 and ~6 m/day). The experimental results and their interpretation suggest that electrostatic gradients can significantly affect the transverse displacement as well as plume dilution of the transported charged species by modifying their diffusive/dispersive fluxes. The nature and magnitude of such modification on the diffusive/dispersive movement (i.e., compared to the "liberated" state) for a particular ion depends, specifically, on the presence of other dissolved charged species, their mobilities, charge, and concentration gradients. Consistent outcomes were also obtained in the experiments presented in other chapters (3, 4, and 6), where the flow conditions were also characteristic of advection-dominated regimes.

- *Effects of heterogeneity*. In Chapter 3, we extended the investigation of multicomponent ionic transport in heterogeneous flow-fields under steady-state flow and transport conditions. Based on the outcomes obtained from the Darcy-scale laboratory experiments, it was confirmed that the micro-scale electrochemical effects, occurring at molecular scale and most commonly related to aqueous diffusion, do not vanish in heterogeneous porous media. Such small-scale effects propagate through the scales and can lead to significantly different observations and transport behaviors for different ionic species in macro-scale domains containing both flow-diverging around low-permeability zones and flow-focusing in high-permeability zones. The effect of heterogeneity at larger scale was also investigated in Chapter 5. Here, numerical simulations, with a newly developed code coupling a multicomponent ionic formulation with the geochemical code PHREEQC (Parkhurst and Appelo, 2013), were

used to assess the influence of physical and geochemical heterogeneity at larger field scales.

- *Effects of solution composition and impact on pH fronts propagation.* Multicomponent ionic dispersion during the transport of charged species was also found to be highly dependent on the composition of the transported electrolyte solution. In the experiments presented in Chapter 4, we specifically focused on the influence of solution composition for the transport of pH under identical hydraulic and transport conditions. The experimental observations demonstrate that the different compositions of the same ionic species lead to remarkably different electromigration effects resulting in distinct transverse displacements of pH fronts and extents of dilution of the acidic plumes. In fact, diffusive/dispersive migration of a specific ion, and in particular of protons, can be significantly accelerated or retarded (compared to its "liberated" state) depending on the concentration of other dissolved charged species in the system. For these particular experimental conditions (Chapter 4), the vertical penetration and dilution of the pH fronts varied by, respectively, up to 36% and 26% solely due to the electrostatic interactions originating from the two different solution compositions.

- *Development of new modeling tools.* In this work we have proposed new two-dimensional numerical modeling approaches able to rigorously account for the electrochemical migration term during multicomponent transport of charged species. Modeling tools were developed in different stages during the work of this dissertation and proved to be invaluable to quantitatively interpret the experimental results. Specifically, Chapter 5 was exclusively dedicated to model development and in particular to the coupling with the geochemical code PHREEQC (Parkhurst and Appelo, 2013). The model accurately describes conservative and reactive multicomponent ionic transport in both homogeneous and heterogeneous porous media. The adopted modeling approach is based on the local charge balance, multicomponent formulation of diffusive/dispersive fluxes (e.g., Lasaga, 1979; Boudreau et al., 2004), and accurate and spatially variable description of local hydrodynamic dispersion coefficients (e.g., Chiogna et al., 2011; Eckert et al., 2012). It is of key importance for accurately capturing the coupled diffusive/dispersive ionic fluxes to recognize the crucial role of aqueous diffusion not only in the pore-diffusion term but also in the mechanical dispersion term (e.g., Guedes de Carvalho and Delgado, 2005; Delgado, 2006; Bijelic and Blunt, 2007; Chiogna et al., 2010; Rolle et al., 2012; Scheven et al., 2014). In Chapter 6, we have verified the transient transport calculations by matching the laboratory breakthrough curves with the model outcomes. The application of this proposed multicomponent reactive-transport model is, however, not limited to laboratory Darcy-scale, and it can also be effectively used in complex field-scale problems with physical and/or geochemical heterogeneity.

- *Maps of multicomponent ionic flux components and electrical potential gradient.* In order to illustrate the ion-specific interactions during the multicomponent ionic transport, we introduced spatial mapping of two quantities: components of diffusive/dispersive fluxes of the transported ionic species, and the distribution of

electrical potential gradient. The first refers to the distribution of different contributions (i.e., pure diffusive/dispersive flux and electrochemical migration flux) of the total flux for the transported ions. As shown in Chapter 3–6, the use of these multicomponent ionic flux maps allows us to quantify and effectively visualize the electrostatic interactions. It is evident that the direction and magnitude of the ions electromigration is determined by the distribution of these flux terms. The second quantity refers to the spatial distribution of electrical potential gradient term, which describes the electrostatic potential (also known as diffusion potential) developed in different parts of the solute plume due to the different mobilities of transported ions. In Chapter 4, we have shown that these potential gradient maps can be useful in illustrating the effects of electrostatic force induced on individual charged species and in explaining the causes behind obtaining a particular flux distribution. Mapping of these quantities is helpful in providing new insights into the fundamental mechanisms of electromigration and also in deepening our process-based understanding of the ion-specific interactions between different species during multicomponent ionic transport.

- *Influence on transient transport and solute breakthrough.* In Chapter 5 and 6 we have shown the influence of electrostatic interactions during the transient transport of multicomponent ionic species. Our numerical simulations in Chapter 5 revealed that the Coulombic effects are also significant for both conservative and reactive transport scenarios under transient conditions. Such processes are important not only at laboratory bench-scale but also at larger field-scales including physical and geochemical heterogeneity. Laboratory experiments conducted in Chapter 6 showed first evidence of electromigration during the transient solute transport and demonstrated the impact of multicomponent ionic dispersion on breakthrough curves of ionic species.

The presented work provides deeper insights into the electrochemical migration effects and improved our capabilities to mathematically include such mechanisms in continuum scale solute transport models describing multicomponent ionic transport in porous media. However, open challenges remain, especially, beyond the experimental conditions tested during this dissertation. With a similar approach and based on the outcomes of the current work, further research should be undertaken to specifically address the following points,

- *Reactive transport experiments.* In our experiments, we only studied conservative solute transport of multicomponent ionic species. As a further step, laboratory experiments should be performed including different geochemical processes along with solution compositions close to natural groundwater systems to identify the impact of charge effects on reactive transport. In the literature, although a few studies included multicomponent diffusion in the treatment of other physical and chemical processes in porous media (e.g., Giambalvo et al., 2002; Maher et al., 2006; Li et al., 2008; Appelo et al., 2010, and Liu et al., 2011), to date, electrostatic effects during multicomponent reactive transport in controlled laboratory experiments (e.g., Bauer et al., 2009; Tartakovsky et al., 2008; Redden et al., 2014; Haberer et al., 2015) have not been investigated in detail.

- *Field-scale investigations.* It would be worth conducting similar controlled experiments or model-based interpretation of experimental datasets in the field sites where aquifer system is extensively explored and well characterized. This would also provide an additional opportunity to test the proposed multicomponent ionic transport model. As a next step, one could also consider addressing field-scale multicomponent reactive transport problems by systematically applying increasing level of complexity in the description of physical and geochemical heterogeneity.

- *Effects of ionic-strength gradients.* The experiments performed in this work used dilute solutions of electrolyte species. The outcomes can be generalized to include the additional influence of activity gradients (e.g., Lasaga, 1979; Appelo and Wersin, 2007) by conducting further experiments with the ionic solutions containing different ionic-strengths. This additional contribution can lead to interesting observations during multicomponent ionic transport and would be of practical interest for applications focused, for instance, on the mixing between fresh water and salt water solutions in porous media.

- *Extension to fully 3-D transport.* The framework used in this work (i.e., experimental studies and numerical modeling) should be extended to fully 3-D setups, in which the effects of compound-specific dispersion were, in fact, found to be more pronounced and plume dilution was remarkably enhanced compared to 2-D transport (e.g., Chiogna et al., 2014; Ye et al., 2015a; 2015b; Cirpka et al., 2015).

Solute transport in natural subsurface conditions is affected by the complex interplay between different factors including heterogeneity, flow topology, anisotropy, interactions with porous matrix, and geochemical reactions. Therefore, it is of utmost importance to establish quantitative descriptions of the fundamental physical and geochemical processes occurring at different scales during solute transport in porous media. This work provided new insights to the understanding of transport processes in porous media and, in particular, to the role of electrochemical mechanisms on multicomponent ionic transport. Experimental evidence was provided in high-resolution Darcy-scale experiments. Such experiments have been performed under flow-through conditions and have been always accompanied by the development of new modeling approaches. The latter have been validated with the experimental data and represent valuable tools that can be used in a wide variety of applications for the rigorous description of multicomponent ionic transport of major ions and charged contaminants at both laboratory and field scales.

References

Appelo, C. A. J., Van Loon, L. R., and Wersin, P. (2010). Multicomponent diffusion of a suite of tracers (HTO, Cl, Br, I, Na, Sr, Cs) in a single sample of Opalinus Clay. *Geochimica et Cosmochimica Acta, 74*(4), 1201-1219. doi:10.1016/j.gca.2009.11.013

Appelo, C. A. J., & Wersin, P. (2007). Multicomponent diffusion modeling in clay systems with application to the diffusion of tritium, iodide, and sodium in opalinus clay. *Environmental Science & Technology, 41*(14), 5002-5007. doi:Doi 10.1021/Es0629256

Bauer, R. D., Rolle, M., Bauer, S., Eberhardt, C., Grathwohl, P., Kolditz, O., and Griebler, C. (2009). Enhanced biodegradation by hydraulic heterogeneities in petroleum hydrocarbon plumes. *Journal of Contaminant Hydrology, 105*(1–2), 56-68. doi:10.1016/j.jconhyd.2008.11.004

Bijeljic, B., and Blunt, M. J. (2007). Pore-scale modeling of transverse dispersion in porous media. *Water Resour. Res., 43*(12), W12S11. doi:10.1029/2006wr005700

Boudreau, B. P., Meysman, F. J. R., and Middelburg, J. J. (2004). Multicomponent ionic diffusion in porewaters: Coulombic effects revisited. *Earth Planet. Sci. Lett*. 222, 653-666.

Chiogna, G., Cirpka, O. A., Grathwohl, P., and Rolle, M. (2011). Relevance of local compound-specific transverse dispersion for conservative and reactive mixing in heterogeneous porous media. *Water Resour. Res., 47*(7), W07540. doi:10.1029/2010wr010270

Chiogna, G., Eberhardt, C., Grathwohl, P., Cirpka, O. A., and Rolle, M. (2010). Evidence of Compound-Dependent Hydrodynamic and Mechanical Transverse Dispersion by Multitracer Laboratory Experiments. *Environmental Science & Technology, 44*(2), 688-693. doi:Doi 10.1021/Es9023964

Chiogna, G., Rolle, M., Bellin, A., and Cirpka, O. A. (2014). Helicity and flow topology in three-dimensional anisotropic porous media. *Advances in Water Resources, 73*, 134-143. doi:http://dx.doi.org/10.1016/j.advwatres.2014.06.017

Cirpka, O. A., Chiogna, G., Rolle, M., and Bellin, A. (2015). Transverse mixing in three-dimensional nonstationary anisotropic heterogeneous porous media. *Water Resources Research, 51*(1), 241-260. doi:10.1002/2014WR015331

Delgado, J. M. P. Q. (2006). A critical review of dispersion in packed beds. *Heat and Mass Transfer, 42*(4), 279-310. doi:10.1007/s00231-005-0019-0

Eckert D., Rolle, M., and Cirpka, O. A. (2012). Numerical simulation of isotope fractionation in steady-state bioreactive transport controlled by transverse mixing. *J. Contam. Hydrol*. 140–141, 95-106.

Giambalvo, E. R., Steefel, C. I., Fisher, A. T., Rosenberg, N. D., and Wheat, C. G. (2002). Effect of fluid-sediment reaction on hydrothermal fluxes of major elements, eastern flank of the Juan de Fuca Ridge. *Geochimica et Cosmochimica Acta, 66*(10),Doi 10.1016/S0016-7037(01)00878-X

Guedes de Carvalho, J. R. F., and Delgado, J. M. P. Q. (2005). Overall map and correlation of dispersion data for flow through granular packed beds. *Chemical Engineering Science, 60*(2), 365-375. doi:http://dx.doi.org/10.1016/j.ces.2004.07.121

Haberer, C. M., Muniruzzaman, M., Grathwohl, P., and Rolle, M. (2015). Diffusive/Dispersive and Reactive Fronts in Porous Media: Fe (II)-Oxidation at the Unsaturated/Saturated Interface. *Vadose Zone Journal, 14(5)*. doi:http://dx.doi.org/10.2136/vzj2014.07.0091

Lasaga, A. C. (1979). The treatment of multi-component diffusion and ion pairs in diagenetic fluxes. *American Journal of Science, 279*(3), 324-346. doi:10.2475/ajs.279.3.324

Li, L., Steefel, C. I., and Yang, L. (2008). Scale dependence of mineral dissolution rates within single pores and fractures. *Geochimica et Cosmochimica Acta, 72*(2), 360-377. doi:DOI 10.1016/j.gca.2007.10.027

Liu, C. X., Shang, J. Y., and Zachara, J. M. (2011). Multispecies diffusion models: A study of uranyl species diffusion. *Water Resources Research, 47*. W12514. Doi 10.1029/2011wr010575

Maher, K., Steefel, C. I., DePaolo, D. J., and Viani, B. E. (2006). The mineral dissolution rate conundrum: Insights from reactive transport modeling of U isotopes and pore fluid chemistry in marine sediments. *Geochimica et Cosmochimica Acta, 70*(2), 337-363. doi:http://dx.doi.org/10.1016/j.gca.2005.09.001

Parkhurst, D. L., and Appelo, C. A. J. (2013). *Description of input and examples for PHREEQC version 3- A computer program for speciation, batch-reaction, one dimensional transport, and inverse geochemical calculations* Vol. book 6, chapter. A43. (pp. 497 p.). doi:http://pubs.usgs.gov/tm/06/a43

Redden, G., Fox, D., Zhang, C., Fujita, Y., Guo, L., and Huang, H. (2014). $CaCO_3$ Precipitation, Transport and Sensing in Porous Media with In Situ Generation of Reactants. *Environmental Science & Technology, 48*(1), 542-549. doi:10.1021/es4029777

Rolle, M., Hochstetler, D. L., Chiogna, G., Kitanidis, P. K., and Grathwohl, P. (2012). Experimental Investigation and Pore-Scale Modeling Interpretation of Compound-Specific Transverse Dispersion in Porous Media. *Transport in Porous Media, 93*(3), 347-362. doi:10.1007/s11242-012-9953-8

Scheven, U. M., Khirevich, S., Daneyko, A., and Tallarek, U. (2014). Longitudinal and transverse dispersion in flow through random packings of spheres: A quantitative comparison of experiments, simulations, and models. *Physical Review E, 89*(5), 053023.

Tartakovsky, A. M., Redden, G., Lichtner, P. C., Scheibe, T. D., and Meakin, P. (2008). Mixing-induced precipitation: Experimental study and multiscale numerical analysis. *Water Resources Research, 44*(6). doi: 10.1029/2006wr005725

Ye, Y., Chiogna, G., Cirpka, O., Grathwohl, P., and Rolle, M. (2015a). Experimental investigation of compound-specific dilution of solute plumes in saturated porous media: 2-D vs. 3-D flow-through systems. *Journal of Contaminant Hydrology, 172*, 33-47. doi:http://dx.doi.org/10.1016/j.jconhyd.2014.11.002

Ye, Y., Chiogna, G., Cirpka, O. A., Grathwohl, P., and Rolle, M. (2015b). Enhancement of plume dilution in two-dimensional and three-dimensional porous media by flow focusing in high-permeability inclusions. *Water Resources Research, 51*(7), 5582-5602. doi:10.1002/2015WR016962

EBERHARD KARLS
UNIVERSITÄT
TÜBINGEN

Mathematisch-Naturwissenschaftliche Fakultät

Erklärung nach § 5 Abs. 2 Nr. 7 der Promotionsordnung der Math.-Nat. Fakultät

-Anteil an gemeinschaftlichen Veröffentlichungen-
Nur bei kumulativer Dissertation erforderlich!

Declaration according to § 5 Abs. 2 No. 7 of the PromO of the Faculty of Science

-Share in publications done in team work-

Name: Muhammad Muniruzzaman

List of Publications

1. Muniruzzaman, M., Haberer, C. M., Grathwohl, P., and Rolle, M. (2014). Multicomponent ionic dispersion during transport of electrolytes in heterogeneous porous media: Experiments and model-based interpretation. Geochimica et Cosmochimica Acta, 141(0), 656-669.
2. Muniruzzaman, M., and Rolle, M. (2015). Impact of multicomponent ionic transport on pH fronts propagation in saturated porous media. Water Resources Research, 51(8), 6739-6755.
3. Muniruzzaman, M., and Rolle, M., (2016). Modeling multicomponent ionic transport in groundwater with IPhreeqc coupling: electrostatic interactions and geochemical reactions in homogeneous and heterogeneous domains. Advances in Water Resources, (*under review*).
4. Muniruzzaman, M., and Rolle, M., (2016). Experimental investigation of the impact of compound-specific dispersion and electrostatic interactions on transient transport and solute breakthrough. (*in preparation*).
5. Rolle, M., Muniruzzaman, M., Haberer, C. M., and Grathwohl, P. (2013). Coulombic effects in advection-dominated transport of electrolytes in porous media: Multicomponent ionic dispersion. Geochimica et Cosmochimica Acta, 120(0), 195-205.
6. Haberer, C. M., Muniruzzaman, M., Grathwohl, P., and Rolle, M. (2015). Diffusive/Dispersive and Reactive Fronts in Porous Media: Fe (II)-Oxidation at the Unsaturated/Saturated Interface. Vadose Zone Journal, 14(5)*.
*(*Publication during the PhD but not included in the dissertation)*

Nr.	Accepted for publication yes/no	Number of all authors	Position of the candidate in list of authors	Scientific ideas of candidate (%)	Data generation by candidate (%)	Analysis and Interpretation by candidate (%)	Paper writing by candidate (%)
1	yes	4	First	80	100	90	90
2	yes	2	First	90	100	90	90
3	no	2	First	90	100	90	90
4	no	2	First	90	100	90	90
5	yes	4	Second	30	80	80	10
6	yes	4	Second	10	20	30	10

I certify that the above statement is correct.

Date, Signature of the candidate

I/We certify that the above statement is correct.

Date, Signature of the doctoral committee or at least of one of the supervisors

Curriculum Vitae

Personal Information

Muhammad Muniruzzaman

Address: Hölderlinstr. 12, 72074 Tübingen, Germany

Email: md.muniruzzaman@uni-tuebingen.de
md.muniruzzaman@gmx.de

Place of birth: Dhaka, Bangladesh | Date of birth: 06/04/1987 | Nationality: Bangladeshi

Education

11/2012 – present
PhD Candidate in Environmental Geosciences
Center for Applied Geoscience
University of Tübingen, Germany

09/2010 – 09/2012
MSc in Applied Environmental Geoscience
Center for Applied Geoscience
University of Tübingen, Germany
Average Grade: 1.3 (excellent) on a scale of 1 to 4 (EU standard)
MSc Thesis: Transport of electrolytes in a 2D saturated porous media: Experimental investigation and numerical modeling

12/2004 – 08/2009
BSc in Chemical Engineering
Department of Chemical Engineering
Bangladesh University of Engineering and Technology, Bangladesh
Average Grade: 3.21 on a scale of 4 (North American standard)
BSc Thesis: Resource recovery and waste treatment in a lead-acid battery plant.

Workshops

30/09/2013 – 04/10/2013 ▪ Fall school on *Reactive Transport Modeling*, Bad Boll, Germany

24/03/2014 – 28/03/2014 ▪ Short course on *Applied Reactive Transport Modelling*, Bordeaux, France

15/08/2015 – 16/08/2015 ▪ Short course on *Pore-Scale Geochemical Processes*, Prague, Czech Republic

07/04/2015 – 10/02/2016 ▪ Integrated Hydrosystem Modelling 2015 Conference, Tübingen, Germany

08/05/2014 – 09/05/2015 ▪ PhD workshop on reactive transport modelling, Karlsruhe, Germany

13/11/2014 – 14/11/2014 ▪ PhD meeting on reactive transport modelling, Tübingen, Germany

15/04/2015 – 30/05/2016 ▪ Research stay at Department of Environmental Engineering
Technical University of Denmark

Award and Scholarships

- Best poster award in competition in *Geosymposium und Quenstedt-Jahresfeier, 2013*
- First prize in the *VisiSens Best TimeLapse Movie Competition 2013* (co-author)
- Baden -Wuerttemberg Landesstiftung Stipendium (scholarship) for MSc studies, 2011-2012
- Merit scholarship at Bangladesh University of Engineering and Technology, Dhaka

Publications

Peer-reviewed articles

- **Muniruzzaman, M.**, and M. Rolle (2016), Modeling multicomponent ionic transport in groundwater with IPhreeqc coupling: electrostatic interactions and geochemical reactions in homogeneous and heterogeneous domains, Adv. Water Res. (*under review*).
- **Muniruzzaman, M.**, and M. Rolle (2016), Experimental investigation of the impact of compound-specific dispersion and electrostatic interactions on transient transport and solute breakthrough (*in prep.*).
- **Muniruzzaman, M.**, and M. Rolle (2015), Impact of multicomponent ionic transport on pH fronts propagation in saturated porous media, Water Resour. Res., 51, doi: 10.1002/2015WR017134.
- Haberer, C. M., **M. Muniruzzaman**, P. Grathwohl, and M. Rolle (2015), Diffusive/Dispersive and reactive fronts in porous media: Fe (II)-oxidation at the unsaturated/saturated interface, Vadose Zone J., doi:10.2136/vzj2014.07.0091.
- **Muniruzzaman, M.**, C. M. Haberer, P. Grathwohl, and M. Rolle (2014), Multicomponent ionic dispersion during transport of electrolytes in heterogeneous porous media: Experiments and model-based interpretation, Geochim. Cosmochim. Acta, 141(0), 656-669.
- Rolle, M., **M. Muniruzzaman**, C. M. Haberer, and P. Grathwohl (2013), Coulombic effects in advection-dominated transport of electrolytes in porous media: Multicomponent ionic dispersion, Geochim. Cosmochim. Acta, 120(0), 195-205.

Conference Proceedings

- **Muniruzzaman, M**. and Rolle, M. (2016), Multicomponent ionic transport and pH fronts propagation, *Goldschmidt Conference Abstracts,* 2641*, Goldschmidt, 2016*.
- **Muniruzzaman, M**. and Rolle, M. (2015), Impact of multicomponent ionic transport on pH fronts propagation in saturated porous media, *EGU General Assembly Conference Abstracts, 18, EGU2016-4035, 2016*.
- **Muniruzzaman, M**. and Rolle, M. (2015), Coulombic interactions and multicomponent ionic dispersion during transport of charged species in heterogeneous porous media, *Interpore, Interpore Conference Abstracts*.
- **Muniruzzaman, M.**, Haberer, C. M., Grathwohl, P., and Rolle, M. (2014), Coulombic effects and multicomponent ionic dispersion during transport of electrolytes in porous media, *EGU General Assembly Conference Abstracts, 16, 6074*.